UNIVERSITÀ DEGLI STUDI DI PALERMO

Dottorato in Ingegneria dell'innovazione tecnologica

Dipartimento dell'Innovazione Industriale e Digitale (DIID)

Ingegneria Chimica, Gestionale, Informatica, Meccanica

Settore Scientifico Disciplinare ING-IND/26

Resource, environmental and economic considerations in the development of a Reverse Electrodialysis Heat Engine

IL DOTTORE

Michail Papapetrou

IL TUTOR

Prof. Ing. Giorgio Micale

CO-TUTORS

Prof. Umberto La Commare

Prof. Andrea Cipollina

IL COORDINATORE:

Prof. Ing. Antonio Chella

Acknowledgements

First of all, I would like to thank my supervisors Giorgio Micale, Andrea Cipollina and Umberto La Commare for their support and guidance. It was a privilege to be part of their group and benefit from cooperating with all members of staff and students there. I have to mention in particular Francesco Giacalone and Bartolomé Ortega for the support they provided to me in the use of the process simulation tool they have developed for the RED Heat Engine and Alessandro Tamburini for the great cooperation and support, especially when it came to scientific publications.

I would also like to thank everyone at WIP-Renewable Energies in Munich. Working for this company has always made it possible to come as close as I could to enjoying my job. In addition to that, I am grateful now to them for allowing me the flexibility to focus on my thesis over the past 3 years. And this would not have been possible without the brilliance and efficiency of my colleague George Kosmadakis.

The work of this thesis was carried out within the framework of the RED Heat-to-Power project. As such, I would like to acknowledge the funding of the European Commission through the H2020 programme and to thank all consortium partners for their cooperation. Below you can see the logos of all partners, together with the link to the project website and the full disclaimer. I would also like to than Prof. Nick Holden and his team in University College Dublin, for the time I spent there and their expert support on my Life Cycle Assessment work.

My parents have always been an inspiration for me and they are the reason that I chose to focus on science.

Throughout my career I have cooperated in projects with many innovators; they have all contributed to forming who I am, and part of the credit for this thesis belongs to them.

Above all, is my family: Claire, Lucas and Alex. I would dedicate that work to them, but I think it is more suitable to dedicate to them more of my time now that the thesis is completed.

Disclaimer:

This work was part of the project “Conversion of Low Grade Heat to Power through closed-loop Reverse Electro-Dialysis” or RED Heat-to-Power for short. The logos of the project partners are shown below. More information is available under www.red-heat-to-power.eu.

This project has received funding from the European Union’s Horizon 2020 research and innovation programme under grant agreement No 640667.

Table of Contents

Summary

Introduction

The RED Heat Engine operates as a closed-loop RED system, where limited amounts of artificial saline solutions are used as working fluids. The solutions exiting from the RED unit are regenerated by means of a separation step, which uses low-temperature heat as its energy source. Essentially the system converts low-grade heat to electricity.

There are two main alternative regeneration strategies: (i) extract solvent from the high salinity solution and move it to the low salinity solution or (ii) extract salt from the low salinity solution and move it to the high salinity solution. In this thesis are considered the Multi-effect distillation (MED) and the Membrane Distillation (MD) under the solvent extraction strategy, while the use of thermolytic salts with distillation and absorption columns are considered for the solute extraction option.

This thesis studied the RED Heat Engine perspectives in terms of:

- the sources that can provide the heat necessary for running the system, indicating the characteristics that the system should have to match the market requirements
- the life-cycle impacts, providing evidence for the environmental credentials of the technology, compared to alternative electricity supply options, and providing direction to system designs with the minimum environmental impacts.
- economic performance, improving the understanding of the factors that affect it, including the design options, operational choices as well as the development over time of the key components in terms of performance and cost

Resource Assessment

The first part of the work focuses on the sources that can provide the heat necessary for running the RED Heat Engine. It presents the collection, processing and assessment of data regarding the heat quantity that is technically possible to be recovered from waste heat sources, from geothermal sources and from solar energy. The analysis is carried out per country and in Europe overall, assessing the overall amount of heat and the temperature level at which this heat is available. The average size of the RED Heat Engine per site has also been assessed in order to guide the technical development, defining the size of systems that should be targeted.

The available waste heat and its potential from various sectors was studied, such as industry, biogas plants, gas compressor stations and marine auxiliary engines. These four sectors show a total waste heat potential of about 700 TWh/year. The heat that is available at temperatures over 200 ^{o}C is still a valuable resource that can be used in other applications. When focusing only at the heat that is available at temperatures lower than that, the overall potential is reduced to 484 TWh/year. The potential at biogas plants and on marine auxiliary engines corresponds to small RED Heat Engines in the range of 7 to 15 kW_e. The potential at gas compression stations is for much larger systems, in the range of 6 to 10 MW_e. Finally, in industry the range can be very wide, but most would fall within the range of 280 to 700 kW_e. These results are summarised in Table A.

Table A: Technical potential of waste heat in all sectors of interest

Sector	Technical potential of waste heat (TWh/year)	Temperature range	Average waste heat per site (GWh/year)	Average range of RED Heat Engine per site (kW_e)
Industry	103.31	Up to 200 °C	100.00	280 – 700
Biogas plants	29.00	80-150 °C	1.70	7-15
Marine	149.40	80-90 °C	1.65	7-15
Gas compressor stations	202.31	Up to 250 °C	660.00	6,000-10,000
Total	**484.02**			

Overall, the industrial waste heat is the most interesting resource, as the size is large enough, the capacity factor is high and there are a lot of such sites in Europe and globally. For assessing in more detail the waste heat that can be recovered from the industry, differentiating per country, per sector and per temperature level, an original methodology was developed and applied. A summary of the results is provided in Fig. A.

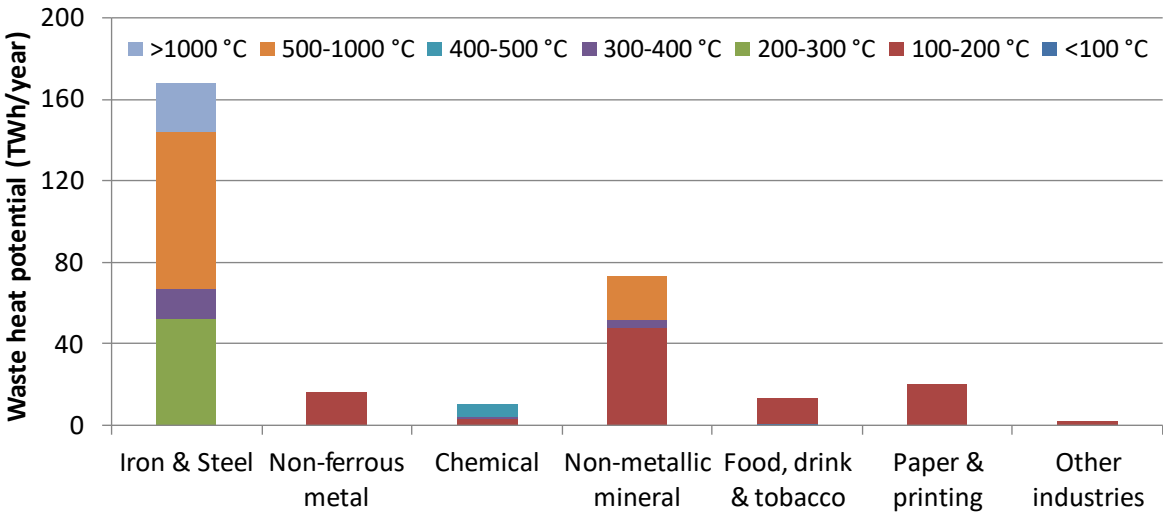

Figure A: Waste heat potential per industrial sector and temperature level for EU industry

The geothermal resource analysis showed that such plants should be of large size, in order to compensate the initial investment costs and produce large amounts of electricity. Even for large plants the costs are still high for being competitive with alternative solutions. The only possibility for reaching costs that are acceptable is to use existing geothermal fields of large scale.

The potential daily and seasonal solar heat production was calculated for different regions in Europe, representing the main climatic zones (south/central/north Europe). As expected, the potential is much higher in Southern Europe than in Central and Norther Europe, while the evacuated tube collectors give significantly higher amounts of heat that the flat plate collectors. However, it has been shown that this is an option that is not feasible, because of the high investment costs for collecting the heat and the low capacity factor.

Environmental Assessment

In order to assess the environmental impacts of the RED Heat Engine, a dedicated analysis has been undertaken. In line with the ISO 14044:2006 the study includes four phases: (i) Definition of goal and scope, (ii) Life Cycle Inventory Analysis, (iii) Life Cycle Impact Assessment and (iv) Life Cycle Interpretation. The assessment was carried out with a model that was built in GaBi, a Life Cycle commercial software provided by the company thinkstep. The flows of the LCA model are expressed as functions of the techno-economic model, allowing to study easily how the environmental impacts vary when changing the system design or operating conditions.

Various scenarios were analysed, with different regeneration systems and operating conditions for the RED Heat Engine, while a sensitivity analysis was also carried out. The analysis focused mainly on the following four impact factors: Global Warming Potential, Eutrophication Potential, Acidification Potential and Ozone Depletion Potential.

The results show that the RED Heat Engine has lower environmental impacts compared to other energy generation technologies and compared to grid electricity. Between the different regeneration technologies, the distillation columns with the thermolytic salts give the highest environmental impacts and the MED gives the lowest environmental impact. The factors that affect mostly the environmental performance of the RED Heat Engine are the system lifetime, the performance of the ion exchange membranes and the metallic parts of the heat exchangers. The system efficiency is not that important from an environmental impact point of view. Reducing the number of MED effects has a positive impact to the environmental performance, even if it reduces the efficiency, because it leads to much lower use of metals for heat exchangers.

A comparison of the CO2eq. emissions of the various RED Heat Engine configurations with the emissions with other generating technologies is shown in Fig. B. This graph illustrates the potential of the RED Heat Engine to be among the electricity generating technologies with the lowest emissions.

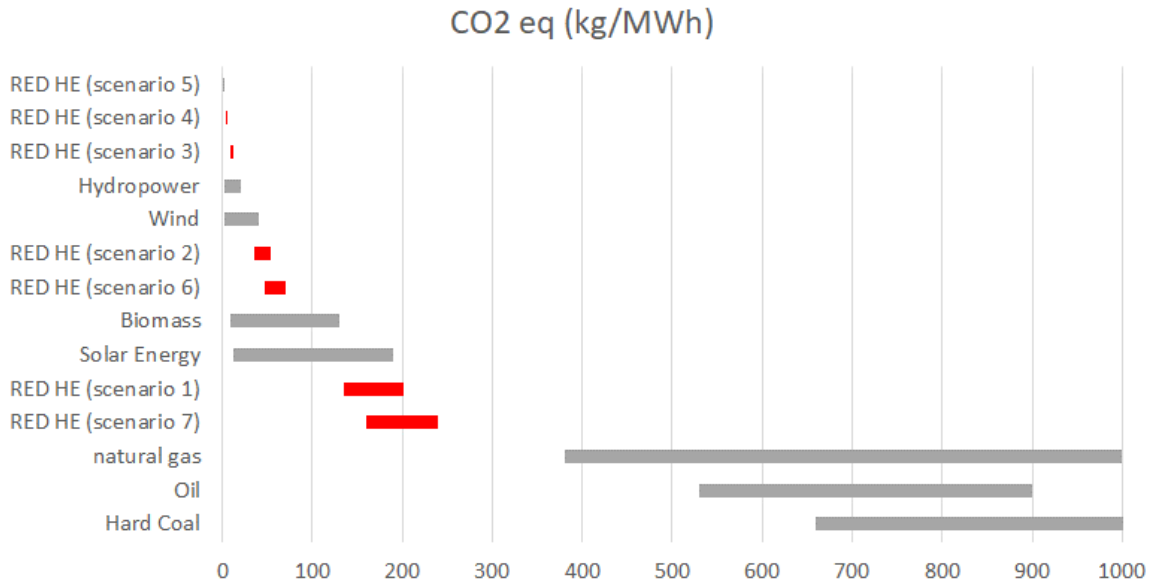

Figure B: Emissions of CO2 eq. from the various RED Heat Engine configurations compared to emissions from other electricity generation technologies

Finally, the comparison with the Osmotic Heat Engine and the Organic Rankine cycle shows that the environmental performance is comparable, but the Organic Rankine Cycle still achieves the lowest environmental impacts.

Economic Assessment

An economic analysis of the RED Heat Engine has been performed. A detailed cost model has been developed, which takes into account all parameters of this technology. All main configurations of the RED Heat Engine are examined, in order to evaluate the most cost-effective one for each type of application. The developed model uses as input results from the process simulator, which are then analysed. The Levelized Cost of Electricity (LCOE) is calculated for each system configuration. This value is used as the criterion for the economic evaluation. The annual balance considers both capital and running costs (e.g. operation and maintenance), as well as the inflation and the discount rate.

A sensitivity analysis has been also conducted, since there are many parameters that have a wide uncertainty range, as well as others that depend on the application itself. Apart from that and to account for the future cost of the components and materials used, appropriate estimations have been developed and used in the model. The outcome is to estimate the LCOE development potential in the future; the years 2020, 2030, and 2050 have been used as the milestones.

When using the RED-MED configuration, the results show that the use of ion exchange membranes that will be optimised for the RED Heat Engine application is necessary for this technology to become cost-competitive. By reducing the number of MED effects, the thermal efficiency is reduced, but at the same time the LCOE is also decreased. The salt that showed the best performance was KAc, while operation of the RED with the working fluid at 50 ^{o}C has also a very positive effect on the LCOE. The LCOE for the RED-MD configuration is higher than the one of the RED-MED, for typical conditions and system sizes. The main advantage of the RED-

MD is that it can be scaled down for use at systems with capacity of few KW without a very negative effect on its LCOE, because the MD specific cost is more or less the same as the MD size is varied, which is not the case for the MED. The result is that the RED-MD is in general most cost-efficient than RED-MED for systems that are below 20-30 kW_e. But the LCOE is at levels that are not competitive with other technologies. For the RED-thermolytic salts configuration it has been shown that the LCOE is much higher than all other combinations for any system size.

The sensitivity analysis and the assessment of future scenarios showed that there is the potential to reach LCOE values below 0.10 €/kWh in various cases and applications in the future. In general, relatively large system sizes and high capacity factor are necessary to reach LCOE values that can make the system competitive. However, when it is necessary to install infrastructure for making the heat available to the RED Heat Engine (or when there is a charge for the heat supply) the values of LCOE are too high for the system to be financially viable.

Some of the LCOE results for the different system configurations for 2020, 2030 and 2050 are provided in Fig. C.

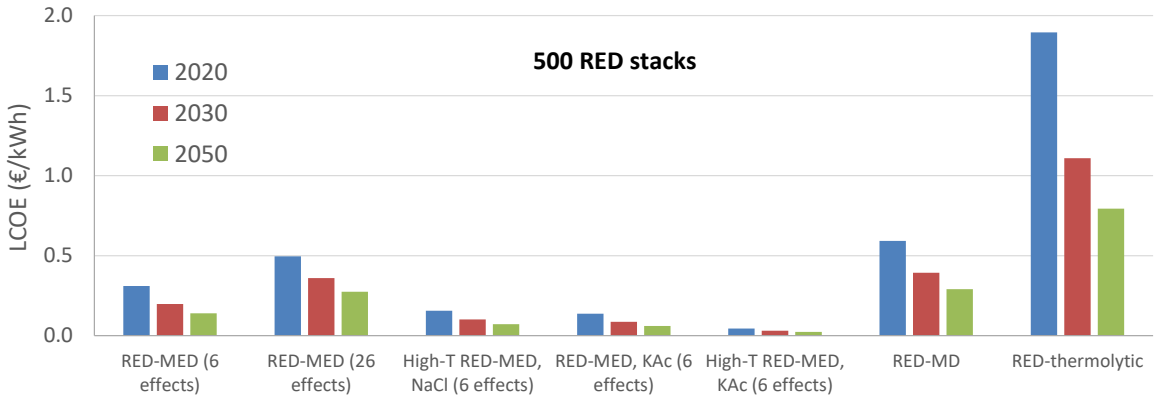

Figure C: LCOE comparison of medium-scale RED with 500 stacks and different regeneration units, including future scenarios

Finally, the operation of the RED-MED at peak power mode can be a very interesting application of this technology, especially as more variable renewable energy sources are connected to the grid, making more volatile the wholesale energy prices and more valuable the provision of flexibility to the system.

Conclusions

A number of case studies have been used with possible applications of the RED Heat Engine in real circumstances in order to better illustrate the results. It has been concluded that the following are among the main conditions that are necessary for the competitiveness of the RED Heat Engine:

- Optimised membranes that at least match the “future membrane” properties
- High capacity factors
- Medium to large scale applications
- Free availability of heat

For future research, the most important priority is the improvement of the ion exchange membranes, aiming for achieving the performance targets of “future membranes” and aiming to make them available at the competitive costs. Once this is achieved, the RED Heat Engine can enter the market, targeting applications where there is more than 1 to 2 MW_{th} of heat available at temperatures of at least 80 ^{o}C, with capacity factors over 60% without any associated costs. The most common setting are the medium or large-scale industrial plants as well as the gas compression stations, provided that they operate with a high capacity factor.

The next priority, for widening the potential applications to sites where smaller systems can be installed, is the research on regeneration systems that are competitive at smaller scale. The one option is to develop MD systems with drastically reduced specific costs, through a combination of increased system performance and reduced costs of the main components. The other option is to develop MED designs suitable for smaller scale applications. One option for reducing the specific costs and the environmental impacts of MED systems would be the development and use of polymeric heat exchangers.

Overall, the RED Heat Engine is a promising technology that could play a role in the future power system contributing to the decarbonisation targets set by the European Union.

Introduction

1. Reverse Electrodialysis

1.1 From natural water streams to electricity

Salinity gradient power (SGP) is the chemical energy potential associated with the "controlled" mixing of two salt solutions at different concentrations. The concept of SGP was described for the first time in 1954 by Pattle [1]. There are different technologies available for recovering this energy and convert it into a more exploitable form. The two prevailing technologies are Pressure Retarded Osmosis (PRO) and Reverse Electrodialysis (RED). Both PRO and RED were described by Loeb already in the 1970s [2,3].

This thesis is focused on reverse electrodialysis (RED). In RED cation exchange membranes (CEM) and anion exchange membranes (AEM) are placed in an alternating way in order to produce diluate and concentrate compartments, as shown in Fig. 1. The concentrate compartment (HIGH) is then filled with the high concentration salt solution while the diluate compartment (LOW) is filled with the low concentration salt solution. The salt concentration difference (salt gradient) between both compartments invokes a Nernst potential across the cell pair which causes an electrical current to flow through the electrical load connected to the electrodes.

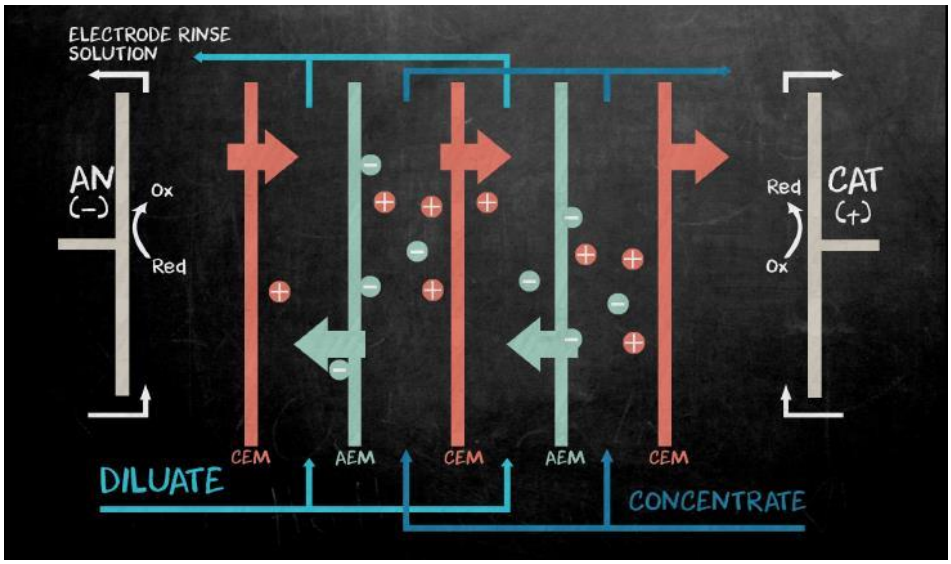

Figure 1: Sketch of a Reverse Electrodialysis stack (credits: Michele Tedesco)

It has been shown in the literature [4–7] that RED is a promising technology that can help harnessing the potential energy available in nature in the form of solutions with different salinities, that are in close proximity to each other, such as seawater with freshwater and brine with brackish water. However, working with natural solutions has limitations, which have already been pointed out in the literature [8]: First of all, the requirement for availability of adequate flow rates of two solutions with different salinities at the same location is an important geographical constraint. Even in the cases where two solutions are available at significant quantities, the potential for energy production is determined by the characteristics of the

available saline streams, such as salinity, temperature and presence of multivalent ions. Finally, the requirements for pre-treatment of the streams for avoiding fouling of the membranes adds costs and increases the energy requirements to the overall process.

1.2 From low-temperature heat to electricity

In order to deal with these limitations, the Reverse Electrodialysis Heat Engine (RED Heat Engine) has been proposed, where RED operates as a closed-loop system. In this concept, limited amounts of artificial saline solutions are used as working fluids. The solutions exiting from the RED unit are then regenerated, in order to restore the original salinity gradient, by means of a separation step, which uses low-temperature heat as its energy source. Essentially the system converts low-grade heat to electricity, as shown in Fig. 2. This technology is particularly interesting, not only because it has the potential to offer higher thermal efficiency compared to Organic Rankine Cycle (ORC) for heat at temperatures between 60 ^{o}C and 120 ^{o}C [8], but also because the salty solutions can be stored in tanks, practically cost-free [9], giving the technology a unique flexibility, an energy storage function, which is getting more and more important in the current energy system with high shares of variable renewable energy sources.

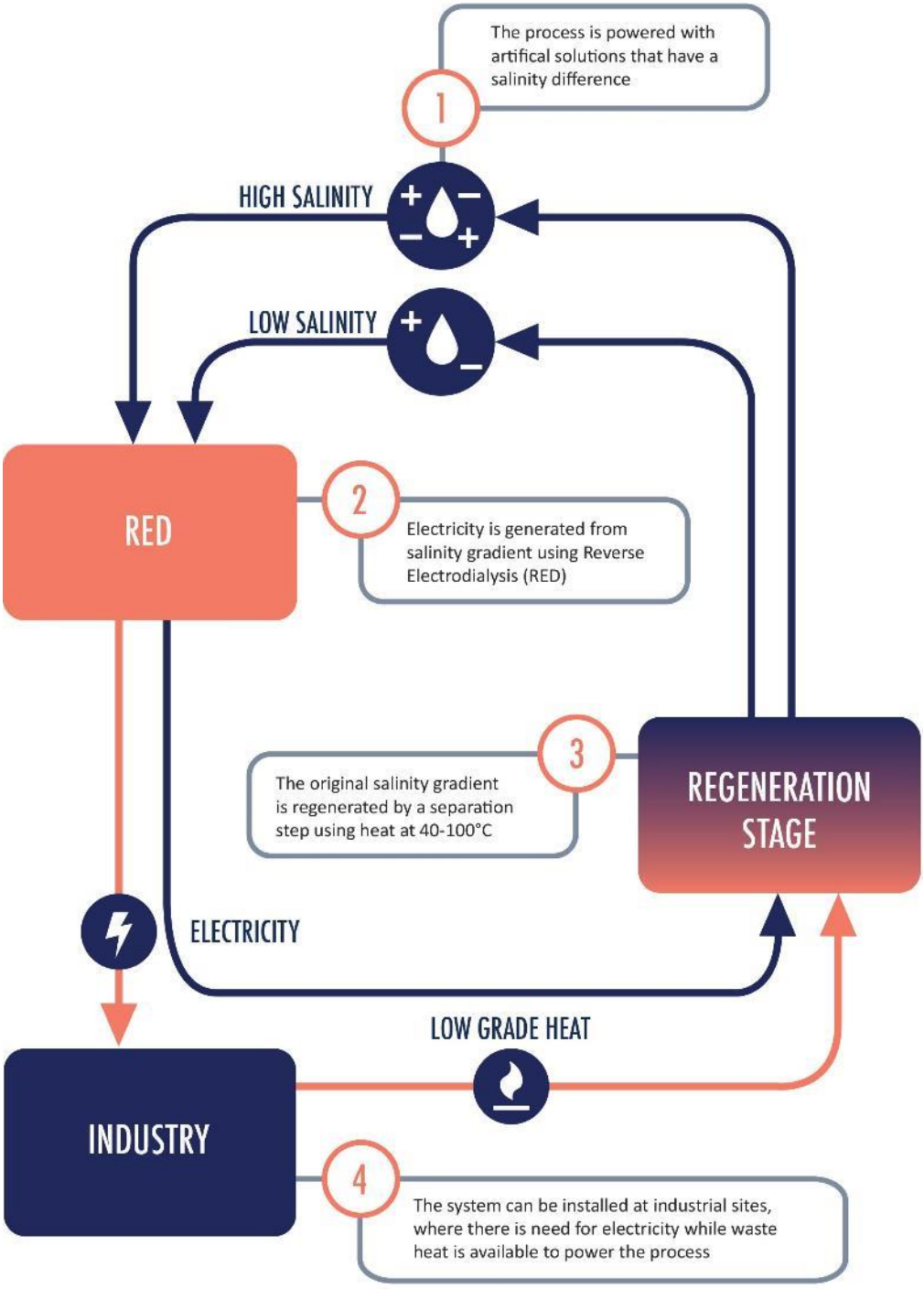

Figure 2: The RED Heat Engine concept

2. Aim and Objectives

This PhD thesis has the overall aim of supporting the fast progression of the RED Heat Engine through the Technology Readiness Level (TRL) scale by linking the technical work with the resource, environmental and economic aspects, guiding the research and innovation work in the route from the laboratory to the market.

The work, after the introduction is structured in three main separate parts, followed by a final part that includes some case studies and the conclusions. Below are outlined the main idea and objectives for each of these three parts.

2.1 Resource Assessment

The limitations of using naturally available saline solutions have been pointed out in section 1.1 and have led to the idea of the RED Heat Engine. The RED Heat Engine builds on the knowledge gained from the development of RED, but it exploits a different source of energy: low-temperature heat. The conviction that this is a promising approach is based on the assumption that heat at low temperatures is widely available and cannot be used easily for other applications. This assumption is indeed shared by several researchers [10–13]. There are also studies offering some assessments and data about actual waste heat availability [14–16], but there is a lack of in-depth analysis of sources where heat is available at suitable conditions for powering the RED Heat Engine.

The objective is to fill this gap, coming up with detailed information on the heat quantity that is technically possible to be recovered (per site, per country and in Europe overall) and the temperature level at which this heat is available. This information will be used for guiding the technical development and the market analysis of the RED Heat Engine.

2.2 Environmental Assessment

The RED Heat Engine will be using an available resource (low temperature heat) and convert it to a useful product (electricity). As it operates in closed loop, there are no associated emissions. Therefore, the initial assumption is that this is an environmentally friendly technology. Typically, in the early stages of developing such technologies, the “green” credentials are used to attract support for research. However, when proceeding without performing a proper environmental assessment in parallel to all stages of development, hurdles can arise later-on to the adoption of the technology. An example of that are the photovoltaics (PV). They were introduced as an environmental friendly technology, but as their market share started growing, studies came out scrutinising the life-cycle energy performance [17], which harmed (temporarily) the popularity of the technology. Another example are the biofuels, which back in 2006 were labelled as the successor to petrol and diesel for transportation [18]. However, very soon the discussions around the social and environmental impacts of biofuel production [19] slowed the developments and dampened the enthusiasm.

In order to avoid such risks with the RED Heat Engine, a comprehensive assessment of the life-cycle impacts will be carried out, providing early warning in case there are environmental issues that might prove to be of concern and identifying strategies for dealing with them. As part of this work, the relative impacts of the different system designs and operating conditions will be studied, providing input to the work of the technology development. The results will be also compared to alternative electricity generation/supply options.

2.3 Economic Assessment

The research during the development stage of renewable energy technologies is often focused on the issue of improving productivity and efficiency. For example, in the field of dye-sensitised solar cells, reaching efficiencies of 15% was deemed as an important milestone [20]. Or in the field of RED for electricity generation, the target is set in terms of power density of the ion exchange membranes [21]. However, the moment at which the transition from the laboratory to the market happens is not associated directly to the moment of achieving any technological objectives. Apart from the case where policies are put in place to support faster introduction of technologies in the market, like in the case of feed-in-tariffs for solar and wind energy in Europe [22], the transition is defined by market forces, which are driven by the competitiveness of the technology. Of course, the improvements in efficiency and productivity can contribute in improving the cost performance of a technology. But the two objectives are not always aligned. Therefore, understanding the factors that drive the costs and developing a strategy for cost minimisation should be an integrated part of developing new technologies. It is common to have "techno-economic analysis" studies for new energy technologies, but as shown in [23], the economic part of the analysis is often done in a simplistic way, with the main focus always placed on the technical model and performance assessment.

The objective of the third part in this thesis is to perform a comprehensive analysis of the RED Heat Engine economic feasibility, improving the understanding of the factors that affect it, including the design options, operational choices as well as cost and performance development of key components over time.

3. RED Heat Engine Configurations

The work on analysing the RED Heat Engine configurations was published in 2017:

A. Tamburini, M. Tedesco, A. Cipollina, G. Micale, M. Ciofalo, M. Papapetrou, W. Van Baak, A. Piacentino, Reverse electrodialysis heat engine for sustainable power production, Appl. Energy. 206 (2017) Pages 1334-1353, *doi:10.1016/j.apenergy.2017.10.008*

3.1 Regeneration

There are various design options for the RED Heat Engine, mostly defined by the different technologies that can be used for the regeneration process. A comprehensive overview of the different options is provided by Tamburini et al. [24] and is described briefly below. There are two main alternative regeneration strategies:

(i) extract solvent from the high salinity solution and move it to the low salinity solution, as shown in Fig. 3

(ii) extract salt from the low salinity solution and move it to the high salinity solution, as shown in Fig. 4

When using the solvent extraction approach, there are a number of technological options that could be employed according to [24]: Evaporative separation processes, Liquid-Liquid extraction process (organic solvent), Azeotropic mixture separation, Absorption/desorption and

adsorption/desorption cycles and Extraction by Forward Osmosis using T-sensitive drawing agents. Regarding the solute extraction process the main alternatives include the use of thermolytic salts and the use of the salt precipitation processes.

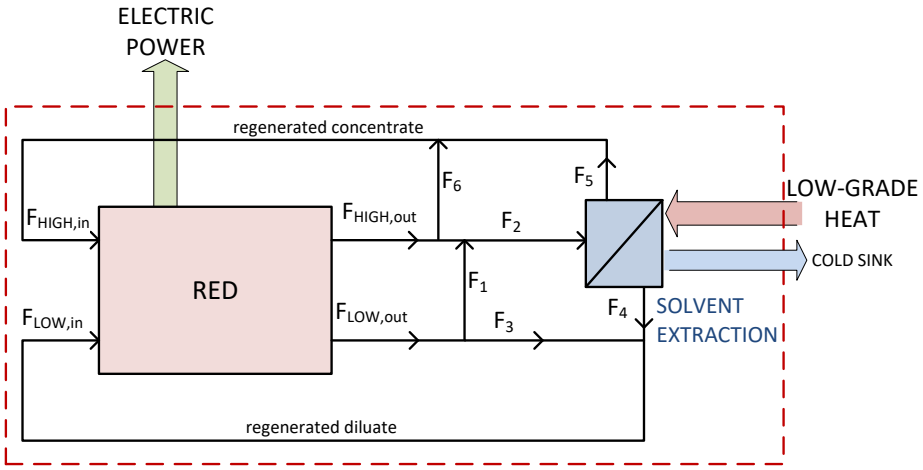

Figure 3: The RED Heat Engine with the solvent extraction process

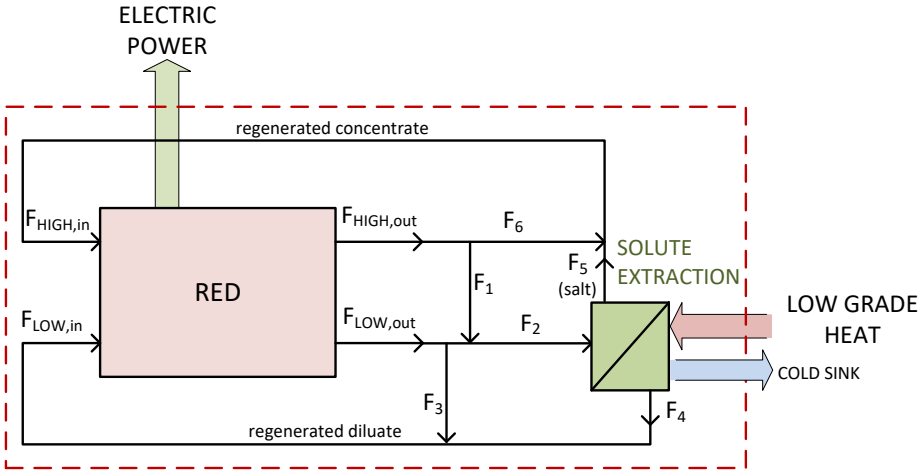

Figure 4: The RED Heat Engine with the solute extraction process

Out of all these options, the most mature one is the evaporative solvent extraction process, as it builds on the many years of development of the thermal desalination industry. More specifically, either the well-established Multi Effect Distillation (MED) process can be used, or the up-coming Membrane Distillation (MD) process. With regards to the salt extraction approach, the option of using thermolytic salts is selected here, which offers the option to regenerate the solution in a two-step process. This includes an air stripping or a distillation column to separate the salt from the diluate in the form of gases and an absorption column for dissolving the salts back in the concentrate. The use of thermolytic salts has attracted attention

as a promising option, both for the RED Heat Engine [25], but also for other similar applications such as forward osmosis [26,27] and the osmotic heat engine [28].

These are the three regeneration options that will be examined as part of this thesis, when alternative options are studied for assessing their environmental impacts (Part II) and economic performance (Part III). More specifically, the following technologies and conditions are considered in this thesis, reflecting the decisions [29] of the RED Heat-to-Power consortium [30].

Three technologies are selected as the most promising for regeneration:

- Multi-effect distillation (MED), which has the potential to reach the highest efficiencies
- Membrane Distillation (MD), which can still benefit from the desalination industry developments, while it is also possible to implement at small-scale, as opposed to MED
- Distillation and absorption columns, for use with thermolytic salts

With regards to the artificial solutions, water has been chosen as the only solvent to consider. Regarding the salts:

- Both sodium chloride (NaCl) and potassium acetate (KAc) will be considered for the solutions to be used with the MED evaporative regeneration option and only NaCl for MD
- The chosen thermolytic salt is ammonium bicarbonate (NH_4HCO_3)

3.2 Reverse Electrodialysis

Throughout the text it is assumed that capacitive electrodes [31] are used at the stacks as well as profiled membranes, which eliminate the need for spacers [32].

With regards to the ion exchange membranes (IEM), two options have been considered, which are termed “current membranes” and “future membranes”.

Table 1: Characteristics of the Ion Exchange membranes considered

Properties	Current Membranes	Future Membranes
Permselectivity [%]	89(1)	95(2)
Water Permeability [ml/(bar·h·m^2)]	8(2)	2(2)
Salt permeability [m^2/s]	4.5 10^{-12}(2)	1.1 10^{-12}(2)
Resistance [Ω·cm^2]	3.53 (1)	0.882 (1)

(1) *reference concentration of 2 M-0.05M NaCl water solutions. Property functions of the solution concentrations.*

(2) *assumed constant in the whole range of concentrations.*

All values here are for solutions at 25 °C

The properties of the *current membranes* are the ones matching the characteristics of the IEM used in the first laboratory tests in the RED Heat to Power project [33]. The future membranes

were defined by referring to the best values among those already achieved and reported in literature [34]. This definition of future membranes assumes that it will be possible to match the best performance already achieved, for all four categories listed in Table 1, in one single membrane optimised for the RED Heat Engine. As will be seen in Part III, we also assume that this future membrane will be made available at the market prices that are now used for the lower performing membranes, which will be also declining over the years.

In Fig. 5 are shown the resistance and permselectivity values for both current and future membranes in comparison with literature values [34]. Similarly, water permeability and salt diffusivity values are in the range of typical literature values: 10^{-11}-10^{-14} m^2/s for salt diffusivity and 1-20 ml/(bar h m^2) for water permeability (see Figure 4 in [35]).

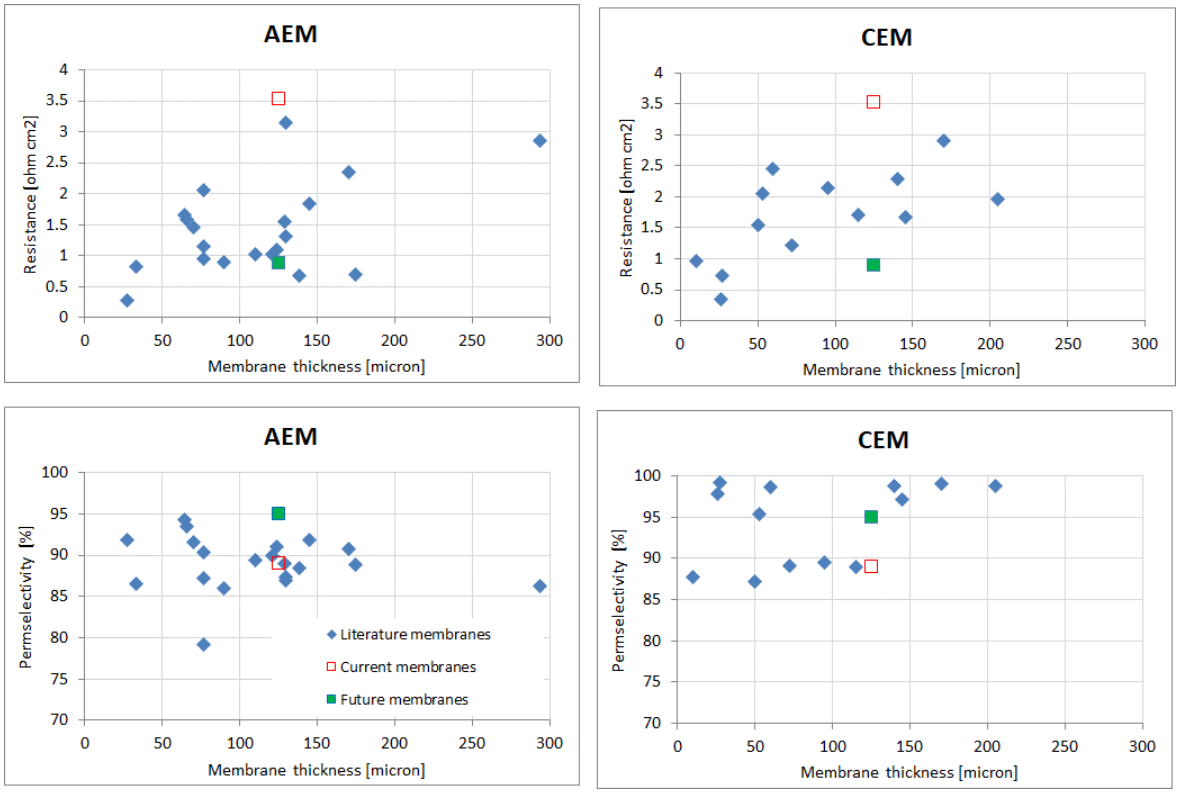

Figure 5: Membrane resistance (up) and permselectivity (down) as a function of membrane thickness for current and future membranes compared to literature [34]. Left: anionic exchange membranes. Right: cationic exchange membranes. Properties are relevant to 0.5M for the resistance and 0.5M-0.05M for the permselectivity.

It has been shown that when operating the RED with solutions at higher temperatures (40 to 80 °C) higher power densities can be achieved [6,7]. This option is considered in this thesis for the cases where the MED regeneration option is adopted. In order to calculate the performance of the system under higher temperatures, the process simulator [36] includes correlations (derived from experimental data) on the effect that the temperature has on IEM resistance (higher temperatures lead to lower resistance), permselectivity (higher temperature leads to lower permselectivity), water permeability and salt permeability.

The option of operating at higher temperatures cannot be applied with the thermolytic salts, as lifting the temperature above the ambient one will lead to salt degradation. In the case of MD it could be applied, but that is not presented in this thesis, as the option was not examined in the process simulator.

3.3 Other equipment and services required

In Fig. 6 is provided a more detailed scheme of the RED Heat Engine, where MED is used as a regeneration system. This illustration is useful for highlighting that only minimal equipment and services in addition to the RED stack and the regeneration system are necessary for the Engine to operate.

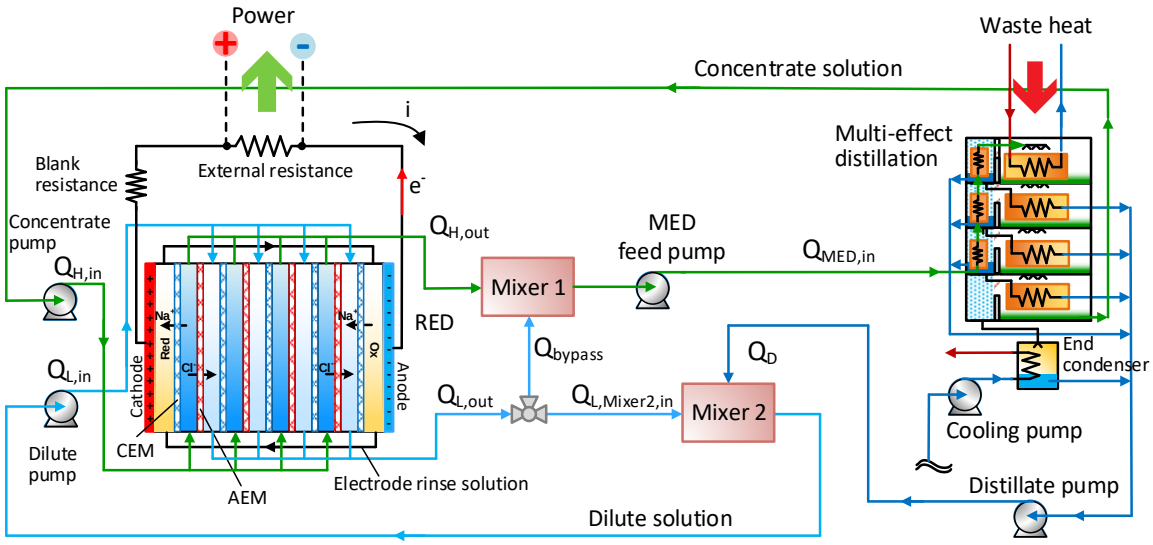

Figure 6: Outline of the RED Heat engine using MED as the regeneration option

The equipment consists mainly of pumps, pipes and mixers, which circulate the solutions between the MED and the RED stack. In terms of services, external AC power will be used in most of the cases for the operation of the pumps. The only other critical factor is the provision of the heat for the operation of the system. This depends on the heat source that will be used, and specialised equipment might be necessary for harnessing the heat and giving it to the regeneration system.

4. Structure of the Thesis

Following the introduction, the thesis is structured in four parts.

Part I includes the work on the identification, quantification and evaluation of the different sources where heat can come from, at adequate quantities and at a suitable temperature to be used at the RED Heat Engine. After an introduction, the first resource to be studied is waste heat. This chapter is broken down into the analysis of waste heat from the industry, from power plants, from ships and finally from gas compressing stations. The next chapter is dedicated to

geothermal heat and the final chapter to solar heat. Within each of these chapters, the methodology that was followed is described first, then the data collection process is presented and finally are provided the results and the conclusions.

The environmental assessment is presented in Part II. The Life Cycle Assessment (LCA) method has been adopted for the analysis. As such, the structure of Part II was determined by the requirements of EN ISO 14044:2006 [37], which includes: (i) Definition of Goal and Scope, (ii) Life Cycle Inventory Analysis, (iii) Life Cycle Impact Assessment, (iv) Life Cycle Interpretation, and (v) Conclusions and Recommendations.

The third part of the thesis is dedicated to the economic analysis. The methodology and the model that was developed are introduced first, followed by a presentation and discussion of all parameters that need to be defined for the calculations. After that, the main results and their evaluation are presented. The following chapter includes a sensitivity analysis, studying how much would the results be affected if the input parameters varied from the estimated values. The chapter after that is dedicated to future scenarios, including assumption on the future development of the components' costs and performance. All results are put together and discussed in a chapter that compares the results for the different system configurations, followed by a chapter that discusses the option of operating the system in a mode, where instead of baseload, it provides peak power.

After the three main parts of the thesis is a section with case studies, which illustrate the main results of the work, followed by the general conclusions and recommendations.

Part I: Resource Assessment

1. Introduction

Part I examines the availability and characteristics of heat sources in Europe. These heat sources are available in various forms, such as waste heat or heat from solar and geothermal sources. It is essential to identify the expected scale and capacity of each source, as well as its temperature level, in order to provide feedback to the cost assessment and the initial business plan that would identify the most promising sectors to employ the RED Heat Engine.

Waste heat sources have the main advantage that they are readily available and the cost for harnessing this source is limited, requiring only heat harnessing equipment, such as heat exchangers. On the other hand, solar thermal and geothermal energy require investments to be made for collecting the heat. This initial investment should be recovered afterwards from electricity sales during the system operation, in order for the integrated plant (solar-RED Heat Engine or geothermal-RED Heat Engine) to be sustainable from the economic point of view.

In Chapter 2, waste heat sources have been identified, especially the ones corresponding to the temperature levels required by the RED Heat Engine (up to 200 ^{o}C). The analysis is implemented for each industry type, temperature level of waste heat, and EU country, in order to have available all necessary data that are required for identifying the most appropriate solutions.

Except from the industrial sector, the study also considers decentralized power plants based on biogas engines, whose main advantage is that their electricity production is currently subsidized in many European countries. The marine sector is also examined, where large amounts heat and co-produced and waste heat recovery technologies are already applied widely.

Finally, the potential from gas compressor stations is examined, which are usually operated with gas turbines with low/moderate efficiency, resulting to very large amounts of wasted heat per station. This heat is at high enough temperature to be recovered with the resulting RED Heat Engine capacity being within the MW scale.

In Chapter 3, the geothermal potential is examined with main parameters being the temperature of the geofluid and the depth of drilling, revealing the high initial costs related to this kind of plants. These aspects require the installation of heat exploitation technologies, such as the RED Heat Engine, at a large scale to compensate the very high initial investment costs.

In Chapter 4, heat production from solar thermal energy is examined. Different types of collector types are considered (flat plate, evacuated tube collector, PV/thermal). The analysis is conducted for representative locations in Europe covering south, central and north regions. Solar heat production is given as a function of temperature level, which has a direct effect on the RED Heat Engine efficiency.

2. Waste heat

2.1 Introduction

Waste heat is the rejected heat from various processes and is included in a thermal carrier. The most common ones are gaseous streams (e.g. exhaust gas, flaring gas, low-quality steam, and cooling air), liquid streams (e.g. hot oil, cooling water), and solids (e.g. commodities and products, such as hot steel). Waste heat is calculated as the heat of the carrier once it is cooled from its initial temperature (e.g. at 250 °C) up to the ambient one (usually 20 °C). There are many challenges involved in abstracting as much heat as possible from a carrier (in other words decreasing its temperature as much as possible), respecting all technical limitations. These limitations have to do mainly with the available equipment for harnessing the waste heat. Different types of heat exchangers are used for that purpose. Their pinch point temperature difference depends on the carrier type and the existing technology. For liquid streams it is usually 10-20 K, for gaseous streams it is increased to about 50 K, and for solids it is above 100 K. These temperature differences can decrease by increasing the effective heat exchanging surface area. That would lead to oversized components with much higher cost (in case of infinite heat exchanging surface, the temperature difference approaches zero). This solution is not favoured, which is also the overall outcome of relevant techno-economic studies [38–40].

As a result, the technical potential of waste heat is much lower than the overall available potential. This is easily illustrated with the standard example of flue gases with initial temperature of 250 °C, with the restriction that their temperature should not decrease below 150 °C (instead of reaching the ambient temperature), in order to avoid condensation of water vapor and the production of sulfuric acid (in case the combustion of fuel leads to the production of sulfur oxides – SO_2, which is the standard case mostly with diesel fuel and biogas/landfill gases). The relation of the technical with the overall potential of waste heat is illustrated in a report dealing with UK industrial waste heat (Ecofys Report) [41], shown in Fig. 2.1, where additionally the economic and commercial potential is depicted.

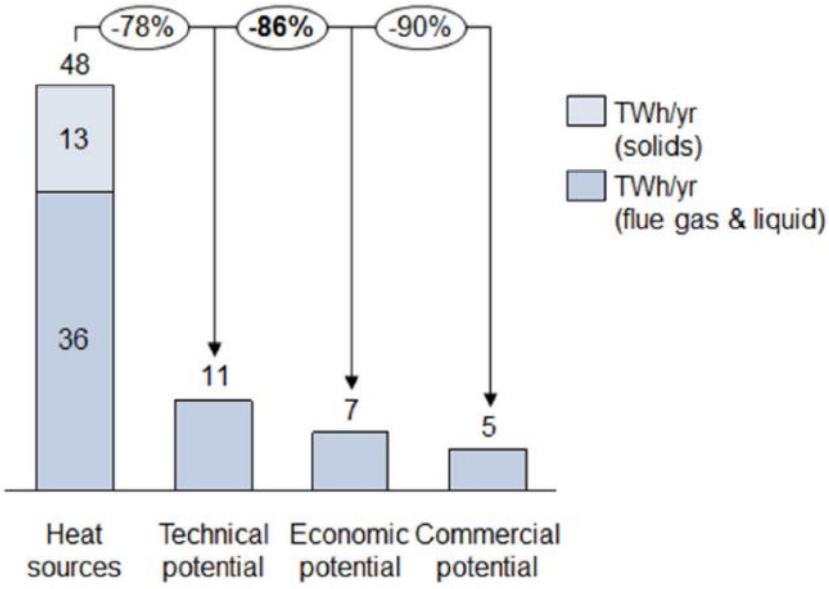

Figure 2.1: Potential of heat sources in UK [41]

The technical potential according to this report includes only gaseous and liquid streams (not solids, since the harnessing of heat from them is a very challenging task), and out of the 48 TWh/year, just 11 TWh/year (78% reduction) can be exploited using the limitations that have been discussed above.

2.2 Potential sectors for waste heat recovery and their energy consumption

There are four main sectors that have been identified and reject large amounts of heat that can be exploited by the RED Heat Engine, namely:

Industrial sector

Industrial waste heat corresponds to heat rejected from industrial processes, in which energy (mostly heat or electricity) is used to produce high-added value products. The amount of waste heat as a fraction of energy consumption varies widely between the various sectors, with a mean value of about 10%. The temperature of this heat also varies within a wide range, from about 50 ^{o}C up to 1000 ^{o}C, depending on the industrial sector (e.g. steel, paper, food, chemical) and the process. It becomes clear that the high diversity of rejected heat within this sector requires an in-depth study and analysis of all available data with the appropriate estimations. Focus is given on all sectors, while in the last sub-section the sectors with temperature of waste heat close to the needs of the RED Heat Engine, up to 150-200 ^{o}C will be examined more closely.

Power generation sector

In the power generation sector, power plants reject large amounts of heat, about 50-70% of the input heat, depending on their type (steam Rankine, combined cycle, nuclear, diesel engine, and gas turbines), technology (subcritical or supercritical steam Rankine, power-only or combined heat and power – CHP) and fuel type (coal, natural gas, oil, biogas). Large power plants usually have thermal efficiency about 35-55% (the highest efficiency is reached with Combined Cycle Gas Turbine (CCGT) plants and the lowest with coal-fired and nuclear plants). An estimation of the rejected heat of centralized power plants considers the electricity generation in EU of about 3000 TWh/year [42]. With a mean conversion efficiency of 40% (taking into account all different power plants: old/new, nuclear plants, steam power plants, etc.) the resulting waste heat from all power plants in EU is about 4500 TWh/year.

In all these plants, the main sources of waste heat are in the condenser (cooling towers) and in the exhaust gases. However, the rejected heat at the cooling system is at very low temperatures [43], about 30-40 ^{o}C, and the temperature of the exhaust gases usually reaches its minimum allowable limit (about 160-180 ^{o}C) and is not technically possible to be exploited. The situation is similar also with Concentrated Solar Power (CSP) plants, which harvest heat from the sun with different solar technologies [44] (e.g. parabolic troughs, heliostats with solar towers, linear Fresnel collectors, parabolic dish), which is then driven to a steam-based Rankine cycle [45], rejecting low-temperature heat at the condenser (at about 30-40 ^{o}C, depending on the season and ambient conditions). A similar case is also for geothermal plants (heat is supplied from the hot geofluid). Finally, gas turbines are mostly used for backup purposes or for covering the peaks of the load, with a very low capacity factor (up to 10%), making the exploitation of their waste heat not attractive.

Although the potential is high and large amounts of waste heat are rejected, their exploitation is not possible, due to technical restrictions or their very low-temperature. Therefore, the above sources from centralized power plants are not suitable to be exploited by the RED Heat Engine and will not be examined further in this thesis.

On the other hand, decentralized power plants based on internal combustion engines with capacity from few hundred kWs up to some MWs show some advantages for use with the RED Heat Engine. The most important one is the waste heat in the cooling circuit. Its temperature is about 80-90 °C, making it ideal for use by the RED Heat Engine. Especially the biogas engines, whose electricity is subsidized, seem an attractive option with their market share and applications steadily increasing over the past few years, although they are usually operated at CHP mode. The waste heat of the exhaust gases is not easily harnessed, since all these engines are supercharged and the hot gases leaving the engine cylinders are directed to turbo-compound devices, where their temperature decreases from about 400-500 °C (depending on fuel type) to about 200 °C, before leaving the engine. The remaining thermal content of this gas is already exploited in CHP biogas plants.

Marine sector

In the marine sector there are numerous ships mostly equipped with diesel engines for the main propulsion and for auxiliaries. In most of the ships there are waste heat recovery systems for steam production from the main engines (from both the exhaust gases and the cooling circuit) and from the exhaust of the auxiliary engines (with the highest potential). However, the waste heat of the cooling water of the auxiliary engines with typical temperature of 80-90 °C remains unexploited with its heat rejected to the sea (cooling is accomplished with seawater). This heat can be exploited by the RED Heat Engine, although there are severe space restrictions on ships.

Gas compression stations

Gas compression stations are used to maintain the pressure in the gas transportation pipes at about 70 bar. The compressors are operated with gas turbines, burning a small portion of the gas. Their exhaust gases with temperature at about 250 °C are readily available for heat recovery and exploitation.

In the next sections is presented the energy consumption of the four sectors identified, in order to gain a first view of the possible amounts of heat that can be recovered and finally exploited.

2.2.1 Energy consumption in the industrial sector

Energy consumption in the industrial sector represents a large fraction of the total energy consumption. In EU-28 it is about 25% according to Eurostat [46], as shown in Fig. 2.2.

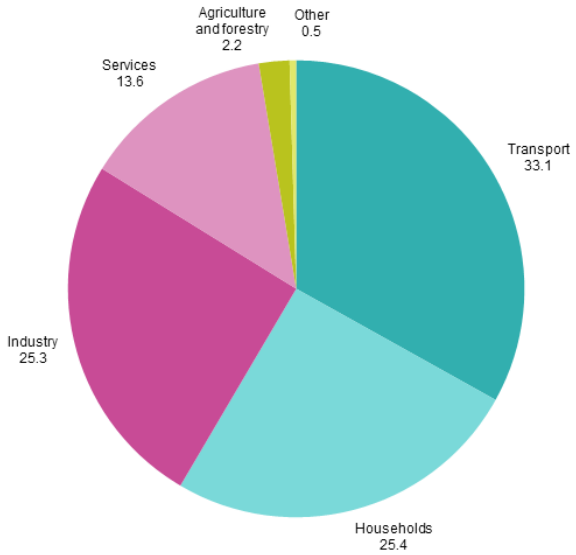

Figure 2.2: Energy consumption per sector in EU for 2015 [46]

This share of energy consumption varies widely among the EU countries, as shown in Fig. 2.3, according to Odyssee-Mure project [47] (depicting 2000 and 2014 data), ranging from 15% in Cyprus, Luxembourg and Denmark up to over 40% in Finland and Slovakia.

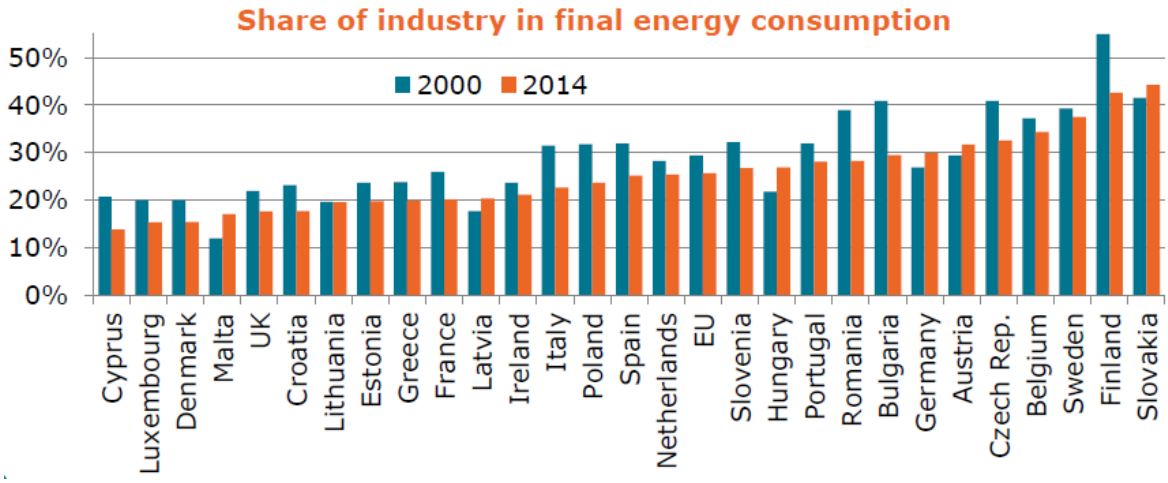

Figure 2.3: Share of industrial energy consumption in EU countries (2000 and 2014 data from [47])

The share of industry in final energy consumption has declined between 2000 to 2014 as the result of the following two reasons: (1) energy efficiency measures have started to be implemented in industry, focusing on reducing energy costs, and (2) rising share of energy consumption in other sectors, mainly in buildings, services and transportation, in which energy consumption in absolute figures has increased.

The evolution over time (from 2005 to 2015) of the industrial energy consumption (in absolute numbers) in the EU countries with medium/high industrial activity is presented in Fig. 2.4, according to Eurostat [42] (data given in TWh per year).

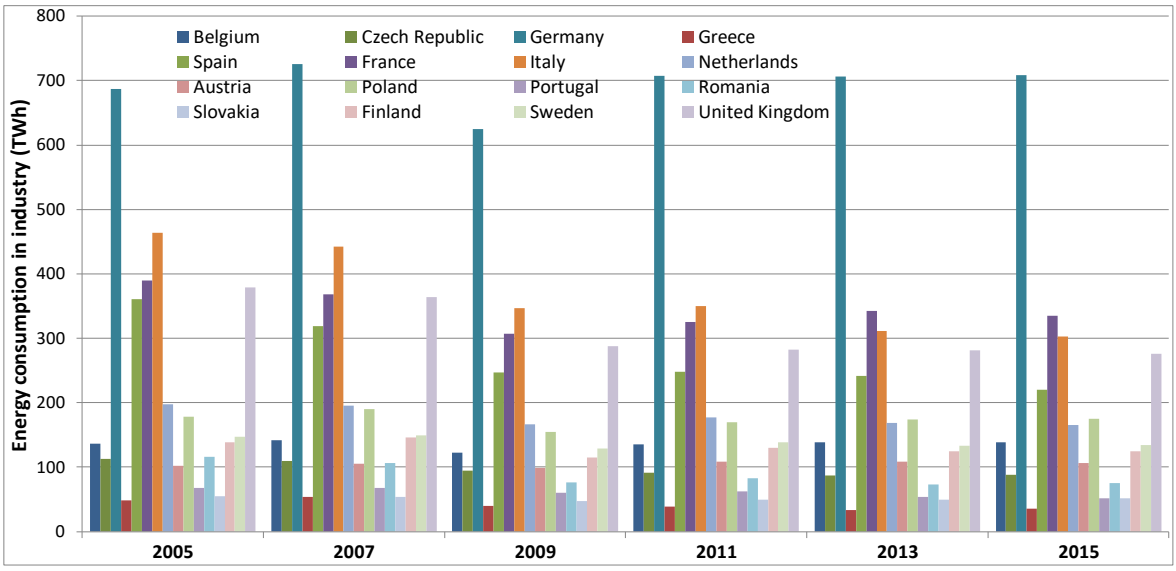

Figure 2.4: Energy consumption in industry in EU countries (2005-2015 data from [42])

The countries with the higher industrial energy consumption are Germany, Italy, France, UK, and Spain. These five countries represent about 60% of the total industrial energy consumption in EU, which is given in Fig. 2.5 (same Eurostat dataset as in Fig. 2.4).

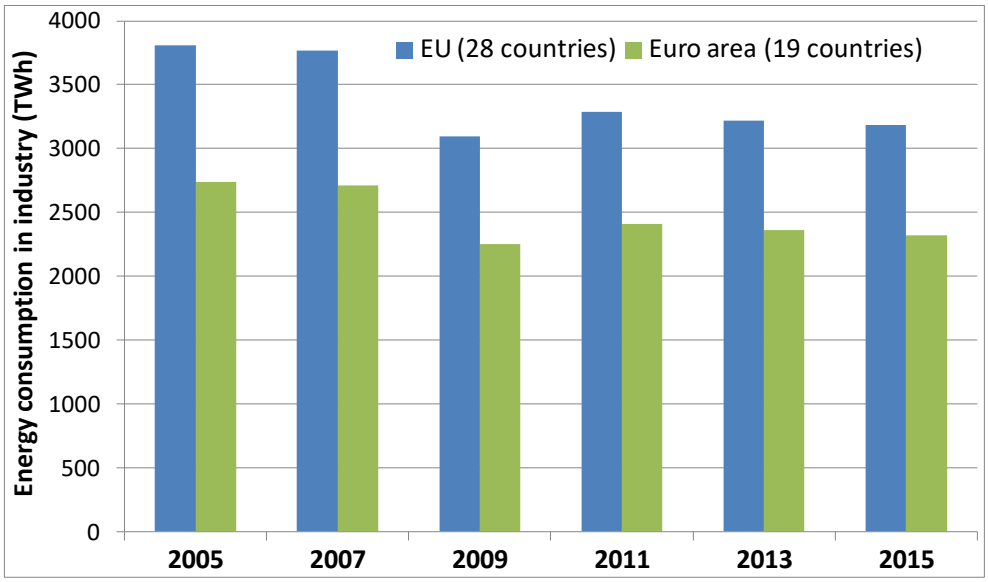

Figure 2.5: Energy consumption in industry in EU (2005-2015 data from [42])

Industrial energy consumption has decreased in 2009, mainly as a direct effect of economic recession, returning to positive growth in 2011 and remaining constant in EU-28 to about 3200 TWh up until 2015 (year with the latest available data).

The decrease in industrial energy consumption since 2000 is reflected with different magnitude in each industrial sector, according to the Odyssee-Mure report [48]. The industrial energy consumption per sector is shown in Fig. 2.6 for the years 2000, 2007 and 2014 (data given in Mtoe[1]).

[1] toe: tonne of oil equivalent (1 toe equals to 11630 kWh).

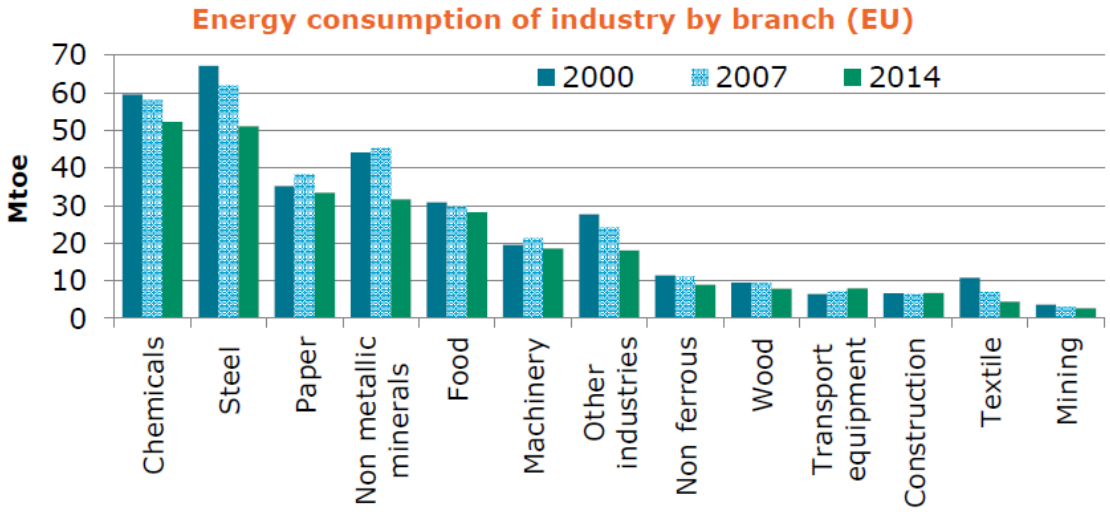

Figure 2.6: Energy consumption in industry per sector in the EU (2000, 2007, 2014 data from [48])

Chemical and steel industries are the largest energy consumers (consumption of about 50 Mtoe=580 TWh each), followed by paper, non-metallic minerals and food (consumption of about 30 Mtoe=350 TWh each). These five sectors represent about two thirds of the total energy consumption in industry. In Fig. 2.6 it is also clear that energy consumption has decreased within the period 2000 – 2014 in all major sectors with chemicals, steel and non-metallic minerals showing the largest decrease of about 20-25%.

A future projection of energy demand in industry is presented in an EC report [49] for different temperature levels (low: up to 100 °C, medium: 100-400 °C, high: over 400 °C). This projection is shown in Fig. 2.7.

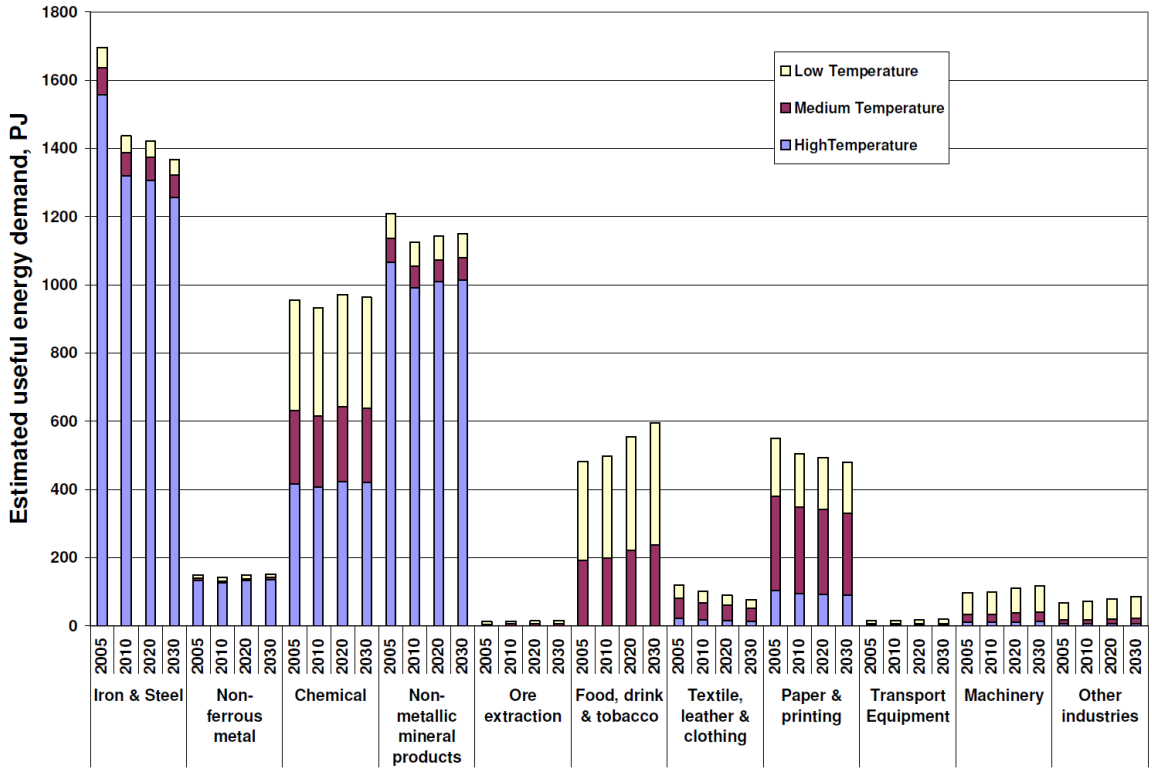

Figure 2.7: Estimation of heat demand in industry per sector in EU [49]

Moreover, each industrial sector has different specifications and temperature of heat demand. Usually, each industry requires heat at different temperature levels, starting from 60 °C (for washing and drying processes) and reaching even more than 1000 °C (in energy intensive industries, such as iron and steel, cement and glass). An illustration of the heat demand fraction of different temperature levels is observed in Fig. 2.8 [50].

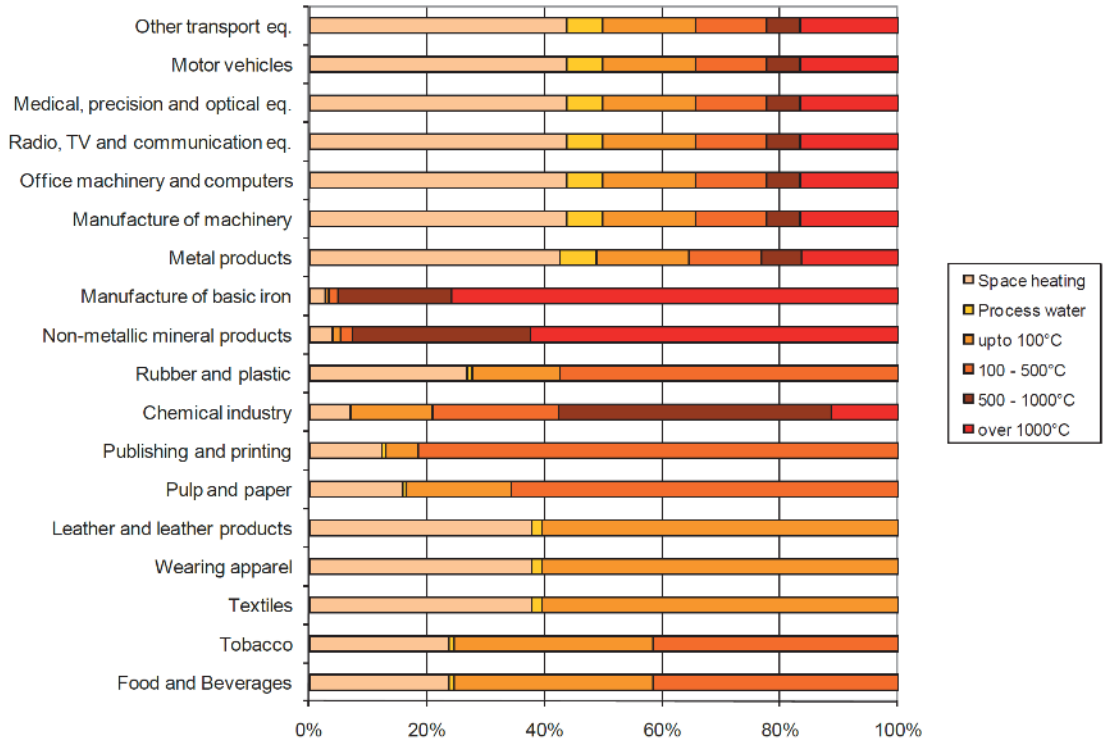

Figure 2.8: Fraction of heat demand according to temperature levels and industries [50]

Most of the industrial sectors require all ranges of heat [51], with food, tobacco, textiles and leather industries showing heat demand mostly up to 100 °C, while industries for manufacturing metals, steel and iron requiring mostly heat with temperature over 500 °C.

In another study, heat demand per temperature level has been calculated, which is given in Fig. 2.9 [52], with a different categorization of temperature levels.

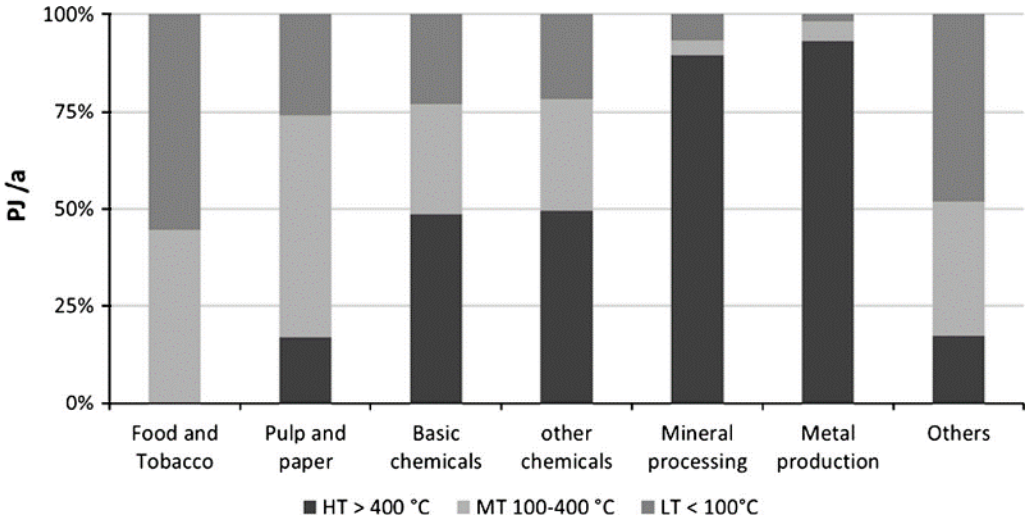

Figure 2.9: Fraction of heat demand according to temperature levels and industries [53]

The same conclusions are also valid here with metal production industries requiring very high temperature heat and food and paper industries much lower.

For the calculation of the waste heat in this thesis, the most recent heat consumption data available are used (2015 Eurostat data [42]). Data regarding the use of primary energy sources in industry (solid fuels, oil, gas, etc.) have been processed, in order to calculate (process) heat consumption in each sector and EU country. The fraction of electricity used for process heating is also added in this consumption (mostly in iron and steel industries). According to this analysis, heat consumption in all EU industries is 1820.73 TWh/year, with the contribution of each industrial sector depicted in Fig. 2.10. The remaining energy consumption of about 1400 TWh/year corresponds to space heating and cooling and electricity for pumps, motors, cooling/refrigeration, office equipment, and lighting [54].

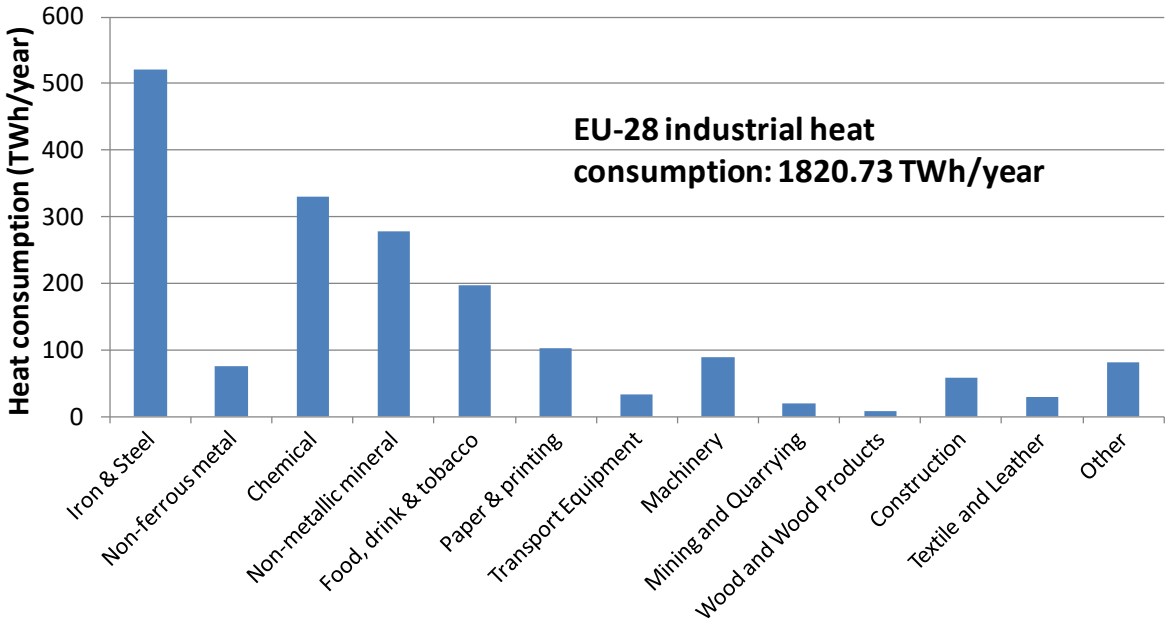

Figure 2.10: Heat consumption in industry in EU countries [42]

Even though Eurostat gives separate data for sectors such as transport equipment, machinery, mining, wood, construction and textiles, many sources/databases used for the calculations in this thesis do not break down the data for these sectors, therefore they are grouped here altogether under the heading “other industrial sectors”.

2.2.2 Energy consumption in decentralized power plants

Decentralized power plants mostly operate based on reciprocating internal combustion engines. There are various types of these engines, capable of burning a large variety of fuels, such as diesel oil, heavy fuel oil, natural gas, biogas, syngas, mining gas, etc. Their capacity starts from some kWs up to some tens of MWs with the advantage that they have the flexibility of adjusting their operating load within a wide range. This is necessary to effectively meet the seasonal changes of electricity demand (e.g. summer/winter), especially in remote areas or islands.

The number of decentralized power plants is increasing over the past few years. Most of the new commissioned engines are up to 2 MW, according to a Diesel & Gas Turbine Worldwide

2016 report [55], with about half of them intended for continuous operation. The capacity of the new installed engines during 2015 in Europe is about 8.2 GWe and their classification according to their size is presented in Fig. 2.11, following the data of the same report.

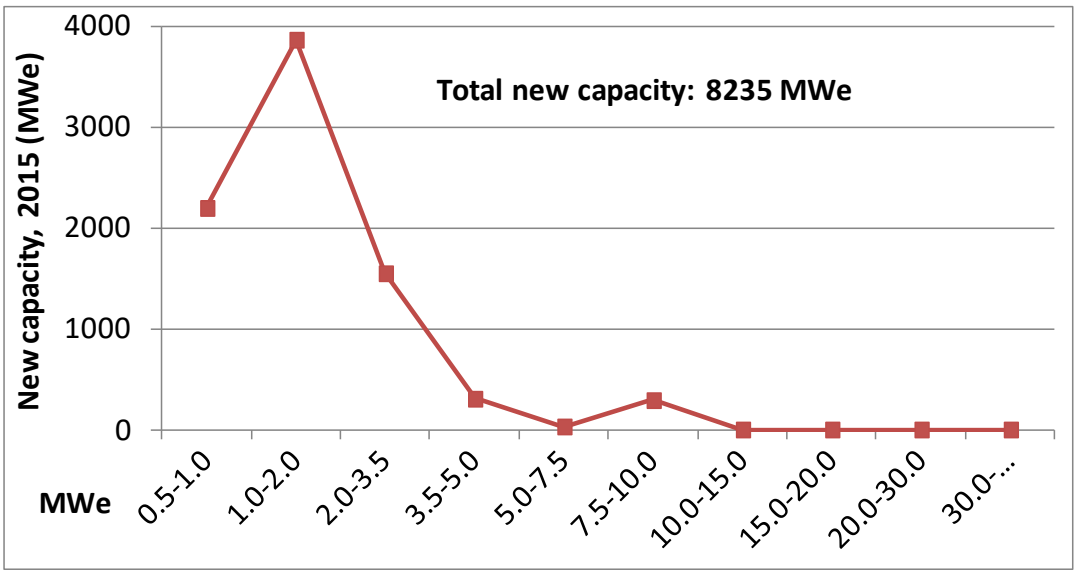

Figure 2.11: Capacity of new engines commissioned in Europe according to their size [55]

The majority of these engines are diesel engines using diesel fuel, with the larger ones using heavy fuel oil. Engines fuelled with gaseous fuels (natural gas, biogas) represent a small fraction of this capacity (about 10%). However, most of the diesel engines are used for backup or peaking purposes, while gaseous engines are mostly used in CHP mode for continuous operation with high capacity factor.

These power plants show a constant growth during the last years (about 4%), according to a GE report [56]. The installed capacity in Europe is estimated to 36.5 GW [57], based on the power plants capacity per fuel type. According to this report, the electric energy that corresponds to this figure is about 138.3 TWh/year, which is in accordance to Eurostat data [58]. The average capacity factor derived from these figures is 43%, which is justified by the large number of engines for backup purposes, while engines for continuous operation show capacity factor over 90%.

With a mean thermal efficiency of 40% (considering gaseous engines with efficiency ~35-40% and modern diesel engines with 40-50% and part load operation with reduced efficiency), the total fuel heat consumption is equal to 345.75 TWh/year.

2.2.3 Energy consumption in marine sector

The estimation of energy consumption of the entire fleet involves uncertainty, since there are not many sources of reliable data available. The analysis here is based on the overall fuel oil consumption and the number of ships. According to a Royal Academy of Engineering report [59], the total (global) fuel oil consumption of the marine sector is more than 350 million tonnes per year. With a global fleet of about 90,000 ships (from small up to very large ones), with a recent

growth rate of about 3.5% [60], this sector represents about 2.5% of the global CO_2 emissions, as shown in Fig. 2.12 [61].

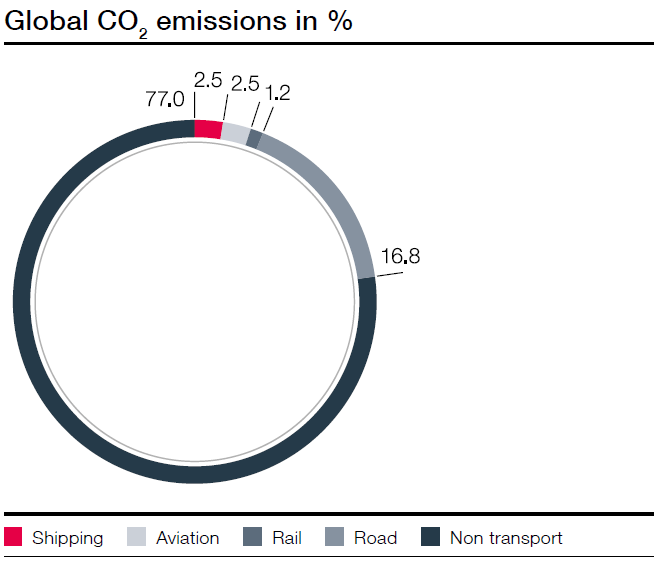

Figure 2.12: Fraction of global CO2 emissions per transportation sector [61]

The energy consumption that corresponds to the fuel oil consumption mentioned is about 4150 TWh per year (with heating value equal to 42.65 MJ/kg [62]). Although the number of ships and their tonnage is increasing, fuel consumption decreases [63] due to the building of new ships with modern engines and higher efficiency (for reducing fuel costs and meeting the stricter emissions standards). This leads to a decrease of fuel/energy consumption and less potential for further waste heat recovery measures, since modern engines already exploit most of the rejected heat from the exhaust gas and cooling water circuits.

2.2.4 Energy consumption in gas compressor stations

Gas compression stations (GCS) are used to maintain the high pressure in natural gas netowrks (due to the pressure losses in the pipes). Gas turbines are coupled with centrifugal compressors with typical capacity of 40 MW each, burning gas from the pipeline. The exhaust gases of these turbines with temperature at about 250-300 ^oC are readily available for heat recovery and further exploitation, since potential heat users are not usually available in these isolated areas, far away from district heating networks.

The installed capacity of such stations in Europe is about 9 GW with 613 stations (and further increasing) and another 50 GW between Russia (44 GW) and Ukraine (6 GW) [64]. Usually, most of these gas turbines operate with capacity factor over 90%, while some others only cover seasonal peaks also influenced by hot ambient conditions that change the density of the compressed gas. All stations are equipped with backup gas turbines in case of any failure or maintenance (a typical station is equipped /with two gas turbines and another one as backup). Their thermal efficiency is about 32-35%, with a single gas turbine of 40 MW rejecting about 80 MW of heat (total combustion heat of natural gas equals to 120 MW per typical gas turbine). Considering a mean capacity factor of 40% (with the backup units and the ones operating at specific seasons), the annual combustion heat in Europe is 94 TWh/year. By adding the

compressor stations in Russia and Ukraine as well, the total heat consumption increases to 616 TWh/year.

2.2.5 Overview of energy consumption in all sectors examined

The summary of the energy consumption for the four sectors presented previously is given in Table 2.1.

Table 2.1: Energy consumption of all sectors examined

Sector	Energy consumption (TWh/year)
EU industry	3200.00
EU decentralized power plants	345.75
Marine	4150.00
Gas compressor stations in Europe	616.00
Total	**8311.75**

The marine sector shows a very large fraction of energy consumption, while also industry is a very promising sector for RED Heat Engine, based on their primary energy consumption.

2.3 Waste heat potential per sector

In this section the waste heat potential per sector will be calculated, in order to identify the most promising segments, in which the RED Heat Engine can be applied. Each sector has different characteristics, temperature, technical limitations, and capacity factors, leading to different technical potentials [14]. These parameters are considered in this analysis, presenting both the available waste heat and the technically exploitable fraction of it.

2.3.1 Waste heat potential in the industrial sector

Introduction

An overview and brief description of the main industrial sectors and their waste heat sources are provided next. Further details for each sector with extensive description are available from Best Available Techniques (BAT) and their Reference Documents in the EC-JRC report [65].

Chemical industry: This sector includes both the chemical and petrochemical industries. It represents a large fraction of European industrial energy consumption, as already presented previously. About half of the heat demand is over 400 ^{o}C, while a large fraction of electricity demand, about 32%, is used for refrigeration and cooling purposes.

Possible waste heat sources are from exhaust gases from boilers, heating systems, thermal oxidizers, or even gases heated from exothermic processes in reactors and heat from flared gas, mainly in the medium temperature range.

Steel and iron industry: There are two main routes to produce steel: the integrated steel route and the recycling route. In the first one, higher specific heat demand is observed (about 20 GJ/ton of hot rolled product), while in the second one, the specific demand is lower - about 4.5 GJ/ton. About 95% of the heat demand lies in the high temperature range (over 400 ^{o}C).

Waste heat recovery from blast furnaces is still a challenging task, due to the contaminants included in the gas, while recovering heat from exhaust gases from boilers (at about 300 ^{o}C) is more technically feasible. Finally, waste heat from rolling mills in the form of exhaust gas from furnaces at temperature about 500 ^{o}C is possible, as the gas is relatively clean and standard heat exchangers can be used for heat recovery purposes.

Paper and pulp industry: There is a wide variation of specific energy consumption (GJ/ton), depending on whether a cogeneration plant is integrated and whether recycling material is used or high-quality specialty papers production is taking place.

Standard waste heat sources are from paper mills and mainly from exhaust air from paper machine dryers at very low temperatures of about 70-80 ^{o}C. Also, waste heat sources from wood refining and grinding processes for the production of mechanical pulp are significant (at similar temperature) and can be recovered with current technology [66].

Non-metallic mineral products industry: The main sectors of these industries are cement, glass and ceramics ones. Their brief description and waste heat assessments are provided next.

Cement industry: In this industry most of the heat demand (around 88%) is over 400 ^{o}C (high temperature), with the rest 12% equally shared in the medium and low temperature levels [49]. A large fraction of process heat is wasted, due to the high temperature required. The two main waste heat sources in cement industries are: (1) the exhaust gases from the rotary kiln, which after passing through the raw material preheater are at a temperature of about 380 ^{o}C, and (2) hot air exiting the clinker cooler at an average temperature of 360 ^{o}C [67].

Glass industry: The main waste heat sources are in the glass melters and curing ovens, which finally reject clean gases of about 200 ^{o}C. Initially their temperature is much higher, but they pass through incinerators and special filters to remove contaminants and organic particles.

Ceramics industry: Similar waste heat sources as in glass industry exist with the same temperature range of heat demand and waste heat.

Food and beverages industry: Available waste heat sources mostly include exhaust gases from boilers, gases from dryers, toast ovens and fryers [68]. Typical temperature range of heat demand is from 60 up to 500 ^{o}C, while waste heat is below 200 ^{o}C, usually with high moisture content, reducing the heat harnessing potential, in order to avoid condensate production.

Non-ferrous industry: The aluminium industry accounts for almost 55% of the energy consumption of this industry type. About 50% of energy demand concerns heat (and the rest electricity), while heat demand of high temperature level is 95% of the total and medium and low levels are 4% and 1% respectively.

A large percentage of the total energy required to produce aluminium is used during the calcination process (refining process) [69]. The waste of the exhaust gas from the calciners contains considerable moisture (about 50% water by volume) and contaminants such as alumina particulates at a relatively low temperature (185-200 ^{o}C), which can cause severe fouling in all heat exchanger types.

Other waste heat sources are from smelting pots (kept at about 400 °C), from exhaust gases during anode baking (at 200-300 °C) and melting furnaces (over 850 °C), and from recycling and secondary melting process (mostly exhaust gas at medium/high temperature).

The second and third industries of this sector are copper and zinc with similar specific energy demand, processes and heat temperature levels.

Overview of waste heat availability

There are many differences between the industrial sectors in terms of both energy consumption, waste heat potential and its temperature level. An overview of energy losses compared to the energy utilized is given in Fig. 2.13 for the US industries[2] (SPIRE Roadmap [70]).

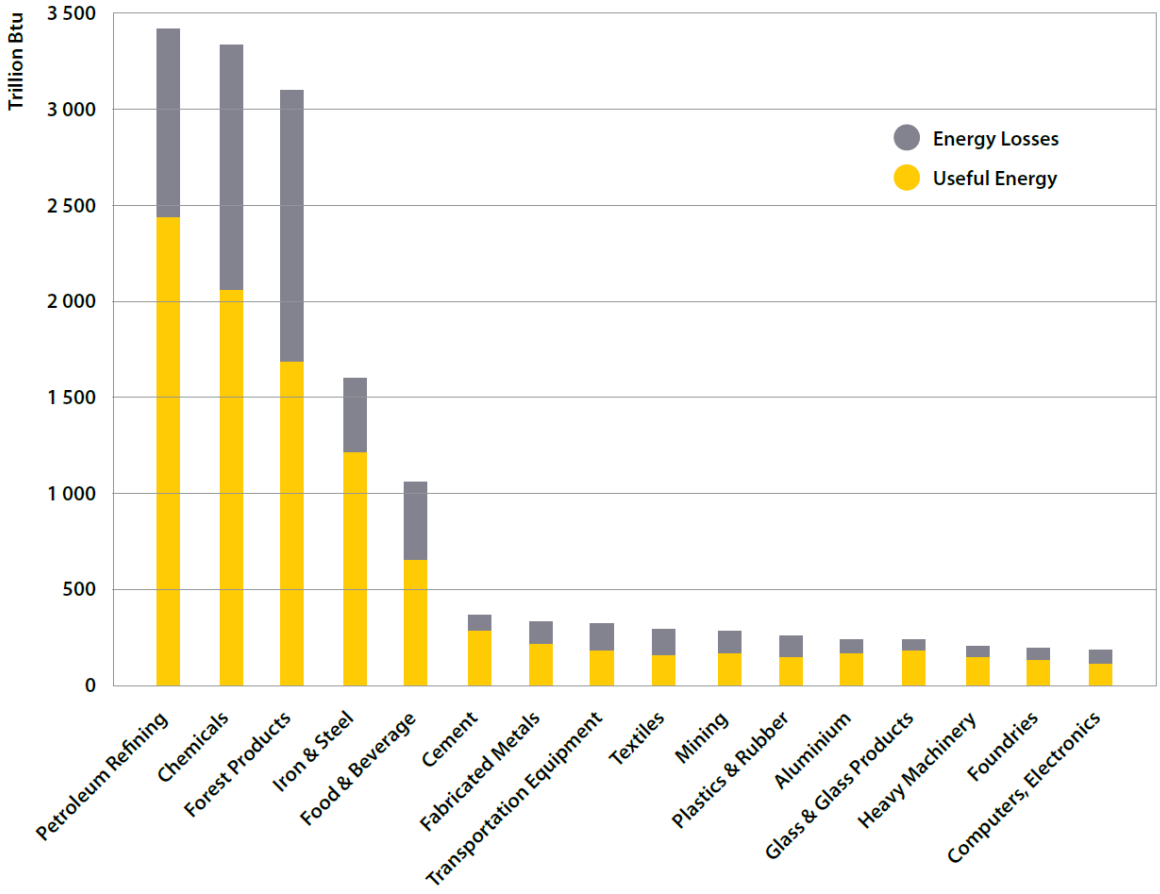

Figure 2.13: Overview of energy losses within industrial sectors [70]

A direct comparison in absolute numbers with EU industry is not possible, but the fraction of energy losses compared to the total energy consumption per sector is of interest. A mean fraction of 20-30% concerns energy losses from various sources, such as exhaust gases, cooling water, low-quality steam, heat losses from the commodities/products (solid streams), as well as energy losses from pumps/motors and other electromechanical equipment. However, waste

[2] 1 trillion BTU equals to about 293 GWh.

heat concerns only a fraction of these losses, estimated at about 10-20% of the total energy input.

Similar studies for the EU have been conducted focusing on waste heat from the industry and have led to results that vary widely. According to Bianchi et al., 2016 [71], industrial waste heat potential in EU is about 370 TWh/year, while according to the "HeatUp" project this figure is 750 TWh/year [72]. Considering that the recent EU energy consumption in industry is about 3200 TWh/year (presented previously), a figure closer to 300-500 TWh/year seems more realistic. Therefore, the value reported in the work of Bianchi et al., 2016 [71] will be considered here. This value refers to the total waste heat availability, which can be partly recovered and utilized.

In the ECOHEATCOOL project [73] waste heat recovery factors have been introduced for some energy-intensive industries, following the findings of a relevant Swedish study [74]. These results have been further processed by Brückner et al., 2014 [53], who identified the waste heat potential at country/region level. They stated that with waste heat recovery factors per temperature level and per industrial sector (see Fig. 2.14) it is possible to estimate the waste heat potential in Europe. This approach is adopted in this thesis, with the methodology described in the next pages.

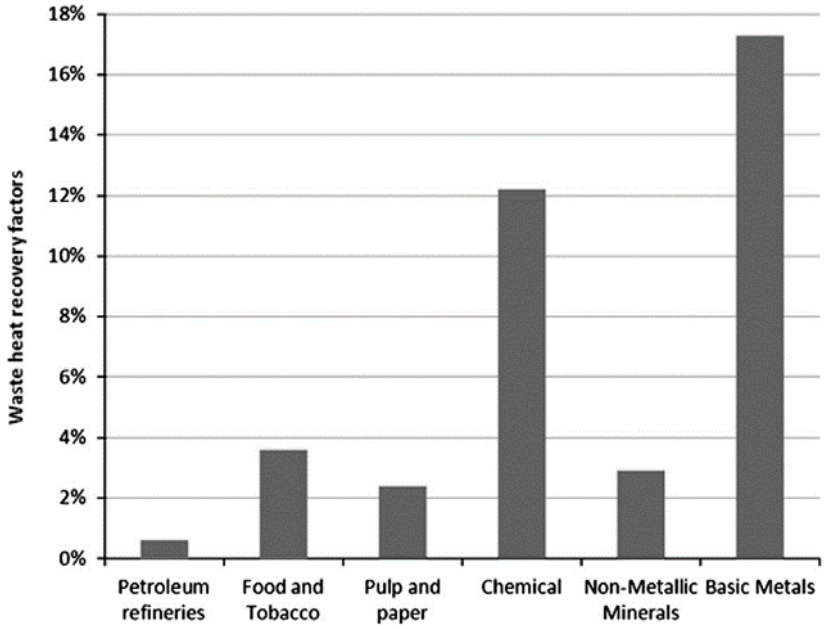

Figure 2.14: Waste heat recovery factors per industrial sector [53]

Moreover, waste heat potential has been studied in Norway, where a detailed report based on questionnaires has been implemented [75], showing that more than 60% of the waste heat is at temperature below 140 °C. These findings from the industrial sector in Norway have been extrapolated in German industry by Pehnt et al. [50], where they directly used the recovery factors from the Norwegian study for metal production, chemicals and processing of stone and earth (30, 8, and 40% respectively), while they used a flat 3% for the other sectors, as shown in Fig. 2.15.

Description	Final Energy	Waste heat percentage above 140 °C of the final energy consumption	Waste heat over 140 °C final energy consumption
	TJ		TJ
Metal production	561,846	30 %	168,554
Basic chemicals	460,104	8 %	36,808
Commercial paper	242,634		
Processing of stone and earth	221,802	40 %	88,721
Food and tobacco	204,328		
Other economic sectors	215,970		
Glass and ceramics	92,501	*3 %*	*2,775*
Metal working	114,476	*3 %*	*3,434*
NF metals, foundries	133,674	*3 %*	*4,010*
Automobile industry	131,117	*3 %*	*3,993*
Other chemical industry	91,138	*3 %*	*2,734*
Machine construction	84,435	*3 %*	*2,533*
Rubber/ plastic products	81,298	3 %	2,439
Mining	17,777		
	2,653,101		**316,001**

Figure 2.15: Waste heat factors per industrial sector in Germany [50]

A more detailed approach for the different waste heat sources and their temperature level is provided by the Ecofys Report [41] mentioned previously. This report identified waste heat sources (and sinks) in the UK industry, differentiated by thermal carrier, as shown in Fig. 2.16. The temperature levels of heat sources are divided into low, medium and high, as follows:

- Low level: From the ambient temperature up to 250 °C.
- Medium level: From 250 °C up to 500 °C.
- High level: over 500 °C.

While for the heat sinks the levels are:

- Low level: From the ambient temperature up to 150 °C.
- Medium level: From 150 °C up to 250 °C.
- High level: over 250 °C.

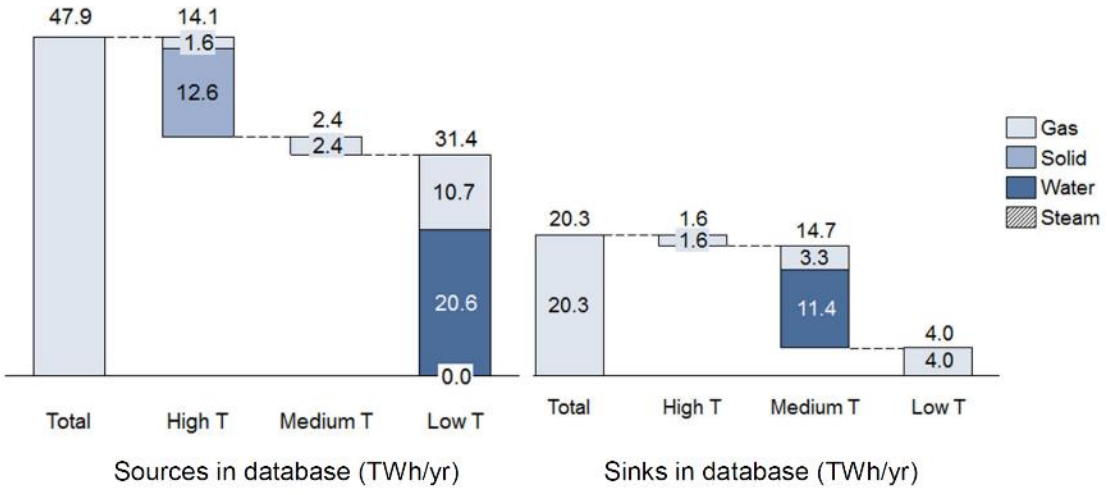

Figure 2.16: Heat source and sink per temperature level and heat carrier in UK industries [41]

High temperature heat sources are mostly available in solid carriers with their recovery being very challenging, as no commercial equipment exists for that purpose. This is the reason that this temperature level is very low in the heat sinks part. The majority of heat sources are below 250 °C (low level) with water and gas being the main thermal carriers, for which there are available heat harnessing equipment.

New methodology for estimating waste heat fractions

The methodology and results presented in that section were published in 2018:

M. Papapetrou, G. Kosmadakis, A. Cipollina, U. La Commare, G. Micale, Industrial waste heat: Estimation of the technically available resource in the EU per industrial sector, temperature level and country, Appl. Therm. Eng. 138 (2018) 207–216. doi:10.1016/j.applthermaleng.2018.04.043

The available studies and data presented in the previous section give a first assessment of waste heat availability in the industry. However, most studies focus on a specific country and/or industrial sector. In this thesis the objective is to build a clear understanding of the available waste heat for all European countries and for all industrial sectors. Such assessments exist, but as presented in the previous section, they adopt a generic top-down approach and their results vary widely. Most importantly, a clear classification of the waste heat per temperature level is lacking in the literature. Therefore, a methodology is developed and applied here, based on the estimation of waste heat fractions per industry, country and temperature level.

The starting point is a study of the UK industry [16] where the technically available waste heat of each industrial sector in the UK was estimated using data from 425 industrial sites from the period 2000-2003. Electricity used for process heat is included in the above study, although it represents a small fraction compared to the total heat consumption. This analysis used data from a large number of industrial sites, bringing confidence that the results are reliable, even though waste heat estimations on a country or continent level are inherently uncertain. In this study they have categorized the heat demand per sector and temperature level, as shown in Fig. 2.17. Moreover, they calculated the technically available waste heat of these UK industrial sectors, as also shown in the same figure.

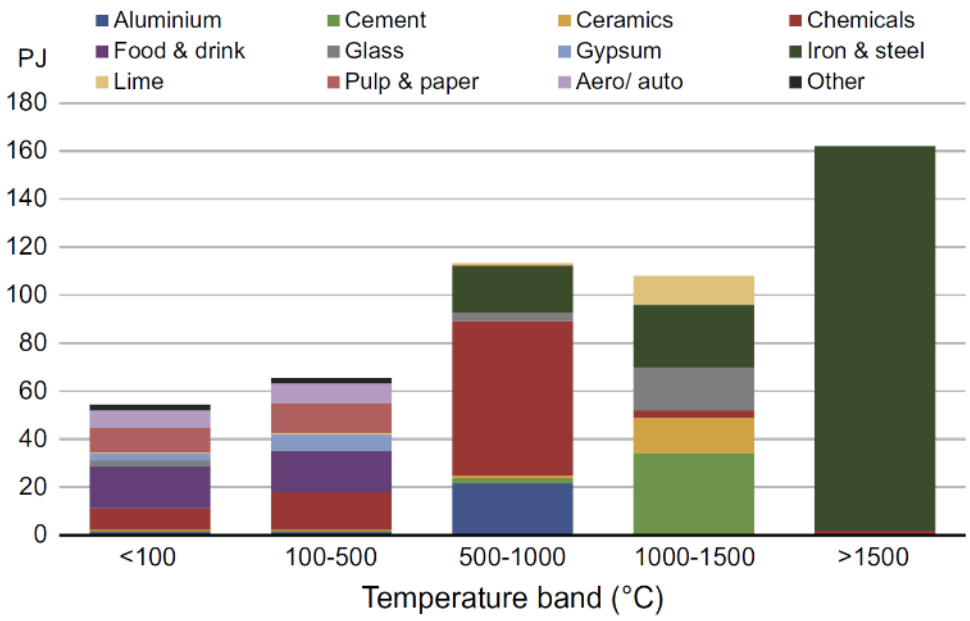

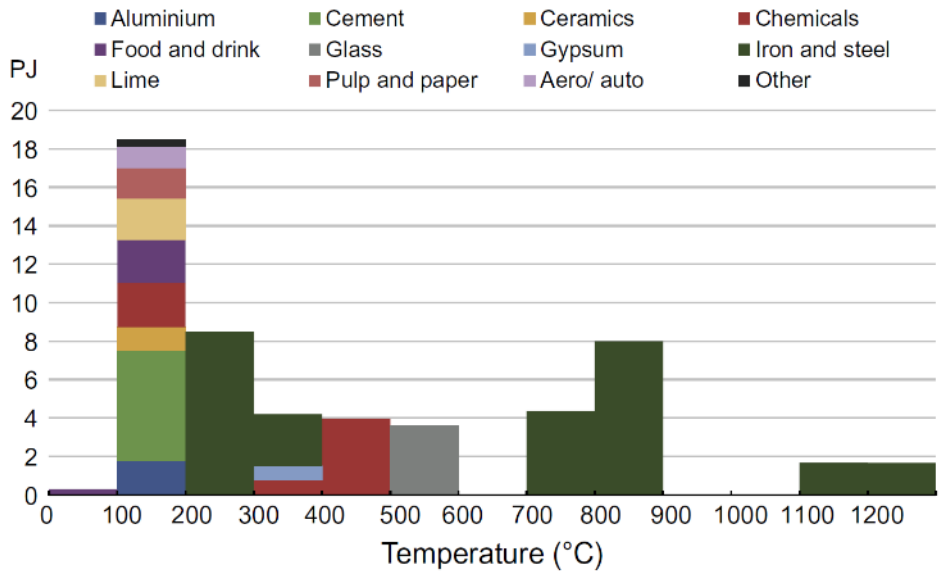

Figure 2.17: Heat demand and waste heat availability per industrial sector and temperature for UK industry [16]

First step

In the methodology developed for this thesis, the first step is to calculate the waste heat fractions (WHFs) for the UK industry in the period 2000-2003, according to Eq. (2.1). The Eq. (2.1) is applied for each temperature band and industrial sector using the data from the UK study about the heat consumption and recoverable waste heat potential. Cement, ceramics, gypsum, lime and glass have been reported separately; here they are grouped together as non-metallic minerals in order to be in line with the classification of the, from where data is used in the next steps of the methodology.

$$\left(WHF_{UK,sector,Temp\ range}\right)_{2000-2003} = \left(\frac{(waste\ heat\ potential)_{UK,sector,Temp\ range}}{(heat\ consumption)_{UK,sector}}\right)_{2000-2003} \quad (2.1)$$

Second step

The second step of the methodology is to adjust the set of WHF that are calculated for each industrial sector and temperature band in the UK (in the first step), to the realities of each of the other members states of the European Union, by multiplying with a factor that indicates the relative energy intensity of each country compared to the UK (country-specific adjustment) and industrial sector (industrial sector-specific) for the period 2000-2003. The annual energy intensity (EI) values per country and per industrial sector have been taken from the Odyssee-Mure database [47]. The average values of the 2000-2003 period have been used for every country and for each industrial sector. The energy intensity values are given in toe/€2005ppp (purchasing power parities), to eliminate any distortions between currencies and market conditions in the different countries.

Then, using Eq. (2.2) a set of WHFs is calculated per EU country, industrial sector and temperature band for the period 2000-2003.

$$\left(WHF_{EU\ country,sector,Temp\ range}\right)_{2000-2003} =$$

$$\left(WHF_{UK,sector,Temp\ range}\right)_{2000-2003}\left(\frac{EI_{EU\ country,sector}}{EI_{UK,sector}}\right)_{2000-2003} \quad (2.2)$$

Third step

The third step of the methodology is to update the calculated sets of WHFs of the second step, accounting for the energy efficiency improvements in each country and industrial sector from the period 2000-2003 to 2015 (year that the most recent heat consumption data are available). For that purpose the ratio of the energy intensity values in 2015 is calculated (per industrial sector and country) using data from the Odyssee-Mure database to the average energy intensity values from the period 2000-2003, which was used in step 2. By multiplying this ratio with the WHF for the same country and industrial sector, the WHFs are updated to 2015 values, as shown in Eq. (2.3).

$$\left(WHF_{EU\ country,sector,Temp\ range}\right)_{2015} =$$

$$\left(WHF_{EU\ country,sector,Temp\ range}\right)_{2000-2003}\frac{\left(EI_{EU\ country,sector}\right)_{2015}}{\left(EI_{EU\ country,sector}\right)_{2000-2003}} \quad (2.3)$$

Fourth step

The final step, consists of multiplying heat consumption derived from 2015 Eurostat data per industrial sector with the WHFs for 2015 for each industry, temperature band and EU country. The result is the estimation of the waste heat potential for 2015, eliminating any major uncertainties related to the differences of energy efficiency levels between countries and years.

Assumptions

Although the above methodology eliminates some major uncertainties, there are several assumptions, which need to be considered when discussing the results. Here are listed the main assumptions:

1. The starting point of this work (the UK study) already includes some uncertainties (waste heat is estimated with a ±33% accuracy). The reported available waste heat in the UK is within the range of 37-73 PJ/year and in this thesis is used the average value of this range.
2. When using the Eurostat 2015 data for heat consumption per industry and country, the derived heat and energy from renewables (mostly biomass in wood industry) is not taken into account. That was done in order to be consistent with the UK study, which also did not consider these heat consumption sources based on their methodology; if these sources were taken into account the adaptation of WHFs for other countries and years would not have been correct. In any case, these heat sources account for about 13% of EU industrial energy consumption, most of it being in the pulp and paper sector. Therefore, the result would not change significantly at least for all other industrial sectors.
3. Electricity consumption that is used for process heat is also considered in the calculations and included in the heat consumption, following a similar methodology as in the UK study.
4. The use of energy intensity values at purchasing power parities for adjusting the WHFs for the different countries and the different periods does not consider different possible forms of the end-product within an industrial sector. For example, the paper and pulp

industry in Sweden and Finland have much higher energy intensities than these industries in other European countries. This is because Sweden and Finland produce mainly pulp, a low value product which requires an energy intensive process. Other European countries might just import pulp and produce paper (less intensive process), a higher value product. We could avoid this by using the specific energy consumption (energy input per volume of industrial production) rather than the energy intensity, however the available data do not allow for a full calculation between all countries, industrial sectors and periods (data are partly available only for steel, cement, glass and paper industries). In any case, a comparison in a small sample of sectors and countries has been made when using specific energy consumption and energy intensity data, with the results being similar and following the same trend.

5. It is assumed that the relative difference of energy intensity in each country and sector and any improvement over time is distributed equally between heat/fuels and electricity.
6. This methodology does not consider the detailed circumstances that might be present at specific industrial sites (e.g. use of combined heat and power – CHP, or industrial symbiosis). The results consider the average energy values of the industrial sector of each country and as such cannot be derived with high accuracy. More accurate estimations of the waste heat potential would require to restrict the study to the industries of a region or even better to a specific site.
7. In steps 2 and 3 of the methodology, energy intensity data from the Odyssee-Mure database [47] are used. As such, the results here are only as good as the reliability of the data. The industrial energy intensity is defined by Odyssee-Mure as "*the ratio between the final energy consumption of the branch (measured in energy units: toe, Joule, etc) and the value added measured in constant monetary units."*. The data for calculating the energy intensity every year and for every country are collected within the Odyssee-Mure project annually by a network of 37 partners from 31 countries, usually national representatives, such as energy agencies or statistical organizations. This process has been on-going since 2001 and the database is widely respected and used, providing confidence that the data is reliable.

The heat demand values are broadly in line with the ones provided in [49] (differences of about 10%, which mainly derive from the data used from different years). After further processing these results from the UK industry, and following the methodology presented above, the waste heat recovery fractions for the period 2000-2003 per sector and temperature level for UK are calculated, shown in Fig. 2.18. Cement, ceramics, gypsum, lime and glass have been grouped to non-metallic minerals, in order to be in accordance to all other studies and reports.

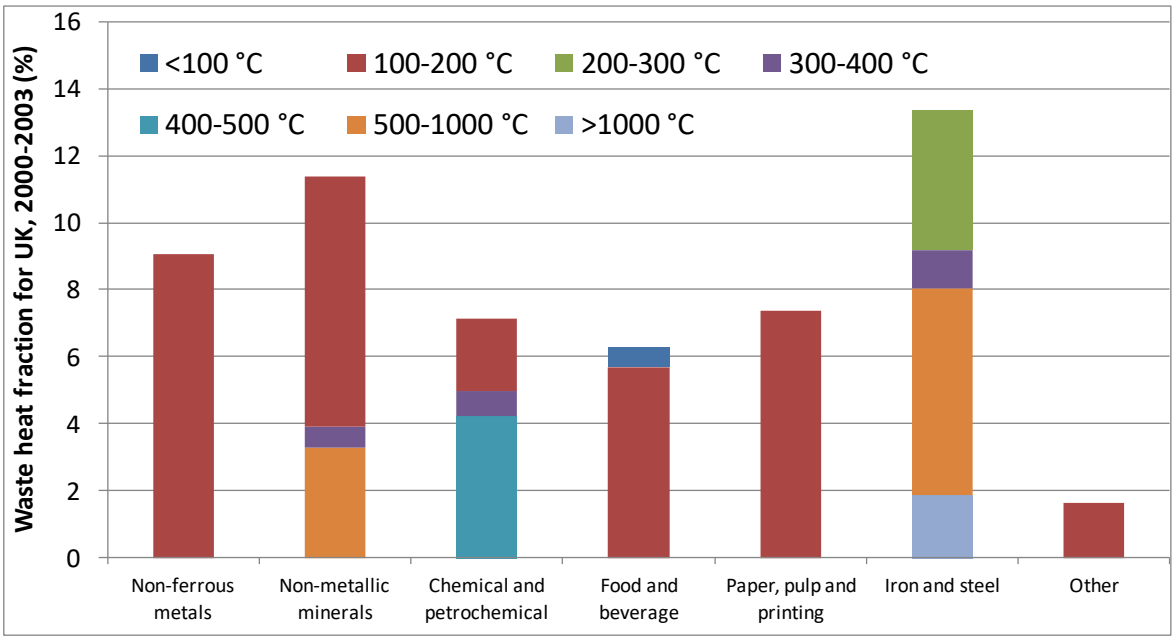

Figure 2.18: Waste heat fraction per industrial sector and temperature level for UK industry for the period 2000-2003 (processed data from [16])

The waste heat potential over 1000 °C is limited and observed only in the iron and steel industries. Even within the 500-1000 °C temperature range, not much waste heat is available, with the potential being restricted in the cement, iron and steel sectors. Within the 200-500 °C range the potential increases, mainly in pulp and paper and iron and steel industries. The majority of waste heat lies in the temperature range of 100-200 °C, spread over most industrial sectors, while below 100 °C the potential is rather limited, concentrated in the food and drink sector, mostly from drying and preheating processes.

The waste heat fractions calculated lie mostly within the 6-9% range, of heat consumption. Only the non-metallic minerals and iron and steel sectors have a higher waste heat fraction (about 11 and 13% respectively), due to the high temperatures at which they require their process heat, resulting to larger heat losses. This result is in-line to a Swedish (ECOHEATCOOL) [74] and a German study [50].

Waste heat fraction calculations

In order to extrapolate the waste heat fractions from the UK industry to the industries of other countries, energy intensity values are used, as explained previously. Energy intensity values correlate the energy input in each country and industry with the added value end-product. Their ratios (energy intensities for each EU country divided by UK industries) provide an estimation of relative energy efficiency of that EU country compared to the UK for the specific industrial sector. The outcome is a set of WHFs for each EU country per industry and temperature band for the period 2000-2003, similar to the one shown in Fig. 2.18.

After that, the ratio of energy intensity between the 2000-2003 period and the one for 2015 are calculated per industry and country, in order to adapt the results to the energy efficiency situation of 2015, as described in section 2.1. The final result is an updated set of fractions per industry and country for 2015. These calculated waste heat fractions are shown in Table 2.2.

These fractions will be used in the next section for estimating the waste heat potential of all industrial sectors in the EU.

Table 2.2: Waste heat fractions per industrial sector and temperature level in EU countries (adjusted to 2015)

		<100 °C	100-200 °C	200-300 °C	300-400 °C	400-500 °C	500-1000 °C	>1000 °C
European Union	Non-ferrous metals	0.00	22.00	0.00	0.00	0.00	0.00	0.00
	Non-metallic minerals	0.00	17.19	0.00	1.45	0.00	7.66	0.00
	Chemical and petrochemical	0.00	0.97	0.00	0.34	1.89	0.00	0.00
	Food and beverage	0.63	6.34	0.00	0.00	0.00	0.00	0.00
	Paper, pulp and printing	0.00	19.73	0.00	0.00	0.00	0.00	0.00
	Iron and steel	0.00	0.00	10.04	2.78	0.00	14.88	4.60
	Other	0.00	0.59	0.00	0.00	0.00	0.00	0.00
Austria	Non-ferrous metals	0.00	24.27	0.00	0.00	0.00	0.00	0.00
	Non-metallic minerals	0.00	15.12	0.00	1.27	0.00	6.74	0.00
	Chemical and petrochemical	0.00	1.02	0.00	0.36	1.99	0.00	0.00
	Food and beverage	0.72	7.23	0.00	0.00	0.00	0.00	0.00
	Paper, pulp and printing	0.00	25.60	0.00	0.00	0.00	0.00	0.00
	Iron and steel	0.00	0.00	11.08	3.07	0.00	16.42	5.07
	Other	0.00	0.61	0.00	0.00	0.00	0.00	0.00
Belgium	Non-ferrous metals	0.00	11.85	0.00	0.00	0.00	0.00	0.00
	Non-metallic minerals	0.00	23.27	0.00	1.96	0.00	10.37	0.00
	Chemical and petrochemical	0.00	1.45	0.00	0.51	2.83	0.00	0.00
	Food and beverage	0.87	8.69	0.00	0.00	0.00	0.00	0.00
	Paper, pulp and printing	0.00	17.43	0.00	0.00	0.00	0.00	0.00
	Iron and steel	0.00	0.00	5.41	1.50	0.00	8.02	2.48
	Other	0.00	1.18	0.00	0.00	0.00	0.00	0.00
Bulgaria	Non-ferrous metals	0.00	11.30	0.00	0.00	0.00	0.00	0.00
	Non-metallic minerals	0.00	10.61	0.00	0.90	0.00	4.73	0.00
	Chemical and petrochemical	0.00	6.12	0.00	2.14	11.93	0.00	0.00
	Food and beverage	0.61	6.06	0.00	0.00	0.00	0.00	0.00
	Paper, pulp and printing	0.00	31.82	0.00	0.00	0.00	0.00	0.00
	Iron and steel	0.00	0.00	5.16	1.43	0.00	7.64	2.36
	Other	0.00	0.64	0.00	0.00	0.00	0.00	0.00
Croatia	Non-ferrous metals	0.00	4.61	0.00	0.00	0.00	0.00	0.00
	Non-metallic minerals	0.00	19.32	0.00	1.63	0.00	8.61	0.00
	Chemical and petrochemical	0.00	0.93	0.00	0.33	1.81	0.00	0.00
	Food and beverage	0.49	4.93	0.00	0.00	0.00	0.00	0.00
	Paper, pulp and printing	0.00	6.97	0.00	0.00	0.00	0.00	0.00
	Iron and steel	0.00	0.00	2.10	0.58	0.00	3.12	0.96
	Other	0.00	0.79	0.00	0.00	0.00	0.00	0.00
Cyprus	Non-ferrous metals	0.00	0.00	0.00	0.00	0.00	0.00	0.00
	Non-metallic minerals	0.00	28.69	0.00	2.42	0.00	12.79	0.00
	Chemical and petrochemical	0.00	0.25	0.00	0.09	0.48	0.00	0.00
	Food and beverage	0.60	6.01	0.00	0.00	0.00	0.00	0.00
	Paper, pulp and printing	0.00	3.72	0.00	0.00	0.00	0.00	0.00
	Iron and steel	0.00	0.00	0.00	0.00	0.00	0.00	0.00
	Other	0.00	1.67	0.00	0.00	0.00	0.00	0.00
Czech Rep.	Non-ferrous metals	0.00	24.65	0.00	0.00	0.00	0.00	0.00
	Non-metallic minerals	0.00	13.08	0.00	1.10	0.00	5.83	0.00
	Chemical and petrochemical	0.00	1.48	0.00	0.52	2.89	0.00	0.00
	Food and beverage	0.64	6.35	0.00	0.00	0.00	0.00	0.00
	Paper, pulp and printing	0.00	13.58	0.00	0.00	0.00	0.00	0.00
	Iron and steel	0.00	0.00	11.25	3.12	0.00	16.67	5.15
	Other	0.00	0.59	0.00	0.00	0.00	0.00	0.00
Denmark	Non-ferrous metals	0.00	9.13	0.00	0.00	0.00	0.00	0.00
	Non-metallic minerals	0.00	21.62	0.00	1.82	0.00	9.64	0.00
	Chemical and petrochemical	0.00	0.21	0.00	0.07	0.41	0.00	0.00

	Food and beverage	1.27	12.70	0.00	0.00	0.00	0.00	0.00
	Paper, pulp and printing	0.00	6.04	0.00	0.00	0.00	0.00	0.00
	Iron and steel	0.00	0.00	4.17	1.16	0.00	6.18	1.91
	Other	0.00	0.71	0.00	0.00	0.00	0.00	0.00
Estonia	Non-ferrous metals	0.00	5.79	0.00	0.00	0.00	0.00	0.00
	Non-metallic minerals	0.00	16.61	0.00	1.40	0.00	7.40	0.00
	Chemical and petrochemical	0.00	1.63	0.00	0.57	3.18	0.00	0.00
	Food and beverage	1.15	11.53	0.00	0.00	0.00	0.00	0.00
	Paper, pulp and printing	0.00	19.37	0.00	0.00	0.00	0.00	0.00
	Iron and steel	0.00	0.00	2.64	0.73	0.00	3.92	1.21
	Other	0.00	0.59	0.00	0.00	0.00	0.00	0.00
Finland	Non-ferrous metals	0.00	25.33	0.00	0.00	0.00	0.00	0.00
	Non-metallic minerals	0.00	15.07	0.00	1.27	0.00	6.72	0.00
	Chemical and petrochemical	0.00	1.60	0.00	0.56	3.12	0.00	0.00
	Food and beverage	1.22	12.20	0.00	0.00	0.00	0.00	0.00
	Paper, pulp and printing	0.00	32.82	0.00	0.00	0.00	0.00	0.00
	Iron and steel	0.00	0.00	11.56	3.20	0.00	17.14	5.29
	Other	0.00	1.03	0.00	0.00	0.00	0.00	0.00
France	Non-ferrous metals	0.00	21.14	0.00	0.00	0.00	0.00	0.00
	Non-metallic minerals	0.00	17.86	0.00	1.51	0.00	7.96	0.00
	Chemical and petrochemical	0.00	1.09	0.00	0.38	2.12	0.00	0.00
	Food and beverage	0.77	7.69	0.00	0.00	0.00	0.00	0.00
	Paper, pulp and printing	0.00	16.40	0.00	0.00	0.00	0.00	0.00
	Iron and steel	0.00	0.00	9.65	2.67	0.00	14.30	4.42
	Other	0.00	0.89	0.00	0.00	0.00	0.00	0.00
Germany	Non-ferrous metals	0.00	22.82	0.00	0.00	0.00	0.00	0.00
	Non-metallic minerals	0.00	16.22	0.00	1.37	0.00	7.23	0.00
	Chemical and petrochemical	0.00	1.06	0.00	0.37	2.08	0.00	0.00
	Food and beverage	0.76	7.63	0.00	0.00	0.00	0.00	0.00
	Paper, pulp and printing	0.00	15.56	0.00	0.00	0.00	0.00	0.00
	Iron and steel	0.00	0.00	10.42	2.89	0.00	15.44	4.77
	Other	0.00	0.50	0.00	0.00	0.00	0.00	0.00
Greece	Non-ferrous metals	0.00	17.11	0.00	0.00	0.00	0.00	0.00
	Non-metallic minerals	0.00	35.04	0.00	2.96	0.00	15.62	0.00
	Chemical and petrochemical	0.00	0.41	0.00	0.14	0.80	0.00	0.00
	Food and beverage	0.83	8.31	0.00	0.00	0.00	0.00	0.00
	Paper, pulp and printing	0.00	11.16	0.00	0.00	0.00	0.00	0.00
	Iron and steel	0.00	0.00	7.81	2.16	0.00	11.57	3.58
	Other	0.00	0.78	0.00	0.00	0.00	0.00	0.00
Hungary	Non-ferrous metals	0.00	56.50	0.00	0.00	0.00	0.00	0.00
	Non-metallic minerals	0.00	15.21	0.00	1.28	0.00	6.78	0.00
	Chemical and petrochemical	0.00	2.30	0.00	0.80	4.48	0.00	0.00
	Food and beverage	0.98	9.84	0.00	0.00	0.00	0.00	0.00
	Paper, pulp and printing	0.00	12.04	0.00	0.00	0.00	0.00	0.00
	Iron and steel	0.00	0.00	25.79	7.15	0.00	38.22	11.81
	Other	0.00	0.53	0.00	0.00	0.00	0.00	0.00
Ireland	Non-ferrous metals	0.00	26.46	0.00	0.00	0.00	0.00	0.00
	Non-metallic minerals	0.00	33.90	0.00	2.86	0.00	15.11	0.00
	Chemical and petrochemical	0.00	0.07	0.00	0.02	0.14	0.00	0.00
	Food and beverage	0.34	3.40	0.00	0.00	0.00	0.00	0.00
	Paper, pulp and printing	0.00	2.34	0.00	0.00	0.00	0.00	0.00
	Iron and steel	0.00	0.00	12.08	3.35	0.00	17.90	5.53
	Other	0.00	1.78	0.00	0.00	0.00	0.00	0.00
Italy	Non-ferrous metals	0.00	13.63	0.00	0.00	0.00	0.00	0.00
	Non-metallic minerals	0.00	18.79	0.00	1.58	0.00	8.38	0.00
	Chemical and petrochemical	0.00	0.81	0.00	0.28	1.57	0.00	0.00
	Food and beverage	0.59	5.93	0.00	0.00	0.00	0.00	0.00
	Paper, pulp and printing	0.00	12.21	0.00	0.00	0.00	0.00	0.00
	Iron and steel	0.00	0.00	6.22	1.72	0.00	9.22	2.85
	Other	0.00	0.75	0.00	0.00	0.00	0.00	0.00

Latvia	Non-ferrous metals	0.00	13.48	0.00	0.00	0.00	0.00	0.00
	Non-metallic minerals	0.00	13.28	0.00	1.12	0.00	5.92	0.00
	Chemical and petrochemical	0.00	0.68	0.00	0.24	1.32	0.00	0.00
	Food and beverage	0.87	8.66	0.00	0.00	0.00	0.00	0.00
	Paper, pulp and printing	0.00	1.96	0.00	0.00	0.00	0.00	0.00
	Iron and steel	0.00	0.00	6.15	1.71	0.00	9.12	2.82
	Other	0.00	0.65	0.00	0.00	0.00	0.00	0.00
Lithuania	Non-ferrous metals	0.00	2.10	0.00	0.00	0.00	0.00	0.00
	Non-metallic minerals	0.00	15.56	0.00	1.31	0.00	6.94	0.00
	Chemical and petrochemical	0.00	1.89	0.00	0.66	3.69	0.00	0.00
	Food and beverage	0.52	5.15	0.00	0.00	0.00	0.00	0.00
	Paper, pulp and printing	0.00	2.82	0.00	0.00	0.00	0.00	0.00
	Iron and steel	0.00	0.00	0.96	0.27	0.00	1.42	0.44
	Other	0.00	0.29	0.00	0.00	0.00	0.00	0.00
Luxembourg	Non-ferrous metals	0.00	28.32	0.00	0.00	0.00	0.00	0.00
	Non-metallic minerals	0.00	9.18	0.00	0.77	0.00	4.09	0.00
	Chemical and petrochemical	0.00	1.76	0.00	0.62	3.44	0.00	0.00
	Food and beverage	0.95	9.47	0.00	0.00	0.00	0.00	0.00
	Paper, pulp and printing	0.00	5.51	0.00	0.00	0.00	0.00	0.00
	Iron and steel	0.00	0.00	12.93	3.58	0.00	19.16	5.92
	Other	0.00	1.85	0.00	0.00	0.00	0.00	0.00
Malta	Non-ferrous metals	0.00	0.00	0.00	0.00	0.00	0.00	0.00
	Non-metallic minerals	0.00	0.00	0.00	0.00	0.00	0.00	0.00
	Chemical and petrochemical	0.00	0.00	0.00	0.00	0.00	0.00	0.00
	Food and beverage	0.00	0.00	0.00	0.00	0.00	0.00	0.00
	Paper, pulp and printing	0.00	0.00	0.00	0.00	0.00	0.00	0.00
	Iron and steel	0.00	0.00	0.00	0.00	0.00	0.00	0.00
	Other	0.00	0.00	0.00	0.00	0.00	0.00	0.00
Netherlands	Non-ferrous metals	0.00	26.20	0.00	0.00	0.00	0.00	0.00
	Non-metallic minerals	0.00	17.13	0.00	1.44	0.00	7.64	0.00
	Chemical and petrochemical	0.00	1.95	0.00	0.68	3.80	0.00	0.00
	Food and beverage	0.87	8.67	0.00	0.00	0.00	0.00	0.00
	Paper, pulp and printing	0.00	10.04	0.00	0.00	0.00	0.00	0.00
	Iron and steel	0.00	0.00	11.96	3.31	0.00	17.72	5.48
	Other	0.00	0.56	0.00	0.00	0.00	0.00	0.00
Poland	Non-ferrous metals	0.00	15.44	0.00	0.00	0.00	0.00	0.00
	Non-metallic minerals	0.00	7.35	0.00	0.62	0.00	3.28	0.00
	Chemical and petrochemical	0.00	1.65	0.00	0.58	3.22	0.00	0.00
	Food and beverage	0.46	4.57	0.00	0.00	0.00	0.00	0.00
	Paper, pulp and printing	0.00	11.68	0.00	0.00	0.00	0.00	0.00
	Iron and steel	0.00	0.00	7.05	1.95	0.00	10.45	3.23
	Other	0.00	0.26	0.00	0.00	0.00	0.00	0.00
Portugal	Non-ferrous metals	0.00	12.90	0.00	0.00	0.00	0.00	0.00
	Non-metallic minerals	0.00	19.82	0.00	1.67	0.00	8.83	0.00
	Chemical and petrochemical	0.00	1.21	0.00	0.42	2.36	0.00	0.00
	Food and beverage	0.53	5.35	0.00	0.00	0.00	0.00	0.00
	Paper, pulp and printing	0.00	48.85	0.00	0.00	0.00	0.00	0.00
	Iron and steel	0.00	0.00	5.89	1.63	0.00	8.73	2.70
	Other	0.00	1.10	0.00	0.00	0.00	0.00	0.00
Romania	Non-ferrous metals	0.00	17.86	0.00	0.00	0.00	0.00	0.00
	Non-metallic minerals	0.00	21.72	0.00	1.83	0.00	9.68	0.00
	Chemical and petrochemical	0.00	2.39	0.00	0.84	4.66	0.00	0.00
	Food and beverage	0.26	2.56	0.00	0.00	0.00	0.00	0.00
	Paper, pulp and printing	0.00	5.15	0.00	0.00	0.00	0.00	0.00
	Iron and steel	0.00	0.00	8.15	2.26	0.00	12.08	3.73
	Other	0.00	0.61	0.00	0.00	0.00	0.00	0.00
Slovakia	Non-ferrous metals	0.00	11.42	0.00	0.00	0.00	0.00	0.00
	Non-metallic minerals	0.00	4.64	0.00	0.39	0.00	2.07	0.00
	Chemical and petrochemical	0.00	2.85	0.00	1.00	5.56	0.00	0.00
	Food and beverage	0.57	5.67	0.00	0.00	0.00	0.00	0.00

	Paper, pulp and printing	0.00	14.85	0.00	0.00	0.00	0.00	0.00
	Iron and steel	0.00	0.00	5.21	1.45	0.00	7.73	2.39
	Other	0.00	0.84	0.00	0.00	0.00	0.00	0.00
Slovenia	Non-ferrous metals	0.00	21.32	0.00	0.00	0.00	0.00	0.00
	Non-metallic minerals	0.00	22.11	0.00	1.86	0.00	9.86	0.00
	Chemical and petrochemical	0.00	0.38	0.00	0.13	0.74	0.00	0.00
	Food and beverage	0.52	5.18	0.00	0.00	0.00	0.00	0.00
	Paper, pulp and printing	0.00	19.07	0.00	0.00	0.00	0.00	0.00
	Iron and steel	0.00	0.00	9.73	2.70	0.00	14.42	4.46
	Other	0.00	0.73	0.00	0.00	0.00	0.00	0.00
Spain	Non-ferrous metals	0.00	12.51	0.00	0.00	0.00	0.00	0.00
	Non-metallic minerals	0.00	21.18	0.00	1.79	0.00	9.44	0.00
	Chemical and petrochemical	0.00	0.74	0.00	0.26	1.45	0.00	0.00
	Food and beverage	0.50	5.00	0.00	0.00	0.00	0.00	0.00
	Paper, pulp and printing	0.00	14.62	0.00	0.00	0.00	0.00	0.00
	Iron and steel	0.00	0.00	5.71	1.58	0.00	8.46	2.61
	Other	0.00	0.52	0.00	0.00	0.00	0.00	0.00
Sweden	Non-ferrous metals	0.00	22.12	0.00	0.00	0.00	0.00	0.00
	Non-metallic minerals	0.00	13.02	0.00	1.10	0.00	5.81	0.00
	Chemical and petrochemical	0.00	0.67	0.00	0.23	1.30	0.00	0.00
	Food and beverage	0.53	5.32	0.00	0.00	0.00	0.00	0.00
	Paper, pulp and printing	0.00	43.17	0.00	0.00	0.00	0.00	0.00
	Iron and steel	0.00	0.00	10.10	2.80	0.00	14.96	4.62
	Other	0.00	0.58	0.00	0.00	0.00	0.00	0.00
UK	Non-ferrous metals	0.00	6.58	0.00	0.00	0.00	0.00	0.00
	Non-metallic minerals	0.00	7.25	0.00	0.61	0.00	3.23	0.00
	Chemical and petrochemical	0.00	0.87	0.00	0.30	1.69	0.00	0.00
	Food and beverage	0.40	3.96	0.00	0.00	0.00	0.00	0.00
	Paper, pulp and printing	0.00	6.08	0.00	0.00	0.00	0.00	0.00
	Iron and steel	0.00	0.00	3.00	0.83	0.00	4.45	1.38
	Other	0.00	1.13	0.00	0.00	0.00	0.00	0.00

Waste heat potential calculations

Heat consumption data have been processed from Eurostat for 2015 per industrial sector and EU country, presented previously. Some industrial sectors with low consumption, such as textiles, machinery, etc. have been grouped under the heading “other industries” for consistency with the other data sources. The waste heat potential per industrial sector and temperature level was calculated for each EU country, using the 2015 waste heat fractions that have been calculated using the new methodology. Figure 2.19 gives the waste heat potential per industrial sector and per temperature range for all EU countries together; the country level analysis is provided in the next section.

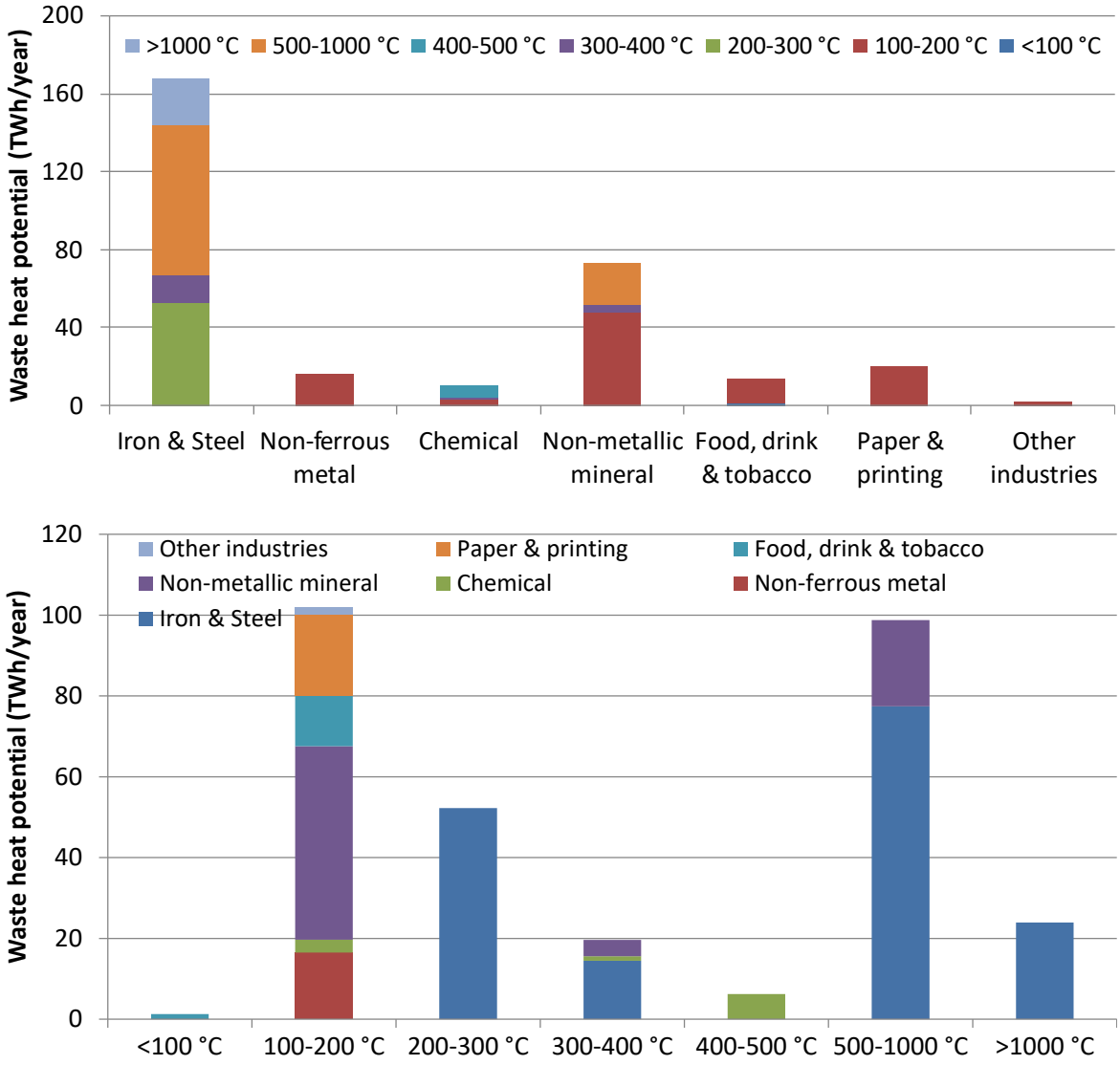

Figure 2.19: Waste heat potential per industrial sector (top) and temperature level (bottom) for EU industry

The waste heat potential at temperature level of 100-200 °C is high (about 100 TWh/year), representing about one third of the total one. It is spread between a variety of industrial sectors, such as non-metallic minerals, food, paper and chemical industries. For higher temperature levels, the amount of waste heat decreases with a waste heat potential over the temperature level of 200-500 °C of about 78 TWh/year. For waste heat with temperatures over 500 °C only industries that use high temperature process heat feature, like the steel industry, with the total potential being quite high at 124 TWh/year.

What is interesting is the very low waste heat potential with temperature below 100 °C, equal to 1.25 TWh/year, when compared to the other temperature levels. One reason for this is the very low temperature difference compared to the reference temperature (ambient temperature), the very low heat consumption within this range, and the very low heat losses (low waste heat fractions).

The sum of waste heat potential in the EU is 304.13 TWh/year, which accounts for 16.7% of the industrial consumption for process heat, and represents 9.5% of the total industrial energy consumption.

The previous analysis has identified the waste heat and its technical potential in the main industrial sectors in EU. Appropriate estimations have been used, which have been verified by regional studies, in order to conclude to waste heat recovery factors for each sector and temperature level. The highest uncertainty lies in the total waste heat, since large quantities are wasted through solid streams (e.g. hot products), which is difficult to quantify. However, the analysis presented provides a first convincing view of the potential for RED Heat Engine in this large sector, although detailed energy audit should be implemented before a feasibility study is conducted for a specific site.

2.3.2 Waste heat potential in decentralized power plants

As was presented in Section 2.2.2, the fuel heat consumption of all engines for decentralized power production is 345.75 TWh/year. The main sources of waste heat are from the exhaust gases and the cooling circuit, as shown in a typical Sankey chart of a heavy duty diesel engine (Fig. 2.20 [76]).

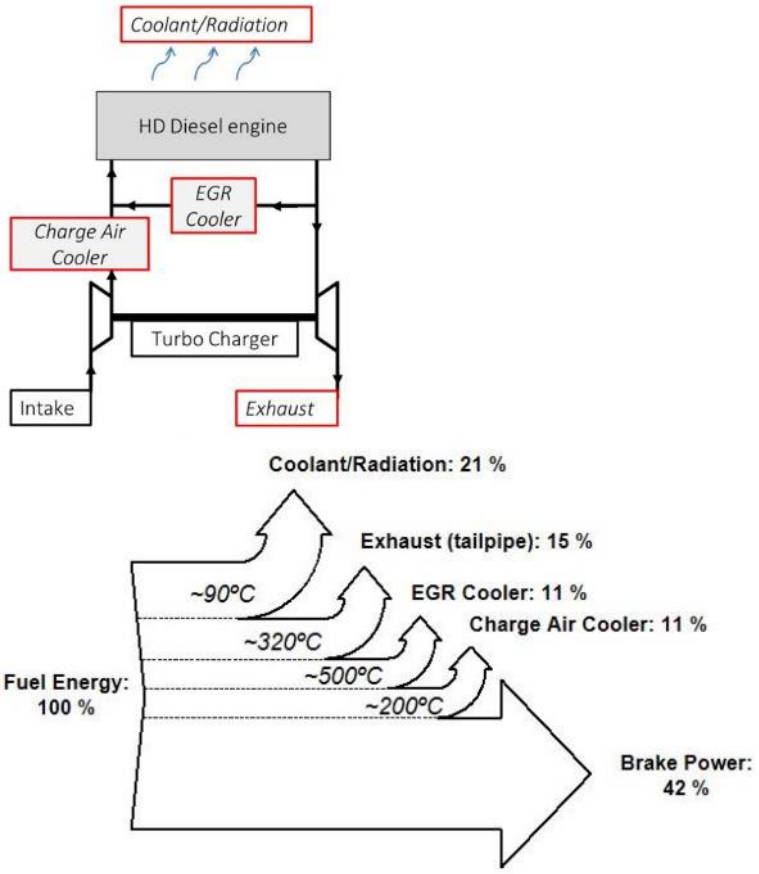

Figure 2.20: Typical diesel engine with energy flows [76]

The rejected heat of the cooling water represents about 30% of the combustion heat (includes jacket water and charge air cooler, both cooled by the same cooling circuit), and exhaust gases about 25% (includes both tailpipe exhaust gases and EGR cooling). In case of even larger engines with heavy fuel oil, a large fraction of the exhaust gas heat is used for preheating the fuel, in order to increase its viscosity, and the heating of lubricant oil. The result is a reduced exhaust gas temperature of about 150-200 ^{o}C, further limiting the potential of this heat source. It should be stressed that its temperature should be kept above the dew point, in order to avoid condensation of water vapour and the production of H_2SO_4 from the SOx emissions of the exhaust gas (creating corrosion on the stack walls [77]), depending on the partial pressure of water vapour and SOx. A high safety temperature margin is also introduced, in order to make sure that the exhaust gas can exit the stack (this gas is also cooled in the stack). On the other hand, the temperature of the cooling water is constant at about 80-90 ^{o}C.

The waste heat potential is thus divided according to the main fuel types: heavy fuel oil (usually over 1 MW), diesel (below 1 MW), natural gas, biogas and other low gaseous calorific fuels. The estimated waste heat sources and typical performance data for the engines with different fuel types are given in Table 2.3 [78–80].

Table 2.3: Efficiency and waste heat sources for engines with different fuel types

Fuel type	Efficiency (%)	Waste heat sources (%)		
		Exhaust gas	Cooling water	Other (radiation, lubricating oil, etc.)
Heavy fuel oil	50	27	20	3
Diesel	42	26	30	2
Natural gas	40	28	31	1
Biogas	38	30	30	2
Other low calorific gaseous fuels	35	34	29	2

Moreover, most of the engines supplied with gaseous fuels (natural gas, biogas, and other low calorific gaseous fuels such as landfill gas) operate at CHP mode, already exploiting the waste heat of the exhaust gas and cooling water. In the cases of biogas plants and landfills a fraction of this heat (mean annual is about 20%) is used for the production of the gaseous fuel itself. Leaving a small part of heat that is currently rejected, which is estimated to about 20%, varying within a large range, depending on the heat consumer.

With the above limitations, the resulting waste heat potential for each engine type is shown in Table 2.4, according to the input energy presented in Section 2.2.2 per fuel type and the conversion factors of Table 2.3. Other minor waste heat sources shown in Table 2.3 (last column) are not included, since they concern minor losses, such as radiation or friction losses, which are difficult to be estimated and harnessed.

Table 2.4: Waste heat potential for engines with different fuel types

Fuel type	Available (TWh/year)		Technical potential (TWh/year)	
	Exhaust gas	Cooling water	Exhaust gas	Cooling water
Heavy fuel oil	14.41	10.68	2.32	10.68
Diesel	5.68	6.55	1.58	6.55
Natural gas	32.02	35.45	8.00	8.86
Biogas	39.38	39.38	7.88	7.88
Other low calorific gaseous fuels	6.10	5.64	1.32	1.13
Total	**98.09**	**97.70**	**21.10**	**35.10**

The available waste heat source in this sector is 195.79 TWh/year, covering a large range of engines and fuel types. The technical potential of waste heat is reduced to 56.2 TWh/year, considering the applications of these decentralized power plants and all limitations, being equal to about 29% of the total available one.

The biogas segment shows the higher potential with an additional important advantage: its electricity is subsidized in most of the EU countries [22], making it very attractive to produce additional "green" electricity from the heat recovery of biogas engines. Therefore, special focus will be given on this segment with further details provided in a next section, where waste heat potential is analysed per country.

The technical potential of this heat source is high, since a large fraction of the whole waste heat of the cooling circuit can be utilized. This potential is observed in the last two columns of Table 2.4. In case of engines operating at CHP mode, the available waste heat is the one not utilized for heating purposes, with exactly the same conclusions reached here. A more detailed view of natural gas engines is provided in Section 2.4, justifying the reasons that this engine type is not suitable for supplying with heat the RED Heat Engine.

Finally, an energy consumption of 2-3% of the gross power output is introduced for rejecting the heat of the cooling water. This self-consumption can be reduced or even eliminated in case of exploiting its waste heat for additional power production.

2.3.3 Waste heat potential in marine sector

The global energy consumption in ships all over the world is 4150 TWh/year as presented previously. Marine engines have large sizes with efficiencies approaching 48-50% (for new large ships even higher efficiency is reached~52%). Auxiliary engines are usually four stroke medium

speed ones with capacity about 0.5-1 MW and lower efficiency, about 45%. A typical energy flow in a cruise ship is shown in Fig. 2.21.

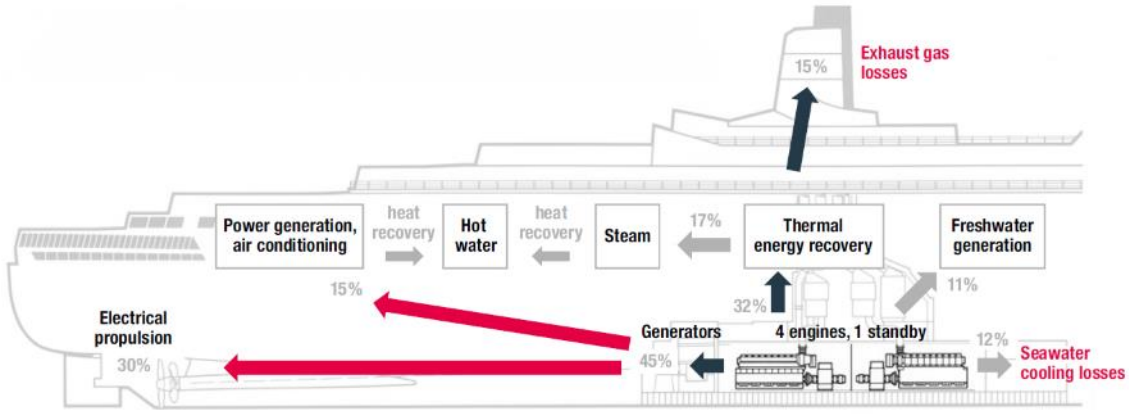

Figure 2.21: Typical energy / heat balance of a cruise ship [61]

Most of the fuel/energy consumption in ships is for the main propulsion engines, while auxiliary engines (and boilers) represent a much lower fraction of this consumption. In Fig. 2.22 is shown for every ship type the fuel consumption and its breakdown to main/auxiliary engine and boiler, according to IMO study, 2014.

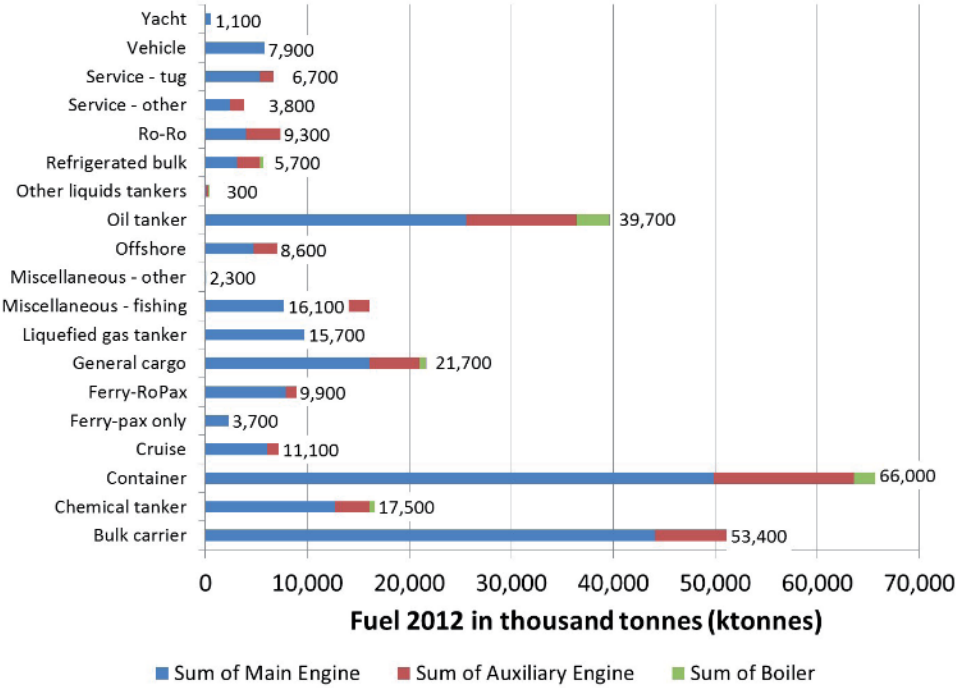

Figure 2.22: Fuel consumption for each ship type (Third IMO Greenhouse Gas Study 2014)

The fuel consumption in the auxiliary engines is 498 TWh/year, and corresponds to about 12% of the total one, according to the IMO report. Using average typical values, the efficiency and

waste heat sources (exhaust gases or cooling water) of the main and auxiliary engines are given in Table 2.5.

Table 2.5: Efficiency and waste heat sources for main and auxiliary engines

Engine type	Efficiency (%)	Waste heat sources (%)		
		Exhaust gas	Cooling water	Other (radiation, lubricating oil, etc.)
Main propulsion engine	50	27	20	3
Auxiliary engine	42	26	30	2

In all ships the waste heat sources from the main engines are already recovered and exploited, for fuel/lubricant preheating, fresh water production, and other heating purposes. The exhaust gas from the auxiliary engines is also utilized in most of the cases, leaving the waste heat of their cooling water to be exploited.

The resulting waste heat potential for the auxiliary engines is shown in Table 2.6, calculated from the total fuel input and the conversion factors of Table 2.5. Other minor waste heat sources shown in Table 2.5 (last column) are not included, since they concern minor losses, such as radiation or friction losses, which are difficult to be estimated and harnessed.

Table 2.6: Waste heat potential for auxiliary engines

Engine type	Available (TWh/year)		Technical potential (TWh/year)	
	Exhaust gas	Cooling water	Exhaust gas	Cooling water
Auxiliary engines	0.00	149.40	0.00	149.40

The available waste heat source is about 149 TWh/year from the auxiliary engines. Moreover, an energy consumption of 1-2% of the gross power output is introduced for rejecting the heat of the cooling water to the sea. This self-consumption can be reduced or even eliminated in case of exploiting its waste heat for additional power production.

Finally, the main drawbacks of waste heat recovery in ships are: (1) the uncertainty of the capacity factor, since every ship operates differently, and (2) the space restrictions in the engine room.

2.3.4 Waste heat potential in gas compressor stations

With the estimations introduced previously, it has been calculated that the annual combustion heat in Europe is 94 TWh/year and considering the compressor stations in Russia and Ukraine as well, the total heat consumption increases to 616 TWh/year.

The mean thermal efficiency of gas turbines is 32-35%, and the resulting waste heat from the exhaust gas (the only waste heat of these plants), is 63 TWh/year for the compressor stations in Europe. By adding the ones in Russia and Ukraine as well, the total waste heat equals to 412.72 TWh/year. This waste heat is available at temperature of about 250-300 ^{o}C, making it appropriate for the RED Heat Engine. Moreover, these stations are located in isolated areas away from heat consumers, and it is not practical to provide their waste heat in district heating networks.

However, the technical potential of this waste heat is reduced, due to technical limitations (not possible to cool the exhaust gas down to ambient temperature). The lower limit is about 150 ^{o}C or even less [81] since the produced sulfur oxides are very low (depending on the natural gas composition). Therefore, the technical potential equals about 50% (exhaust gas cooled from 275 ^{o}C to 150 ^{o}C, dT=125 ^{o}C, instead of reaching ambient temperature of 20 ^{o}C, dT_{max}=255 ^{o}C). The resulting available and technical potential of waste heat of this sector is shown in Table 2.7.

Table 2.7: Waste heat potential for gas compressor stations

Power plant type	Available waste heat of exhaust gas (TWh/year)	Technical potential of the waste heat of exhaust gas (TWh/year)
Gas turbine for gas compressor stations	412.72	202.31

About 200 TWh/year is the technical potential of this waste heat, and out of this about 30 TWh/year is available in EU countries and the rest (170 TWh/year) in Russia and Ukraine.

2.3.5 Overview of waste heat potential in all sectors examined

The available waste heat and its technical potential are summed here for the four sectors presented previously, presented in Table 2.8.

Table 2.8: Waste heat potential in all sectors examined

Sector	Available waste heat (TWh/year)	Technical potential of the waste heat (TWh/year)
Industry	370.42	304.13
Decentralized power plants	195.79	56.20

Marine	149.40	149.40
Gas compressor stations	412.72	202.31
Total	**1128.33**	**712.04**

The marine sector shows a very large fraction of available waste heat at temperature about 80-90 °C, while also gas compressor stations and industry are very promising sectors for the RED Heat Engine with different levels of temperature.

2.4 Waste heat potential per EU country

The available waste heat potential per sector has been estimated in the previous sections for the EU as a whole. This potential is broken down here on the level of each EU country, in order to identify the most promising ones. The marine sector is not examined in this section, since the potential is not exploitable within the territory of a specific country. Thus, the analysis only considers the industrial sector, decentralized power plants and gas compressor stations.

2.4.1 Waste heat potential in the industrial sector in EU countries

The share of energy consumption of each industrial sector in EU countries is presented in Fig. 2.23 (2012 data), indicating the increasing participation of energy-intensive industries in the final mix (according to Odyssee-Mure project).

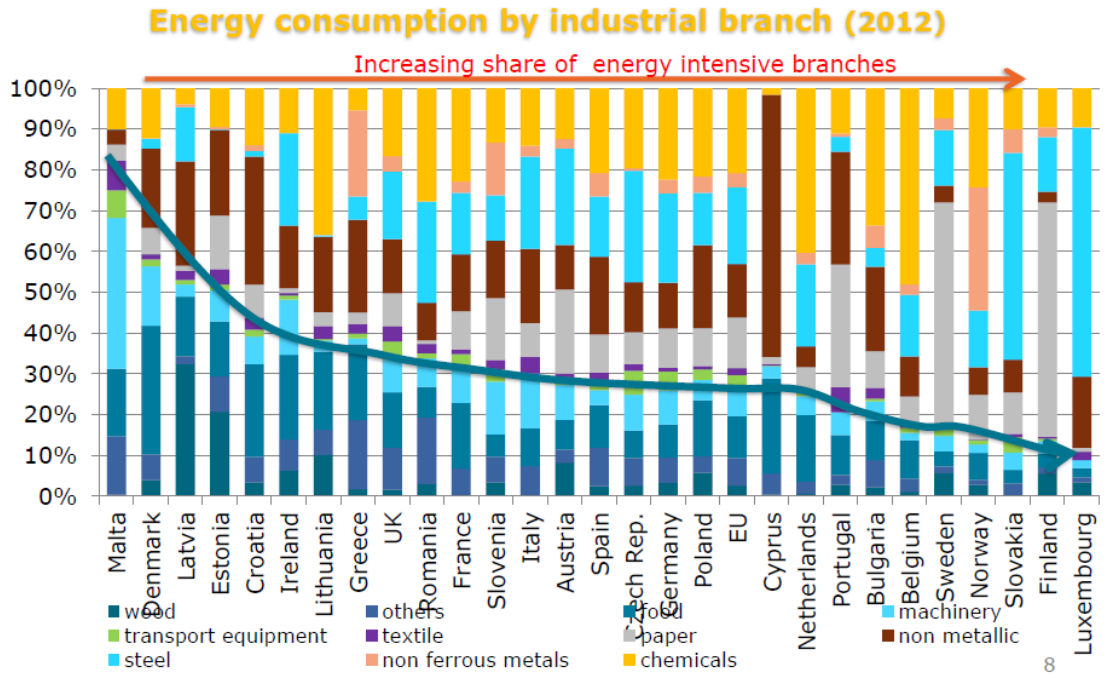

Figure 2.23: Share of energy consumption in industry per sector in EU countries [48]

In all EU countries there are food, paper, non-metallic, machinery, and chemical industries. Usually the smaller countries show large fraction of energy consumption in a single sector, such as in Malta (machinery industry with 40% of energy consumption), Cyprus (non-metallic industry with 60% of energy consumption), and Luxembourg (steel industry with 60% of energy consumption). In the larger countries (e.g. France, Germany) there is a higher balance between industries, showing that their industrial sector is highly diversified.

An overview of waste heat potential in each EU country is provided in Fig. 2.24 [71]. The values of each country in TWh/year correspond to the total waste heat availability.

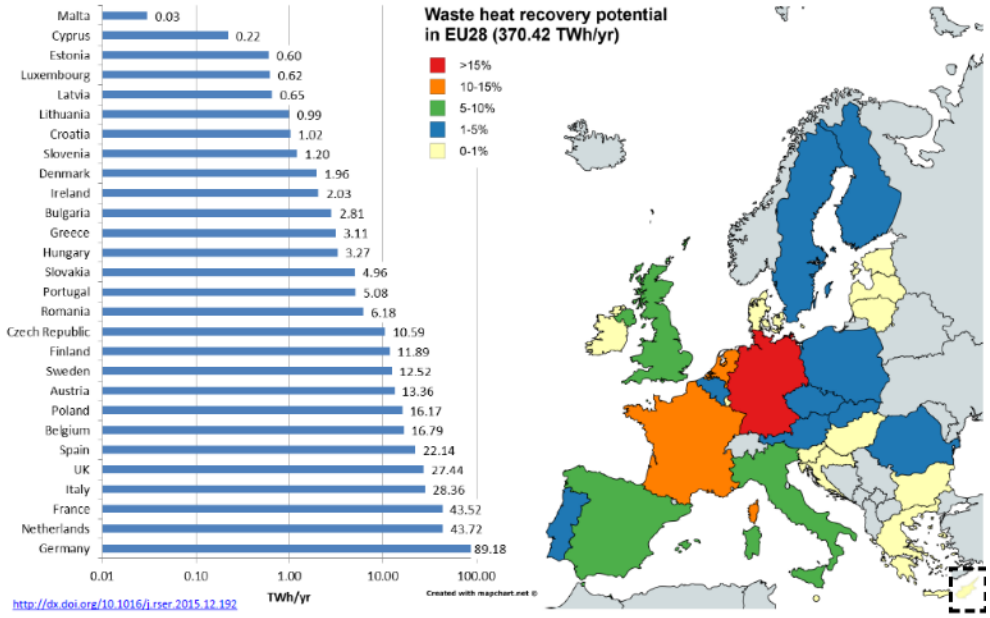

Figure 2.24: Waste heat potential in each EU country [71]

A similar map is given in Fig. 2.25, showing the exact location and type of industries. This map has been developed in the framework of the STRATEGO project [82], in which heating and cooling streams have been identified.

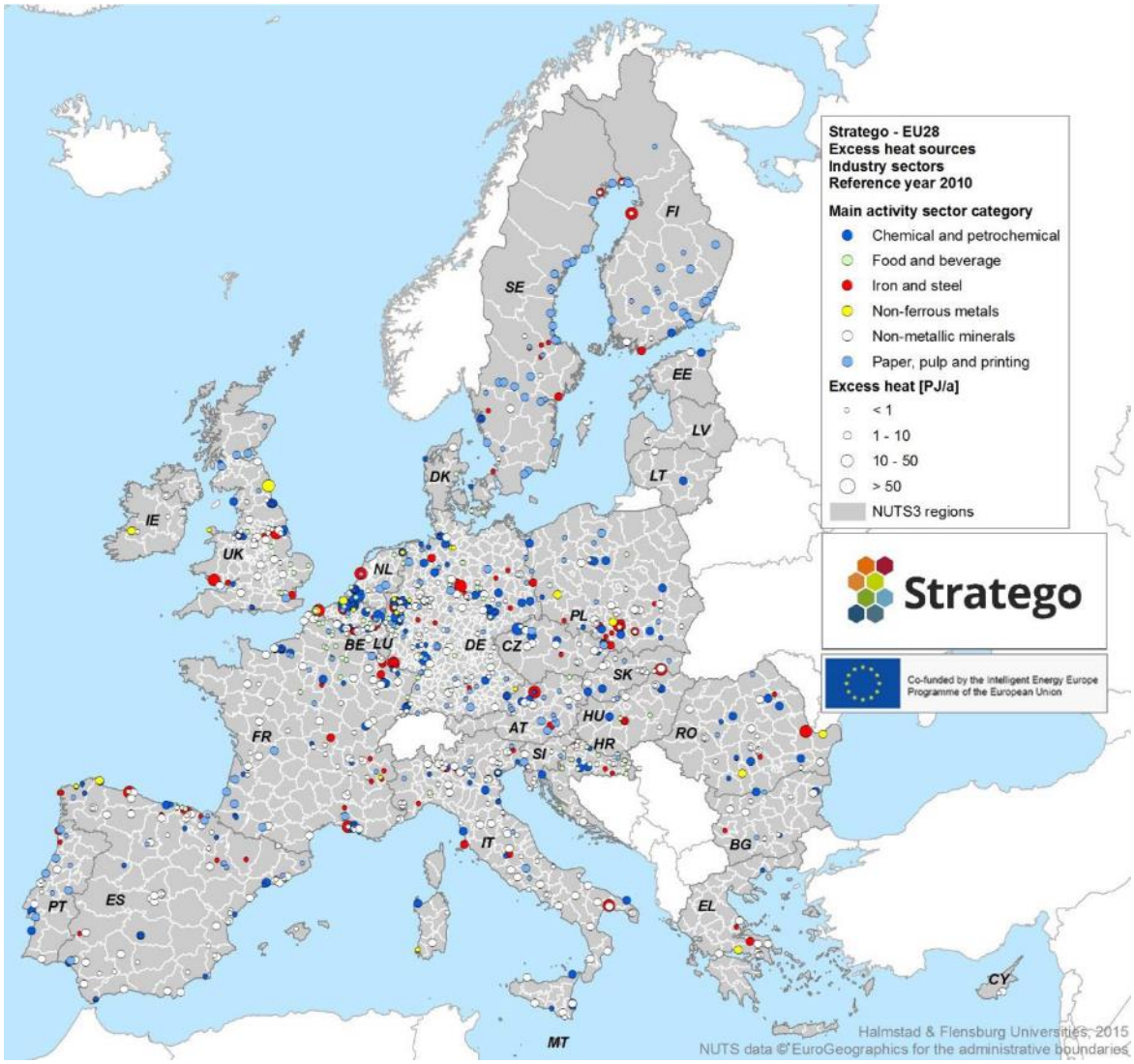

Figure 2.25: Excess heat in each EU country [82]

In the Scandinavian countries there are plenty of paper industries, due to the large quantities of wood availability. On the other hand, in central Europe there are many industrial sites of various types, spread in many countries. Most of them are located in Germany, Belgium, the Netherlands, France and Poland.

The number of medium/large industrial sites is about 1200 in the EU, according to the STRATEGO project. In Fig. 2.26 is shown how this number is distributed per EU country.

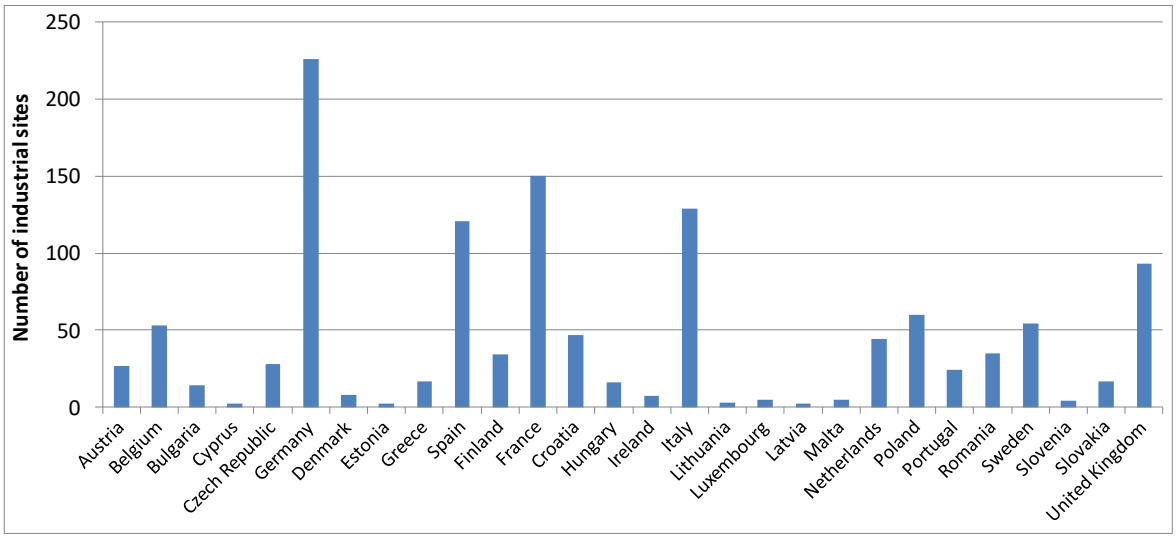

Figure 2.26: Number of industrial sites in each EU country [82]

Following the methodology presented previously, using appropriate waste heat recovery fractions for each industry and temperature level, the waste heat potential in each EU country has been calculated. Heat consumption data for each country were available from Eurostat, which have been further processed, as already described.

The results are presented for each industrial sector separately and per EU country, since the amount of data is large. These results are shown in Figs. 2.27-2.33 for iron and steel, non-ferrous metal, chemical, non-metallic mineral, food, paper and pulp, and other industries respectively.

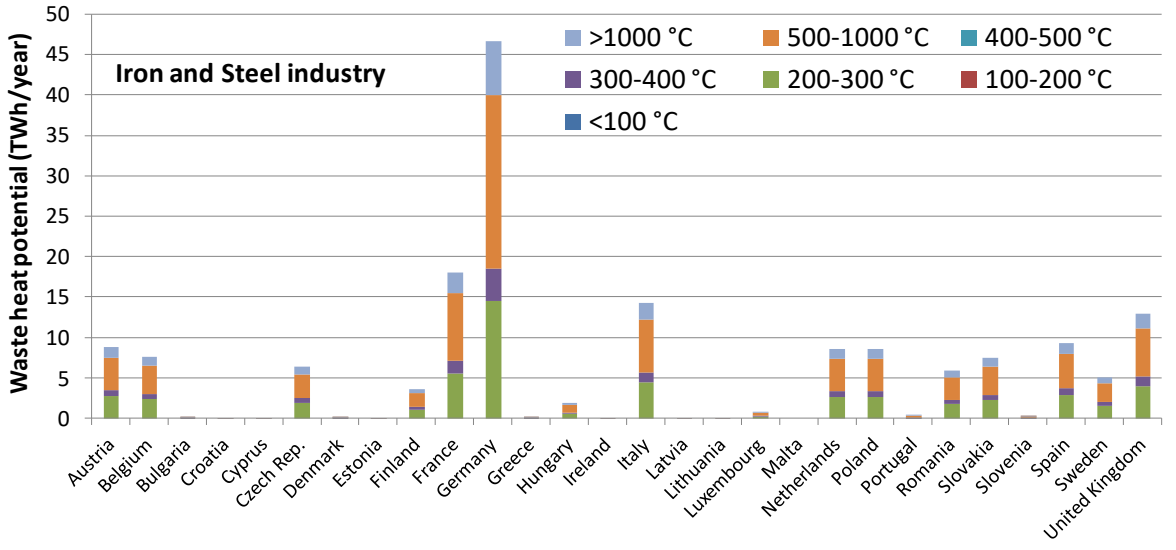

Figure 2.27: Waste heat potential in each EU country per temperature level in iron and steel industry

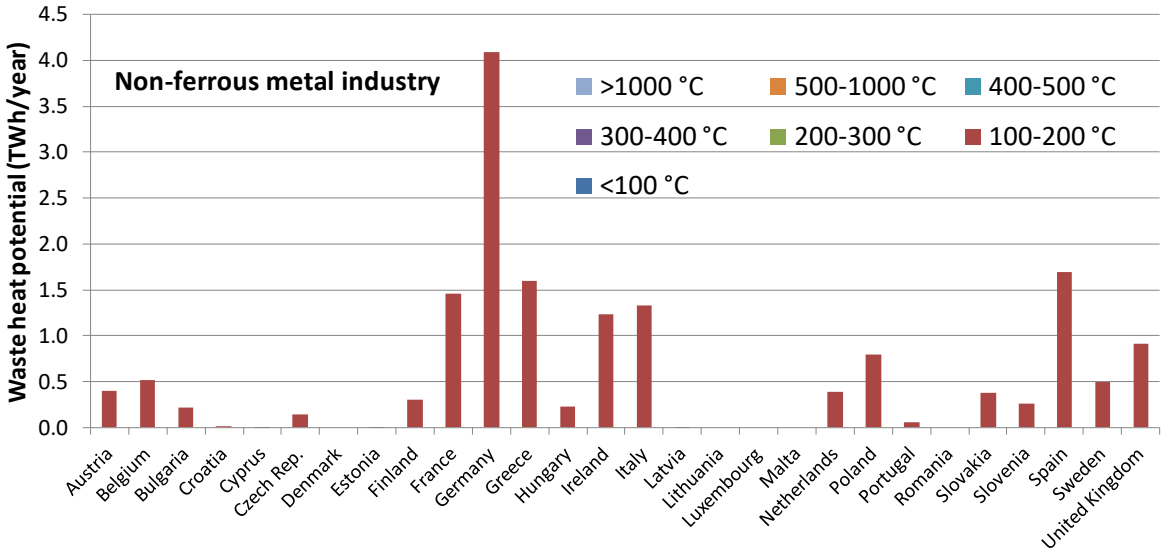

Figure 2.28: Waste heat potential in each EU country per temperature level in non-ferrous metal industry

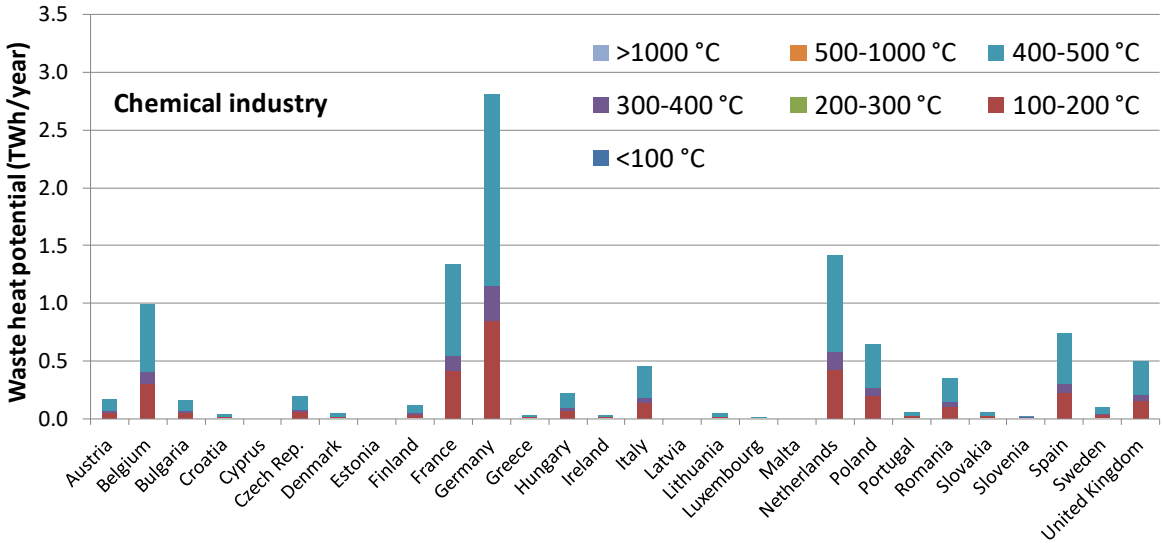

Figure 2.29: Waste heat potential in each EU country per temperature level in chemical industry

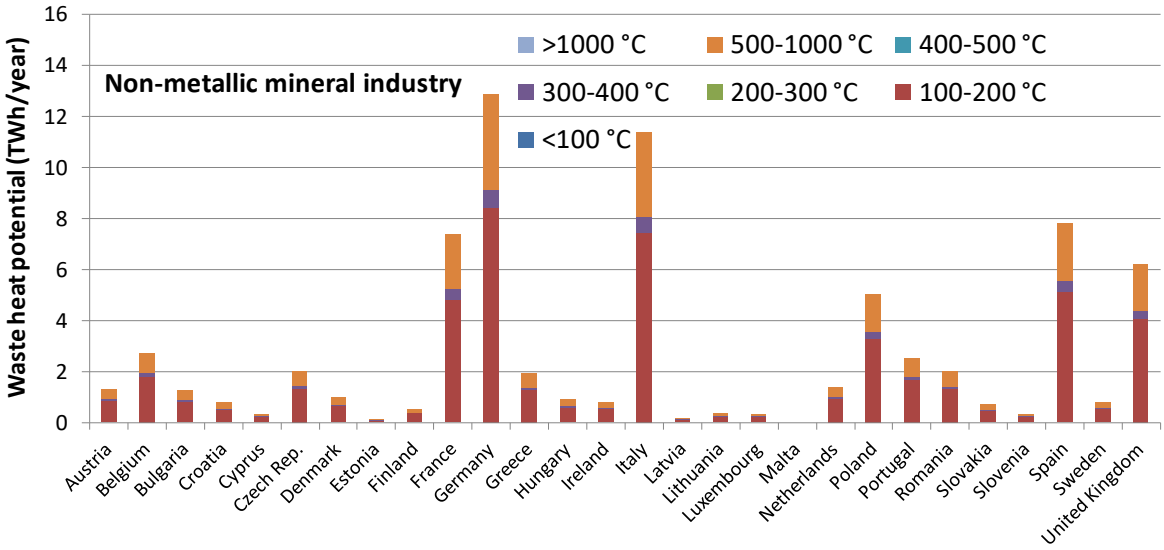

Figure 2.30: Waste heat potential in each EU country per temperature level in non-metallic mineral industry

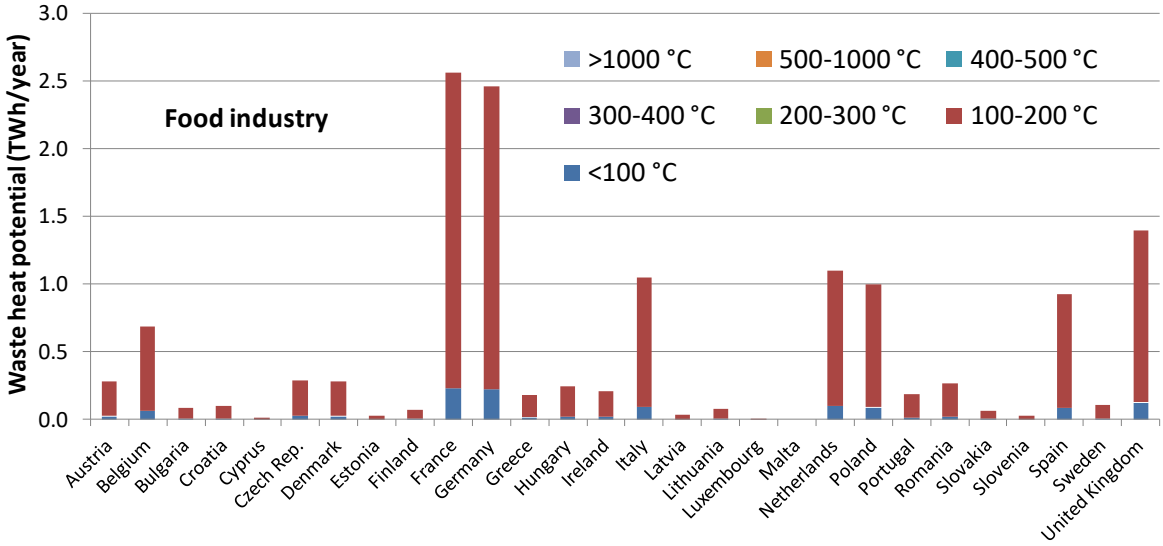

Figure 2.31: Waste heat potential in each EU country per temperature level in food industry

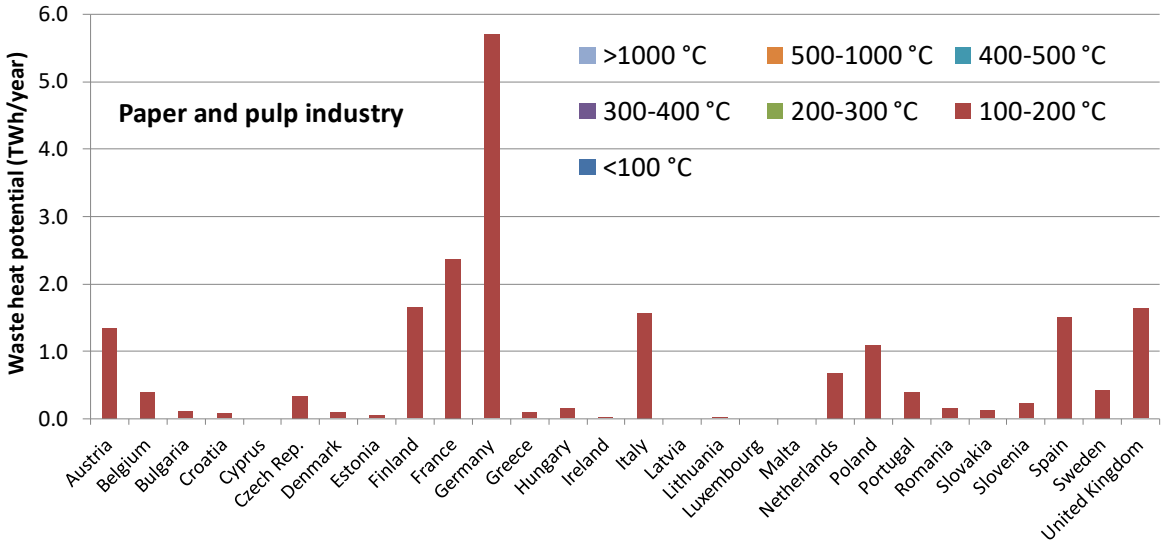

Figure 2.32: Waste heat potential in each EU country per temperature level in paper and pulp industry

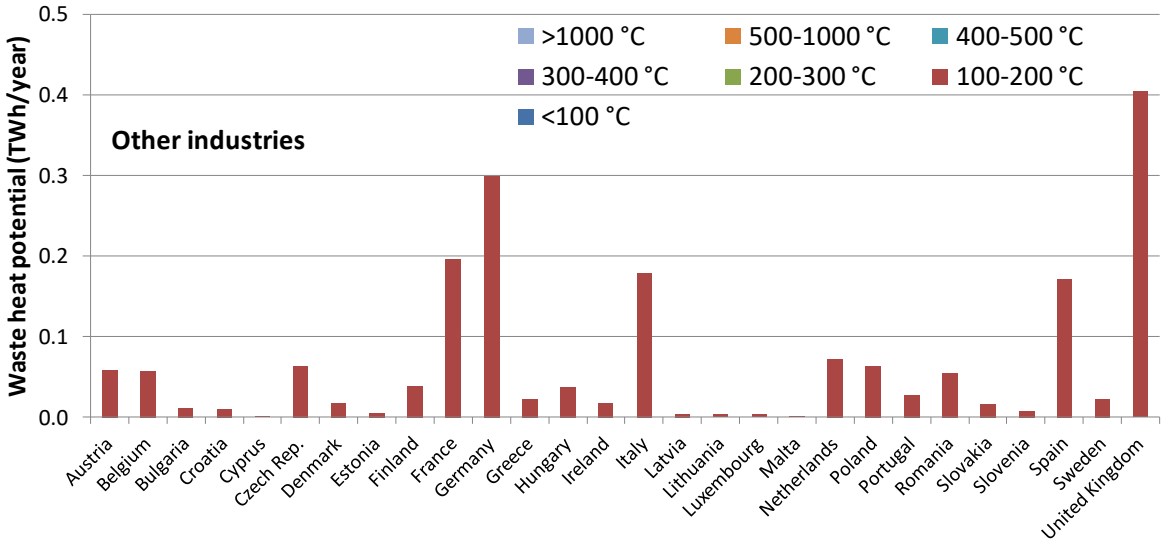

Figure 2.33: Waste heat potential in each EU country per temperature level in other industries

In most sectors the highest potential exists in Germany. This was expected as Germany is the largest EU Member State and has intensive industrial activity. However, in food industry the leading country in waste heat potential is France followed by Germany, and in the category "other industries" the leading country is UK.

Moreover, the waste heat of most sectors is within the temperature level of 100-200 °C, which matches the temperature of the exhaust gases of boilers and standard heating equipment. The temperature of the waste heat is increased to more than 500 °C in only three industrial sectors: chemical, iron and steel and non-metallic mineral.

Finally, the sum of waste heat potential in each EU country from all industrial sectors per temperature level is shown in Fig. 2.34.

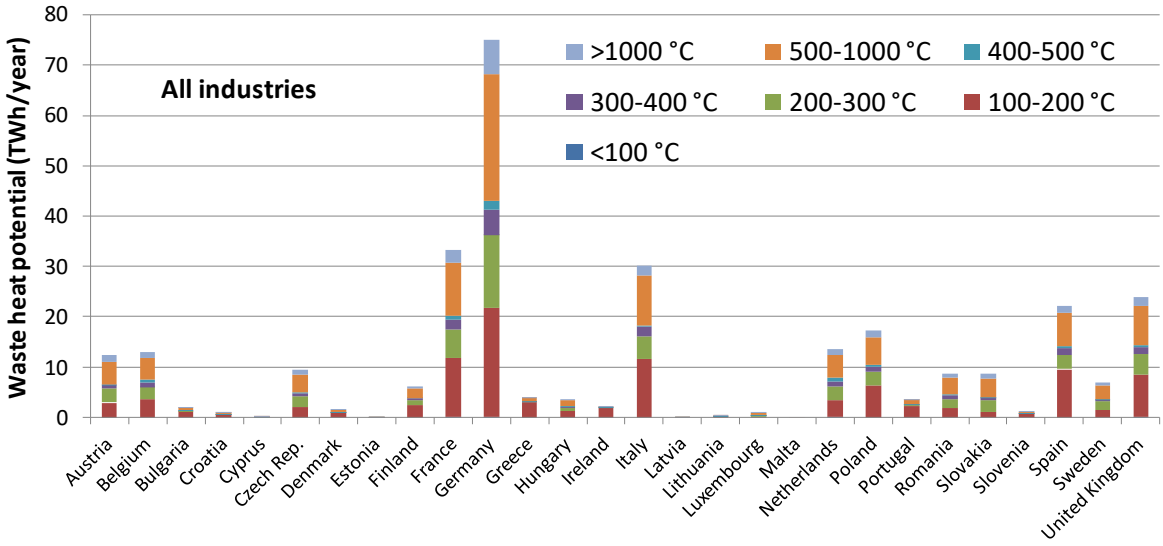

Figure 2.34: Waste heat potential in each EU country per temperature level in all industries

The highest waste heat potential exists in the industrial sectors of Germany, Italy, France, Spain and UK, and if summed it represents about 60% of the total one.

Comparison of results

The results of this methodology compare well with results from similar previous studies. In the UK a waste heat potential of 24 TWh/year was calculated here, which is within the range of 10-40 TWh/year estimated by various studies for UK industry [83]. The waste heat potential in Sweden was calculated here to be 7.09 TWh/year, while in a Swedish report [84] the waste heat potential in Sweden was estimated to about 9 TWh/year (using 2002 data [85]). But the energy efficiency index has decreased since 2002 by about 16% in Sweden (1.24%/year for the period 2000-2015, according to Odyssee-Mure database); taking that into account, we come to 7.56 TWh/year for 2015 which is very close to the 7.09 TWh/year calculated by our methodology.

There are also cases where differences with previous studies are observed. Pehnt et al., 2011 [50] calculated a waste heat potential for Germany of about 132 TWh/year, which is about 43% higher than the 74.85 TWh/year calculated here. Considering energy efficiency improvement in Germany (0.87%/year over the period 2000-2015) the resulting waste heat potential is 117 TWh/year, reducing this difference to 36%. When exploring the reasons for this difference, it was noticed that while there are no significant differences in the average fractions used in the two studies, in this thesis the waste heat fraction is applied only on the heat consumption of each industry (since this is how the waste heat fractions were calculated), while Pehnt et al. [50] apply it on the total energy consumption including both heat and electricity.

In terms of studies covering the whole of Europe, an estimation of waste heat potential has been recently conducted within the framework of the I-Therm EC-funded project [86], which calculated a potential of 370.42 TWh/year using 2012 data. In their study, there was no

differentiation between energy efficiency levels among the different countries. Also in terms of temperature ranges, they grouped the waste heat to temperatures below 100 °C, from 100 to 300 °C and over 300 °C for calculating the waste heat fractions, but the reported waste heat potential is not divided into any temperature levels. The potential they calculated for each country is very close to the one calculated here, and the somewhat lower values reached in this thesis could be well attributed to the improvement of industrial energy efficiency over the period 2012-2015. A large difference was observed for the case of the Netherlands; this comes down to a very high value that they have used for energy consumption in the category "other industries" and it is not clear where that comes from as it is not in-line with the Eurostat data. In case the I-Therm results at country level are adjusted considering the difference of energy intensity of each country's industry from the year 2012 to 2015, and the potential in the Netherlands is corrected, then the total waste heat potential is reduced to 321.86 TWh/year (5.8% difference from the results in this thesis). Fig. 2.35 provides a more detailed comparison per country among the current results and the I-Therm ones (the reported and the adjusted ones).

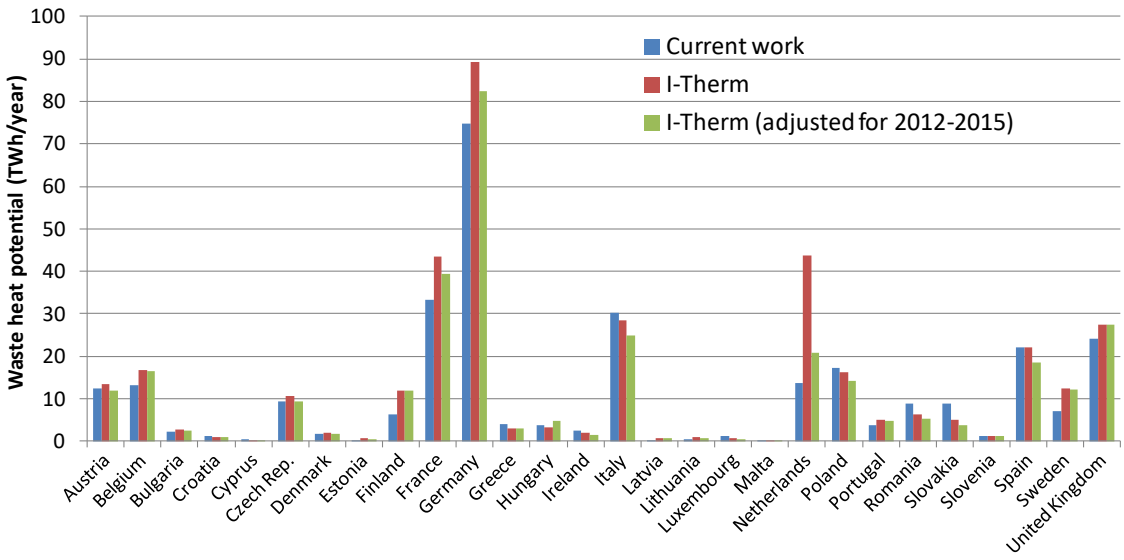

Figure 2.35: Comparison of the current results with the I-Therm data (original and adjusted) per EU country

In general, the results in this thesis are at similar levels with the results from previous studies. The main advantage of the present work is that waste heat potential has been also adjusted to take into account the different energy efficiency levels between European countries. In addition, a more detailed breakdown of the waste heat potential is provided breaking it down per temperature level, which makes it interesting for exploring the applicability feasibility of different recovery technologies.

2.4.2 Waste heat potential in decentralized power plants in EU countries

The analysis in each EU country is divided into two main segments:

- Fossil-fuelled internal combustion engines. The fuel used in this segment is heavy fuel oil, diesel oil and natural gas.
- Biogas engines. This segment includes all types of biogas, from adiabatic digesters, landfills, waste water, etc.

Especially for the first segment, there are very few available data in each EU country, since some plants are commercial ones and others are used only for backup purposes. Therefore, the potential for only a few EU countries has been identified and is presented here. On the other hand, biogas engines have been the subject of many EU projects and the available literature on this is extensive. Therefore, detailed and recent information is available, which will be presented next.

Diesel engines:

As mentioned before, very few data are available in each EU country for this type of power plant. Most of them exist on islands, which however have started to install modern power plants, while interconnection with the mainland using submarine power-cables is ongoing. This is the case in Greece with its numerous islands, some of which are already interconnected, while for some others (e.g. Crete) this procedure has been initiated. Moreover, Malta has been interconnected with Sicily, Italy [87]. In the above cases, the existing power plants are not decommissioned, but are rather used for covering the base loads or as backup units.

Some available power plants in some countries from Global Energy Observatory [88] database are presented next.

Greece: Most of the Greek islands in the Aegean Sea are not connected with the mainland electricity grid, having many distributed power plants using heavy fuel oil or diesel oil. The installed capacity is about 1.76 GWe (2016 data) [89], with Crete and Rhodes islands sharing about 60% of this capacity. The electric energy produced from these thermal plants is about 326.3 GWh. The installed power plants in Crete and Rhodes are mostly steam power plants, which are not of interest for the RED Heat Engine (in Crete only one power plant based on diesel engines exists with capacity 102 MW).

On the other hand, all other power plants in the Greek islands are based on medium/large diesel engines, with total capacity 714.51 MW_e and total electricity production during 2016 of 116 GWh. This production is shared in 11 medium islands (e.g. Lesvos, Kos, Samos, Paros, Santorini) and 19 small ones (e.g. Ikaria, Kythnos, Patmos) [90].

The waste heat potential is estimated, using the methodology presented in a previous section, considering a mean thermal efficiency of the power plant equal to 42%. The waste heat of the cooling water is then equal to 58 GWh/year at temperature of 80-90 ^oC.

Cyprus: The installed capacity is about 1.74 GWe with some power plants based on steam cycle and some others on internal combustion engines with heavy fuel oil [91] (4 total in number: a 100 MW at Dhekelia and three smaller ones with total capacity of 20 MW).

The resulting waste heat potential is estimated to about 260 GWh/year at temperature of 80-90 ^oC, considering a capacity factor of 80% and mean operating load at 70%.

France: Corsica island is equipped with modern diesel engines with capacity of 131 MW for covering the main electricity loads. It is connected with Sardinia to increase flexibility.

The resulting waste heat potential is estimated to about 200 GWh/year at temperature of 80-90 ^oC, considering a capacity factor of 80% and mean operating load at 50% (reduced due to the interconnections).

The use of diesel engines for continuous electrical generation is gradually decreasing. This type of power plant is preferred in remote areas, such as isolated areas or islands. However, most of these sites have started to examine technical solutions for extending the grid and establishing connections, in order to increase flexibility. The existing diesel engines usually remain operational and used as backup or peaking units, operating few hours per year. Therefore, the waste heat potential from this type of power plants is not of interest for the RED Heat Engine, which requires continuous heat supply, in order to produce significant amounts of electricity per year.

Natural gas engines:

Natural gas engines of spark-ignition type mostly operate as CHP units (NG-CHP). Their sustainability depends on the utilization of heat production, since only the exploitation of their generated electricity (supplied to the grid or used by the plant operator) is not adequate to secure a reasonably short payback period. The smaller engines with capacity below 0.5 MW_e have a typical power to heat ratio of 0.6-0.8, while larger gas engines have a ratio of 0.8-1, due to their higher electrical efficiency of 40% and thermal efficiency around 40-45% (resulting to total cogeneration efficiency reaching 85%).

Their use is increasing throughout Europe, and most of their heat production is utilized. Some engines even operate at tri-generation mode (power, heat and cold production), such as in the Munich airport in Germany [92], to maximize heat utilization during the summer season when heating is not required.

In EU about 155 TWh/year of electricity is produced from NG-CHP units and another 326 TWh/year of heat (2014 data). In Fig. 2.36 is shown the electricity and heat from these units in each EU country (processed data from Eurostat [93]).

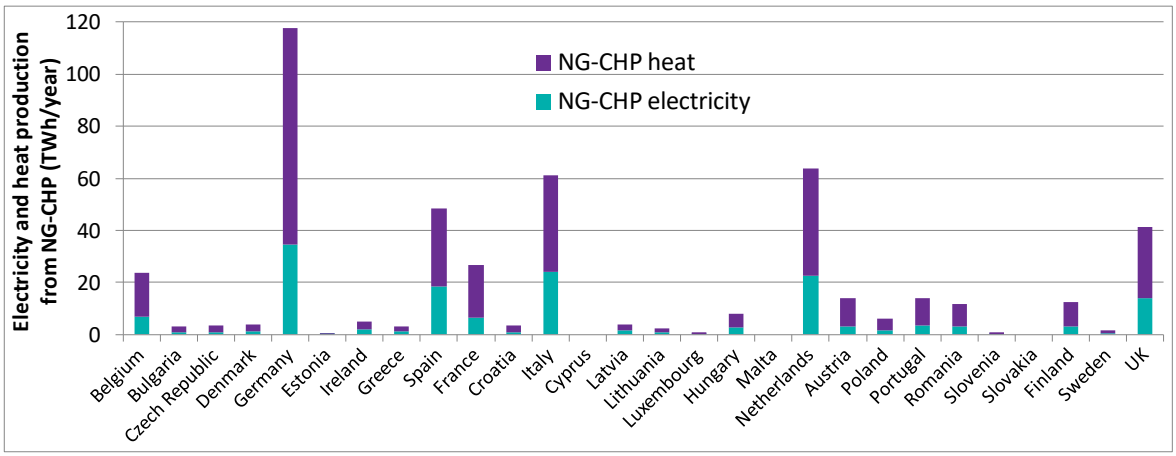

Figure 2.36: Electricity and heat production from NG-CHP units in EU

Although the potential of these engines is high, low amounts of heat production are rejected, as most of it is utilised for other purposes. Therefore, these engines are not considered as a sustainable power plant to feed with heat the RED Heat Engine.

Biogas plants:

Biogas production and share of use in each EU country are shown in Figs. 2.37 and 2.38 respectively, according to EurObserv'ER [94].

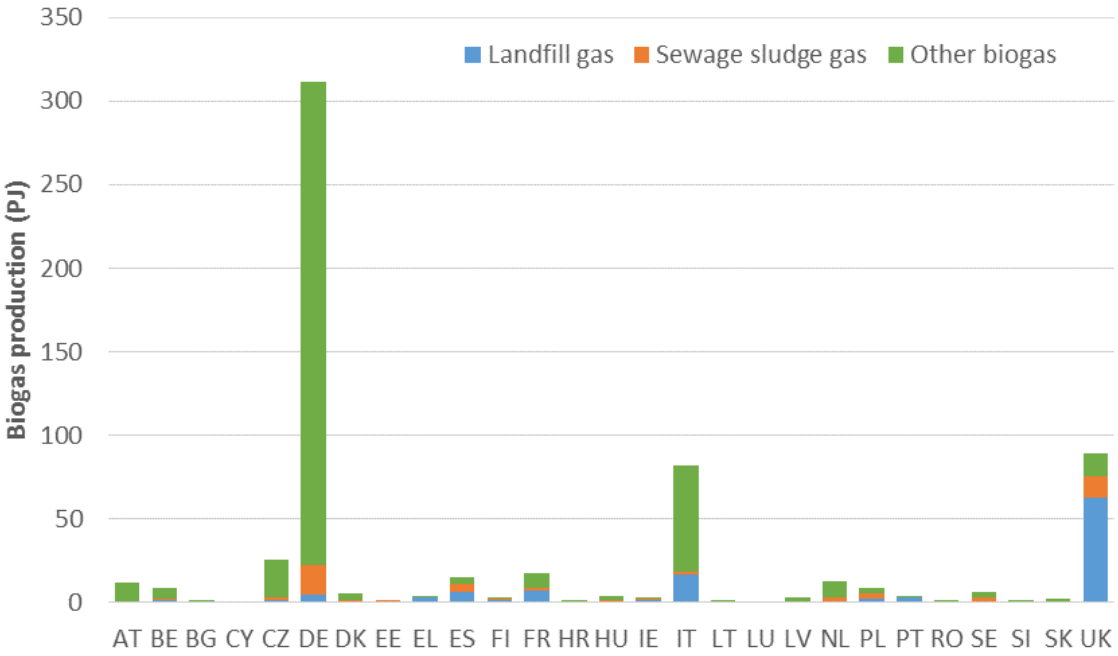

Figure 2.37: Biogas production from each source and per country [94]

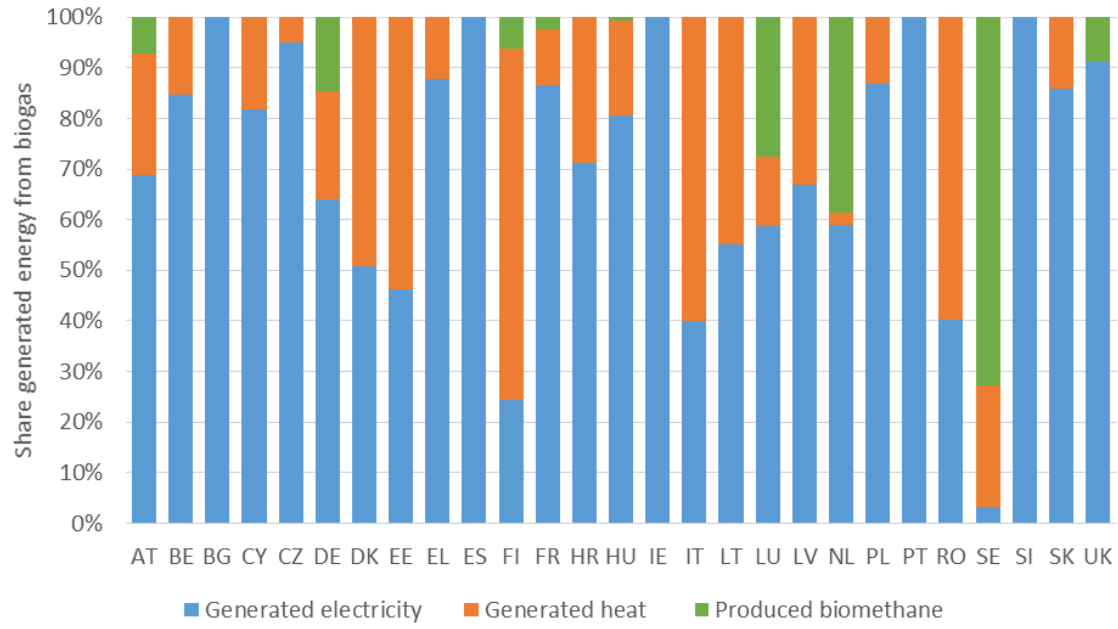

Figure 2.38: End use of biogas per country [94]

Germany, Italy and UK are the countries with the higher biogas exploitation, and adequate incentives provided to biogas energy. Czech Republic, France and Spain are also well developed markets for biogas.

Electricity production from biogas was 57 TWh, while heat utilization (either in district heating networks or self-consumed in the plants) was 34.75 TWh (2014 data, EurObserv'ER, 2015). Considering that a biogas engine has electrical efficiency of about 40% and converts to heat about 45% of fuel combustion heat, about 54% of heat available is utilized, and the rest is

rejected (equal to about 29 TWh). Most of this rejected heat comes from electricity-only plants, which produce about 37% of the total electricity (about 21 TWh).

Concerning the use of biogas, most of it is intended for electricity production in CHP plants. Usually in north Europe a large fraction of biogas is used for heat production (feeding mostly district heating networks), whereas in south Europe lower fraction is used for heating, due to the lower heating demand, resulting to the rejection of large amounts of heat that can be exploited by the RED Heat Engine.

The number of biogas plants per country is shown in Fig. 2.39 [95][96] , using the most recent available data, with many new plants commissioned each year, due to the high growth of this sector. The total number of biogas plants is about 17,000.

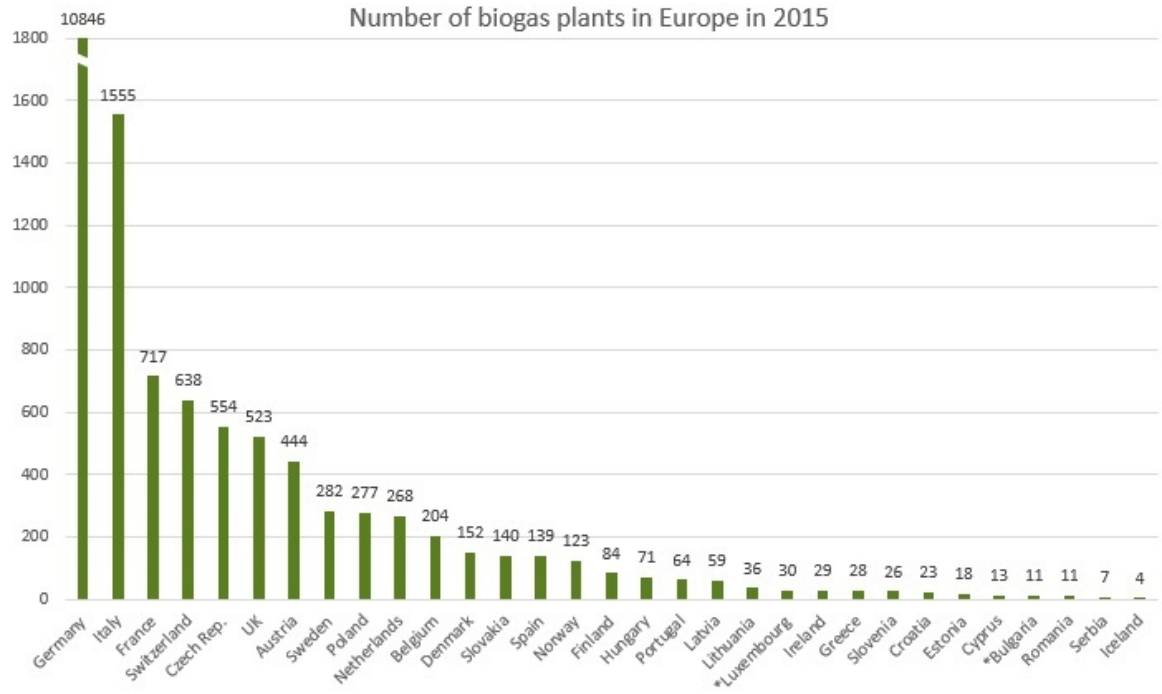

Figure 2.39: Number of biogas plants in EU countries [96]

The waste heat potential is estimated according to the energy production from biogas, using appropriate conversion factors, as presented in previous sections. The results are given in Fig. 2.40 for each EU country.

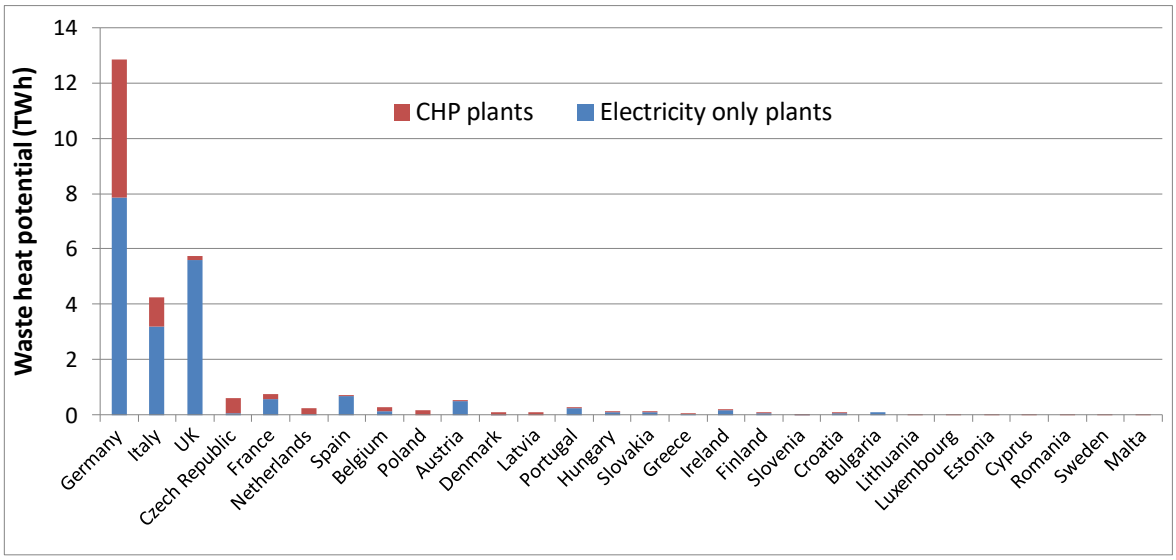

Figure 2.40: Waste heat potential from biogas plants (CHP and electricity only plants) in each EU country

In Germany the potential is very high, about 13 TWh, while also in UK and Italy there are many opportunities for waste heat recovery from the biogas sector. In other countries, the potential is much lower, but still significant, considering that this sector has high growth (see Fig. 2.41), and is supported with strong incentives.

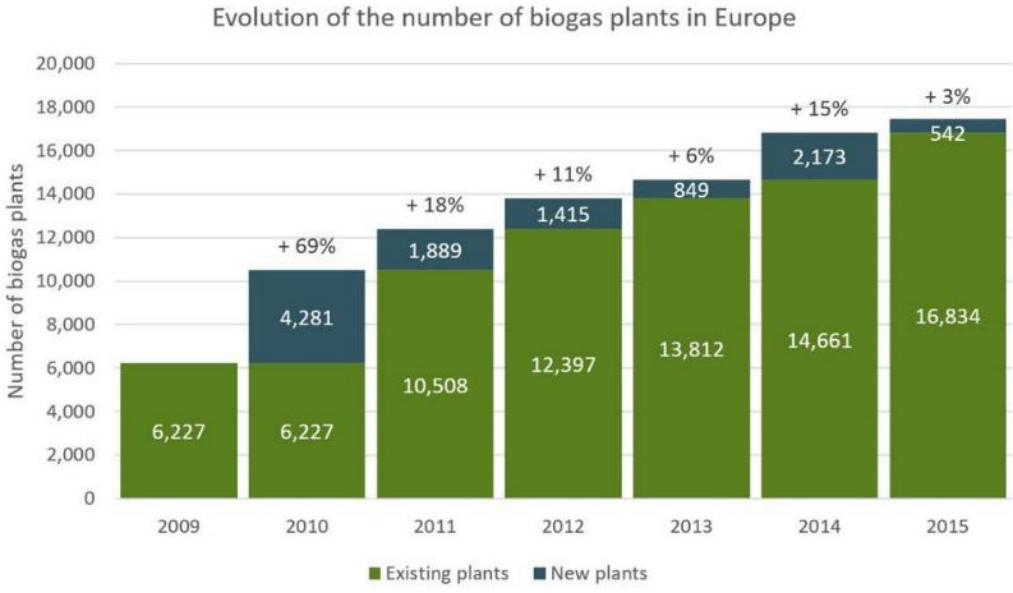

Figure 2.41: Existing and new biogas plants in EU [96]

2.4.3 Waste heat potential in gas compressor stations in EU countries

In the work of Campana et al., 2013 [64], the number and location of gas compressor stations has been examined and updated with 613 identified sites in Europe (including Russia and Ukraine). A map showing the number of sites in Europe is given in Fig. 2.42.

Figure 2.42: Number of gas compressor stations in Europe [64]

The capacity of these stations per country is given in Fig. 2.43. This capacity is then processed, in order to estimate the potential waste heat in each country, which is shown in Fig. 2.44.

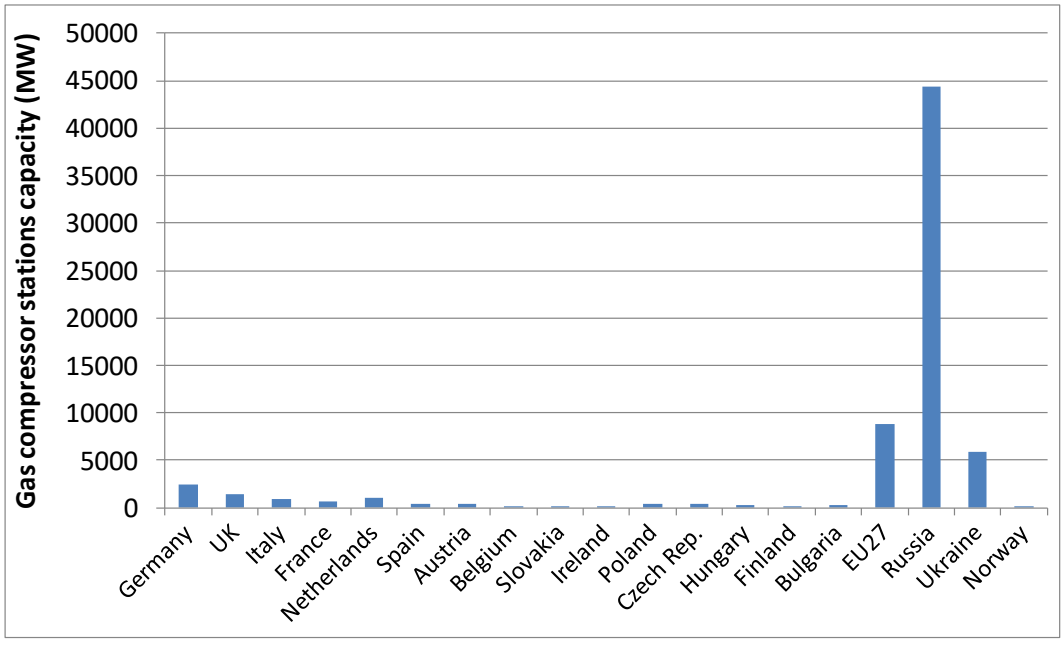

Figure 2.43: Capacity of gas compressor stations per country

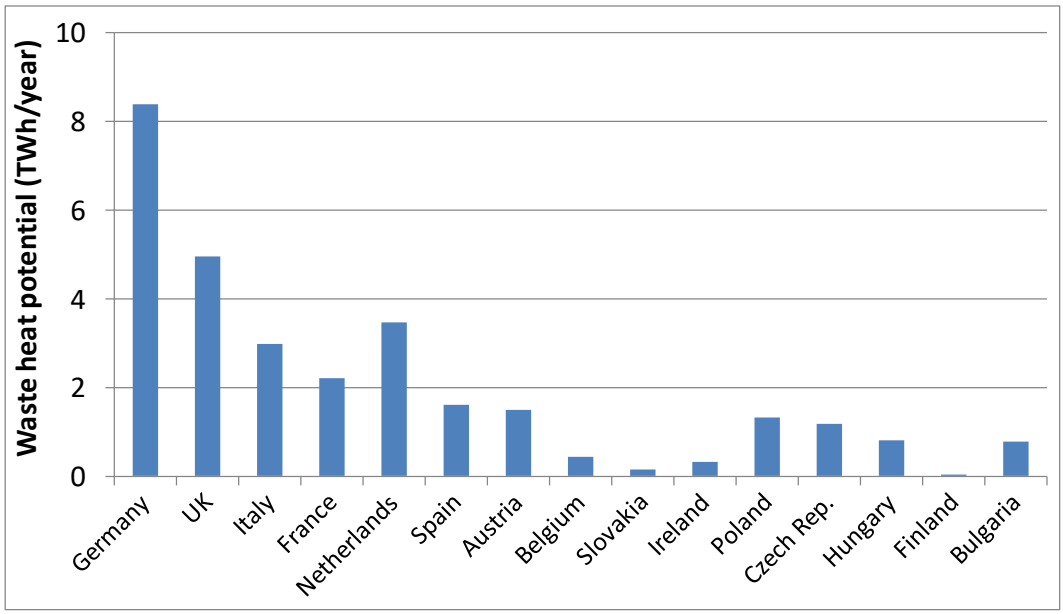

Figure 2.44: Waste heat potential from gas compressor stations in EU countries

Most of the available waste heat exists in the stations in Germany, UK, Italy, France and the Netherlands. Moreover, significant amounts of waste heat also exist in Poland and Czech Republic, from where large pipelines cross feeding Europe with gas.

In case the potential from Russia, Ukraine and Norway is also added, the waste heat greatly increases, as observed in Fig. 2.45.

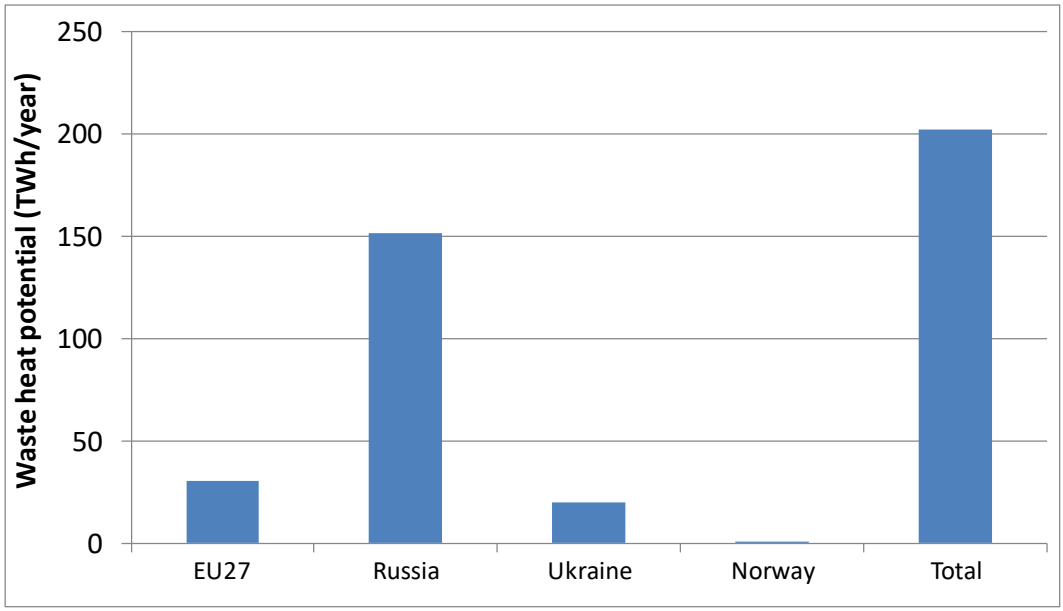

Figure 2.45: Waste heat potential from gas compressor stations in EU and other countries

The waste heat potential in EU27 is about 30 TWh/year (shared among the EU countries as shown in Fig. 2.44), which increases to about 200 TWh/year, mainly from the stations that exist in Russia and Ukraine.

2.5 Waste heat potential for the RED Heat Engine

In the previous sections the waste heat potential from four identified sectors has been analyzed and presented. This analysis has been implemented per sector (including industrial sector) and per temperature level, revealing the huge untapped potential.

In order to harness this heat, a separate heating network is necessary, which mainly includes a number of heat exchangers (their type and size depends on the thermal carrier type, flow rate and composition, and temperature level), piping and pumps, bypass sections (in order to isolate the RED Heat Engine unit in case of maintenance), safety and measuring/control equipment.

Here, the most promising sectors are identified and discussed, estimating the available heat for each site. An average size of the sites is considered for each of the four main sectors examined previously, in order to estimate the available heat for each application and to get an initial idea of the average size of the RED Heat Engine size that will be more suitable in the market.

2.5.1 Waste heat potential for the RED Heat Engine in industry

Industrial waste heat is available in a very wide range of temperature levels. As the temperature of this heat increases, the cost and complexity of heat harnessing equipment (heat exchangers, piping, etc.) increases as well. Therefore, it is preferable to harness heat sources with temperature close to the one required by the RED Heat Engine. The industrial sectors with large amounts of waste heat at temperature level up to 200 ^{o}C are the most promising, which are the following:

- Food and beverage.
- Paper and pulp.
- Chemical.
- Non-metallic minerals.
- Non-ferrous metals.
- Other (e.g. textiles, machinery, etc.)

The iron and steel industry (with about 200 industrial sites in Europe, according to Campana et al., 2013 [97]) is not included in the above list, since its waste heat sources are above 200 ^{o}C (with waste heat potential of about 42 TWh/year), and is not suitable for the RED Heat Engine.

The resulting actual waste heat potential is then reduced to 103.31 TWh/year. In Table 2.9 is shown the technical potential of waste heat per industrial sector with temperature below 200 ^{o}C.

Table 2.9: Technical potential of waste heat with temperature below 200 °C in industrial sectors

Industrial Sector	Technical potential of the waste heat (TWh/year)	Fraction (%)
Food and beverage	13.74	13.3
Paper and pulp	20.15	19.5
Chemical	3.20	3.1
Non-metallic minerals	47.87	46.3
Non-ferrous metals	16.48	16.0
Other	1.87	1.8
Total	**103.31**	**100.0**

In order to estimate the average waste heat potential per industrial site, the potential is divided with the number of remaining industrial sites except from iron and steel ones, equal to about 1000. The outcome is about 100 GWh/year per site at a temperature below 200 °C to be harnessed by the RED Heat Engine. With an average capacity factor of 80%, this corresponds to a capacity of 14.3 MW_{th} per site. However, in each site there are various waste heat sources (e.g. boilers with different exhaust gas temperature and capacity, which could have a distance of even few hundred meters) and it is extremely complicated to harness all available sources. A reasonable fraction concerns the exploitation of about half the available waste heat, resulting to a capacity of about 7 MW_{th} from few different sources.

2.5.2 Waste heat potential for the RED Heat Engine in decentralized power plants

As presented previously, diesel engines and natural gas-fired CHP units are not considered as plant types with a sustainable potential for supplying with heat the RED Heat Engine. The most promising sector of decentralized power plants is biogas power plants, which includes both CHP and electricity-only units.

The number of biogas plants in Europe is about 17000 and following a similar methodology as before, the average waste heat potential per biogas plant is 1.7 GWh/year. With a mean capacity factor of 85%, the thermal capacity available for the RED Heat Engine is 230 kW_{th} per plant. This capacity is low and there could be the option to focus on larger biogas plants that could lead to significant electricity generation by the RED Heat Engine.

2.5.3 Waste heat potential for the RED Heat Engine in marine sector

A similar methodology is followed in the marine sector (about 90,000 ships with about 149 TWh/year waste heat potential). The average waste heat potential per ship is about 1.65 GWh/year, which is similar to the one in biogas plants. Again, the resulting capacity of the RED Heat Engine is relatively low and a detailed analysis should be implemented for selecting ships

with large or many auxiliary engines for installing multiple RED Heat Engine units and increasing the recovery potential and conversion to electricity.

2.5.4 Waste heat potential for the RED Heat Engine in gas compressor stations

The available waste heat per site is much higher in gas compressor stations, since the gas turbine capacity of each station has capacity of more than 40 MW. The resulting waste heat per gas turbine is 330 GWh/year and usually each station is equipped with two or more gas turbines operating continually with high capacity factor (except from the backup ones). Therefore, the waste heat per site is more than 660 GWh/year, resulting to a thermal capacity available for the RED Heat Engine of up to 80 MW_{th}. This makes it possible to install large RED Heat Engine units (in the range of 1-8 MW_e) and reduce specific costs, due to the economy of scale.

2.5.5 Overall waste heat potential for the RED Heat Engine

The waste heat potential from all sectors is summed in Table 2.10. Although the marine sector shows the highest potential, this is shared among numerous ships, resulting to a small capacity in each vessel. On the other hand, the number of gas compressor stations is rather low in EU, resulting to large-scale plants for the utilization of their wasted heat. In the same table is also shown the average heat-to-power size, resulting from the total waste heat potential and the number of sites per sector, as described in the previous sub-sections.

Table 2.10: Technical potential of waste heat in all sectors of interest

Sector	Technical potential of waste heat (TWh/year)	Temperature range	Average waste heat per site (GWh/year)	Average range of RED Heat Engine per site (kW_e)
Industry	103.31	Up to 200 °C	100.00	280 – 700
Biogas plants	29.00	80-150 °C	1.70	7-15
Marine	149.40	80-90 °C	1.65	7-15
Gas compressor stations	202.31	Up to 250 °C	660.00	6,000-10,000
Total	**484.02**			

3. Geothermal heat

Geothermal energy is stored in the subsurface in a variety of concentrations and modes, which influence the extraction method and final application of this heat. Geothermal energy involves drilling and pumping water from depth, accompanied by the development of production and re-injection wells. The cost fractions related to drilling and wells development are usually the largest ones. After having available the heat, various technologies and applications can be used to exploit it [98], such as for power generation, direct use of heat, water desalination [99], and heat pumps.

Geothermal heat has the advantage over other renewable energy sources of being available all day and in all seasons. This fact makes geothermal energy an attractive option for project developers, supplying various processes with low/medium temperature heat. The main drawback is the availability at specific locations, which makes the success of a relevant project development depending highly on the local conditions and quality of geothermal heat and temperature.

In this section, geothermal availability in Europe is examined and presented, according to available resource maps. Focus is given on low-enthalpy fields that can be cost competitive (e.g. at small depth, since drilling is costs are high and increase with depth) and could supply the RED Heat Engine with adequate heat for operation.

3.1 Geothermal fields and availability in Europe

Geothermal energy is the natural heat of the earth, which is transferred from the interior towards the surface mostly by conduction. This heat has higher temperature at larger depth in the crust with an average thermal gradient in the range of 25-30 ^{o}C/km [100] (in areas with no volcanic activity or ground waters that affect heat conduction). At a depth of about 3 km the temperature usually reaches 80-90 ^{o}C. Drilling costs for reaching such depth though are high and represent a large fraction of the total investment for developing a system to extract and use this heat [101]. Therefore, when looking to exploit geothermal energy the focus is on the identification of sites that could provide heat at adequate temperature (water flowing to the surface) at low depth. Apart from that, the development of production and re-injection wells in case of binary plants (the most common technology) substantially contributes to project costs. This fact makes it necessary to develop large scale projects for geothermal applications (in the range of some MW_{th}), in order to reduce the fraction of drilling costs [102], which is about 1000-1500 €/m for small depths (about 1 km), increasing to 2500 €/m for depth of about 2-3 km, and reaching even 4000-5000 €/m for over 4 km [103], as presented in detail later in this section.

Geothermal energy has many different applications according to the temperature and usually it is divided into two main categories: high (temperature over 150 ^{o}C) and low enthalpy fields (temperature below 150 ^{o}C). High enthalpy resources are mostly suitable for electricity generation with steam power cycles. Sites with such resources are found in few countries, such as in Italy, Greece, Turkey, and Iceland. On the other hand, low enthalpy resources are mostly utilized for direct uses (e.g. district heating, agricultural use) and power generation with ORC, which is preferred for heat-to-power applications at low temperature, widespread over most of the EU countries. The possible applications of geothermal energy according to its temperature are provided in Fig. 3.1 [101].

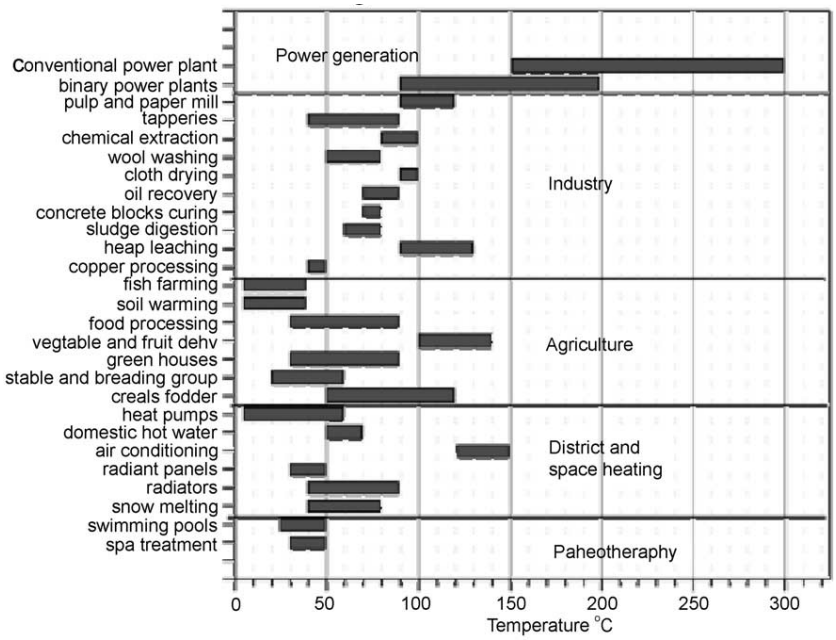

Figure 3.1: Applications of geothermal resources according to temperature [101]

It is observed that most of its uses are within the temperature range of 50-150 °C, while only geothermal conventional power plants (based on steam Rankine cycle) exploit temperatures over 150 °C, in order to increase thermal efficiency and reduce the Levelized Cost of Energy (LCOE) to acceptable values [104], even if geo-electricity is subsidized in some countries.

Moreover, the global utilization of geothermal energy for various applications during the last 20 years is clearly depicted in Fig. 3.2, showing the intense evolution of geothermal heat pumps [105].

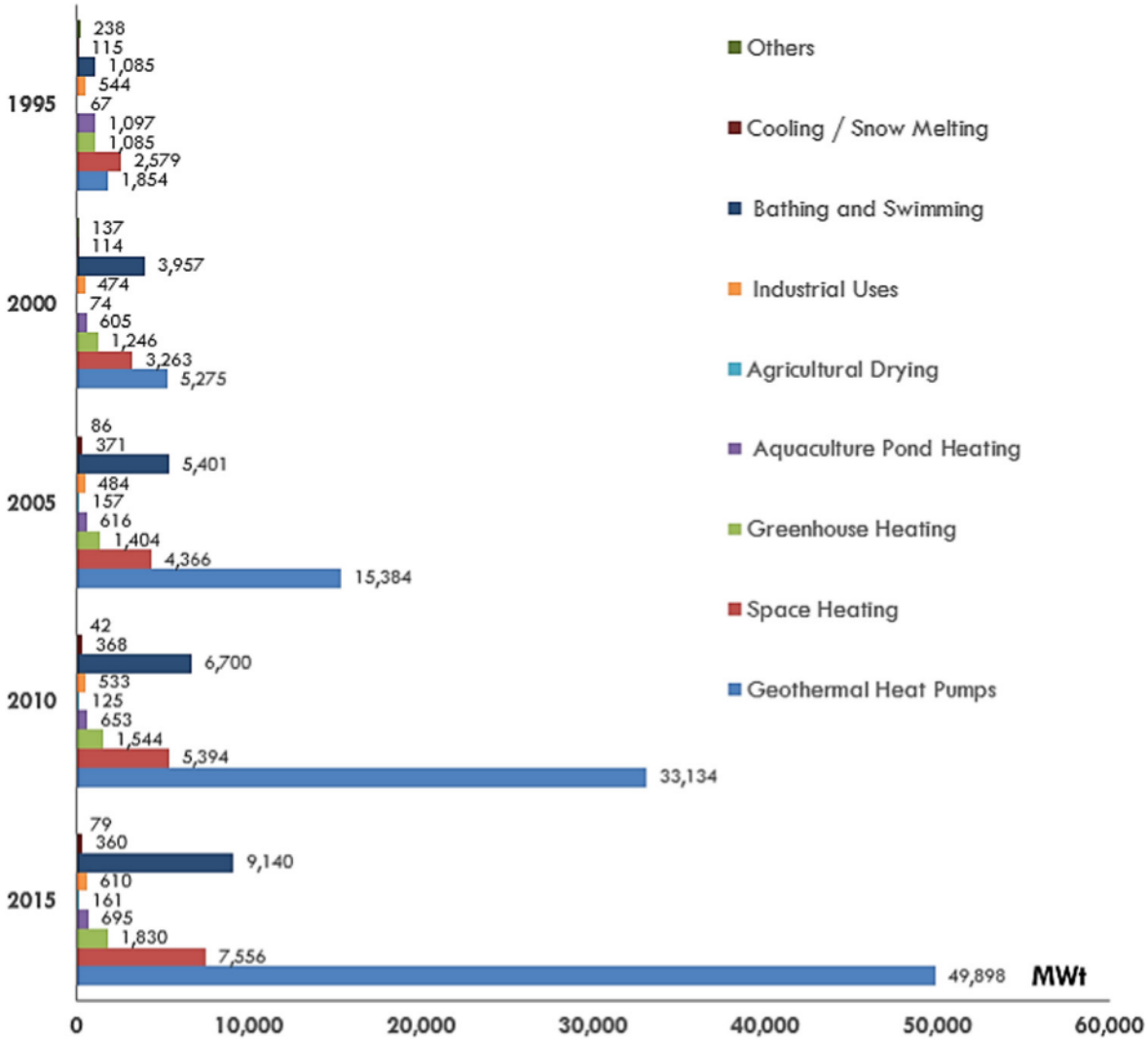

Figure 3.2: Geothermal energy utilization globally [105]

Except from geothermal heat pumps, bathing/swimming in spas and space heating are the other mainstream applications of geothermal energy, in terms of installed capacity (in MW_{th}).

The core parameters of geothermal resources are the following:

- Depth (with effect on drilling costs).
- Available temperature (with effect on the RED Heat Engine conversion efficiency).
- Reservoir type and size (with effect on amount of heat in the geothermal reservoir and the number of production and re-injection wells).

These define the heat availability (amount of thermal energy and temperature), while the main advantage of geothermal energy is its constant availability, making it possible to operate the thermal consumer continuously, reaching a capacity factor over 85% (capacity factor is defined as the fraction of normal operation; total operating hours during a year divided by 8760 h). This is not the case with solar energy, which has a large temporal variation (during each day and season), as will be demonstrated in a next section.

The RED Heat Engine requires heat at temperatures at about 60 to 120 °C (for operation at about 50 to 100 °C), therefore the main focus is given on available geothermal resources within that range.

This section is further divided into two main cases, depending whether a new drilling installation is implemented (requiring large investment) or not:

1. New drilling installations for exploiting geothermal heat of newly explored wells. In this case, drilling costs and wells development represent a large proportion of the investment.
2. Existing wells, which might be operating (e.g. oil-/gas-fields) or abandoned and (waste) heat is co-produced, which can be utilized for the RED Heat Engine.

3.1.1 New exploration of geothermal wells

The available geothermal fields in Europe and their heat availability (e.g. temperature, depth, etc.) are presented here for the case of new drilling installations. The analysis considers the available maps that have been developed mainly as a function of depth, considering regional data.

The temperature distribution in Europe at 1000 m depth is presented in Fig. 3.3, according to the "Atlas of geothermal resources in Europe" and further processed by Chamorro et al., 2014 [106], who used these data and extrapolated the resources to even larger depths (up to 10 km) for unexplored geothermal resources.

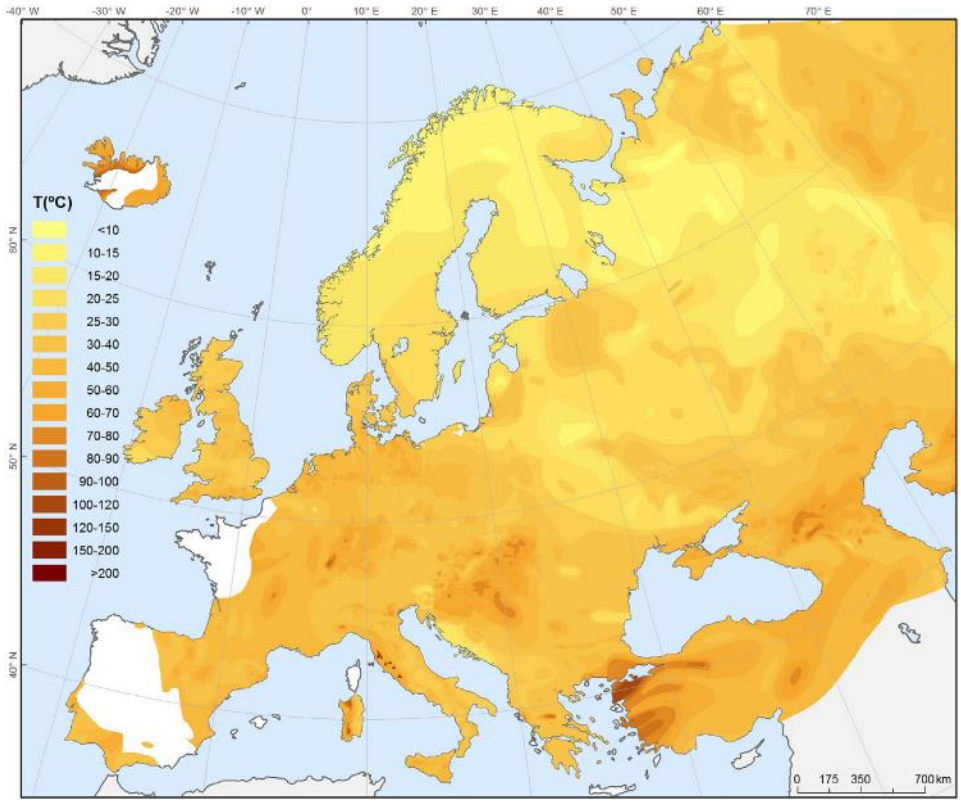

Figure 3.3: Geothermal resources: temperature distribution at 1000 m depth [106]

A depth of 1 km is relatively small for geothermal applications. This is clear in Fig. 3.3, since locations with adequate temperature (about 100 °C) are rather limited and exist only in few parts of Italy, Greece, Germany, Iceland and especially Turkey.

Similar maps at larger depths of 2, 3.5, 4.5, 5.5, 6.5, 7.5, 8.5 and 9.5 km have been processed in the same study and are shown in Figs. 3.4-3.11. These maps have been produced for the investigation of "Enhanced Geothermal Systems – EGS" [107], which focuses on large depths (up to 9.5 km) with high temperatures (usually up to 650 °C) for operating high efficiency power plants [108]. However, the results of this study are mostly valuable for small depths, about 2-3 km.

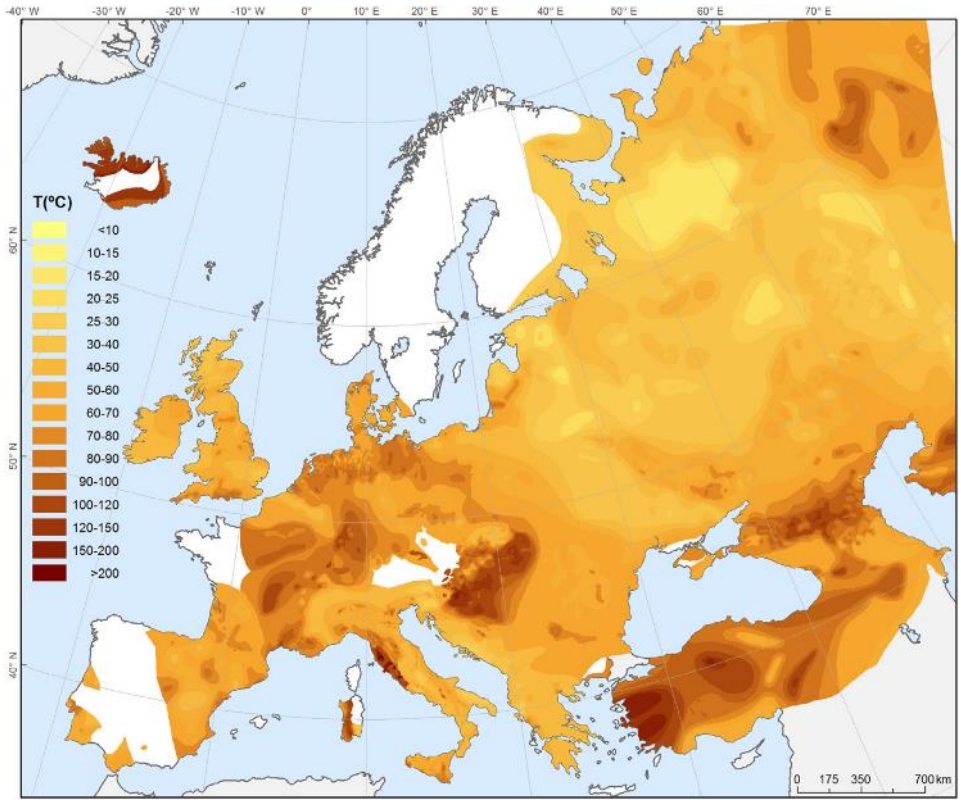

Figure 3.4: Geothermal resources: temperature distribution at 2000 m depth [106]

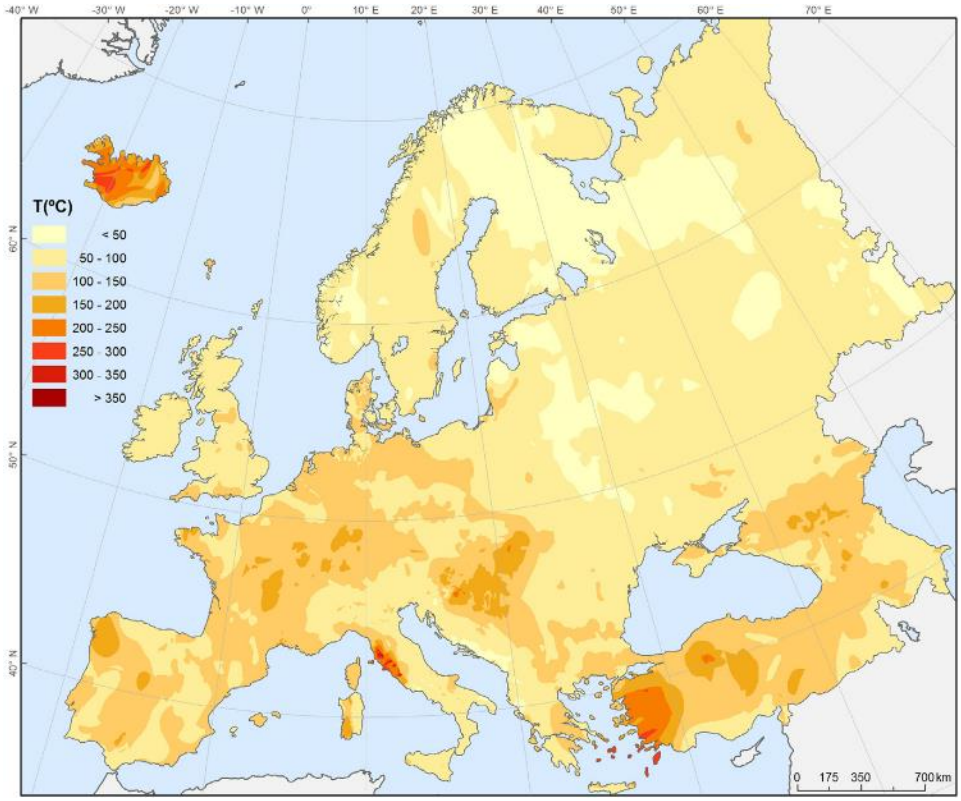

Figure 3.5: Geothermal resources: temperature distribution at 3500 m depth [106]

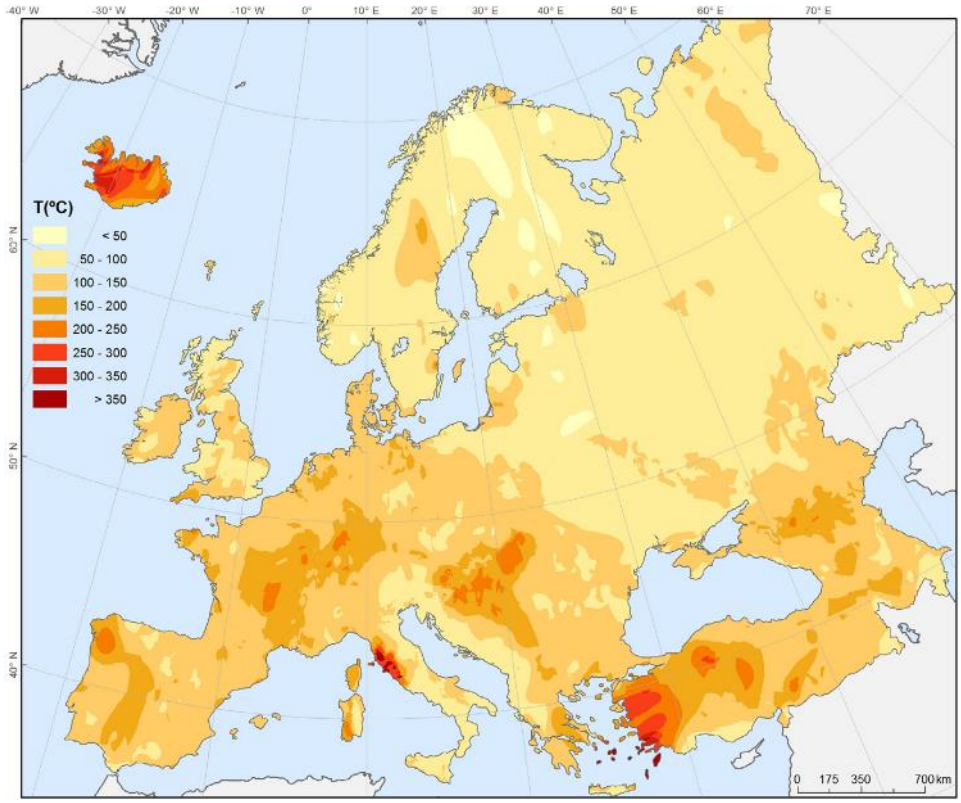

Figure 3.6: Geothermal resources: temperature distribution at 4500 m depth [106]

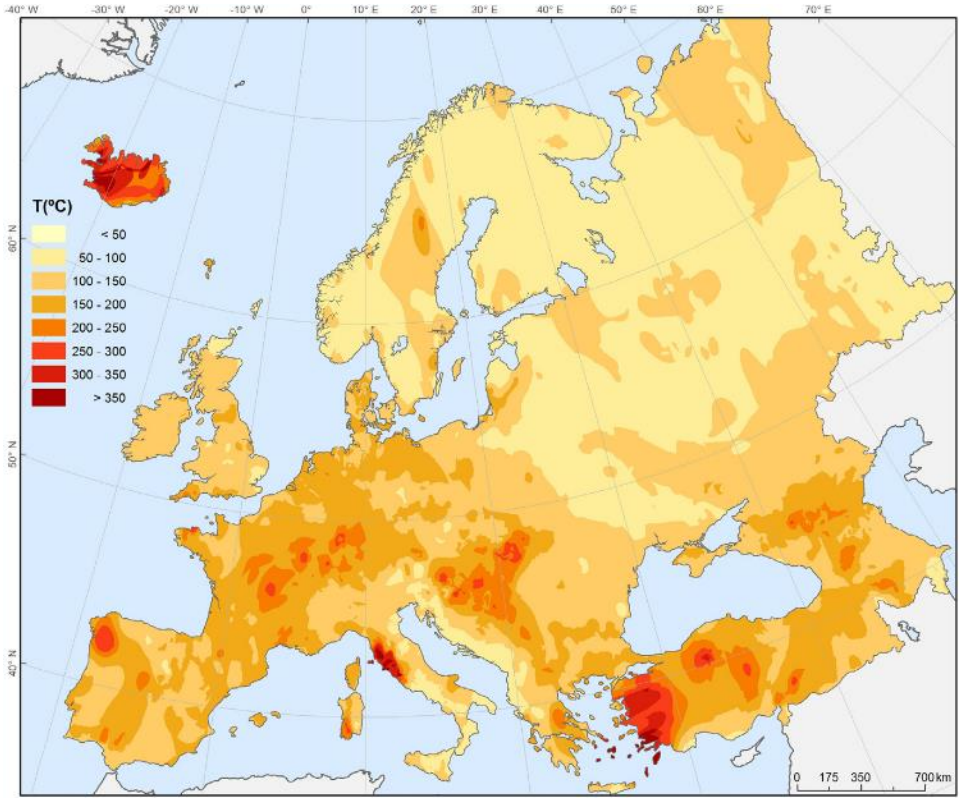

Figure 3.7: Geothermal resources: temperature distribution at 5500 m depth [106]

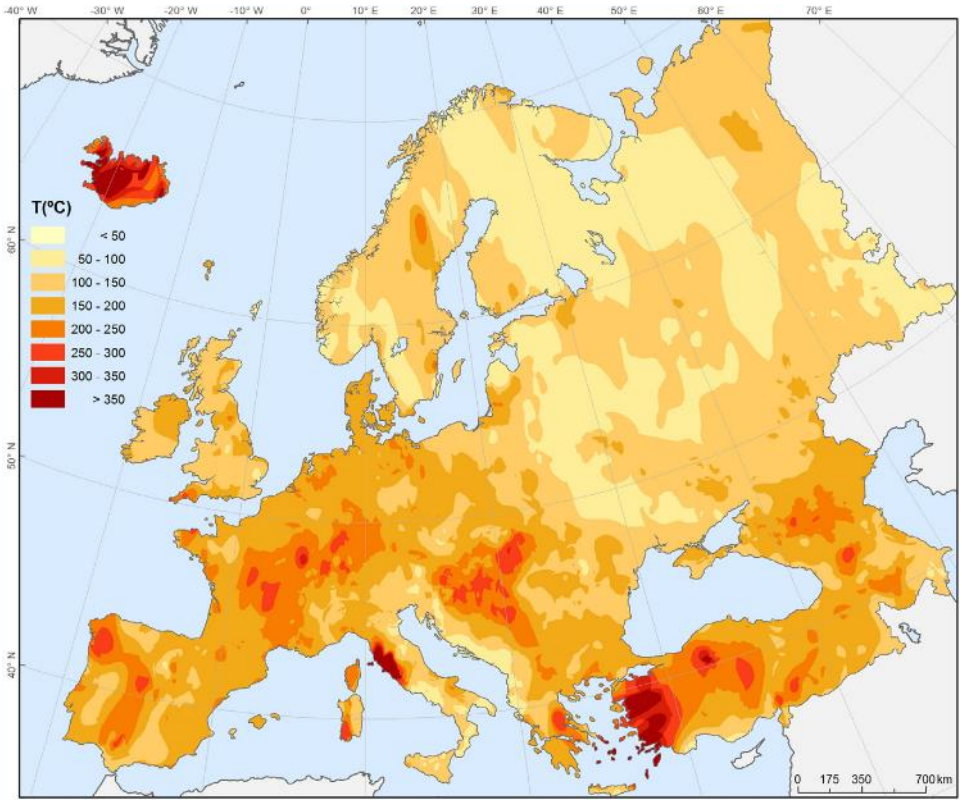

Figure 3.8: Geothermal resources: temperature distribution at 6500 m depth [106]

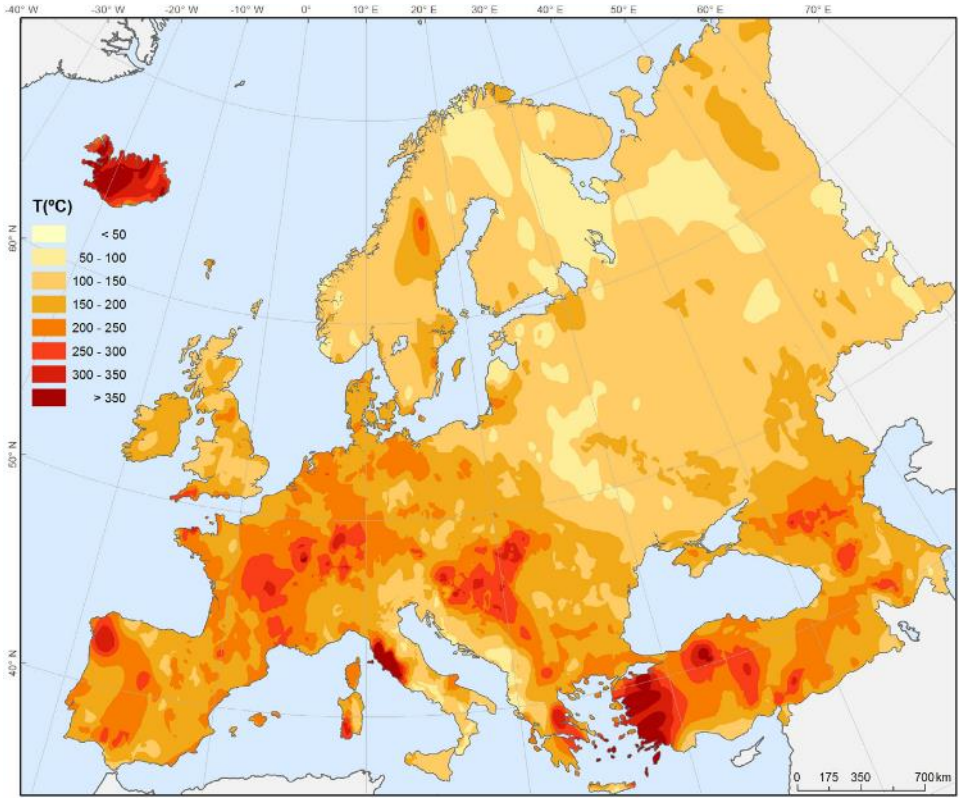

Figure 3.9: Geothermal resources: temperature distribution at 7500 m depth [106]

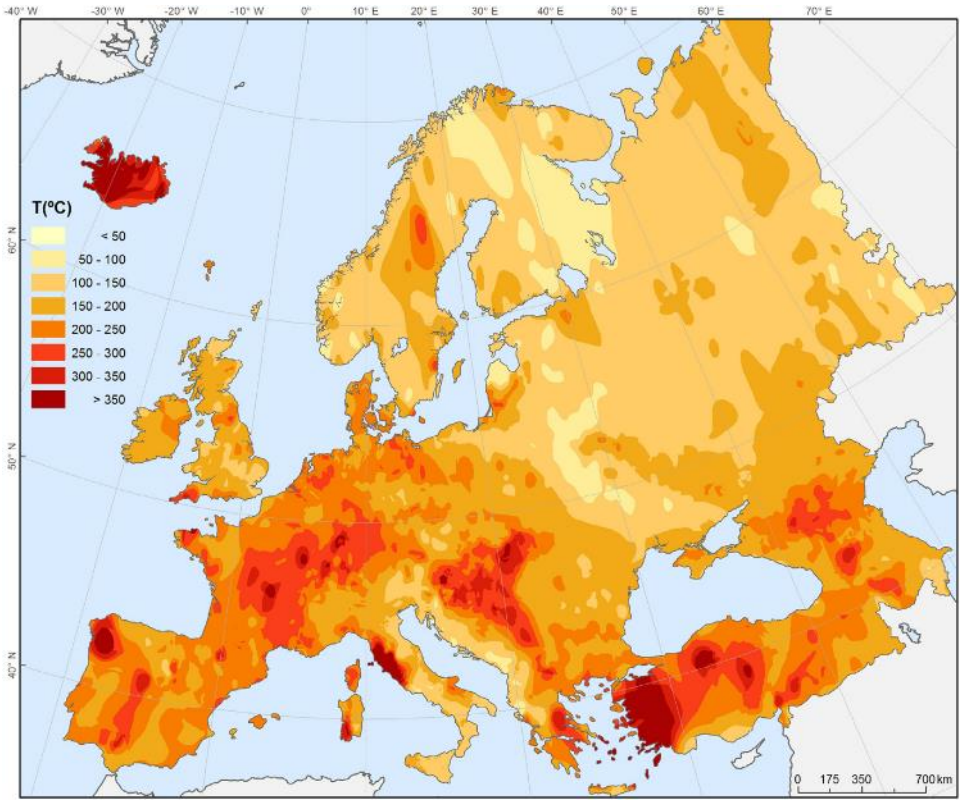

Figure 3.10: Geothermal resources: temperature distribution at 8500 m depth [106]

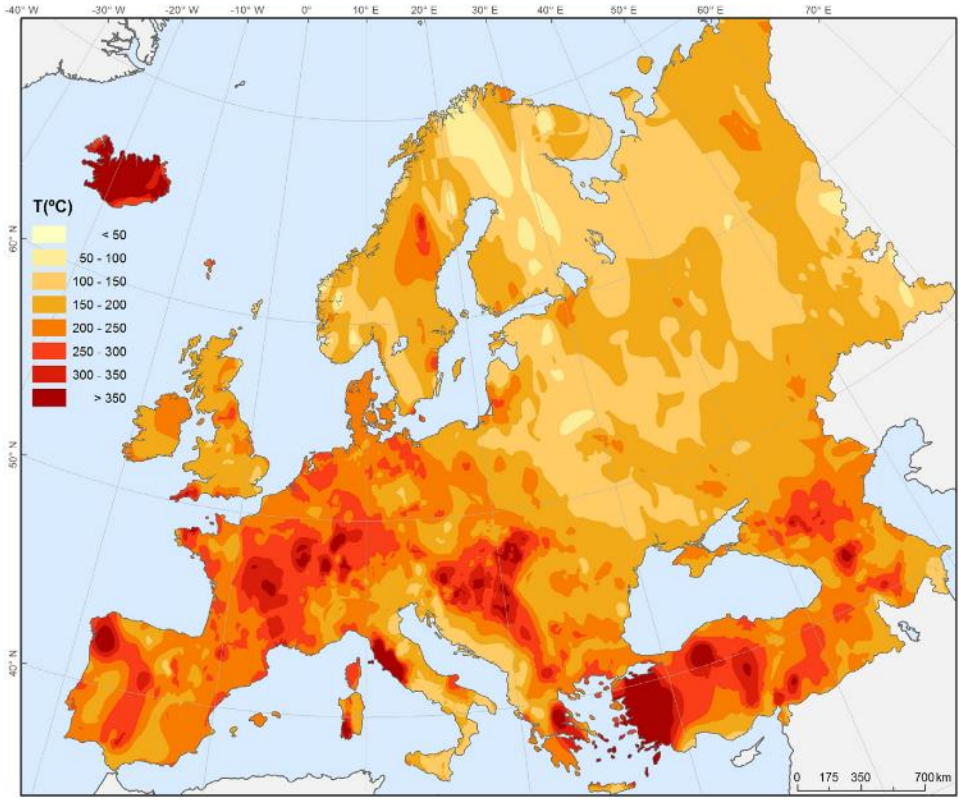

Figure 3.11: Geothermal resources: temperature distribution at 9500 m depth [106]

Similar resource maps have been produced in another study following the same methodology [109], again based on data for 1 and 2 km of the Geothermal Atlas of Europe with same results.

From the previous figures is clear that for very large depths of more than 6500 m, the available areas with geothermal resources of about 100 °C cover a large fraction of Europe, mostly in central and southern EU countries. However, this depth requires a very large investment for drilling, about 30 million € (considering a drilling cost of about 5000 €/m for this depth), which is extremely high, while the costs for the well development (for production and re-injection of the geofluid) increases further the required investment. In most cases a production well has a thermal capacity of 4-5 MW_{th}, and the number of re-injection wells is about half of the production ones. Such project would require a very high-efficiency power plant (over 15-20%), in order to reach a sustainable geothermal investment, which is not the case for the RED Heat Engine that has other important advantages (focusing mainly on low/very low temperature heat sources). Therefore, the work here will identify the promising areas that could supply the RED Heat Engine with heat and have the potential of being profitable.

3.1.2 Existing geothermal wells

Some possibilities have been identified that can provide geothermal heat in very specific cases, which do not involve the high cost of drilling and infrastructure. These cases are adequate to provide low-enthalpy geothermal heat at minimum cost, but they are scarce, not easily available, and possibly with a reduced capacity factor. They mainly concern the exploitation of existing/abandoned oil-/gas-fields and/or geothermal drilling installations. These are described next, indicating the temperature range of the possible heat supply.

Oil-/gas-fields: During hydrocarbon exploitation activities, large quantities of hot water are usually produced in temperature range 50-100 °C, as a by-product of the explored oil or gas. The management of this waste water requires high-cost treatment and water cooling [110]. This heat can reach a temperature of 100 °C [111], which is ideal for the RED Heat Engine. Exploiting it would also remove the need for costly cooling of this wastewater. There are some relevant studies [112], aiming to reduce the quantity and cost for treatment of this wastewater and at the same time exploit the available resources, which can lead to sustainable solutions [113]. There are even cases where there are limited hydrocarbon resources and as a result the drilling installation has been sealed and abandoned [114]; this offers still the opportunity to use the existing infrastructure for recovering the geothermal heat without investing in drilling facilities.

However, in both previous cases (operational or abandoned oil-/gas-fields) the available temperature of geothermal heat depends on the depth and location of the site [115], requiring a case-by-case study to determine whether it is interesting for further analysis. Many oil/gas fields of this type have been reported mainly in USA, China, Canada, and UK, with limited data available on their production capacity/potential [116]. Similar data in EU countries are still not available.

Another possible option is to exploit existing wells that have been drilled for either geothermal or hydrocarbon exploitation without succeeding in their original goal (adequate hydrocarbon resources or high temperature geothermal energy), and the infrastructure already exists. There is also the possibility the oil–field to be mature, approaching the end of its lifetime [117] and its use to be adjusted. However, data for all these sites are not easily available and detailed studies are necessary, in order to estimate the available geothermal energy that can be exploited.

These options will be further examined for supplying with heat the RED Heat Engine, estimating in section 3.2 their costs, although the temperature level and its thermal content (in MW_{th}) depend on the specific location.

Operational geothermal fields: Finally, there is the possibility that the binary fluid from existing and fully operational geothermal power plants is not occasionally used [118], due to maintenance/failure of the main power block or to temporal reduced temperature of some production wells (lower than about 120 °C, which is still suitable for the RED Heat Engine). Instead of re-injecting the fluid underground, without exploiting its thermal content, it can be used for supplying with heat the RED Heat Engine. However, this option is not favourable, since the heat-to-power conversion unit will be operating with a low capacity factor, about 10-15%, with a questionable profitability, even if the generated electric energy is incentivized. Therefore, it will not be further examined in the next section.

3.2 Geothermal potential for the RED Heat Engine

In the previous sections the geothermal availability in Europe has been presented, which is of interest to this project. Here, the potential to supply with heat the RED Heat Engine is presented, accompanied with cost figures that can provide data that are necessary for assessing the possible profitability of such coupling. Only the geothermal sources of interest are further examined that show high capacity factor and adequate temperature. Geothermal sources are divided into two main groups, following their distinction in the previous section: (1) geothermal fields with new drilling installation, (2) exploitation of existing drilling infrastructure.

3.2.1 Geothermal potential for RED Heat Engine with new geothermal fields

In case of investing in new geothermal drilling and production wells, the preferred areas and depth are depicted in Figs. 3.4-3.11 in section 3.1 above. For reasonable depths of up to 3-4 km and areas that can supply geothermal heat at adequate temperature, the available heat to be converted to electricity depends on the amount of production wells (and the re-injection wells), the piping, and the thermal content of the well. In case of well projected installations, the total amount of heat depends on the geofluid temperature, its specific heat capacity, and its (total) flow rate. These parameters define the available heat, according to Eq. (3.1).

$$Q_{geo} = \dot{m}_{geo} c_p \left(T_{geo,out} - T_{geo,in}\right) \quad (3.1)$$

, where Q_{geo} is the available heat, $\dot{m}_{geo}$ the total mass flow rate of the geofluid from all production wells, c_p its specific heat capacity (usually lower than water), and T_{geo} the outlet/inlet temperature of the geofluid from the well.

The temperature difference of the geofluid is usually about 20-30 ^{o}C for the temperature ranges considered here and with specific heat about 3.5 kJ/kg/K, the available heat is mostly defined by the geofluid mass flow rate. Common flow rates are about 50 kg/s for a single production well, resulting to a heat of about 5 MW_{th} per well.

The cost of a geothermal well (in million USD) is extrapolated with the following Eq. (3.2) as a function of depth (given in m), according to current costs of existing geothermal wells [119]. This correlation against real cost data and the specific drilling cost are also clearly reported in the same study and are shown in Fig. 3.12.

$$Geothermal\ well\ cost = 1.72\ 10^{-7}(depth)^2 + 2.3\ 10^{-3}(depth) - 0.62 \quad (3.2)$$

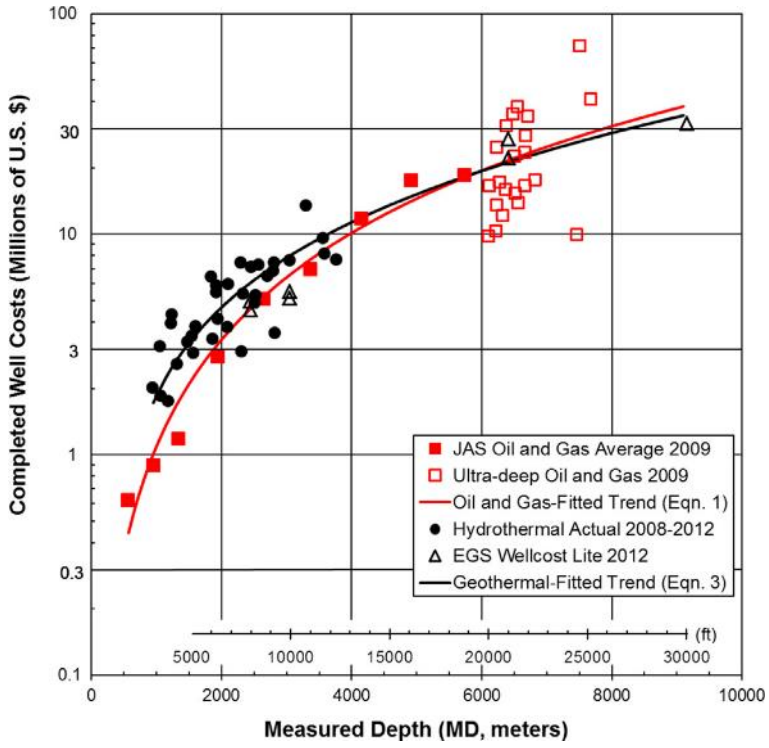

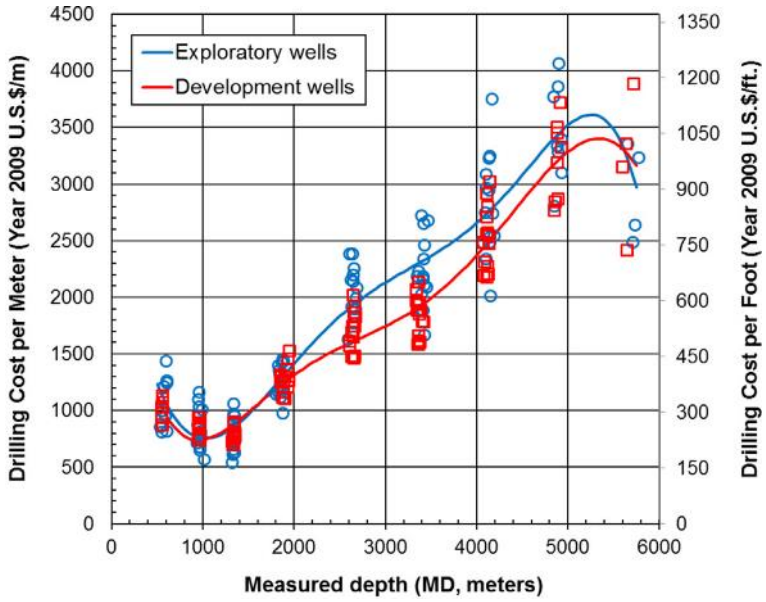

Figure 3.12: Geothermal drilling and well cost [119]

For a reference case with drilling depth of 3 km and total heat capacity of 10 MW_{th} (requiring two production wells and a single re-injection one), the estimated costs for delivering heat of about 100 °C are shown in Table 3.1. These cost figures are obtained and processed from various relevant studies [99,120] with the drilling and well costs presented in Fig. 3.12.

Table 3.1: Cost of geothermal infrastructure for new field (10 MW_{th}, 3 km depth)

Component	Cost (€)	Comments
Drilling development	3,900,000	Depth of 3 km. Cost per meter: 1,300 €/m (2009 USD to EUR: 1.3).
Geothermal production and re-injection wells	18,000,000	For binary plants, two production wells are required (each of 5 MW_{th} capacity) and a re-injection one at reduced geofluid temperature. Three in total (6 million € each according to Fig. 3.12).
Geofluid pumps and heat exchangers	330,000	Pump for pumping geofluid at the required flow rate and temperature (capacity 100 kW, lifetime: 6-7 years). One for each production well (two in total), 115,000 € each. Heat exchangers for delivering the heat of the geofluid in the power plant (cost: 100,000 €).
Building infrastructure and auxiliaries	500,000	Includes the building that houses all surface components, safety equipment, and electrical panels.
Total:	**22,730,000**	

It is observed from Table 3.1 that the cost of geothermal plant development largely depends on the depth and the number of wells. Drilling and production/re-injection wells development represent about 95% of the costs, as shown in Fig. 3.13.

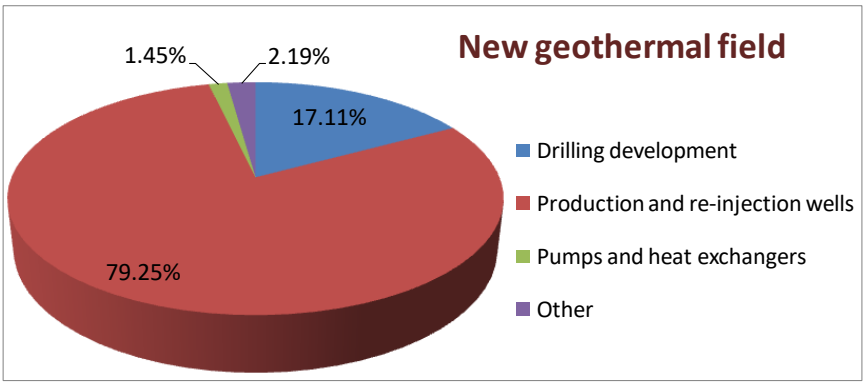

Figure 3.13: Costs breakdown for 10 MW_{th}, 3 km depth, geothermal infrastructure (new field)

In all previous cost figures, some additional costs exist, such as the land rent for the power plant installation, permit, and trial drilling facilities and exploratory wells development. Especially the latter ones are essential, in order to make sure that the estimated geothermal potential exists in terms of both temperature and capacity. These costs can vary widely, depending on local conditions (mostly for permit and land) and depth (mostly for exploratory wells and trial drilling, requiring a case by case study).

3.2.2 Geothermal potential for RED Heat Engine with existing fields

The high costs for extracting geothermal energy are limited in case of using existing fields that are either abandoned (oil/gas/geothermal fields) or under operation (oil/gas fields) [121]. A case-by-case study is required to evaluate the thermal content, capacity, and related costs. However, the estimated costs for infrastructure are reduced compared to the development of new geothermal fields, presented in the previous sub-section.

The cost breakdown for a field of similar capacity (10 MW_{th}, depth 3 km) in case of exploiting existing fields that are abandoned is presented in Table 3.2, together with a brief discussion of each main component.

Table 3.2: Cost of geothermal infrastructure for existing field (10 MW_{th}, 3 km depth) that is abandoned

Component	Cost (€)	Comments
Drilling development	-	Depth of 3 km. Drilling has been already developed for the existing field.
Geothermal production and re-injection wells	9,000,000	Production wells exist. However, their restoration is required, including costs of removing the production tubing, repairing or replacing the casing, and perforating a larger section of the well to restore the well to production (1,500,000 € per production well) [122]. Only one re-injection well is required, as in the previous case (Table 3.1).
Geofluid pumps and heat exchangers	330,000	As in the previous case (Table 3.1).
Building infrastructure and auxiliaries	500,000	As in the previous case (Table 3.1).
Total:	**9,830,000**	

In case of abandoned fields, the cost is reduced from about 22.7 million € (for new wells) to 9.8 million €. The main difference is that no drilling development and production wells are necessary (only restoration of the production wells). The cost fraction of each main component is presented in Fig. 3.14.

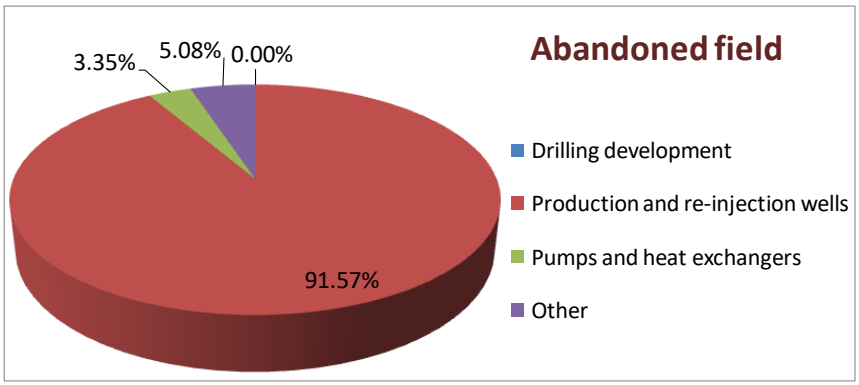

Figure 3.14: Costs breakdown for 10 MW_{th}, 3 km depth, geothermal infrastructure (abandoned field)

Finally, in case of an existing oil/gas field that is operating, no production and re-injection wells are required, and the infrastructure costs are further reduced, as shown in Table 3.3 for the same capacity field.

Table 3.3: Cost of geothermal infrastructure for existing field (10 MW_{th}, 3 km depth) that is operating

Component	Cost (€)	Comments
Drilling development	-	Depth of 3 km. Drilling has been already developed for the existing field.
Geothermal production and re-injection wells	-	Production and re-injection wells exist.
Geofluid pumps and heat exchangers	100,000	Pumps of the geofluid exist. Only heat exchangers are necessary for harnessing the thermal content of the geofluid.
Building infrastructure and auxiliaries	200,000	Limited additional infrastructure is required, estimated to 200,000 €.
Total:	**300,000**	

The costs for this case are low (0.3 million €), since the existing infrastructure of an operating field can be utilized and heat is readily available at the surface. The cost fraction of each main component for the operating oil/gas fields is presented in Fig. 3.15.

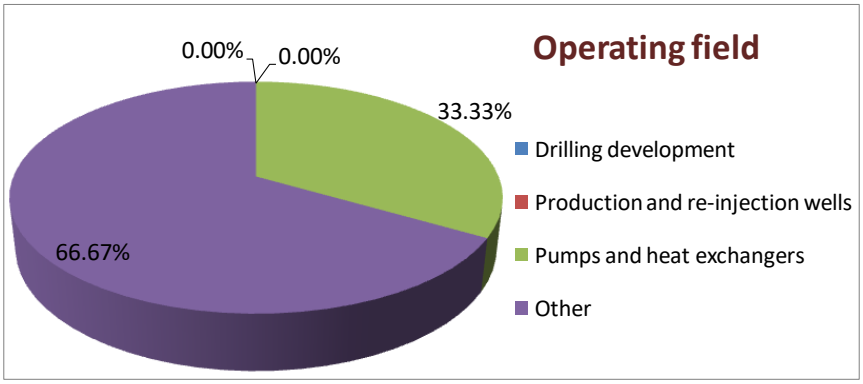

Figure 3.15: Costs breakdown for 10 MW_{th}, 3 km depth, geothermal infrastructure (operating field)

Although this option seems to have the highest interest and potential, there are some limiting parameters, which are highlighted next:

1. The available heat of the geofluid depends on the operation of the oil/gas field. In case of maintenance or any failure, the field will not be operating and no heat will be available.
2. Operating oil/gas fields are scarce and in rural areas.
3. The hot water temperature is sufficiently high only in few cases.
4. The available heat is usually low, resulting to small capacity power plants.
5. The available heat is fluctuating and it is difficult to predict whether its availability will sustain over a period of a few years (fluctuates as a function of the oil/gas production).

3.2.3 Geothermal potential for RED Heat Engine with new/existing fields as a function of depth and thermal capacity

According to the previous analysis and methodology, various cases are considered here, in order to provide an overview of the potential and the related costs as a function of the following parameters, covering the whole range of applications of interest:

- New, existing or abandoned field.
- Depth of drilling (from 0.5 up to 4 km).
- Thermal capacity of the field (from 1 up to 50 MW_{th}).

The main results of this analysis are the costs of infrastructure for having available the geothermal energy on the surface, presented in Fig. 3.16.

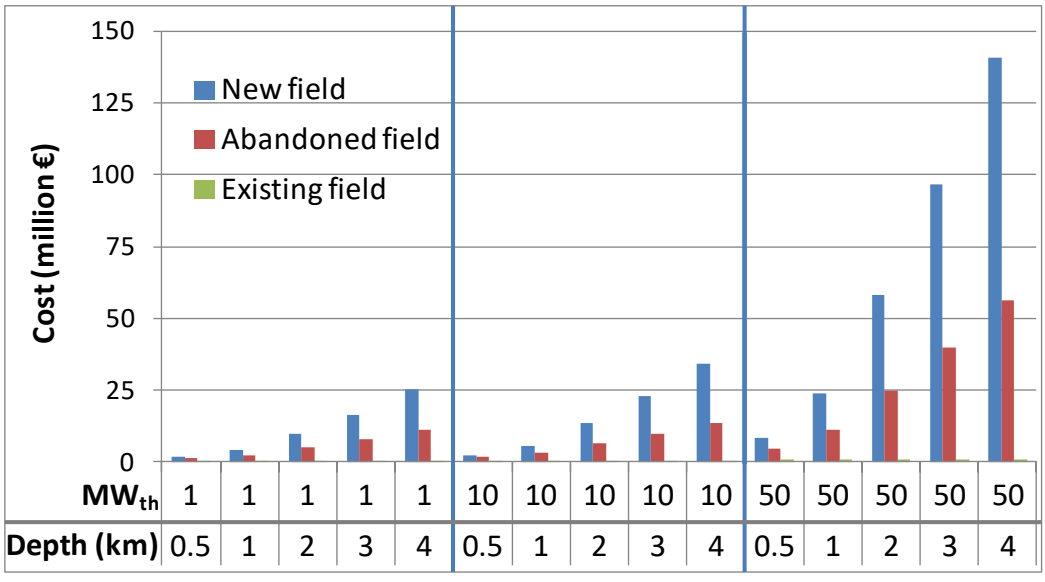

Figure 3.16: Cost of infrastructure (in million €) of new, abandoned and existing fields for various thermal capacities and depths

The costs of existing fields is very low compared to the other two cases, and ranges from 0.16 million € for the 1 MW case up to 0.8 million € for the 50 MW case, with the main contribution on this the heat exchanging equipment and few other costs.

On the other hand, the costs for new fields reaches 140 million € for large depths and 50 MW of heat (requiring the development of 10 production wells and 5 re-injection wells), reducing to about 25 million € for 10 MW of heat (with 2 production wells and a single re-injection one).

An interesting parameter is the specific cost of heat, expressed in €/kW_{th}, making more clear the size of geothermal plants that are of interest. The specific cost as a function of capacity and depth is presented in Fig. 3.17.

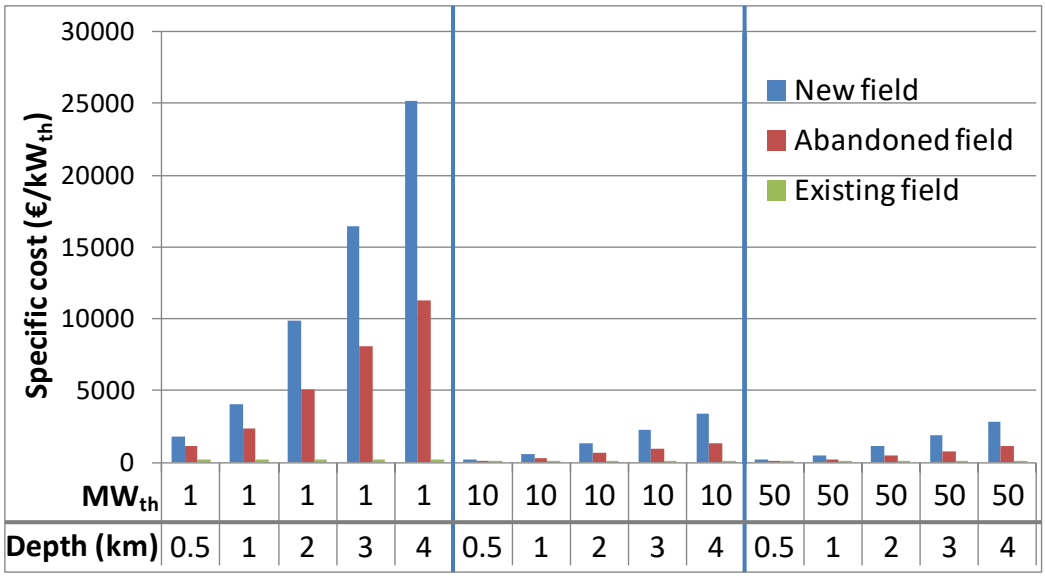

Figure 3.17: Specific cost of infrastructure (in €/kW_{th}) of new, abandoned and existing fields for various thermal capacities and depths

It is very clear that for small plants, the specific cost reaches a very high value of 25000 €/kW_{th}, whereas for larger installations this cost reduces to more reasonable values of about 500-3000 €/kW_{th} [123]. A main reason for this is that for small fields two wells are required (one production and one re-injection one), with each having a maximum thermal capacity of about 4-5 MW, while for the 10 MW case also just the two production wells and one re-injection one are necessary.

The outcomes of Fig. 3.17 make it clear that geothermal plants have to use economies of scale in order to compensate the high costs of drilling and well development.

3.3 Annual production of geothermal heat for the RED Heat Engine

In this last section of this chapter, the annual production of geothermal energy is presented. This energy mostly depends on the capacity factor and the drilling/well capacity. For the reference cases described previously (heat capacity of 1, 10, 50 MW_{th}), the available geothermal heat and pumps electricity consumption as a function of capacity factor are given in Figs. 3.18 and 3.19 respectively.

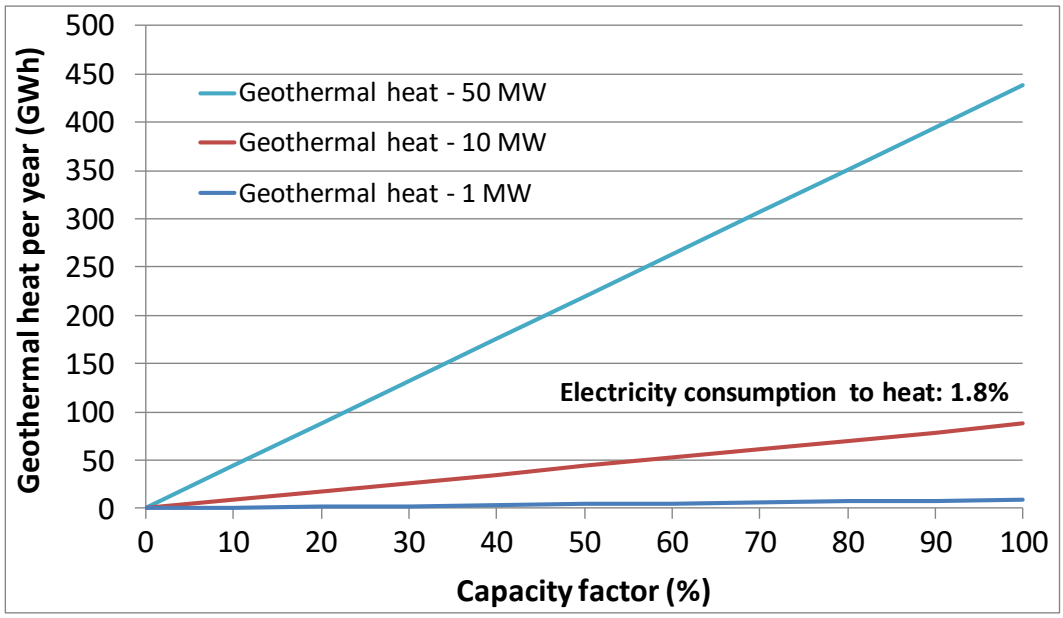

Figure 3.18: Annual geothermal heat as a function of capacity factor for 1, 10 and 50 MW_{th} plant

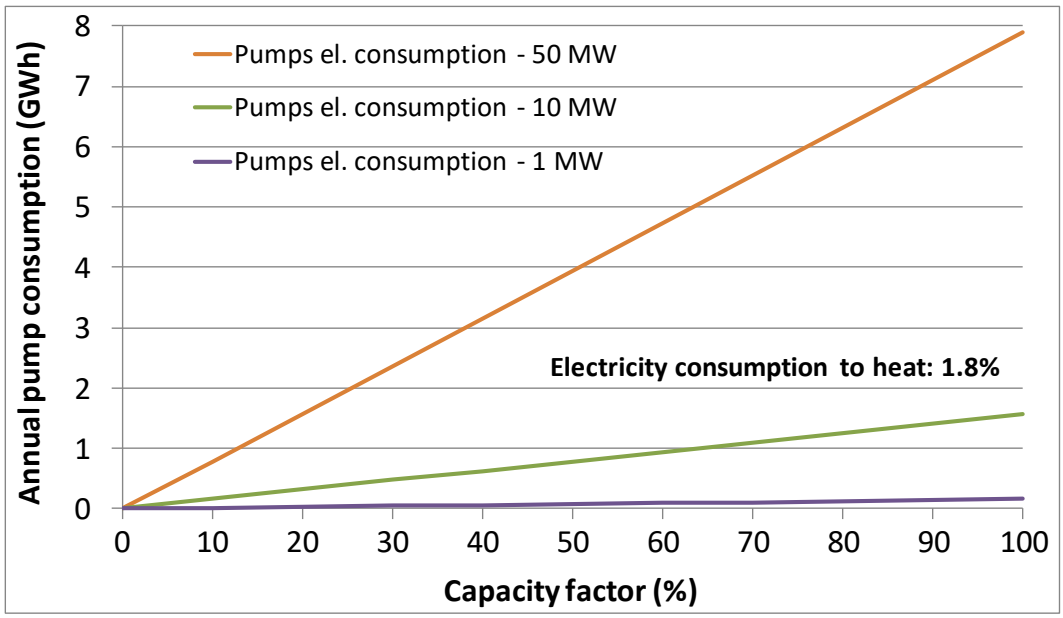

Figure 3.19: Annual pumps electricity consumption as a function of capacity factor for 1, 10 and 50 MW_{th} plant

The pumps are considered to operate at 90% of their load with the resulting ratio of pumps electricity consumption to available heat equal to 1.8% for all cases. This ratio has a major role in the net power production, introducing an important constraint for low efficiency systems. This issue can be critical, since significant amount of own-consumption reduces the net power production and the potential profitability of such coupling.

4. Solar thermal heat

In this section, the potential of solar heat is presented that can be produced by low-cost solar thermal collectors. This potential mostly concerns the following parameters:

- Solar availability in Europe
- Solar collector type and technology
- Temperature of heat production
- Daily and seasonal fluctuation of solar heat

The daily and seasonal fluctuation of solar availability and heat are also presented for selected areas, which represent the main geographical locations within Europe (south/central/north Europe). Finally, the annual production in selected locations is given, exhibiting the collectors' performance at various weather conditions and production temperatures.

4.1 Solar availability in Europe

Solar availability is usually illustrated using solar maps that depict the global solar irradiation on a surface. Most of the times the horizontal and inclined irradiation values are presented, which are the most important ones and clearly provide an overview of solar intensity.

These maps have been obtained after processing recorded data over a long period of time from numerous weather stations and then extrapolated to annual sum of global irradiation on horizontal and optimally inclined surface [124]. The data values are given in kWh/m^2. The available solar maps are from EC's Joint Research Centre (JRC) – Institute of Energy and Transport (IET) with average data over the period 1998-2011. The solar availability (annual sum of global irradiation on optimal inclined surface at each location, orientation: south) in Europe is observed in Fig. 4.1. The values in the map are shown in kWh/m^2. There are similar maps for global solar irradiation on horizontal surface or direct normal irradiation (DNI) [125]; the conclusions from those maps would have been the same.

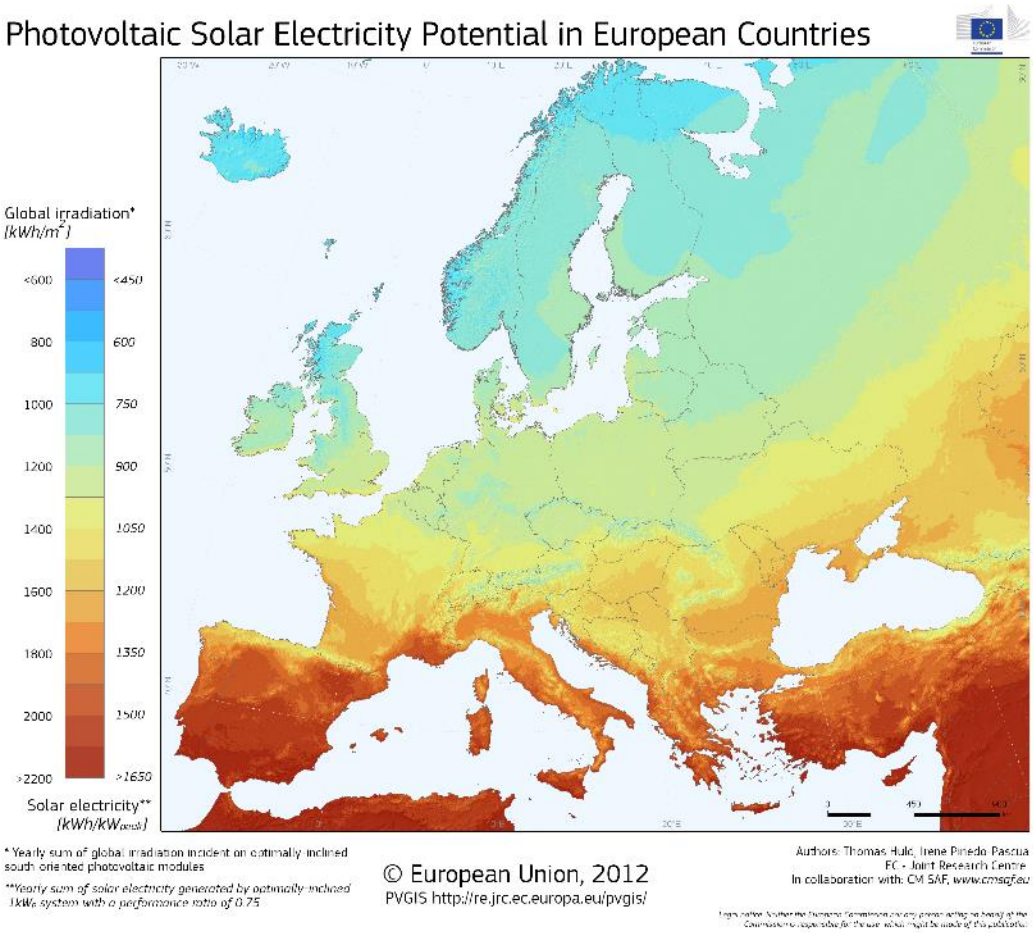

Figure 4.1: Solar irradiation map of Europe [126]

There are also similar maps available for each EU country that illustrate with higher detail the potential sites and areas [126].

It is clear that areas with global irradiation over about 1500 kWh/m^2 have the greater potential to supply with heat the RED Heat Engine. This geographical region extends from central France and to the south. Moreover, in these areas the ambient temperature is moderate/high, which contributes to adequate solar heat production even during the winter season with more heating hours per year. The most promising countries, as expected, are Spain, Portugal, Italy, Greece, Malta and Cyprus.

However, the solar heat production will be calculated for various EU countries, since the framework conditions and energy prices significantly vary over the countries and there is the possibility that the RED Heat Engine to be profitable even in a northern European country.

The solar potential in some representative areas is provided. It should be stressed that only the available solar irradiation is presented, while the collectors that harness solar energy and convert it to useful heat will be presented in the next section. In Table 4.1 is provided the solar potential with additional parameters that affect the solar heat production in 6 selected (representative) areas. The calculations have been accomplished with the interactive online tool of PVGIS [126].

Table 4.1: Solar potential in selected areas

Area / country	Annual solar potential on optimum inclined surface (kWh/m^2)	Mean ambient temperature (^{o}C)	Optimum angle (^{o})
Palermo, Italy	2048	19.0	32
Almeria, Spain	2237	18.7	34
Athens, Greece	2088	18.6	32
Munich, Germany	1332	11.1	36
Amsterdam, the Netherlands	1256	11.4	37
Stockholm, Sweden	1330	7.8	44

It becomes clear that the annual solar potential in south Europe is more than 50% higher than in areas of central/north Europe.

A similar trend is also observed for the monthly radiation, which is presented in Fig. 4.2 for the selected areas of Table 4.1. The average daily temperature during each month is given in Fig. 4.3.

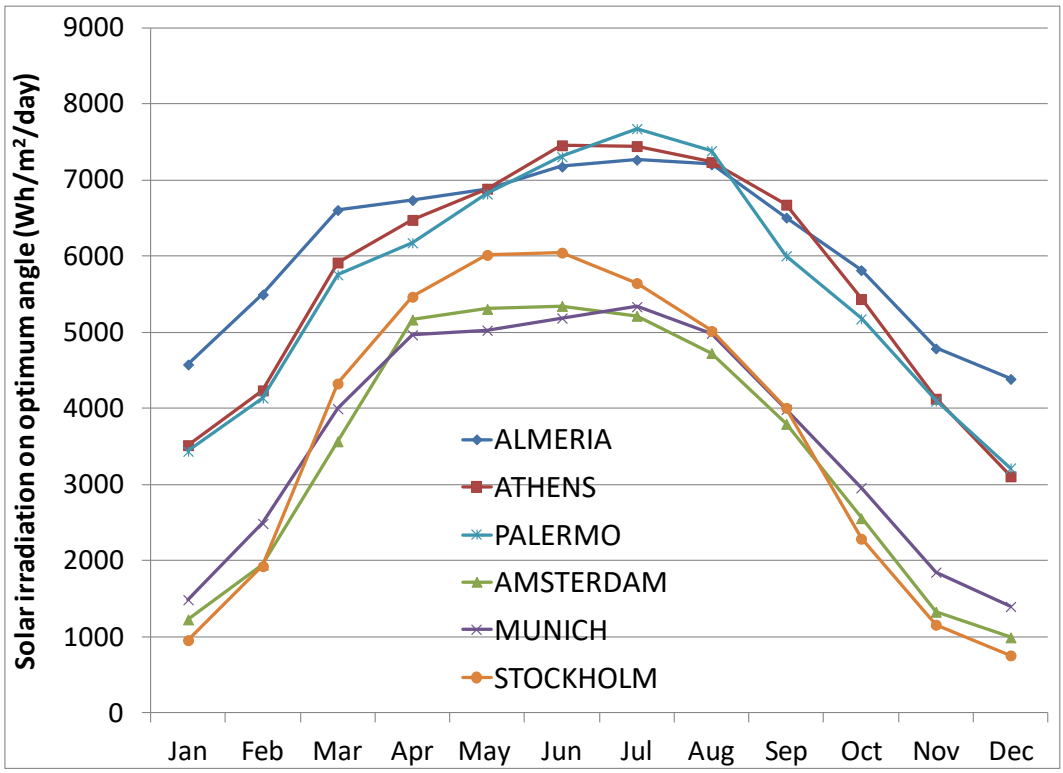

Figure 4.2: Monthly solar irradiation on surface with optimum angle in selected areas (in Wh/m²/day)

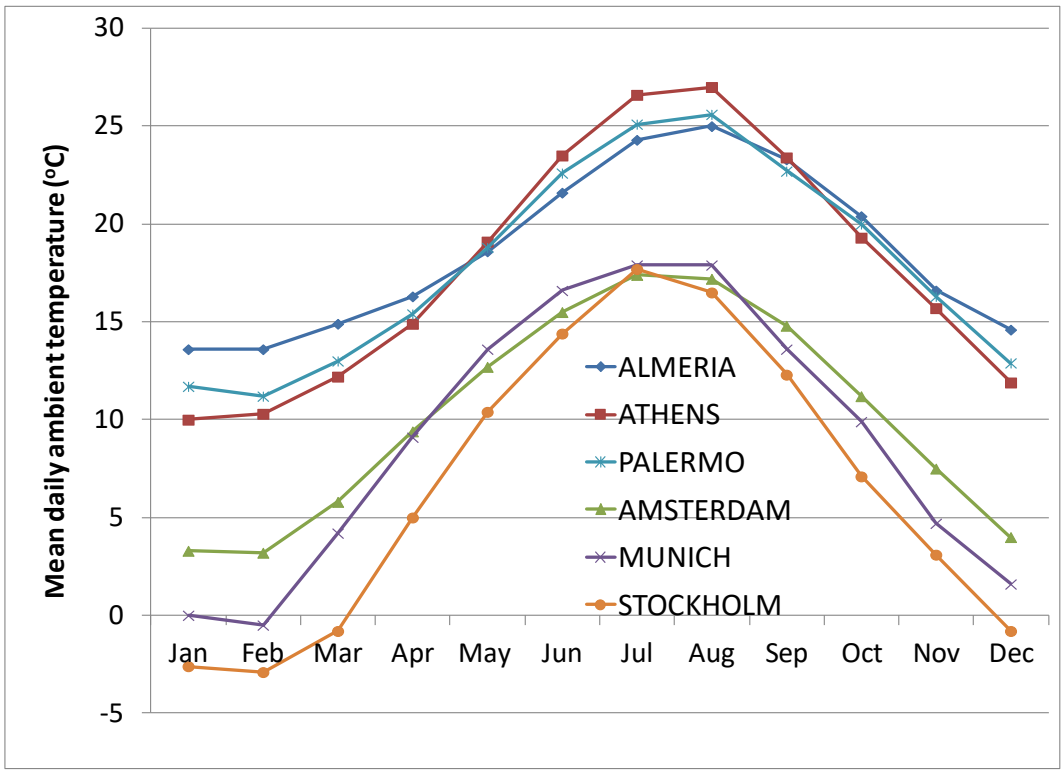

Figure 4.3: Average daily ambient temperature in selected areas

There is a very large variation of solar potential during each month, especially in central/north Europe, where the lowest potential is observed in December (about 1000 Wh/m²/day) and the highest in June (about 5500 Wh/m²/day), which is 5.5 times higher. On the other hand, in south Europe the potential profile is smoother with the lowest value being about 4000 Wh/m²/day and the highest 7500 Wh/m²/day (fraction of almost 2). This fact favours the solar heat production over the whole year, avoiding strong fluctuations that can have a major effect on the RED Heat Engine performance and efficiency.

The mean monthly ambient temperature shown in Fig. 4.3 is also higher in south Europe, as expected. This fact has a positive impact on solar collector efficiency, which will be presented in the next section.

Next, the daily solar irradiation during two days with extreme weather conditions (winter day in January and summer day in July) is presented for the selected areas. The processed data are shown in Fig. 4.4.

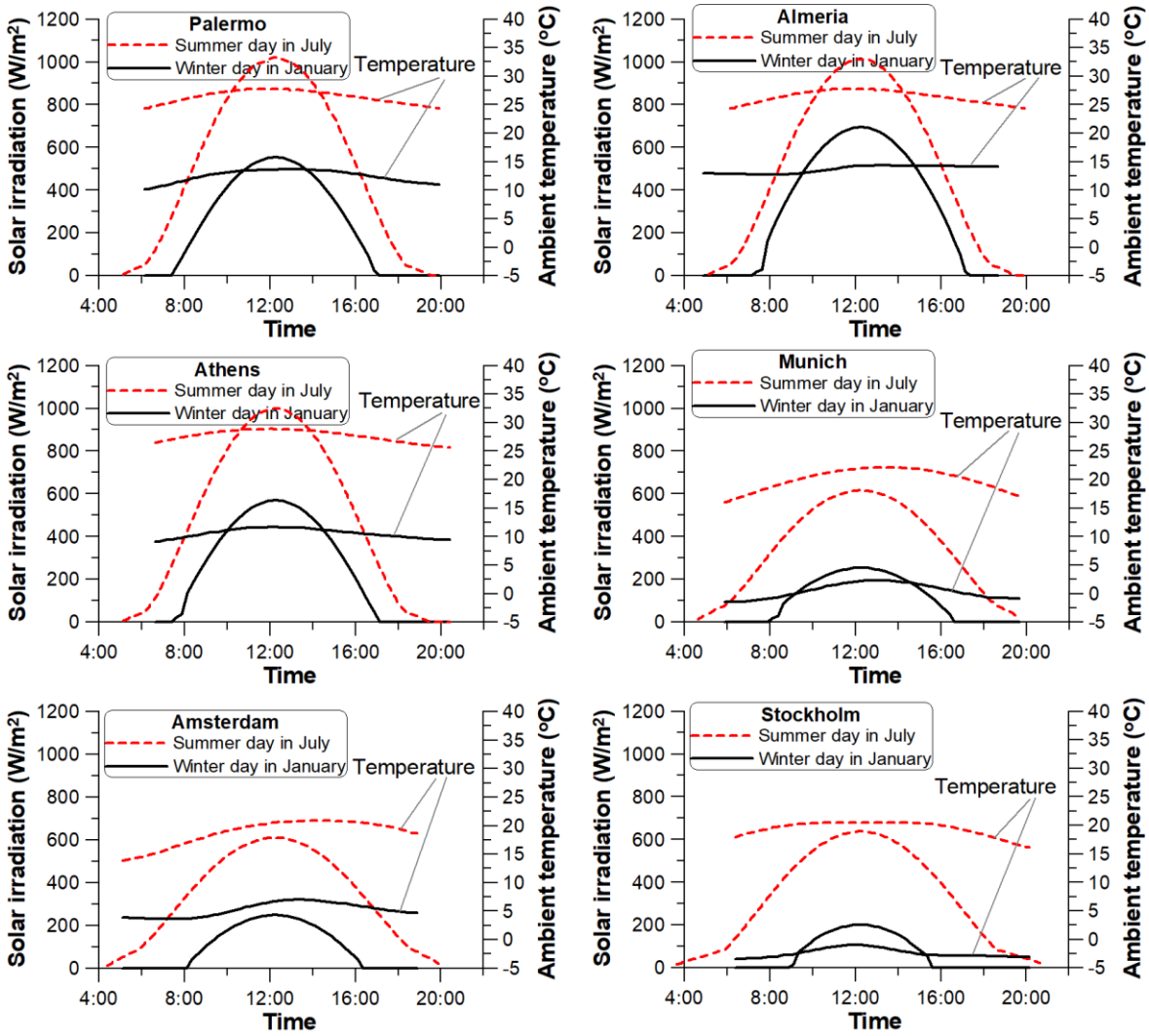

Figure 4.4: Daily solar irradiation and ambient temperature in selected areas during a winter and summer day

The solar and temperature profiles for Palermo, Athens and Almeria are very similar and the expected heat production in these three locations is very similar. The maximum solar irradiation reaches 1000 W/m^2 during summer and about 500 W/m^2 during winter (in Almeria it reaches close to 700 W/m^2 even in the winter). On the other hand, for central and northern European climates, the maximum solar potential comes close to 600 W/m^2, while the winter potential is extremely low.

With the previously presented data, the high solar potential in south Europe is quantified, which is also evident from the solar thermal market in EU, according to ESTIF [127,128].

Up to now, only the solar potential has been presented. The available solar collectors that can actually harness this solar energy and convert it to useful heat are presented in the next section.

4.2 Solar thermal collectors

Solar thermal collectors harness the incident solar irradiation and convert it to useful heat. This heat is then transferred to a fluid (usually water for the current application) that flows through

the collector. The circulating fluid is then heated and either carries directly this heat to the thermal consumption (the heat exchanger of the RED Heat Engine) or to a thermal energy storage tank.

Focus here is given on non-concentrating collectors (stationary) that have simpler structure, lower cost and are used for low-temperature heat applications, usually below 100 ^{o}C, compared to concentrating collectors, which usually produce heat of temperature higher than 150-200 ^{o}C.

There are two main collector types/technologies for such applications [129], which are also highlighted in Table 4.2:

- Flat-plate collectors
- Evacuated tube collectors

Both solutions are readily available with many local manufacturers and large industries commercializing these products.

Table 4.2: Solar thermal collectors for low temperature heat production

Solar thermal collectors	Temperature range (^{o}C)	Availability	Cost range (€/m^2)	Core applications
Flat-plate collectors	30-80	Many local manufacturers in most EU countries	100-150	Domestic hot water production, space heating
Evacuated tube collectors	50-200	Few manufacturers	250-400	Domestic hot water production, space heating, process heat, solar cooling

The cost figures presented in Table 4.2 are mean commercial prices for the purchase of a single unit (usually collectors come with a gross area of 2 m^2). In case of a large solar field of hundreds or even thousands of collectors, the cost per m^2 can substantially decrease even up to 50% (for both collector types). Additional costs can be applied, such as land rent, permit (mostly for large scale power plants), and equipment for thermal energy storage, but a case by case analysis of the costs is required for reaching reliable conclusions.

In general, flat-plate collectors are used for very low temperature applications, mostly in buildings for hot water production and space heating, being very common in south Europe. On the other hand, collectors with vacuum tubes can produce heat of higher temperature and their applications are extended to industrial and commercial environment as well. Moreover, they are suitable in locations with low ambient temperatures, since they decrease heat losses mainly due to the vacuum tubes (elimination of convection and conduction to the ambient air).

The main features, types, and specifications of both collectors are briefly presented in the next two sub-sections.

4.2.1 Flat-plate solar collectors

A typical configuration of flat-plate collectors is considered here, which is appropriate for supplying heat to the RED Heat Engine. Glazed collectors are examined only, which protect the absorbing surface from dust, humidity, etc. and reduces convection and radiation losses from the absorber plate. Water (or water/glycol mixture) is used as the heat transfer medium to decrease pinch point temperature difference and increase specific capacity (kW per m^2). The core components of a standard flat plate collector are shown in Fig. 4.5. In Fig. 4.6 is shown a typical flat-plate collector.

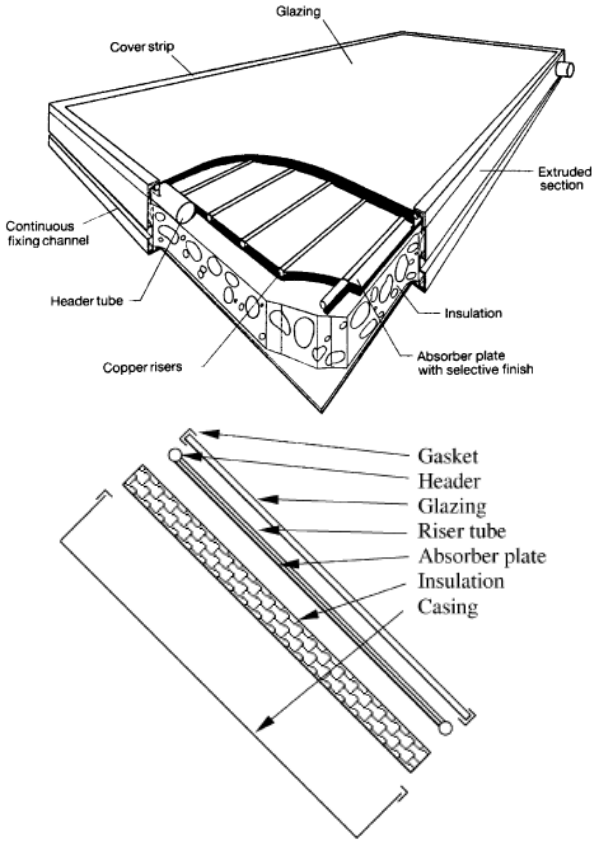

Figure 4.5: Flat-plate collector components [129]

Figure 4.6: Installed flat-plate collectors (source: http://calpak.gr/)

The most important specification of a collector is the expression describing its efficiency. This is given as a function of mean collector temperature (inlet and outlet), ambient temperature, incident solar irradiation, with input parameters the constants of each collector. Most of the times, second-order terms are included, requiring three parameters, which are available from certification organizations that issue a "Solar Keymark"[130]. Out of the exhaustive Solar Keymark database [131], high-quality collectors can be identified. From this database, the analysis here considers a high-quality flat-plate collector (commercially available, Calpak M4 200 [132]) [133]. The efficiency of this collector is given by Eq. (4.1).

$$n_0 = 0.755 - 3.89\frac{(T_c - T_{amb})}{G} - 0.013\frac{(T_c - T_{amb})^2}{G} \quad (4.1)$$

, where T_c is the mean collector temperature: $(T_{out} - T_{in})/2$, T_{amb} the ambient temperature and G the incident (global) irradiation on collector surface.

The heat gain of the collector (Q_c) is given by Eq. (4.2).

$$Q_c = n_0 G = \dot{m}_c c_p (T_{out} - T_{in}) \quad (4.2)$$

, where $\dot{m}_c$ is the mass flow rate of the heat transfer fluid, c_p its heat capacity, and T_{out}, T_{in} the outlet/inlet water temperature respectively.

The FPC performance is presented and compared with ETC at various weather and operating conditions in section 4.2.3.

4.2.2 Evacuated tube solar collectors

Standard flat-plate solar collectors are mostly appropriate for use in sunny and warm climates, such as in south Europe. Their benefits however are greatly reduced when conditions become unfavourable, such as in cold, cloudy and windy conditions. Furthermore, conditions such as condensation and moisture will cause early deterioration of internal materials resulting in reduced performance and system failure. Evacuated tube collectors operate differently than the other collectors available on the market.

They include an effective convention suppressor that minimizes heat losses to the environment, even at high temperature operation. The vacuum envelope reduces convection and conduction losses, so the collectors can operate at higher temperatures than FPC with a much higher efficiency. They collect both direct and diffuse radiation, similar to the flat-plate ones, while their efficiency is higher at low incidence angles. This effect tends to give ETC an advantage over FPC over the period of a day.

A typical ETC and its main components are shown in Figs. 4.7 and 4.8. An ETC usually includes 20 to 30 vacuum tubes, connected with a common manifold.

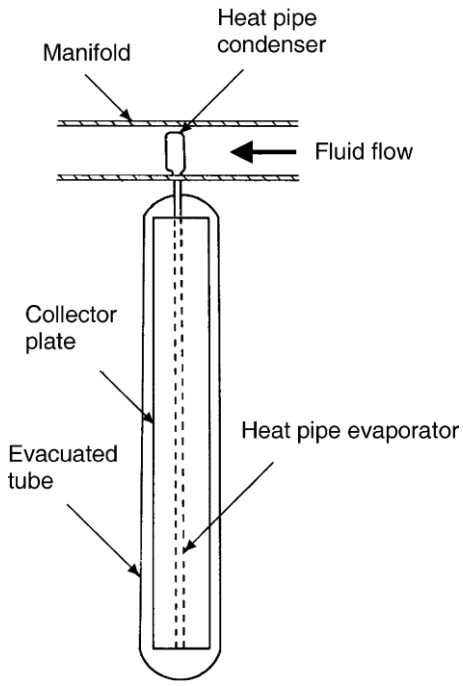

Figure 4.7: Vacuum tube components [129]

Figure 4.8: Installed evacuated tube collectors [134]

Similar as before, a high-quality evacuated tube collector is considered, manufactured by Kingspan Renewables [134] with its efficiency given by Eq. (4.3) [135].

$$n_0 = 0.768 - 1.36\frac{(T_c - T_{amb})}{G} - 0.0053\frac{(T_c - T_{amb})^2}{G} \quad (4.3)$$

4.2.3 Comparison of FPC and ETC performance

In this section, a performance comparison between the two main collector types is presented. This is based on the critical parameters that have to do with the weather and operating conditions of the collector.

In order to evaluate the solar heat potential at various conditions, the most important parameter is the collector efficiency, which expresses the fraction of solar energy that is converted to useful heat. Efficiency for various solar irradiation levels, ambient temperature and inlet/outlet water temperatures is presented in Figs. 4. 9-4.11.

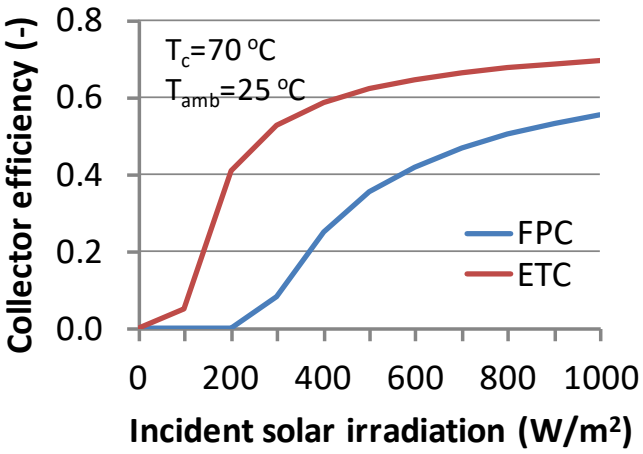

Figure 4.9: Effect of incident solar irradiation on collector efficiency for both collector types

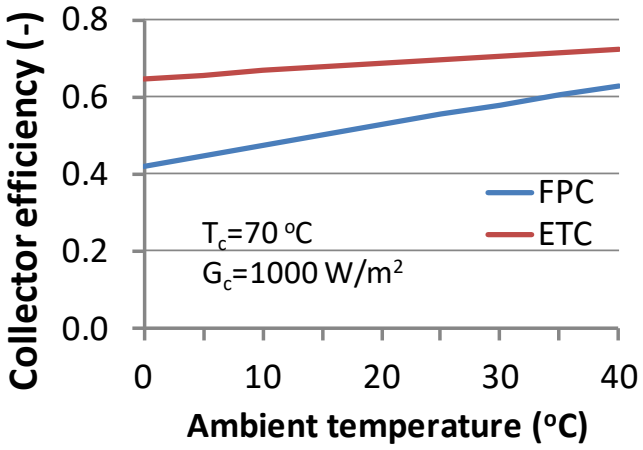

Figure 4.10: Effect of ambient temperature on collector efficiency for both collector types

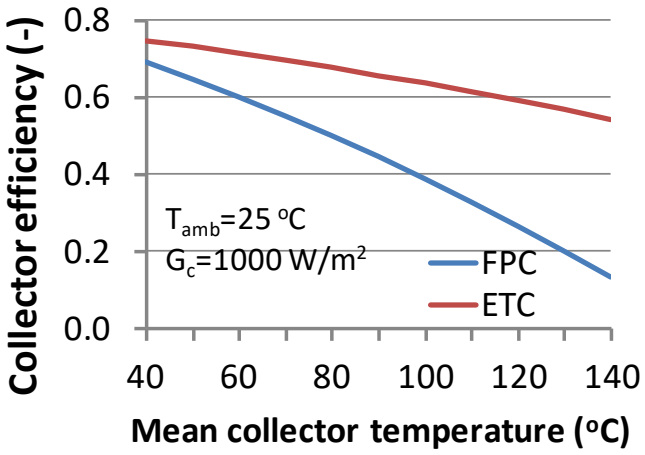

Figure 4.11: Effect of mean collector temperature on collector efficiency for both collector types

Solar irradiation has a major role on the collector efficiency as shown in Fig. 4.9. Flat plate collectors can produce some heat of adequate temperature for irradiation over 200 W/m^2, reaching about 55% efficiency, while evacuated tube collectors start production from just 100 W/m^2 with efficiency reaching even 70%.

Moreover, high ambient temperatures boost solar heat production, with the reduction of heat losses at such conditions. This is clearer for flat plate collectors, with their performance greatly enhanced for higher ambient temperatures, while evacuated tube collectors show less steep increase, since the use vacuum tubes allows to reach higher efficiencies already at lower temperatures.

Finally, mean collector temperature has a significant role on performance as well (see Fig. 4.11). At favourable weather conditions (high solar irradiation and ambient temperature) the efficiency of FPC decreases to below 35% for temperature higher than 100 °C. On the other hand, ETC holds a high efficiency over the whole range of collector temperatures, usually in the range of 60-70%.

In conclusion, FPC seem to be ideal for very low temperature production, below 60-70 °C, being suitable only for operating the RED Heat Engine at temperature up to 50-60 °C. On the other hand, ETC can supply heat of temperature up to 120 °C or even higher with sufficient efficiency.

4.2.4 CPV/T and PV/T for low temperature heat production

Except from the FPC and ETC that have been presented previously, there are also other types of thermal collectors that can produce heat up to about 100 °C. The most common ones are Concentrating PV/Thermal (CPV/T) and PV/Thermal (PV/T). These collectors are equipped with PV cells as well, producing electricity and heat from the same unit. However, their operation is usually restricted to temperature below 70 °C [136], in order not to decrease their electric efficiency [137]. Typical examples of those collectors are shown in Figs. 4.12 and 4.13 for a CPV/T and PV/T respectively.

Figure 4.12: CPV/T collector manufactured by Absolicon (source: www.absolicon.com)

Figure 4.13: PV/T collector manufactured by Solarus (source: www.solarus.com)

The main advantage of these two types is that they also produce electricity from the PV cells. However, their thermal properties are moderate, and they perform similar to a low-quality thermal collector. This is because the PV cells absorb a fraction of incident solar irradiation for electricity production leaving a smaller part of the solar energy available for actual heat production. Another disadvantage of CPV/T collectors is that they harness only the direct solar irradiation, restricting their use only in south Europe, where the DNI potential is high. Apart from that, their cost is high with current prices over 600 €/m^2 with a negligible market share.

A typical thermal efficiency of a PV/T collector [138] is observed in Fig. 4.14 for variable collector temperature and for two solar irradiation values (600 and 1000 W/m^2). In the same figure, the efficiency of FPC and ETC is also presented for comparison purposes.

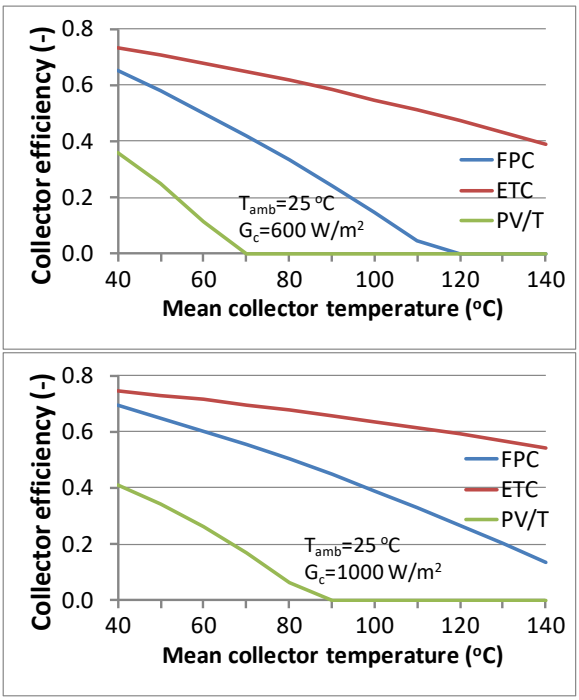

Figure 4.14: Efficiency of typical PV/T collector and comparison with FPC and ETC for variable collector temperature and two solar irradiation levels (left: 600 W/m^2, right: 1000 W/m^2)

It is clear that the PV/T collector efficiency is low and suitable only for very low temperature heat production, up to about 50 °C. The thermal performance of CPV/T is even lower than PV/T by about 20%, since they harness only direct solar irradiation, as mentioned earlier, although their tracking mechanism partly compensates for the lower solar irradiation harnessed.

Moreover, their market potential is limited only to specific applications, such as pool heating, domestic hot water production and space heating, making them inappropriate for the technology developed in this project. Combined with their very high costs, these solutions are not favoured and will not be further examined in this thesis.

4.3 Solar heat potential for the RED Heat Engine

The solar heat potential of both collector types (FPC, ETC) for the selected areas is presented here. The analysis is initially made for two typical days during summer and winter, as previously. Then, the annual yield is presented for the same locations, in order to gain an overview of the potential.

4.3.1 Daily production

The values of the solar availability and ambient temperature in the selected areas have been processed, in order to calculate the daily yield during a typical winter and summer day. This analysis is implemented for both FPC and ETC.

The daily results for both collectors are presented in Fig. 4.15, where the solar heat production (in W/m^2) is calculated using the solar availability, ambient temperature, and collector efficiency at each location. The mean collector temperature is considered equal to 70 ^{o}C.

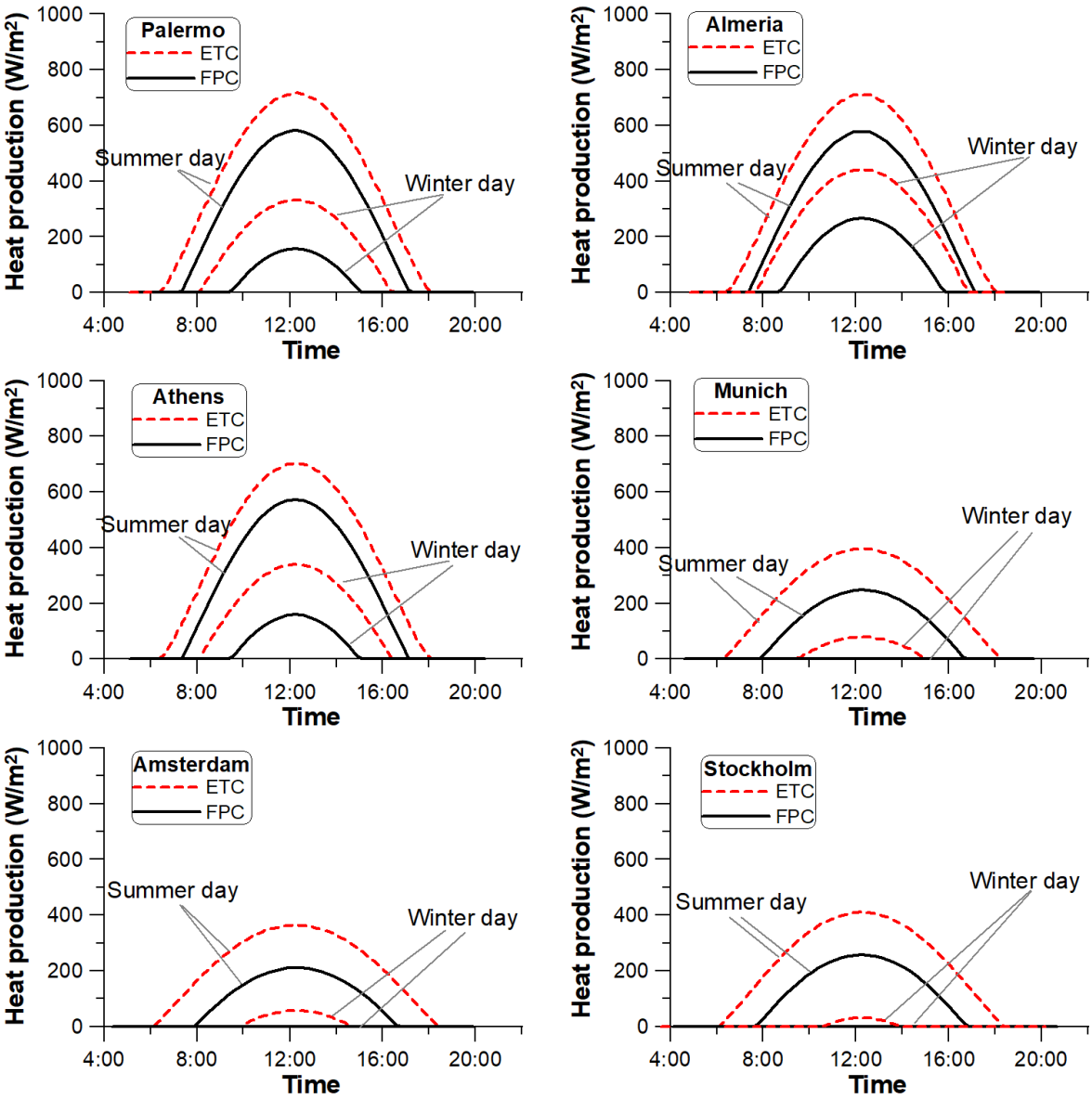

Figure 4.15: Solar heat production for FPC and ETC during a typical winter and summer day at the selected areas (mean collector temperature of 70 ^{o}C)

At all cases, the ETC produces more heat than the FPC, which was expected. Moreover, the maximum of solar heat during summer is about two times higher than the winter one.

In south Europe the maximum solar heat is about 750 W/m^2, whereas in central/north Europe is about 400 W/m^2. In central/northern Europe there is no heat production during the winter

day with a FPC at the 70 °C temperature level, while even with an ETC the production is very low.

Next, the solar heat production as a function of collector temperature is presented. This range represents the core interest of the project, with the lower one (70 °C) being able to operate the RED Heat Engine at 50-60 °C (with a reasonable pinch point temperature difference of 10-20 K) and the higher one (110 °C) for operation of the RED Heat Engine at 90-100 °C.

The results are summed and are given as daily thermal energy produced per collector surface. The results are shown in Figs. 4.16 and 4.17 for winter and summer day respectively (straight lines: FPC, dashed lines: ETC).

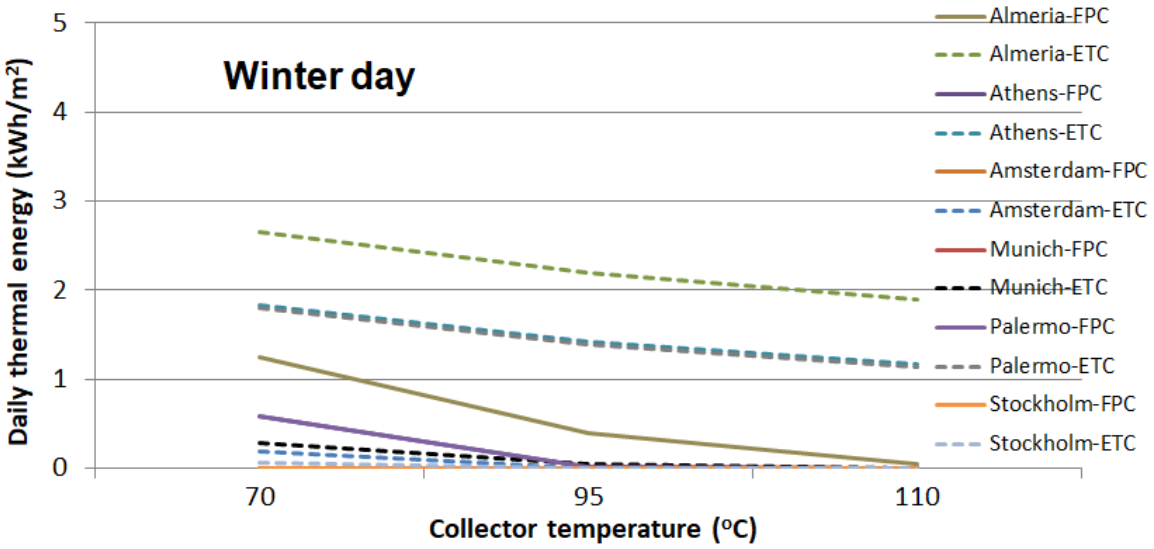

Figure 4.16: Daily thermal energy production for FPC and ETC during a typical winter day at the selected areas for a range of mean collector temperature

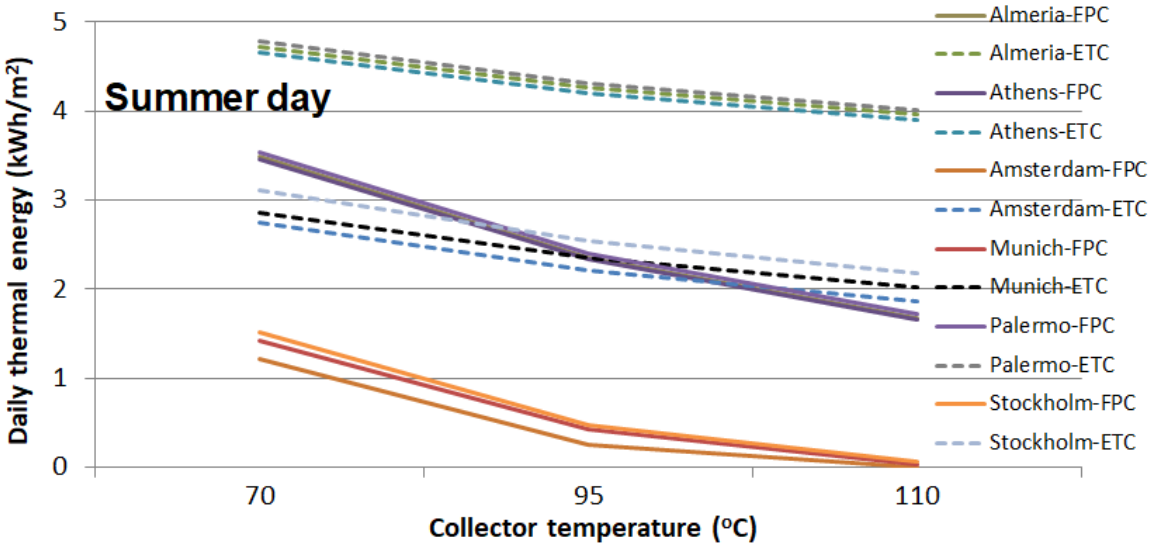

Figure 4.17: Daily thermal energy production for FPC and ETC during a typical summer day at the selected areas for a range of mean collector temperature

The superior performance of ETC can be easily observed, reaching a production of almost 5 kWh/m^2/day in summer for south Europe. In general, ETC in central/north Europe has similar performance as FPC in south Europe. Moreover, for high collector temperatures, heat production decreases, becoming negligible with FPC in central/north Europe.

4.3.2 Annual production

For the calculation of the annual yield of both collectors in the selected areas, TRNSYS software [139] has been applied. A simple model has been developed within this environment using built-in components (solar radiation processor, solar collector and data processing) to calculate the annual yield based on the collector efficiency curves presented previously. The local weather data are considered (built-in from TM2 database) as well as the optimum inclination angle. This analysis has been implemented for three different collector temperatures (70, 90, 110 °C), as previously. The annual data are shown in Fig. 4.18.

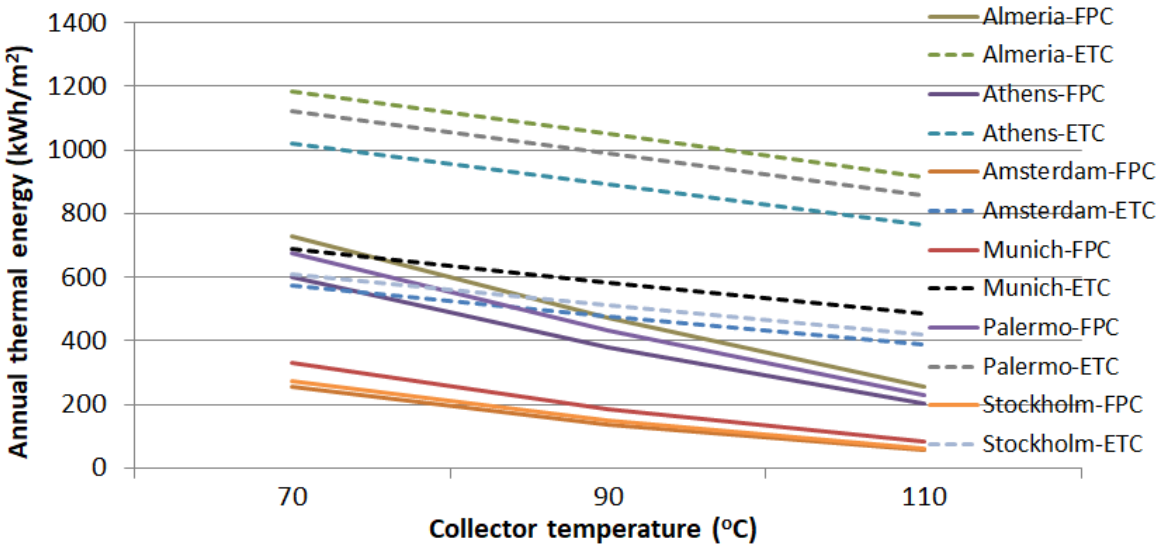

Figure 4.18: Annual thermal energy production for FPC and ETC at the selected areas for a range of mean collector temperature

Annual yield of about 1000 kWh/m^2 is common for south Europe with ETC, reducing to below 600 kWh/m^2 with FPC. On the other hand, in central/north Europe the solar production decreases to about 200 kWh/m^2 for FPC (around 2.5 times lower than in south Europe with the same collector). Moreover, FPC and ETC show different slope of the yield for variable collector temperature (FPC slope is steeper).

5. Conclusions

All possible heat sources that could feed the RED Heat Engine have been examined, identifying their potential, as well as their key features, such as temperature level, availability/intermittency, and costs for heat production in case of solar and geothermal energy. The analysis was based on available waste heat and its potential from various sectors, such as industry, biogas plants, gas compressor stations and marine auxiliary engines. These four sectors show a total waste heat potential of about 700 TWh/year.

Large focus was given on industrial waste heat, due to the variety of temperature of waste heat sources and different types of sectors. A detailed methodology using waste heat fractions has been developed and successfully applied per temperature level and industrial sector. The results showed that a very large potential exists in the temperature range of 100-200^{o}C, which is within the heat requirements of the RED Heat Engine.

The estimation of waste heat potential in biogas plants, marine sector and gas compressor stations was more straightforward, since the most recent available data have been used and then processed considering average efficiency values for calculating the potential.

All previous studies have been also conducted per EU country (except from the marine sector), in order to identify the amount of heat availability. As expected, in Germany exists the largest fraction for all three sectors, followed by Italy, France, UK and Spain. However, the potential is extremely large and concrete opportunities could exist in all EU countries.

The work then focused on renewable energy sources that could be used for heat production. Geothermal energy was examined and its potential has been presented with main parameters the drilling depth and temperature level in different EU countries. Different cases were considered, such as the development of new geothermal fields or existing ones. Their main difference is the investment cost, since very high initial costs are related to exploration and drilling.

Typical cases with various capacity sizes have been calculated, in order to provide a preliminary overview of the associated costs and heat production potential. The analysis showed that geothermal plants should be of large size, in order to compensate the initial investment costs and produce large amounts of electricity.

Finally, solar thermal collectors and their potential has been examined, which can provide low-temperature heat to the RED Heat Engine. Solar availability and heat production were assessed, considering the two most promising collector types (evacuated tube collector and standard flat-plate collector), while PV/thermal or even CPV/thermal collectors have still very large costs and poor thermal performance and were not further examined.

Daily and seasonal solar heat production was calculated for different regions in Europe, representing the main climatic zones (south/central/north Europe). This analysis concluded to the calculation of the annual solar heat production per square meter of collector, showing that about 1000 kWh/m^2 can be produced with ETC in south Europe, reducing to below 600 kWh/m^2 with FPC. This production is reduced by about 2.5 times in central/north Europe, showing that the RED Heat Engine could be combined with solar collectors only in regions with high solar availability, and especially in south Europe (e.g. Italy, Spain, Greece, Portugal).

Part II: Environmental Assessment

1 Introduction

In order to assess the environmental impacts of the RED Heat Engine, a dedicated analysis has been undertaken. The Heat Engine, once commercialised, similar to any other product, starts with the design phase. After that, resources are extracted, and they are transported to a site where they are processed into materials that are subsequently used in the manufacturing process. The product is then transported to the site where it operates, transforming heat to electricity, for a number of years. When the decision is taken to decommission the plant, the end-of-life phase starts, which includes collection/sorting, reuse, recycling and waste disposal of all materials and any necessary site remediation activities.

All these stages taken together are defined as the life cycle of the product. The basis of the life cycle thinking when assessing the merits of a product, is to account for its whole life cycle. Out of that approach has emerged the Life Cycle Assessment (LCA), the method which "*addresses the environmental aspects and potential environmental impacts (e.g. use of resource and the environmental consequence of releases) through a product's life cycle from raw material acquisition through production, use, end-of-life treatment, recycling and final disposal*" [37].

In this analysis the LCA approach is adopted. By including the impacts throughout the product life cycle, the risk is avoided of missing any environmental trade-offs that could occur between the different life cycle phases [140]. For example, a system might seem "greener" compared to a polluting alternative if it has no emissions during operation (like PV or the RED Heat Engine). However, no conclusions can be reached before taking into account also the impacts linked to the manufacturing of the materials required for the system construction and the associated emissions.

2 Literature review

LCA is a well-established methodology for assessing the impacts of products or processes, gaining significantly in popularity over the past 20 years with an increasing number of relevant papers, as shown in Fig. 2.1, which is based on data from [141].

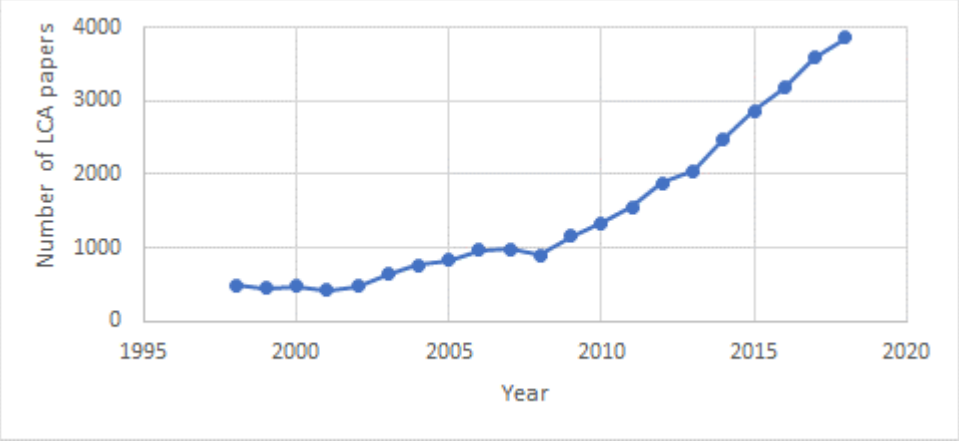

Figure 2.1: Number of LCA related papers per year

The trend is similar focusing at LCA applied to energy technologies, with several thousands of papers published over the past few years. In 2013, Turconi et al. [142] critically reviewed 167 LCAs of electricity generating technologies, based both on fossil fuels and renewable energy. This review resulted in a range of emission data for each case, which forms a very useful basis for comparison of any LCA applied in technologies in the electricity generation field.

When looking specifically at the conversion of low-temperature heat to electricity (e.g. industrial waste heat, solar thermal), most LCA studies are related to the Organic Rankine Cycle (ORC), focusing either at design aspects, such as in Ref. [143] where the impacts of using different working fluids are compared, or on the application context, such as in Ref. [144] where the impacts of using ORC to convert the waste heat from a biogas plant to electricity is explored.

Previous research including LCA of desalination technologies is also relevant, because two out of the three regeneration options considered for the RED Heat Engine are thermal technologies used for desalination and water treatment. Even though the environmental impacts are among the main concerns of desalination technologies and there are several relevant studies in the literature, most do not apply the LCA method. Early works were dedicated to the impact of brine discharge on aquatic environments in particular in relation to the chemicals in the brine [145]. Eventually, the wider impacts of brine discharge and the impacts associated to the energy use during operation were studied [146]. But even where the LCA approach was adopted, the focus was still mainly on the operation phase; Vince et al. [147] highlighted how an LCA tool developed in 2001 (based on SimaPro software [148]) for dedicated potable water production, used as default assumption that the impacts from the construction and the decommissioning phases are negligible and all the impact comes from the operational phase. One study in 2006 by Raluy et al. [149] performed an LCA of the three main desalination technologies (RO, MSF and MED), where the whole life-cycle was indeed considered. This confirmed that the impact of the operational phase accounted for at least 90% of the total plant impact. This study also indicated that the use of waste heat or renewable heat in thermal desalination technologies could make a big difference compared to the option of dedicated fossil fuel combustion.

The use of LCA as a tool for providing direct input to the design process at the early stages of developing a new energy technology has been proposed before. Gerber et al. [150] integrated LCA in the design models of a new process, which involved the co-generation of synthetic natural gas and electricity. In that study they concluded that "*considering the environmental impact at an early stage of design allows the engineers to efficiently propose pertinent impact mitigation measures and modifications in the process design*". This conclusion is fully in line with the approach adopted in this thesis.

There are no studies on the environmental impacts of the RED Heat Engine. Some general aspects of potential environmental concerns of RED and other Salinity Gradient processes have been outlined before in [151], but the focus was mostly on open loop applications and the impacts from the use of natural streams to power the process (e.g. river water with seawater). The only previous study that is closely related to the work in this part of the thesis is the paper on an osmotic heat engine [152], where Pressure Retarded Osmosis is used for power generation, operating in a closed loop and using membrane distillation powered by waste heat for the regeneration process. In that paper the impacts from converting waste heat to electricity are assessed, comparing the options of using an osmotic heat engine or an ORC for converting waste heat to electricity.

3 Methodology

This part of the thesis adheres to the International Standard EN ISO 14044:2006 [37] and as such the study includes the four standard phases, which are illustrated in Fig 3.1.

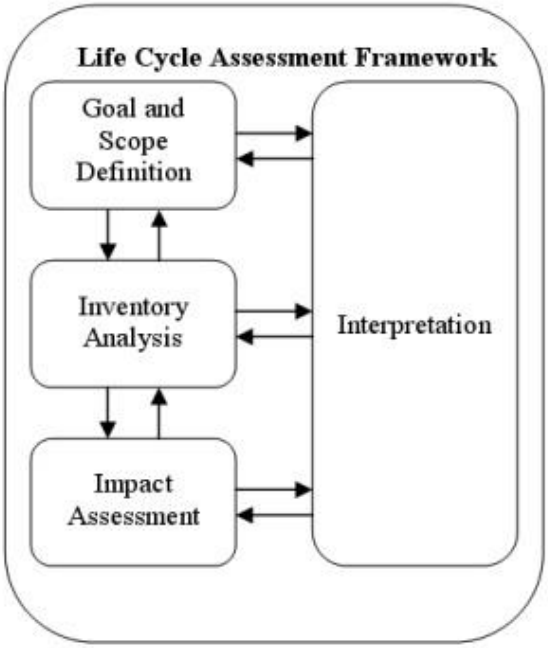

Figure 3.1: The four phases of the LCA framework [153]

A separate section has been dedicated to each of these four phases: (i) Definition of goal and scope, (ii) Life Cycle Inventory Analysis, (iii) Life Cycle Impact Assessment and (iv) Life Cycle Interpretation.

The methodology proposed by Gerber et al. [150] was adopted. The main improvement of that approach compared to standard LCAs is that the flows of the LCA model are expressed as functions of the techno-economic model, allowing to study easily how the impacts are affected when changing the system design or operating conditions.

This approach has been implemented within a model that was built in GaBi, a Life Cycle commercial software provided by the company thinkstep [154]. More details about the methodology are provided in the next section (*Definition of Goal and Scope*).

4 Definition of Goal and Scope

4.1 Goal

Intended application

The RED Heat-to-Power project [30] develops a new technology, to convert low temperature heat to electricity. The RED Heat-to-Power consortium is considering different design configurations and operating conditions for the RED Heat Engine. The goal of this study is to inform them about the relative environmental impacts of each design option and compare them to other electricity generation options.

Reasons for carrying out the study

The RED Heat Engine offers a lot of flexibility, in terms of the components, materials and design options, each having their advantages and disadvantages. Eventually, the market conditions will define which configurations will prevail. However, at the current early stage of development, the RED Heat-to-Power [30] consortium is taking decisions related to the technological options that will be further developed and about the concepts that seem to have lower potential. This study is carried out in order to contribute information about the expected environmental impacts of the different design options, supporting the decision process.

Intended audience, i.e. to whom the results of the study are intended to be communicated

The intended audience for this study is the RED Heat-to-Power consortium members and the scientific community with an interest in the field.

Whether the results are intended to be used in comparative assertions to be disclosed to the public

Part of the result of this study will be used for comparative assertions to be disclosed to the public.

4.2 Scope

The product system to be studied

The technology to be studied is the RED Heat Engine, which converts low grade heat to electricity. More specifically, the application of the RED Heat Engine will be studied assuming its application at an industrial setting where waste heat is available, and electricity is needed.

The functions of the product

The electricity generated by the RED Heat Engine will be used to cover part of the industrial plant's electricity needs.

The functional unit

As a functional unit is defined the net electric energy generated by the RED Heat Engine (1 MJ).

The system boundary

This is a "cradle to grave" study. Within the boundaries are included all components of the RED Heat Engine, with all equipment necessary to collect the heat rejected by the industrial plant and all equipment needed to treat the electricity and deliver it back to the industrial unit. The industrial unit itself that provides the heat and uses the electricity is outside the boundaries of this study, as the purpose is to compare different design configurations of the RED Heat Engine and to compare the best configuration in terms of environmental impact with alternative electricity supply/production options that the industrial unit has.

Allocation procedures

There are no allocation decisions to be made.

LCIA methodology and types of impacts

In Fig. 4.1 is illustrated the distinction between the midpoint and the endpoint impact assessment models. In this study, midpoint assessment models are used, since using endpoint impact assessment would require more value choices.

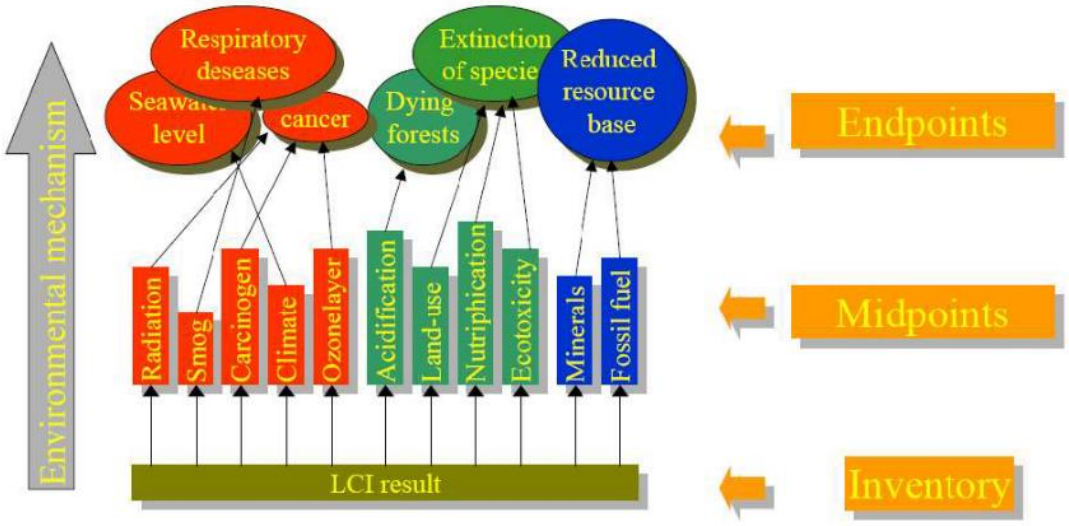

Figure 4.1: The distinction between midpoint and endpoint impact assessment models [155]

According to Turconi et al. [142], the most important impact categories for electricity generation technologies are global warming, eutrophication and acidification. For this reason, these three impact categories are considered throughout the study. In addition to that, the Ozone Depletion Potential (ODP) is also considered in most of the cases analysed. The four impact categories are used as defined in Exhibit 4-1 (page 49) of the SAIC document [140], and are shown in Table 4.1.

Table 4.1: The four impact categories examined

Impact Category	Characterization factor
Global warming	Global Warming Potential (Converts LCI data to carbon dioxide (CO_2) equivalents – 100 years potential)
Eutrophication	Eutrophication Potential (Converts LCI data to phosphate (PO4) equivalents.)
Acidification	Acidification Potential (Converts LCI data to hydrogen (H+) ion equivalents.)
Stratospheric Ozone Depletion	Ozone depleting potential (converts LCI data to trichlorofluoromethane (CFC-11) equivalents.)

In addition, when comparing our results to the grid electricity, all the impact categories listed below are used, in order to identify if there are any important factors that might have been omitted at the initial analysis:

- CML2001 - Jan. 2016, Freshwater Aquatic Ecotoxicity Pot. (FAETP inf.)
- CML2001 - Jan. 2016, Human Toxicity Potential (HTP inf.)
- CML2001 - Jan. 2016, Marine Aquatic Ecotoxicity Pot. (MAETP inf.)
- CML2001 - Jan. 2016, Photochem. Ozone Creation Potential (POCP)
- CML2001 - Jan. 2016, Terrestric Ecotoxicity Potential (TETP inf.)
- EN15804 - Total use of non-renewable primary energy resources (PENRT)
- EN15804 - Use of net fresh water (FW)
- Land use LANCA v2.3 2016 - Biotic Production Loss Potential (Occupation)
- EF 1.8 - Ionising radiation - human health
- Particles to air
  - Aluminium oxide (dust)
  - Dust (> PM10)
  - Dust (PM10)
  - Dust (PM2.5 - PM10)
  - Dust (PM2.5)
  - Metals (unspecified)
  - Silicon dioxide (silica)

Interpretation to be used

The results will be discussed, studying different scenarios and sensitivities, explaining the limitations, reaching conclusions and formulating recommendations

As mentioned, three different options for the regeneration technology are considered:

a) Multi Effect Distillation (MED): This has been chosen by the RED Heat-to-Power project as the most promising option. Therefore, a few alternative configurations are studied with regards to the MED number of effects, the performance characteristics of the Ion Exchange Membranes, the type of salt used and the temperature level at which the solution enters the RED unit. (Scenarios 1 to 5)

b) Membrane Distillation (MD): One option is considered, with the design as provided by the RED Heat-to-Power consortium. (Scenario 6)

c) Distillation column for thermolytic salts: One option is considered, with the design as provided by the RED Heat-to-Power consortium. (Scenario 7)

The specific conditions for each of the 7 scenarios are provided in sections 7.1 to 7.3.

A sensitivity analysis was also carried out in order to examine how the results vary, when some key input parameters change. The sensitivity analysis is carried out only for the scenario that gives the best results in terms of environmental performance. The parameters that were chosen for the sensitivity analysis are:

- the distance that all materials have to be transported between manufacturing and use
- the technical life-time of the system
- the capacity factor
- the frequency at which we need to change the Ion exchange membranes.

The details about the sensitivity analysis are provided in section 7.6.

Data requirements

The process simulator of the RED Heat-to-Power project was used for calculating the main technical data of the RED Heat Engine performance for each scenario. This process simulator is based on a model [36] that has been validated with experimental data.

The industrial partners of the RED Heat-to-Power consortium (FUJIFILM and REDstack) provided information about the exact materials used to construct the components of the RED Heat Engine and the relevant quantities. Finally, the GaBi database was used for the data on the resources used and the emissions associated with the extraction and processing the raw materials required as input for the components of the RED Heat Engine.

Assumptions

It is assumed that the RED Heat Engine will operate as foreseen by the validated technical model. There is no specific location or end-user defined. It is assumed that the industrial user has available large amounts of waste heat at 100 ^{o}C and uses all electricity that is generated by the Heat Engine.

Value choices and optional elements – Limitations

The following limitations/value choices were made in this study:

- The manufacturing of all main materials required was considered, but the energy required for the assembly of the regeneration system was ignored because of lack of data.
- The following materials were ignored, following cut-off rule, because their mass is less than 0.3% of the total system mass: The water (0.4 kg) and salt (0.07 kg) used to create the working fluid and the titanium (3.2 kg) used for the electrodes
- The mass of the platinum used in the electrodes (0.04 kg) is very low compared to the total system mass. The cut-off rule cannot be applied as platinum is critical and scarce resource. However, no data was available therefore it was ignored. This is a limitation that has to be addressed in future research.
- The Poly(diallyldimethylammonium chloride) used for the cation exchange membrane (CEM) was ignored as no data was available for its manufacturing. But in most scenarios examined, the total mass was below the 1% of the total system mass, so the impact of ignoring it is negligible.

5 Life Cycle Inventory Analysis

5.1 Data collection procedures

The RED Heat-to-Power consortium provided the data as follows:

The research team of the University of Palermo has provided access to the process simulator of the system [36], which has been validated through extensive experimental campaigns. This model has been used for sizing the system components and quantifying the performance for each scenario examined.

The company REDstack provided the bill of materials required for constructing one reverse electrodialysis stack. In this study, linear scaling was assumed, which is reasonable since the reverse electrodialysis stacks is a modular technology, i.e for larger systems we use more stacks rather than larger stacks.

The company FUJIFILM provided the bill of materials used for the anion exchange membranes and the cation exchange membranes and the electricity required for their production.

In addition to that, literature references have been used to fill-in some gaps in the bill of materials for the overall system, especially for the regeneration systems: for MD data from Ref. [156] was used and from Hickenbottom et al. [152], for the MED from Raluy et al. [149] and for the thermolytic salts from Bevacqua et al. [157] and Giacalone et al. [33].

5.2 Description of unit processes, sources of data and calculation procedures

In this section are described the unit processes one-by-one, explaining the assumptions, sources and calculations that were used during the Life Cycle Inventory Analysis. The Process Flow Diagram is provided on Fig. 5.1.

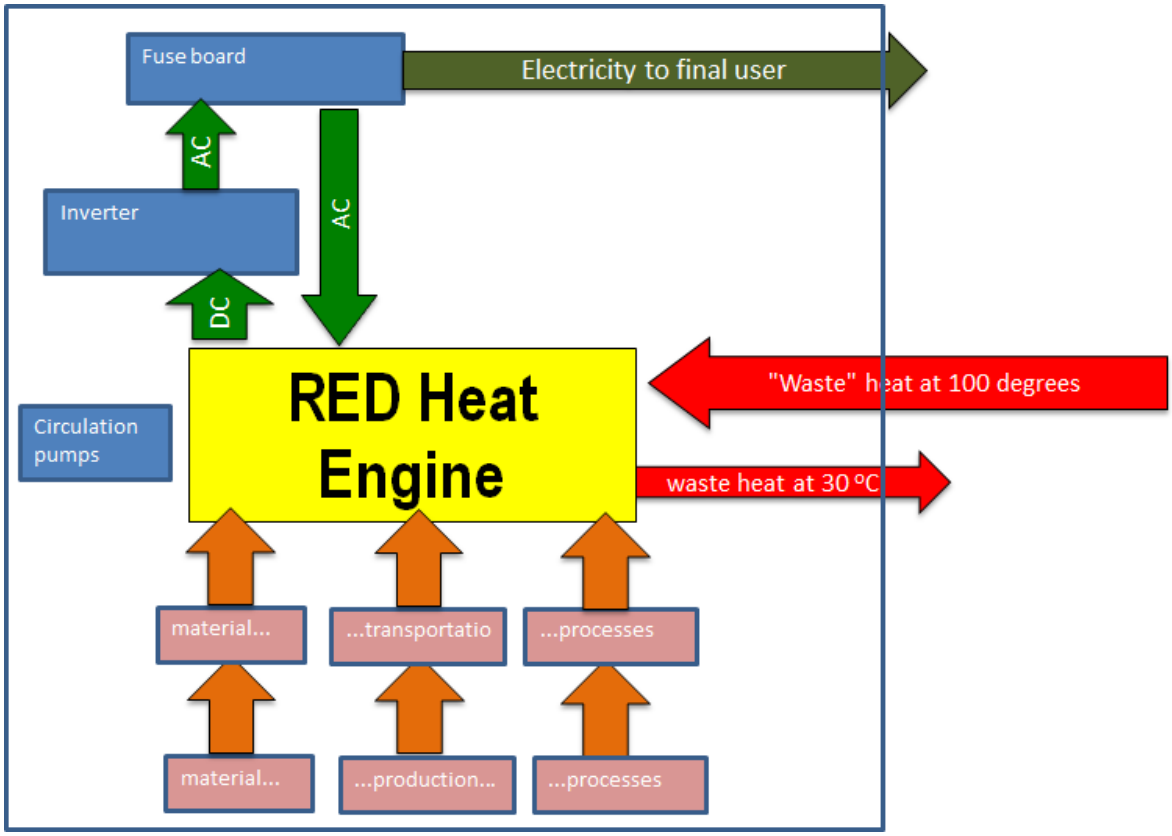

Figure 5.1: The main concept of the RED Heat Engine

I. RED Heat Engine process

For the purpose of this LCA, the whole RED Heat Engine has been considered as one single unit process, where heat comes in and electricity plus waste heat comes out. The reverse electrodialysis and the regeneration system that constitute the heat engine operate together in a closed loop, therefore there is no need to consider them as separate processes. Only the pumps used to circulate the working fluid around the heat engine are considered as a separate process as shown in Fig. 5.1, which will be explained in the next paragraph.

In the model of scenarios 1 to 5 where the regeneration system is a MED, a RED stack is used where each membrane has a surface of 0.25 m^2, and the stack consists of 1000 cell pairs. The size of the RED is kept constant between all these 5 scenarios and within the sensitivity analysis. The amount of heat and the size of the regeneration system change between scenarios to adapt to the performance of the system, for making full use of the specific stack that was considered. For that reason, the amount of material associated with the RED system is constant and is provided in the table 5.1. This is the bill of materials for one stack. The total material used over the lifetime of the system can vary, depending on the assumption on how often the membranes are changed as will be explained below.

The only exceptions with regards to the size of the stack are for scenarios 6 and 7. In scenario 6, the size of the MD system is pre-defined as the module AS-24 provided by Aquastill is considered. The stack is sized to match the MD module capacity, which leads to a stack with 162 cell pairs with membrane length of 0.1 m and width of 0.88 m. In scenario 7, the multi-column approach is used. In order to have 4 distillation columns, maximising the efficiency the size of each membrane in the stack is doubled to 0.5 m^2, keeping the number of cell pairs to 1000. For

these two scenarios with the different stack sizes, the amount of materials from table 5.1 is scaled proportionally.

Table 5.1: Material associated with the RED stack

Symbol	Amount	Unit	Explanation
RED st steel	7.20	kg	Amount of stainless steel used for the RED system
RED steel	200.00	kg	Amount of steel used for housing the RED system
PDAC	8.75	kg	Poly(diallyldimethylammonium chloride) used for CEM
PE	7.50	kg	Polyethylene used as support for the CEM and the AEM
PLS	8.75	kg	Polystyrene sulphonated used for the AEM
Mem el	45.00	MJ	Electricity to produce the membranes for 1 stack
PVC	142.01	kg	Amount of PVC used in the RED stack
Silic	2.00	kg	Amount of silicone used in the RED stack
PVC pipes	0.81	kg	Pipes used for the whole heat engine

Table 5.2 gives the parameters that have been used in all 7 scenarios and have been varied in the sensitivity analysis.

Table 5.2: Parameters that vary in the sensitivity analysis

Symbol	Amount	Unit	Explanation
Cf	0.9	-	Capacity factor
mem frq	10	years	Frequency of IEM replacement
N	20	years	System lifetime

Table 5.3 gives the parameters that are calculated by the validated technical model and vary between the different design options. The amounts provided in this table are for scenario 1. The various scenarios are described in sections 7.1 to 7.3, where the associated figures are also provided.

Table 5.3: Parameters that vary between scenarios

Symbol	Amount	Unit	Explanation
Cu	1,791.27	kg	Amount of copper used in the MED heat exchangers
Ni	199.03	kg	Amount of nickel used in the MED heat exchangers
MED el in	143.20	W	Pumping power required for the MED operation
MED H in	23,630.00	W	Heat input at 100 degrees C
MED H out	23,181.20	W	Heat rejected from the system at 30 degrees C
MED steel	298.54	kg	Amount of steel for the housing of the MED system
RED el in	53.05	W	Pumping power required for the RED operation
RED el out	448.80	W	DC electricity generated from the RED system

Finally, based on all input data in the previous tables, the GaBi model that was developed calculates the total material used over the lifetime of the system, the total electricity produced, the resources used within the system and the materials that go to waste. Table 5.4 gives the equations used for these calculations. The flows listed in table 5.1 are not variable and therefore

no equation needs to be developed and inserted in the model. The quantity is inserted to the model directly as a fixed parameter and can change between scenarios but is fixed in the sensitivity analysis.

Table 5.4: Equations used for the GaBi model calculations

Symbol	Equation	Unit	Explanation
TL AC el in	(MED el in + RED el in) *30.7584* cf* y + Mem_el *(y/mem_frq)	MJ	RED-MED electricity requirements over lifetime of the system
TL MED H in	MED H in *30.7584* cf* y	MJ	MED Heat input over lifetime of the system
TL MED H out	MED H out *30.7584 * cf* y	MJ	Heat rejected from the MED over lifetime of the system
TL PDAC	PDAC * (y/mem frq)	kg	Poly(diallyldimethylammonium chloride) over lifetime of the system
TL PE	PE * (y/mem frq)	kg	Polyethylene over lifetime of the system
TL PLS	PLS * (y/mem frq)	kg	Polystyrene sulphonated over lifetime of the system
TL RED el out	RED el out *30.7584 * cf* y	MJ	RED electricity generation over lifetime of the system
TL_steel	MED steel + RED steel	kg	Total amount of steel used in the system

II. Other auxiliary processes

The RED Heat Engine is the main process. For the model to work properly and for switching easily between scenarios and sensitivity analysis options, a number of auxiliary processes are introduced.

First of all, the GaBi software offers the option to use pumps as a pre-defined process. For that reason, the pump has been introduced as a separate process, allowing to account fully for the material used for the pump construction (the energy used by the pumps during operation has been included as internal consumption in the RED Heat Engine process). The GaBi process “EU-28: Circulating pump 50-250W (EN15804 A1-A3)” has been used. This pump is for radiators. As the RED Heat Engine uses corrosive solutions, within that pump process the stainless steel was replaced with duplex stainless steel to consider the corrosion effect of salt water.

An inverter has also been included as a separate process for converting the DC electricity that is generated by the RED system to AC electricity. There is no pre-defined inverter process in GaBi, therefore a new one was created, assuming the efficiency to be 98%. Regarding the materials of the inverter data from table 45 on page 111 in the Palanov study [158] was used, for a 2.5 kW inverter, which the model scales to match the system size.

An “empty” process was also introduced, which was termed “fuse board” for splitting the AC electricity that is provided by the inverter to the part that is used to power the internal requirements of the RED Heat Engine, while the rest is the net electricity generated that is

provided to the end-user. This final process of the end-user is used to scale the whole model to the functional unit of 1 MJ of net AC electricity generated.

Construction and decommissioning

In addition to these processes that are directly associated with the operational phase of the system, there are separate processes included, associated with the production of the materials required for the construction of the system, the transportation of these materials to the site they are used and then similarly, separate processes for the transportation of the materials after the heat engine's end-of-life and for the disposal of the materials. For all these, standard processes have been selected from the GaBi software.

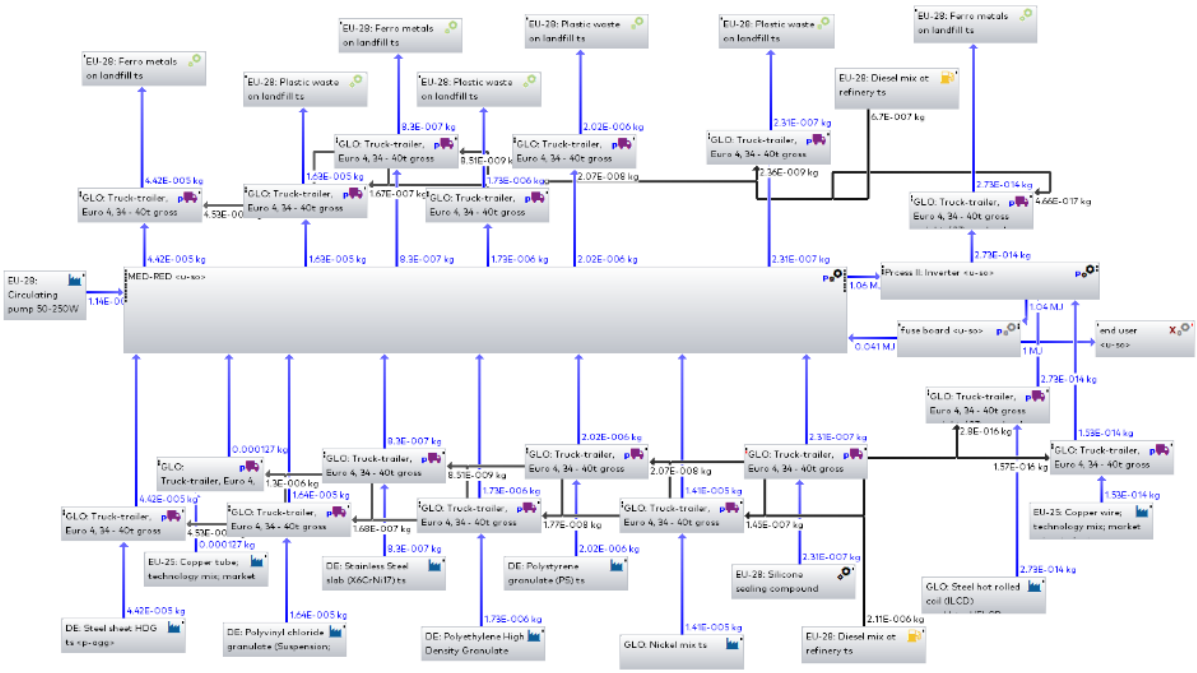

Figure 5.2: Screenshot of the GaBi model

Figure 5.2 shows a screenshot of the model. For most production processes it was assumed that they take place in Germany, with the exception of:

- the nickel production process where the global average was available
- the copper production processes where the EU average was available
- the silicon production process where the EU average was available

For all transportation processes (from production to use and from use to end-of-life) it was assumed that they take place by truck (Truck-trailer, Euro 4, 27 t payload capacity), which is fuelled by diesel (the option "EU-28 diesel at refinery" was used). As there are no specific production, assembly and use locations, a distance of 600 km was assumed, which was used for all transportation processes. The transportation process distance has been used as a variable in the sensitivity analysis, to check if it affects significantly the results.

Regarding the end-of-life phase, landfill disposal was assumed for all materials. The average EU landfill option was chosen for each of the materials. For all these processes, the default GaBi

data and assumptions were applied. For copper and nickel, no disposal option was included as it was not available in the model. In any case, the main option for these materials is recycling. If credits for recycling were included though there is a very positive impact on the results. However, a conservative approach was preferred, therefore no end- of life option was chosen for these two materials.

5.3 Allocation procedures

The RED heat engine uses as input large amounts of heat. That heat comes from an industrial process. This heat is regarded as waste at the industrial process because it is at low temperature (100 °C) and cannot be used for any other purpose. As a result, all emissions from the industrial process are allocated to the industrial products and none is allocated to the heat. There are no other allocation decisions necessary for this LCA, as all other flows are fully allocated to the RED Heat Engine.

6 Life Cycle Impact Assessment

6.1 Classification

Each emission/consumption is allocated here to the one of the impact categories, as indicated in Table 6.1. Here the four main impact categories are listed that will be used throughout the current analysis.

Table 6.1: Classification table allocating emissions to impact categories

Impact Category	Classification
Global warming	Carbon Dioxide (CO_2), Nitrogen Dioxide (NO_2), Methane (CH_4)
Eutrophication	Phosphate (PO4), Nitrogen Oxide (NO), Nitrogen Dioxide (NO_2), Nitrates, Ammonia (NH_4)
Acidification	Sulfur Oxides (SOx), Nitrogen Oxides (NOx), Hydrochloric Acid (HCL), Hydroflouric Acid (HF), Ammonia (NH_4)
Ozone depletion	Chlorofluorocarbons (CFCs), Hydrochlorofluorocarbons (HCFCs), Halons, Methyl Bromide (CH_3Br)

6.2 Characterization

The characterisation was run for all scenarios for the main four impact categories. For one of the scenarios also the impacts for a range of other categories were characterised and compared them to other electricity supply options. The classification and characterization in all cases was done by the Gabi Software by selecting the following options:

Global warming: The CML2001 - Jan. 2016, Global Warming Potential (GWP 100 years) option was used (Unit kg CO2 eq.)

Eutrophication: The CML2001 - Jan. 2016, Eutrophication Potential (EP) option was used (Unit: kg Phosphate eq.)

Acidification: The CML2001 - Jan. 2016, Acidification Potential (AP) option was used (Unit: kg SO2 eq.)

Ozone depletion: The CML2001 - Jan. 2016, Ozone Layer Depletion Potential (ODP, steady state) option was used (Unit: kg R11 eq.)

Freshwater Ecotoxicity: The CML2001 - Jan. 2016, Freshwater Aquatic Ecotoxicity Pot. (FAETP inf.) option was used (Unit: kg DCB eq.)

Human toxicity: The CML2001 - Jan. 2016, Human Toxicity Potential option was used (Unit: kg DCB eq.)

Marine ecotoxocity: The CML2001 - Jan. 2016, Marine Aquatic Ecotoxicity Pot. (MAETP inf.) option was used (Unit: kg DCB eq.)

Terrestic ecotoxicity: The CML2001 - Jan. 2016, Terrestric Ecotoxicity Potential (TETP inf.) option was used (Unit: kg DCB eq.)

Photochemical ozone creation: The CML2001 - Jan. 2016, Photochem. Ozone Creation Potential (POCP) option was used (Unit: kg Ethene eq.)

Resource depletion: The EN15804 - Total use of non-renewable primary energy resources (PENRT) option was used (Unit: MJ)

Water use: The EN15804 - Use of net fresh water (FW) option was used (Unit: m^3)

Land use: The LANCA v2.3 2016 - Biotic Production Loss Potential (Occupation) option was used (Unit: kg)

Ionising Radiation: The EF 1.8 - Ionising radiation - human health option was used (Unit: kBq U235 eq.)

Emission of particles: The Particles to air section of the inorganic emissions group under the technical results option was used (unit kg)

7 Life Cycle Interpretation – Results

7.1 Scenario 1

The LCA results are included in a paper that is under submission:

M. Papapetrou et al "Techno-economic and Environmental analysis of the RED Heat Engine"

The input data presented in section 5.2 was used in the model. This data represent scenario 1, as described below:

- The regeneration technology is Multi Effect Distillation (MED) and has 26 effects. The large number of effects was the result of the technical optimisation which was seeking to maximise the efficiency of the heat engine.
- The waste heat is available at 100 ^{o} C
- The salt used for the working fluid is NaCl
- The Ion Exchange Membranes have the performance of currently available low cost-membranes that are not optimised to operate in the RED Heat Engine conditions
- The working fluid is at room temperature (assumed to be 25 ^{o}C).

The results of the four impact categories are provided in Table 7.1 for the net production of 1 MJ of electricity.

Table 7.1: Results for Scenario 1 for 1 MJ of net electricity production

Category	Total
GWP potential (kg CO_2 eq.)	0.046667
Eutrophication Potential (kg Phosphate eq.)	1.63×10^{-5}
Acidification Potential (kg SO_2 eq.)	9.86×10^{-4}
Ozone Depletion Potential (kg R11 eq.)	1.33×10^{-9}

In Fig. 7.1 are illustrated the relative contributions of each material to each impact category. The operation phase has negligible impact as the heat engine operates in a closed loop. Practically all impact is associated with the manufacturing phase, this is why it has been broken down to the relative contributions of the main materials and processes used. The full results are provided in Annex I.

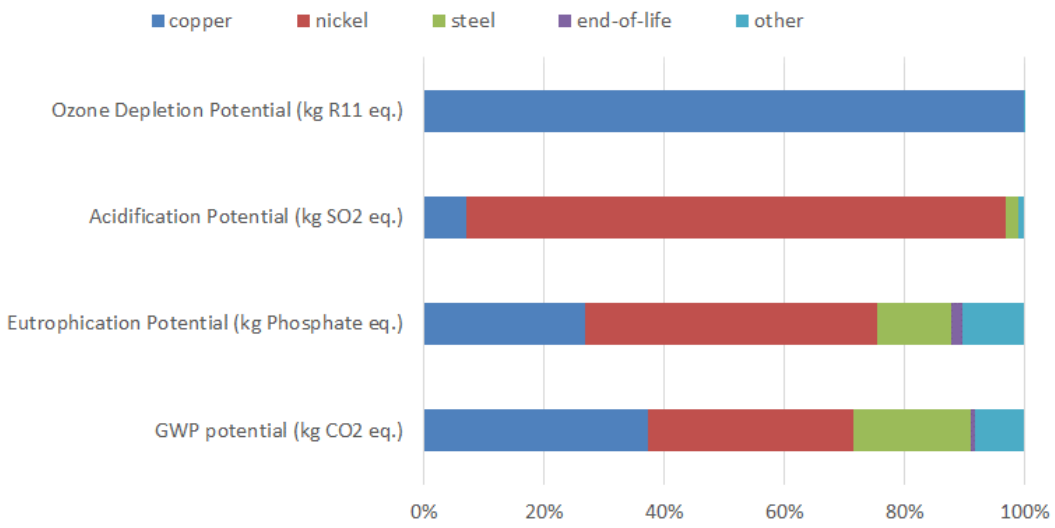

Figure 7.1: Relative contribution to the calculated impacts

It can be seen that the major part of the impacts is attributed to the production processes of the metals used in the heat engine (primarily for the heat exchangers). It is only in the global warming and the eutrophication categories where the plastic production, but also the transportation processes do have a more noticeable role, but even there the metal production processes account for more than 91% and 87% of the total impact, respectively.

For the case of global warming the impact is relatively balanced between copper, nickel and steel. In acidification the main impact is attributed to nickel while in ozone depletion the main impact is because of the copper production. Finally, for eutrophication almost half the impact comes from the nickel production process and the rest is shared between copper, steel and the transportation processes.

These results put a clear focus to the MED unit and more specifically to its copper-nickel 90-10 heat exchangers.

7.2 Scenarios 2 to 5

As explained, in Scenario 1 the model that was used to size the system and to calculate its' performance assumed that the ion exchange membranes used are the ones commercially available today. Based on that assumption, the system was designed by the model for maximising its efficiency. In order to examine different scenarios, which might reduce the environmental impacts, the following will be considered:

- The use of improved ion exchange membranes in the RED stack, referred to as "future membranes".
- The reduction of the number of effects in the regeneration process from 26 to 6. This reduces the efficiency of the heat engine, requiring more heat for generating the same amount of electricity. But it also reduces the heat exchanger material required for the same amount of electricity. This is positive, as we have seen in scenario 1 that the

materials of the MED heat exchangers is directly associated with the bulk of the environmental impacts.

- The use of KAc rather than NaCl in the working fluid and the operation of the RED stack at higher temperature (re-heating option). Both have shown to improve the RED performance. Both have shown to improve the RED performance (see [24] for the KAc and [7] for the higher temperatures)

An overview of the five RED-MED scenarios considered is given in Table 7.2, all supplied with waste heat at a temperature of 100 °C.

Table 7.2: Description of the main scenarios analysed

	Number of MED effects	IEM performance	Salt used	RED solution T
Scenario 1	26	Current	NaCl	25 ° C
Scenario 2	6	Current	NaCl	25 ° C
Scenario 3	6	Future	NaCl	25 ° C
Scenario 4	6	Future	KAc	25 ° C
Scenario 5	6	Future	KAc	50 ° C

For each of these scenarios the performance of the system was calculated obtaining the input figures required by the developed model for the different scenarios. Using the symbols introduced in table 5.1, the input data for each scenario are provided in table 7.3.

Table 7.3: Input data for the different scenarios

Symbol	Scenario 1	Scenario 2	Scenario 3	Scenario 4	Scenario 5
Cu (kg)	1,791.27	336.72	480.49	280.73	1,100.48
Ni (kg)	199.03	37.41	53.39	31.19	122.28
MED el in (W)	143.20	98.76	99.92	43.00	514.60
MED H in (W)	23,630.00	110,200.00	111,607.00	92,772.00	269,711.00
MED steel (kg)	298.54	56.12	80.08	46.79	183.41
RED el in (W)	53.05	53.04	54.26	40.17	127.10
RED el out (W)	448.80	448.80	1,611.00	2,998.00	16,638.00

By running the model for all these different scenarios, the results for the four main impact categories are shown in table 7.4 per one MJ of electricity produced (net). The full results, including the breakdown of the relative contributions from the various materials and processes are provided in Annex I.

Table 7.4: Main impact results for the different scenarios for 1 MJ of net electricity production

	GWP potential (kg CO2 eq.)	Eutrophication Potential (kg Phosphate eq.)	Acidification Potential (kg SO2 eq.)	Ozone Layer Depletion Potential (kg R11 eq.)
scenario 1	0.046667	1.63×10^{-5}	0.000986	1.33×10^{-9}
scenario 2	0.012331	4.02×10^{-6}	0.000168	2.12×10^{-10}
scenario 3	0.003034	1.01×10^{-6}	4.72×10^{-5}	6.12×10^{-11}
scenario 4	0.001138	3.67×10^{-7}	1.44×10^{-5}	1.78×10^{-11}
scenario 5	0.000488	1.68×10^{-7}	9.51×10^{-6}	1.27×10^{-11}

We see that all scenarios give much lower impacts than scenario 1. Actually, every improvement introduced in each scenario, brings extra environmental benefits. By reducing the number of MED effects from 26 to 6 when moving from scenario 1 to scenario 2, the GWP and eutrophication potential are reduced by a factor of 4, while the acidification potential and the ODP by a factor of about 6. The replacement of the commercial ion exchange membranes with the optimised membranes for the RED Heat Engine application (as we move from scenario 2 to scenario 3), the GWP and eutrophication potential are reduced again by a factor of about 4, while the acidification potential and the ODP by a factor of about 3.5. When moving from scenario 3 to scenario 4, i.e replacing NaCl with KAc, the GWP and eutrophication potential are reduced by a factor of about 2.7, while the acidification potential and the ODP by a factor of about 3.3. Finally, by increasing the temperature of the RED solution from 25 to 50 ^{o}C (from scenario 4 to scenario 5) the GWP and eutrophication potential are reduced by a factor of about 2.3, while the acidification potential and the ODP by a factor of about 1.4. The improvement when going from scenario 1 to scenario 5 is about 100 times for all four impact categories.

7.3 Scenarios 6 and 7

As explained before, the scenarios 6 and 7 use different regeneration technologies. In both scenarios the RED system operates at 25 ^{o}C, the IEM have the improved characteristics that were assumed also for scenarios 3 to 5 (“future membranes”) and the waste heat is available at 100 ^{o}C. In scenario 6, the regeneration system is membrane distillation (MD - module AS-24) and the salt used is NaCl. In scenario 7, the regeneration system consists of four distillation columns and the salt used is NH_4HCO_3.

The same model was used for these scenarios, after some necessary adaptations. More specifically, three new processes were created for the production of materials use for the MD spacers (polypropylene (PP)) and the condensation area (PET and aluminium production for the aluminium foil coated on both sides with Polyethylene terephthalate (PET-AL-PET)). All other materials used in the MD or the distillation columns was already included in the model, appropriately adjusting the amounts. For example, the MD membrane is made of polyethylene (PE), which is already in the model as the material used for support of the IEM. Also the packing material of the distillation columns which is stainless steel, is already used as a construction material of the RED stack.

The main input figures that were calculated are provided in Table 7.5. For both scenarios, the data from the experimental systems built [33] and from the technical model were used. For the

case of MD (scenario 6), the details about the materials and their dimensions are also provided in [156].

Table 7.5: Results of scenarios 6 and 7

Symbol	Scenario 6	Scenario 7
Cu (kg)	15.48	0
Ni (kg)	1.72	0
Reg. el in (W)	10.52	314.97
Reg. H in (W)	3600	45,330
steel (kg)	8.6	2,143
RED el in (W)	0.44	7.01
RED el out (W)	103.48	620.14
PVC	33.46	283.21
PP	31.1	0
PET	0.52	0
AL	3.63	0

The main materials in MD have to do with the heat exchangers (copper-nickel 90-10), the MD membrane (PE), the spacers (PP) and some PVC and steel for housing the system and the heat exchangers. In the case of distillation columns, the columns, the packing material, the heat exchangers and reboilers are all made of stainless steel.

The impact category results are presented in Table 7.6. The full results are provided in Annex I. The impacts are three to five times lower when using the MD system for regeneration compared to the distillation columns with thermolytic salts. The only exception is the ozone depletion potential, where in scenario 6 the impacts are two orders of magnitude higher than in scenario 7.

Table 7.6: Impact results of scenarios 6 and 7 for 1 MJ of net electricity production

Category	Scenario 6	Scenario 7
GWP potential (kg CO_2 eq.)	0.016168	0.055395
Eutrophication Potential (kg Phosphate eq.)	4.44×10^{-6}	2.215×10^{-5}
Acidification Potential (kg SO_2 eq.)	6.10×10^{-5}	3.43×10^{-4}
Ozone Depletion Potential (kg R11 eq.)	3.12×10^{-11}	3.56×10^{-13}

In order to interpret better the results, the relative contributions of the different components of the system and the different life cycle stages were analysed. As was the case in Scenario 1, the operational phase has no contribution in scenarios 6 and 7, therefore the focus was mostly on the material manufacturing phase. The results are presented in Fig. 7.2 and 7.2 for scenario 6 and scenario 7 respectively.

It can be seen that the reversal of the general trend in the case of ozone depletion potential is because the main contributor is copper, which is not used in scenario 7 (because copper does

not work well with NH_4HCO_3). Apart from that, it is clear that the steel (stainless steel for the most part) is responsible for the bulk of the impacts.

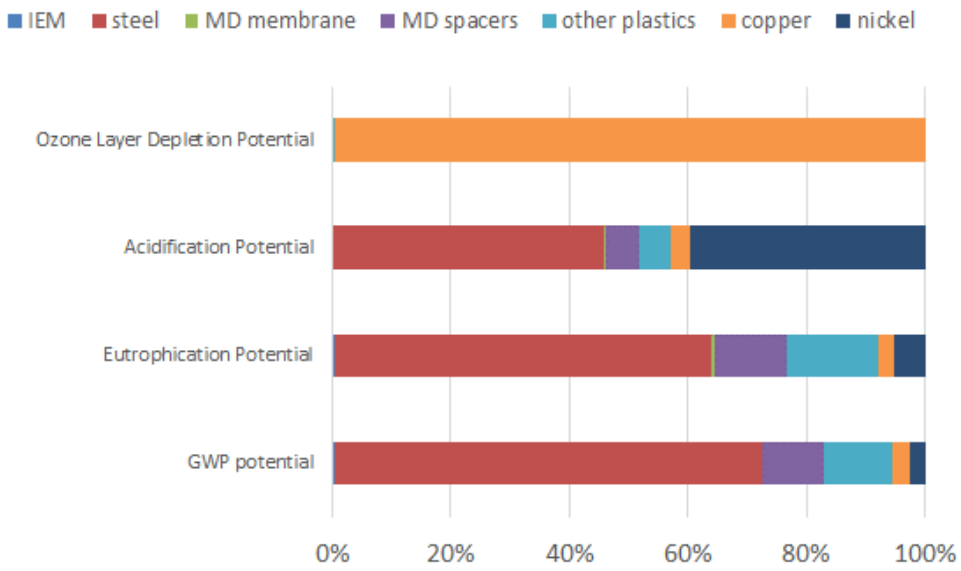

Figure 7.2: Relative contribution to the calculated impacts of scenario 6

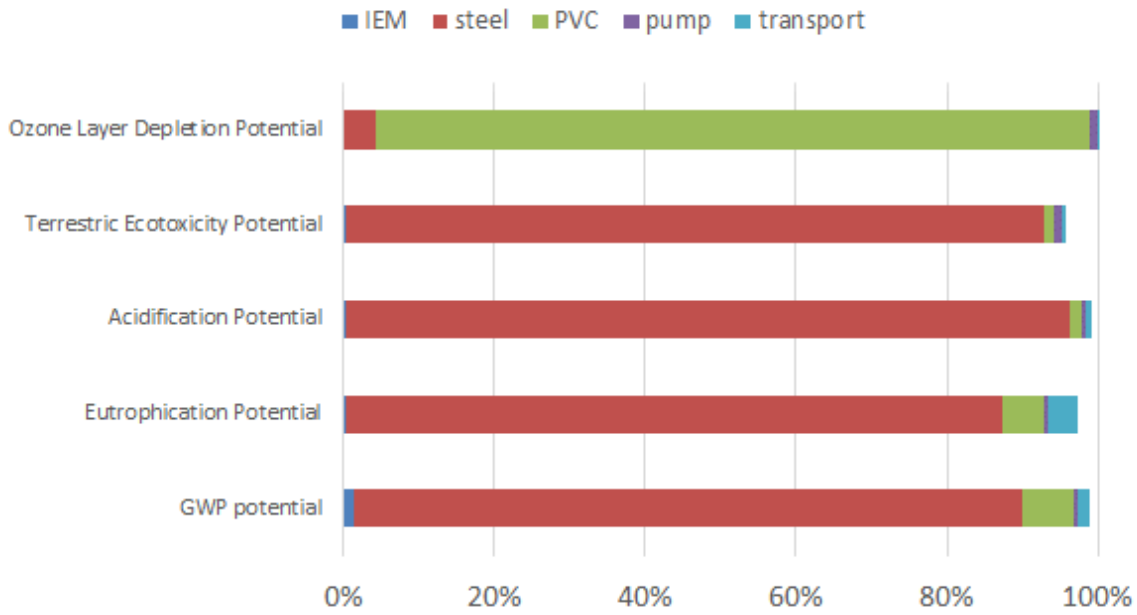

Figure 7.3: Relative contribution to the calculated impacts of scenario 7

7.4 Comparison between all scenarios

In order to get a better picture of the relative results between the various scenarios, scenario 2 was used as a basis and the relative changes between that and the other scenarios were calculated for each one of the 4 impact categories. The results are presented in table 7.7.

Table 7.7: Results of all scenarios, relative to scenario 2

	GWP potential (kg CO2 eq.)	Eutrophication Potential (kg Phosphate eq.)	Acidification Potential (kg SO2 eq.)	Ozone Layer Depletion Potential (kg R11 eq.)
scenario 1	278%	306%	487%	529%
scenario 2	0%	0%	0%	0%
scenario 3	-75%	-75%	-72%	-71%
scenario 4	**-91%**	**-91%**	**-91%**	**-92%**
scenario 5	-96%	-96%	-94%	-94%
scenario 6	**31%**	**10%**	**-64%**	**-85%**
scenario 7	**349%**	**451%**	**104%**	**-100%**

In order to compare the impacts of the three different regeneration systems on an equal basis, it makes sense to select scenario 6 for the RED-MD, scenario 7 for the RED-thermolytic and scenario 4 for the RED-MED (highlighted bold in the previous table), as all these 3 scenarios have the same type of IEM (future membranes) and operate the RED system at room temperature. It is clear that the RED-MED system configuration has the lowest impacts in all categories examined, while the use of thermolytic salts shows the highest impacts (the ozone layer depletion is an exemption as mentioned above). Based on those results it is clear that from an environmental point of view the best regeneration technology is MED and it is preferable to use a MED with a low number of effects. The use of KAc is preferable over NaCl in the working fluid, and it is preferable to heat up the fluid up to 50 ^{o}C before it enters the RED system. Finally, it is clear that from an environmental point of view it is better using IEMs optimised for the RED Heat Engine ("future membranes"), rather than commercial IEMS.

7.5 Data quality assessment

The table 7.8 provides an assessment of the data, giving a grade from 1 (best) to 5 (worse). Also a colour code has been added, ranging from dark green (1) to red (5).

Table 7.8: Data Assessment

	Reliability	Completeness	Geographical correlation	Technological correlation
RED Heat Engine	2	2	1	1
production processes	1.5	1.5	2.5	3.5
end -of-life processes	1.5	1.5	2.5	3
transportation	1.5	1.5	2.5	2

It can be seen that all production, end-of-life and transportation processes, score well in terms of reliability and completeness. This is because for all these cases pre-defined processes were used, with the data from the GaBi database. Geographically, most of these plants were assumed to be located in Germany, which was available in the database, and therefore the correlation does not score that high. Also, the technological correlation is not that high since the actual process that will be used is not easy to be defined always in advance. For example, all transportation was assumed to take place by truck. In reality there might be trains and boats involved if the materials move between countries and continents. Also, for the system's end-of-life landfill disposal was assumed for all material, while the options of incineration and/or recycling might be preferable.

For the RED Heat Engine, the situation is different. The process was developed from scratch, therefore the technological correlation is high, while the geographical correlation is not really relevant as a theoretical plant is studied. The reliability and completeness of the data is high enough because it comes from the industrial partners developing the technology. However, as the technology is in early stages of development, the data assessment includes assumptions and the accuracy will increase as the technology develops further and there is experience with industrial sized plants.

7.6 Sensitivity Analysis

As we have seen, Scenario 5 is the option with the lowest environmental impacts. Therefore, this scenario is examined further through a sensitivity analysis. The four variables used are the capacity factor, the frequency of replacing the Ion Exchange Membranes, the system lifetime and the transport distance. In table 7.9 are provided the "low" and the "high" values used for each variable to test the impact it has on the results.

Table 7.9: Parameters that vary in the sensitivity analysis

Variable Explanation	Symbol	Unit	Low	Base Case	High
Capacity factor	Cf	-	60%	90%	100%
Frequency of IEM replacement	mem frq	years	5	10	15
System lifetime	N	years	15	20	30
Transport Distance	TD	km	100	600	1800

The outcomes of the sensitivity analysis are illustrated in Fig. 7.4 (The full results are provided in Annex I).

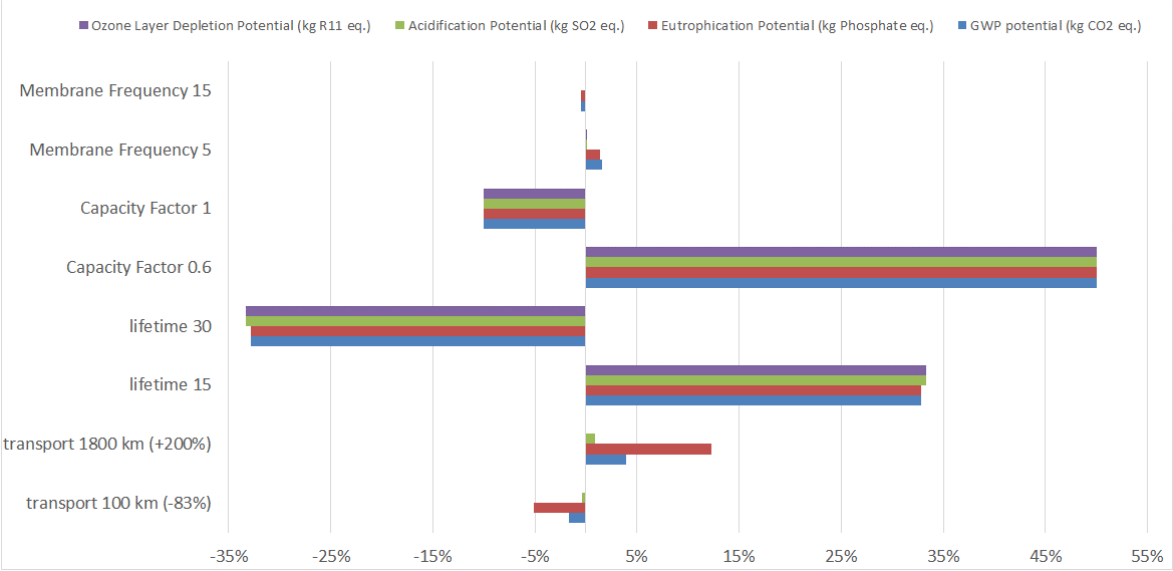

Figure 7.4: Outcomes of the sensitivity analysis

Membrane Frequency: It is not known how often it will be required to change the membranes as this kind of system has never operated for longer periods and this is why it has to be studied in the sensitivity analysis. However, as we see in the results, this does not affect the results much. This does not come as a surprise, since in Figure 7.1 we had already shown that the contribution of the plastic materials (where the membrane materials were classified) to the impacts is very small.

Capacity factor: The capacity factor does affect directly the amount of electricity generated and therefore it is expected that the results will be very sensitive to its variations. The value used in the model was 90%, assuming that the industrial unit is working around the clock, making waste heat available all the time. The 10% of the time was allowed for maintenance and other unforeseen stoppages. The results confirm that the effect is proportional – a 50% decrease of the capacity factor leads to a 50% increase of the environmental impacts in all categories.

System lifetime: The lifetime of the system was assumed to be 20 years. This is a very common assumption for renewable energy systems (see for example Ueckerdt et al. [159]). As the RED Heat Engine is still at early stages of development, the expected system lifetime is difficult to assess. For the regeneration component that was used in the design of the RED Heat Engine examined here (MED – Multi-effect Distillation), which is a mature technology when used for seawater desalination, it is common to have longer lifetime periods, of 25 or even 30 years (see for example Wittholz et al. [160]). In contrary, for the RED system, there is no operational experience over long periods of time. Still, in the literature where the RED levelized cost of electricity is assessed, as by Daniilidis et al. [161], a period of 30 years was assumed.

The results clearly indicate that the impacts are very sensitive to the lifetime of the system. This outcome was expected, since the longer the system operates, the more electricity will be generated using the same input material. As a result, the impacts from 15-year lifetime are about double compared to the impacts from a 30-year lifetime.

Transportation distance: We see that for the transportation, in the “high” option a distance 3 times higher (1800 km) is assumed and in the “low” option a distance 6 times shorter (100 km),

compared to the base scenario of 600 km. Even though the distance changes significantly, the results did not change more than 3-5% or less; the only exception is the eutrophication category where the impact is increasing by more than 12% because of the diesel fuel used by the trucks.

7.7 Comparison with other energy generating technologies

The LCA analysis has shown an interesting trend of significantly reduced impacts as potential improvements are introduced to the system design and operating conditions. However, just with these results it is difficult to assess if the impacts are actually important or negligible. For a more meaningful assessment, our results should be compared to those of other electricity generating technologies or electricity supply options.

In a 2013 paper, Turconi et al. [142] collected and compared the results of 167 different LCAs covering all main electricity generation technologies. As part of this work, a range of figures for the CO2 eq., NOx and SO2 emissions for each of the technologies has been presented.

The comparison of the results in this thesis with the figures reported on that table is shown in Fig. 7.5 for the case of CO2 eq. (the results in this thesis were calculated per MJ, so they were converted to a per MWh basis for the comparison). In order to consider the possible variations of our results (shown in the sensitivity analysis) a range of +/- 20% was taken into account here.

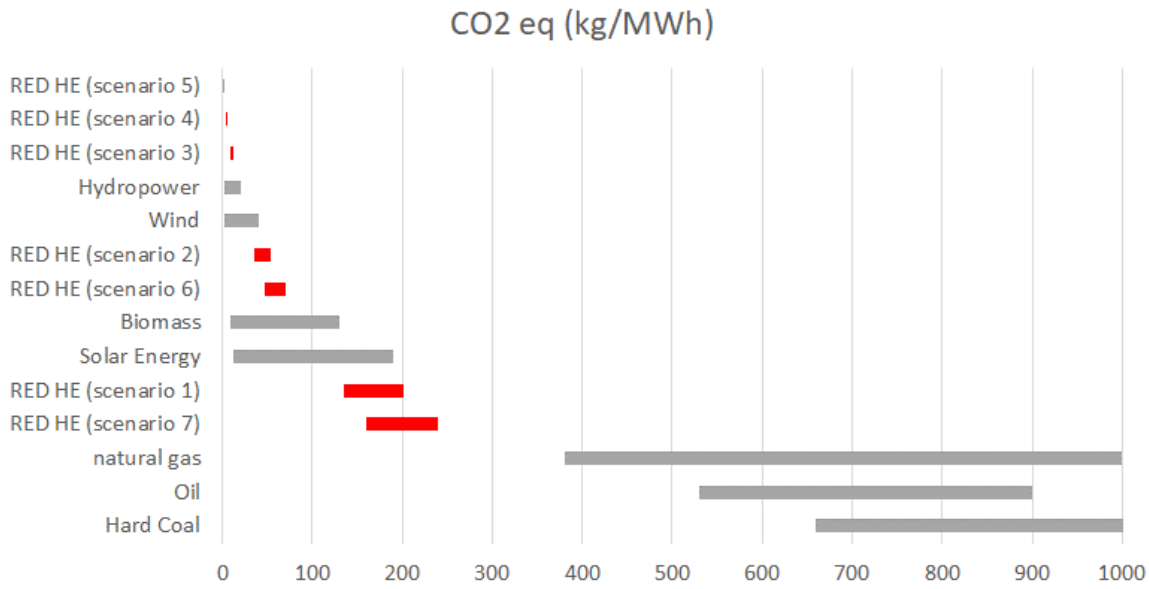

Fig 7.5: The RED Heat engine global warming impacts relative to other technologies

It can be seen that the scenarios 1 and 7 results are better than all fossil fuel generated electricity but have higher global warming impacts than all renewable energy technologies. When moving to scenarios 2 and 6, the global warming impacts are within the same range as the ones from solar energy and biomass, but still higher than the ones of wind energy. But for scenarios 3, 4 and 5 the impacts are significantly reduced and are even lower than the ones from wind energy and hydropower.

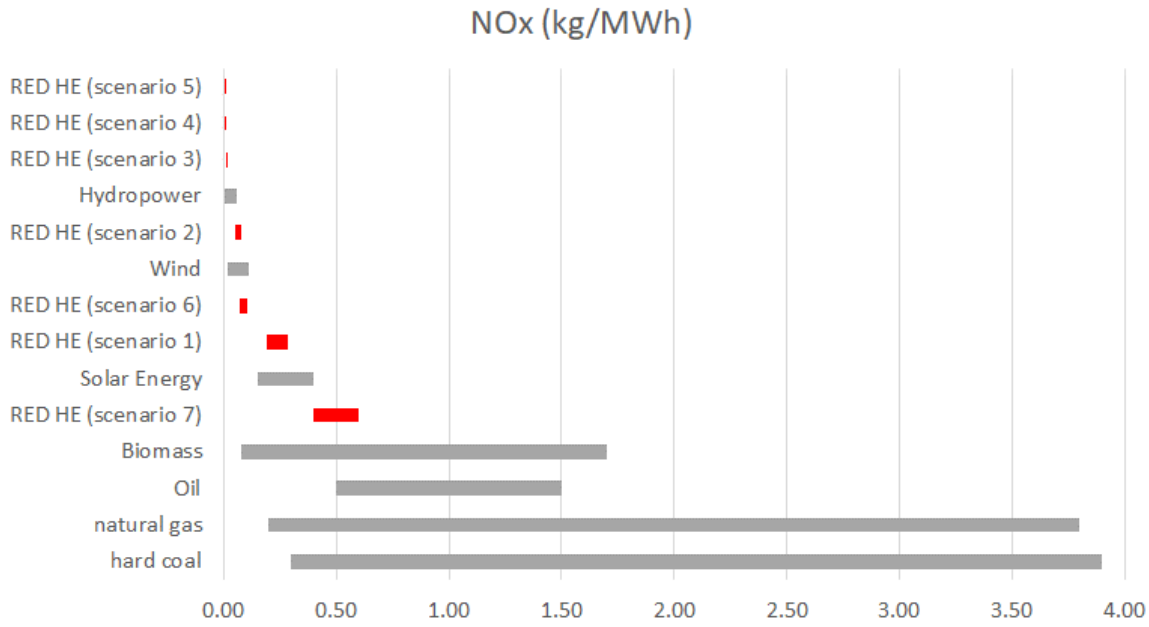

Fig 7.6: The RED Heat engine NOx emissions relative to other technologies

Fig 7.6 shows the comparison of the NOx emissions from the RED Heat Engine and those of other technologies. In this case we scenarios 1 and 7 are already within the same range as solar energy, while scenarios 2 and 6 are on similar levels with wind energy. Then scenarios 3, 4 and 5 bring the NOx emissions down to very low levels, on par with the lower part of the range of hydropower.

When comparing the SO_2 emissions of the RED Heat Engine with those of other electricity generating technologies scenario 1 results are high, on similar levels with the most polluting fossil fuel results, and even higher than those of modern plants that burn coal, lignite or oil, as seen on Fig. 7.7. The results are presented in two different graphs (Fig 7.7 and Fig 7.8), where different scales are used, allowing to read easier the details when moving to less polluting options.

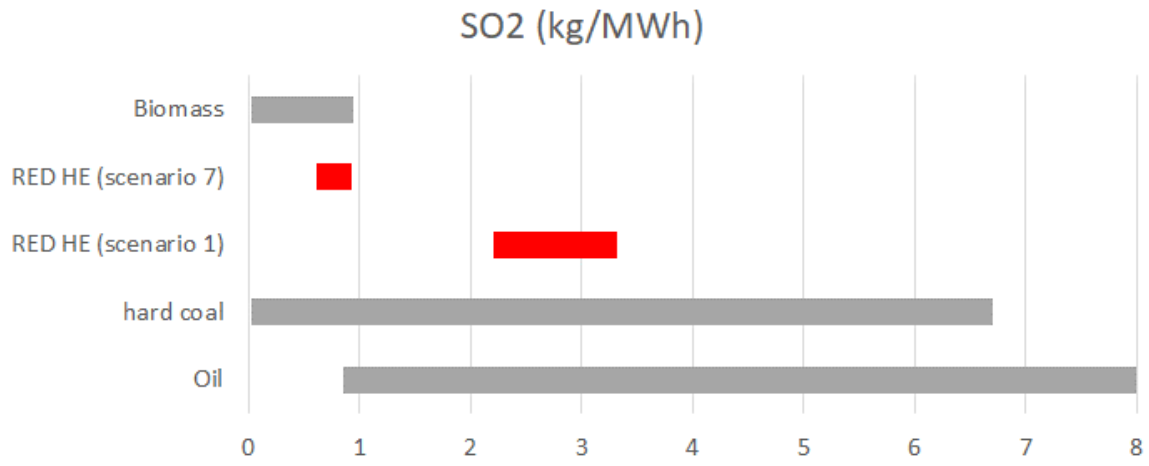

Fig 7.7: The SO_2 emissions of scenarios 1 and 7 relative to other technologies

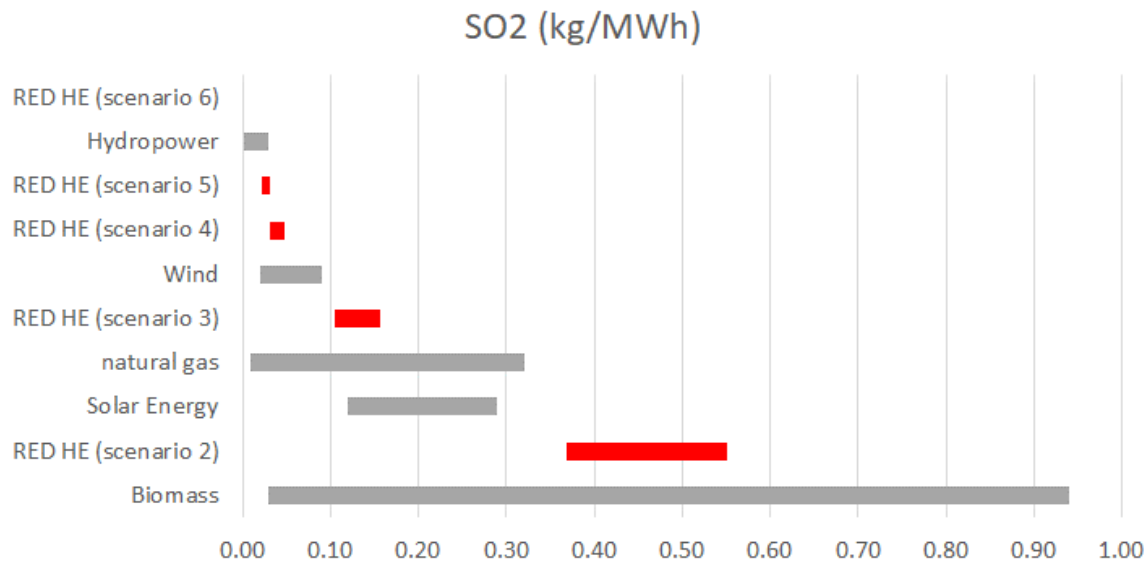

Fig 7.8: The SO_2 emissions of scenarios 2-6 relative to other technologies

Fig 7.8 shows that for scenario 2 the results are better, but still higher than the emissions from natural gas plants. It is only on scenario 3 that the SO2 emissions are on levels similar to the ones of solar energy and natural gas. Finally, for scenarios 4 and 5 the results are within the range of the emissions associated with wind energy, but still higher than the ones of hydropower and nuclear energy and only for scenario 6 we achieve lower emissions than the other technologies.

7.8 Comparison with grid electricity

The comparison to other electricity generating technologies is interesting. However, in most cases, the RED Heat Engine would be installed at an industrial site, converting waste heat to electricity and displacing electricity supplied by the grid. For that reason, it is interesting to compare directly the impacts of the various scenarios of the RED Heat Engine, to the impacts of the grid electricity, as supplied to the end user. For that purpose, the data directly from GaBi is used for the 4 selected impact categories in 6 large EU countries with important industrial activity [162]. In Fig 7.9, are plotted the relative results, using the average EU-28 impacts as the baseline. Almost in every case, substituting electricity supplied by the grid with electricity generated on-site by the RED Heat Engine represents an important reduction of environmental impacts. The mitigated emissions are much more pronounced in countries like Poland that rely heavily on solid fossil fuels for their electricity supply and much lower in countries like France that rely primarily on nuclear energy.

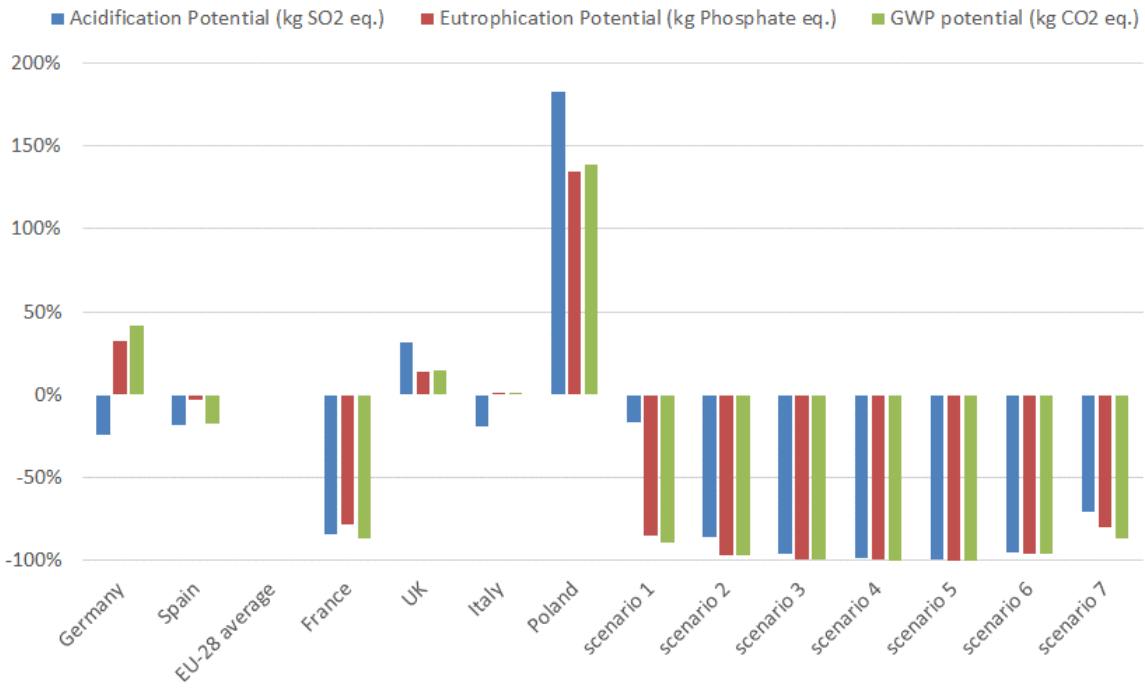

Fig 7.9: The RED Heat engine impacts relative to electricity from the grid in main EU countries

In the graph of Fig 7.9 the category of Ozone layer depletion was not included. This is because the average R11 eq. emissions for EU-28 is 1.84 x 10^{-12}, while the results for scenarios 1 to 6 (as presented above**)** range between 1.33 x 10^{-9} to 1.27 x 10^{-11}, i.e. even in the best case the ozone depletion potential associated to the RED Heat Engine is two orders of magnitude higher than the average EU-28 grid electricity (the only exception is scenario 7, which has similar ODP with the grid electricity). As we have seen in Fig. 7.1 and 7.2, the ODP of the RED Heat Engine is associated with the use of copper. Indeed, in scenario 7 where no copper is used, the R11 eq. emissions are 3.56 x 10^{-13}, an order of magnitude below the ODP associated with the average electricity supply in EU-28.

7.9 Screening of the other impact categories

The analysis up to now was focused on the 4 main impact categories. In table 7.10 are compared the results of scenario 2, which is the RED-MED as it would be operate with the components available commercially today, with the impacts of the average EU-28 grid electricity, for all categories introduced in section 6.2. In all cases, the scenario 2 gives results that are lower by 60 to 99.7%. This result confirms that the decision to focus on the four impact categories did not lead to missing any important impacts of the RED Heat Engine.

Table 7.10: Comparison of scenario 2 and EU-28 grid electricity environmental impacts

Category	unit	scenario 2	EU-28 grid	difference
CML2001 - Jan. 2016, Abiotic Depletion (ADP fossil)	MJ x 10^{-x}	0.1669	4.4168	-96.22%
CML2001 - Jan. 2016, Abiotic Depletion (ADP fossil)	kg DCB eq.	0.0002	0.0009	-78.21%
CML2001 - Jan. 2016, Abiotic Depletion (ADP fossil)	kg DCB eq.	0.0092	0.0232	-60.39%
CML2001 - Jan. 2016, Marine Aquatic Ecotoxicity Pot. (MAETP inf.)	kg DCB eq.	1.8343	49.7225	-96.31%
CML2001 - Jan. 2016, Photochem. Ozone Creation Potential (POCP)	kg Ethene eq.	8.19×10^{-6}	7.38×10^{-5}	-88.89%
EN15804 - Total use of non-renewable primary energy resources (PENRT)	MJ	0.1813	7.5804	-97.61%
EN15804 - Use of net fresh water (FW)	m3	0.0002	0.0039	-95.55%
Biotic Production Loss Potential (Occupation)	kg	0.0001	0.0238	-99.39%
Particles to air	kg	1.04×10^{-5}	9.52×10^{-5}	-89.08%
Aluminium oxide (dust)	kg	1.46×10^{-15}	1.03×10^{-14}	-85.90%
Dust (> PM10)	kg	5.26×10^{-6}	5.90×10^{-5}	-91.09%
Dust (PM2.5 - PM10)	kg	3.23×10^{-6}	1.69×10^{-5}	-80.86%
Dust (PM2.5)	kg	1.28×10^{-6}	1.94×10^{-5}	-93.37%
Silicon dioxide (silica)	kg	1.86×10^{-12}	5.25×10^{-10}	-99.65%
Ionising radiation - human health	kBq U235 eq.	0.0006	0.2042	-99.70%

7.10 Comparison with other heat engines

As a final step, the results for scenarios 2 to 6 are compared with the results of Hickenbottom et al. [152] for the Osmotic Heat Engine (OHE) and the ORC. The OHE uses a very similar principle to the RED Heat Engine, with Pressure Retarded Osmosis to generate electricity and MD to regenerate the salinity difference. Moreover, the results are also compared to the ones of commercially available ORC systems, which convert waste heat to electricity. The results from Hickenbottom [152] and from Bai [163] are used for the ORC systems. We focus the comparison only to the two impact categories where all studies reported results (acidification potential and global warming potential). The comparison is presented in Table 7.11.

Table 7.11: Comparison with OHE and ORC impacts

	Acidification (kg SO2 eq/MWh)	Global warming (kg CO2 eq./MWh)
base case OHE [152]	0.294	68.83
improved case OHE [152]	0.029	8.64
ORC [152]	0.004	1.20
ORC [163]	0.015	0.90
RED HE (Scenario 2)	0.605	44.39
RED HE (Scenario 3)	0.170	10.92
RED HE (Scenario 4)	0.052	4.10
RED HE (Scenario 5)	0.034	1.76
RED HE (Scenario 6)	0.220	58.21

The OHE base case gives similar results to scenario 2 and scenario 6, while the improved OHE case gives similar results with the RED Heat Engine scenario 5 and between scenarios 3 and 4 for Global warming potential. The ORC results are lower for both categories compared to all scenarios of the heat engines. However, the results for scenario 5 are in the same order of magnitude with the ORC results and final conclusions can be reached only when comparing them carefully for the specific conditions of possible projects considered.

8 Conclusions

It was seen that the CO_2 eq., NOx and SO_2 emissions of the RED Heat Engine are lower than most other electricity generating technologies. As a result, by substituting grid electricity with electricity generated by the RED Heat Engine using waste heat would lead to reduced environmental impacts, in terms of global warming, eutrophication and acidification. The level of the improvement depends on the baseline, as the different countries have very different generation mixes feeding into their grids.

Between the different regeneration technologies, the distillation columns with the thermolytic salts give the highest environmental impacts and the MED gives the lowest environmental impact.

The ion exchange membranes performance affects significantly the results as can be seen by comparing the reduction when moving from scenario 2 to scenario 3, where the environmental impacts are reduced by a factor of 4 just by changing from current membranes to future membranes (ion exchange membranes with properties optimised for this application). Therefore, future R&D should focus on reducing the electrical resistance and increasing the ion selectivity of ion exchange membranes for the RED Heat Engine conditions.

The system efficiency is not that important from an environmental impact point of view. Reducing the number of MED effects should be considered in future system designs, even if it reduces the efficiency, because it leads to much lower environmental impacts as can be seen by comparing the results of scenario 1 to the ones of scenario 2. This conclusion contrasts with the work of Bernier et al. [164] that suggested to maximise the efficiency of power generation for minimising the environmental impacts. The main reason for that difference is that Bernier assumes a fossil fuel powered system, while our fuels (waste heat) is assumed to be impact free.

The technical life-time of the system and the capacity factor are parameters that affect proportionally the magnitude of the system's environmental impact. The design should be as robust as possible for extending the technical lifetime of the system, while priority should be given to applications where waste heat is available continuously and the system can operate 24/7.

Most impacts are associated to the metals used at the heat exchangers and other components of the regeneration process (especially in the MED and the distillation columns with thermolytic salts). The recommendations above will help to reduce the overall amount of metal used per unit of electricity generated and hence reduce also the overall environmental impacts. However, relatively important eutrophication potential impacts were seen and are directly associated to the nickel production process; there are also very high ozone depletion potential impacts compared to grid electricity; these impacts are associated to the copper production process. For that reason, it is recommended in future research to explore alternative heat exchanger materials. A recent review of research in polymeric heat exchangers [165] has concluded that they are a promising alternative but still a lot of research is required before they can enter the market.

Part III: Economic Assessment

1. Introduction

In this part of the thesis, a detailed cost model has been developed, which takes into account all parameters of this technology. All main configurations of the RED Heat Engine are examined, in order to evaluate the most cost-effective one for each type of application, mostly matching it to the available heat source.

As in Part II, the developed model uses as input results from the process simulator [36], which are then analysed. These results lead to the capacity and productivity of each set-up, and finally to the detailed annual balance and the calculation of the Levelized Cost of Electricity (LCOE). This value is used as the financial criterion for the economic evaluation. The annual balance considers both capital and running costs (e.g. operation and maintenance), as well as the inflation and the discount rate.

A sensitivity analysis has been also conducted, since there are many parameters that have an uncertainty range (e.g. cost of the RED membranes), as well as others that depend on the application itself (e.g. capacity factor). Apart from that and to account for the future cost of the components and materials used, appropriate estimations have been developed and used in the model. These estimations concern the cost of the components with the higher uncertainty and for which exists a significant room for improvement, such as the RED membranes and the regeneration unit. The outcome is to estimate the LCOE development potential in the future; the years 2020, 2030, and 2050 have been used as the milestones.

The different configurations that have been examined cover an extended version of the scenarios examined in Part II, while an additional one relevant to the operation for peak power production has been considered, by storing the two solutions in tanks and operating the RED stacks for a fraction of the time. The list of the configurations that were considered is provided below:

- **RED-MED**. With both current and future membranes at various heat source temperatures, MED designs (number of effects) and RED specifications (membrane geometry). The working fluids considered are NaCl and KAc solutions and the pre-heating option (high-temperature operation of the solution) at two temperatures (50 and 80 ^{o}C) has been also examined. Operation at peak power mode is also presented. The results for the RED-MED configuration are presented with detail, since it serves as the reference, in order to identify the most promising conditions, including only these in the other combinations.
- **RED-MD**. With only future membranes, using the most promising RED stack specifications.
- **RED-thermolytic salts**. The use of distillation columns has been the regeneration unit. Future membranes have been considered, examining the effect of the number of columns.

2. Description of the cost analysis model

The background work carried out for developing the main approach of the cost analysis model was published in 2017 [23]:

M. Papapetrou, A. Cipollina, U. La Commare, G. Micale, G. Zaragoza, G. Kosmadakis, Assessment of methodologies and data used to calculate desalination costs, Desalination. 419 (2017) pages 8 - 19. doi:10.1016/j.desal.2017.05.038.

2.1 Introduction

The cost analysis has been implemented in a spreadsheet (MS Excel©) and has been carefully adjusted for directly receiving the results and parameters from the process simulator [36] (e.g. stack and membrane specifications, regenerator dimensions/sizing, etc.). These technical results are combined with the necessary cost and financial figures, in order to conduct the cost analysis. The main results concern the key financial criteria, which are the payback period (PBP) in years and the Levelized Cost Of Energy (LCOE) in €/kWh, and once combined they can identify the possible profitability and cost-effectiveness of a RED Heat Engine.

The technical parameters are calculated for a single stack from the process simulator. Therefore, the number of stacks is a free parameter, which defines the final capacity (in kW) of the system, appropriately adjusting the size of the regeneration system. Thus, the resulting sizing of all other components (e.g. pumps, regenerator, pipes, etc.) is calculated as a function of the RED total capacity. This brings a high flexibility for conducting various case studies of varying sizes, as will be presented later.

2.2 Overview of the cost analysis model and financial criteria

The cost analysis model considers both running and capital costs. These are presented next, with their detailed description provided in subsequent sections.

2.2.1 Running and capital costs

The primary aim of the cost analysis model is to calculate the annual income from electricity sales and the annual costs, which are divided into annual fixed operation and maintenance (O&M) costs and heating costs. The annual income and costs are then summed-up to derive to the net annual balance. The above cost amounts and balances are defined in Eqs. (2.1)-(2.4).

$$Annual\ income = \left(\frac{Capacity\ factor}{100}\right) 8760\ (El.price)(P_{net}) \quad (2.1)$$

$$Annual\ fixed\ O\&M\ costs = Operating\ costs + RED\ maintenance\ costs + RED\ labour\ costs \quad (2.2)$$

$$Annual\ costs = [Annual\ fixed\ O\&M\ costs] + [Heating\ costs] = [Annual\ fixed\ O\&M\ costs] + \left[\left(\frac{Capacity\ factor}{100}\right) 8760(Cost\ for\ heat)(Heat\ input)\right] \quad (2.3)$$

$$Annual\ net\ balance = Annual\ income - Annual\ costs \quad (2.4)$$

Except from the above running costs, for assessing the financial performance, the plant capital cost (I_t) is required. This is calculated by Eq. (2.5), summing up all component costs.

$$I_t = RED\ cost + \sum(Pumps\ cost) + Inverter\ cost + \\ + Regeneration\ cost + Civil\ \&\ el.infrastructure\ costs + Piping\ cost \quad (2.5)$$

All related costs shown in the above equations are presented in the next sections.

2.2.2 Financial criteria

The payback period (PBP) and the Levelized Cost of Electricity (LCOE) are then calculated, which are used as financial criteria for evaluating any potential case study. PBP is defined as the number of years necessary to retrieve the initial investment/capital cost [166], while LCOE is the price at which the generated electricity should be sold for the system to break even [167]. LCOE and PBP are given by Eqs. (2.6) and (2.7) respectively.

$$LCOE = \frac{\sum_{t=0}^{n} \frac{I_t + M_t}{(1+r)^t}}{\sum_{t=0}^{n} \frac{E_t}{(1+r)^t}} \quad (2.6)$$

where *t* refers to the year "t" with t=0 the start of the plant construction (it is considered that this construction requires one whole year), *n* the plant lifetime, I_t the investment expenditures in year "t", M_t the running costs (fixed and variable) in year "t", *r* the discount rate, and E_t the electricity generation (in kWh) in year "t".

$$\sum_{t=0}^{PBP} \frac{I_t + M_t}{(1+r)^t} = \sum_{t=0}^{PBP} \frac{En_t}{(1+r)^t} \quad (2.7)$$

where En_t is the income in year "t" from electricity sales.

Both financial parameters, LCOE and PBP, will be used for the investigation of the economic performance of various RED Heat Engine configurations, and also compared with other electricity generation technologies for heat to power, with the prevailing one the organic Rankine cycle – ORC [168].

In order to calculate the financial performance of the system during its lifetime, all cash flows are considered, which are depreciated with the use of the discount factor that is included in this cost model. The use of the discount factor is necessary in order to account for the time value of money, even if it adds complexity to the calculations. This is particularly important considering the long lifetime of such systems of more than 20 years. This depreciation is accomplished with the use of the discount factor defined for each year, given by Eq. (2.8).

$$Discount\ factor\ of\ year\ t = \frac{1}{(1+r)^t} \quad (2.8)$$

2.2.3 Parameters of the cost model

The parameters that are then processed for the calculation of the financial performance of a RED Heat Engine over its lifetime are provided in Table 2.1. These parameters are given per year corresponding to year "t".

Table 2.1: Calculated parameters during the system lifetime

Nr	Parameter	Description and calculation/estimation method
1	Year	Installation during year t=0. Operation during years 1 ≤ t ≤ (*lifetime*).
2	Discount factor	From Eq. (2.8) for the year "t".
3	Investment	Capital cost from Eq. (2.5).
4	Income from electricity sales	Calculated from the capacity factor, electricity price and net power production, including the inflation of the annual income: $El.sales == \frac{Cap.factor}{100} 8760(P_{net})(El.price) \frac{1}{(1+inf_{in})^t}$
5	Discounted income from electricity sales	Parameter nr. 4 multiplied by the discount factor of the year "t" from Eq. (2.8).
6	Annual costs	Annual costs of year "t" from Eq. (2.3) multiplied with the term: $\frac{1}{(1+inf_c)^t}$, for considering the inflation of the annual costs (inf_c is the inflation factor of the costs).
7	Discounted annual costs	Parameter nr. 6 multiplied by the discount factor of the year "t" from Eq. (2.8).
8	Annual balance (EBITDA)	Balance of annual electricity sales and costs (not discounted), from the above parameter nr. 4 and 6.
9	Depreciation	Investment cost of Eq. (2.5) divided equally in each year over the depreciation period.
10	EBIT (after depreciation)	Annual balance minus depreciation cost, from parameters nr. 8 and 9.
11	Taxes	Tax percentage of EBIT (parameter nr. 10) in case it is higher than zero.
12	Static cash flows	Net cash flows without depreciation, including electricity sales, investment, annual costs and taxes, given by: $Static\ cash\ flows = El.sales - Investment - Annual\ costs - Taxes$
13	Discounted cash flows	Static cash flows (parameter nr. 12) multiplied by the discount factor of Eq. (2.8) for the year "t".
14	Cumulative cash flow	Sum of discounted cash flows from the year t=0 over the system lifetime (including the initial capital cost), given by: $Cumulative\ cash\ flows == \sum_{t=0}^{n}(Discounted\ cash\ flows)$

15	Payback period	The year that the cumulative cash flow (parameter nr. 14) becomes positive, defining the necessary amount of years that are required for the return of the initial capital cost.

It should be mentioned that the value of cumulative cash flow at the end of the system lifetime (t=n) is equal to the Net Present Value (NPV), which is also used in some economic analysis studies [137]. NPV shows the present value of all discounted cash flows during the economic lifetime of a system. The use of the NPV parameter is popular with investors considering specific projects, but it is not favored here, since it is not a direct way of examining the financial viability of new technologies, especially when comparing systems of different assumed size. The financial parameters that will be used for the criteria of the economic performance are the LCOE and the PBP, which combined can provide enough evidence on the potential profitability of an electricity generation system.

In the following section is presented calculation process, starting from the technical parameters that were used in this cost model, the variables calculated and finally the costs of:

- the RED stack
- the regeneration technology
- the auxiliary equipment

The financial performance of the different cases examined are then provided in Section 3, presenting all costs, while focusing on the LCOE value, since in many cases no payback is achieved.

2.3 Technical model results – input parameters

The outputs from the process simulator are fed into the different tabs of the economic spreadsheet model. These parameters are listed in Table 2.2 for the RED stack, and in Tables 2.3-2.5 for the MED, MD, and thermolytic salts regeneration technologies respectively. Table 2.6 provides the input parameters related to the auxiliaries considered. All parameters correspond to a single RED stack.

Table 2.2: Input technical parameters for the RED stack

Nr.	Technical parameter (per stack)	Units
1	Number of cell pairs	-
2	Membrane width	m
3	Membrane length	m
4	Pumping power of RED	W
5	Pump efficiency	%
6	Gross power production	kW

Table 2.3: Input technical parameters for the MED

Nr.	Technical parameter (per stack)	Units
1	Temperature of heat input	^oC
2	Pumping power of MED inlet pumps	kW
3	Pumping power of MED outlet pumps	kW
4	Specific heat exchangers area of MED	$m^2/(kg/s)$
5	MED distillate flow rate	kg/s
6	Heat input	kW
7	MED number of effects	-
8	Preheat temperature in case of high-temperature operation of the RED part	^oC
9	Heat capacity of the two preheaters of high-temperature operation of the RED part	kW

Table 2.4: Input technical parameters for the MD

Nr.	Technical parameter (per stack)	Units
1	Specific electricity consumption	kWh/m^3
2	Specific thermal consumption	kWh/m^3
3	Heat Exchanger Area	m^2
4	MD distillate mass flow rate	kg/s
5	Heat input	kW
6	Membrane surface	m^2

Table 2.5: Input technical parameters for the thermolytic salts

Nr.	Technical parameter (per stack)	Units
1	Number of columns	-

2	Column packed height	m
3	Column diameter	m
4	Column void fraction	%
5	Column volume of packing	m^3
6	HEX surface	m^2
7	Reboiler HEX surface	m^2
8	Pumps' flow rates	m^3/s
9	Heat input	kW

Table 2.6: Input technical parameters for the auxiliaries

Nr.	Technical parameter (per stack)	Units
1	Concentration of high concentration working fluid	mol/kg
2	Concentration of low concentration working fluid	mol/kg
3	Density of liquid working fluid	kg/m^3
4	Salt molar weight	kg/kmol

The concentration and density of the working fluid of Table 2.6 are required, in order to calculate the total amount of salt of the system. It is considered that half of the fluid has the high concentration and the other half the low one. This amount is included in the cost analysis, in order to examine its contribution and effect on the total cost, especially if high-costs salts are used, except from sodium chloride (NaCl), which is of very low cost. The cost of Potassium acetate (KAc) is about two times higher, but it still has a negligible effect on the costs.

As mentioned earlier, the process simulator gives the results for 1 stack. Then the economic assessment model, according to the number of stacks that are selected, calculates the overall input parameters (e.g. the total membrane surface of all pairs and stacks), and an overall energy balance of the system, resulting to gross (total) power production by the RED stacks (P_{gross}), own consumption for pumping (P_{pumps}), and finally to the total net power production (P_{net}) and heat input (Q_{in}). The main performance value defined is the thermal efficiency, according to Eq. (2.9).

$$n_{th} = \frac{P_{gross} - \sum P_{pumps}}{Q_{in}} = \frac{P_{net}}{Q_{in}} \quad (2.9)$$

2.4 Variables of the cost analysis

In this section are presented all variables that are used in the cost analysis . These have to do with the sizing (e.g. number of stacks), equipment cost (e.g. specific cost of IEM), and financial parameters (e.g. economic lifetime, discount rate). The list of the variables used in the analysis is shown in Table 2.7, divided into each main component of the RED Heat Engine.

Table 2.7: Variables of the cost analysis model

Nr.	Variable	Units	Comments
RED stack			
1	Total number of stacks	-	This number defines the size of the RED Heat Engine, in order to examine the cost-effectiveness of different configurations and for various applications (industrial waste heat recovery, solar, etc.).
2	Increase of thermal efficiency	-	It expresses how many times the thermal efficiency can be increased. With its use it is possible to artificially examine future scenarios in case the RED membranes and/or the regeneration system have improved performance. This variable is used only in the sensitivity analysis and for the extraction of future scenarios, based on current and future performing membranes.
3	Membrane pair specific cost	€/m^2	Estimated based on the system size and market prices (presented with detail later). This specific cost is included in the sensitivity analysis and for the extraction of future scenarios.
4	Stack casing specific cost	€/m^2	Estimated based on the system size and market prices (presented with detail later). This specific cost is included in the sensitivity analysis and for the extraction of future scenarios.
5	Electrode/electrolyte specific cost	€/m^2	Estimated based on the system size and market prices (presented with detail later). This specific cost is included in the sensitivity analysis and for the extraction of future scenarios.

MED regeneration			
6	Reduction of MED cost compared to desalination units	%	Estimation of MED cost reduction, because it is not used for desalination (no intake, pre-treatment, etc.) with a standard value of 35% according to a breakdown of MED costs (Sommariva [169]). This parameter is included in the sensitivity analysis and for the extraction of future scenarios.
7	Evaporator cost fraction in MED	%	Cost fraction of the evaporator in MED regeneration technology with standard value of 40%, according to Sommariva. This fraction is used for the MED correlation that has been developed.
MD regeneration			
8	MD membrane specific cost	€/m^2	Estimated based on market prices (presented with detail later). This specific cost is included in the sensitivity analysis and for the extraction of future scenarios.
Auxiliaries and financial variables			
9	Civil & electrical infrastructure specific cost	€/kW_e	Estimated to 250 €/kW of net power production, according to standard values of power plants for electricity generation [170].
10	Cost of heat supply (solar, geothermal)	€	Installation costs of solar collectors and geothermal fields that add-up to the capital cost of RED Heat Engine, according to the analysis in D9.3.
11	Salt specific cost	€/kg	Specific cost of the salt charged in the system. An average cost of sodium chloride of 0.2 €/kg is considered.
12	Capacity factor	%	Fraction of operational hours per year. Estimated with a standard value of 90% corresponding to industrial waste heat or geothermal applications. Capacity factor is included in the sensitivity analysis, ranging from 40 (typical for solar applications without storage) up to 100%.
13	Depreciation period	Years	Estimated to a standard 10-year period. The initial investment is depreciated equally over this period and decreases the annual net

			income. It affects the amount of taxes applied on the net profits.
14	Economic lifetime	Years	Lifetime of the power plant. Estimated according to the design of this technology and is equal to 30 years. It is included in the sensitivity analysis, ranging from 15 to 40 years.
15	Discount rate	%	Discount rate reflecting the return that investors expect for such projects. An average value of 5% is considered as a standard value. This rate is included in the sensitivity analysis, ranging from 2 up to 10%, covering all possible cases.
16	Inflation for annual income	%	Inflation applied on the income/electricity sales. An estimated value of 1.5% is used, according to Eurostat [42].
17	Inflation for annual costs	%	Inflation applied on the annual costs. An estimated value of 1% is used, according to average inflation in EU [171].
18	Cost for heat	€/kW_{th}	Cost for installing the heat supply system (solar, geothermal). Calculated according to the available heat source. In case of industrial waste heat, this cost is zero.
19	Other project costs	%/capital cost	Estimated as a fraction of the initial investment (includes allowances, project design and management). An estimated value of 0.5%/ capital cost is considered.
20	Electricity price/feed-in-tariff	€/kWh	Price that the produced electricity is provided to the grid or to a user. Such data is available from statistic agencies or other sources, according to the application and end-user. A standard value of 0.10 €/kWh is considered, which corresponds to electricity price for industries. This value is included in the sensitivity analysis, ranging from 0.08 up to 0.26 €/kWh. The lowest price corresponds to large industries and the highest to feed-in-tariff of biogas plants.
21	Taxes	%	Taxes applied on the net profits, considering the depreciation period as well. Estimated according to the application. A standard value of 0% is considered.

22	Number of RED membrane replacements	-	Estimated according to standard value in membrane desalination systems and considering that all membranes are replaced twice during the plant lifetime of 30 years (every 10 years). It is included in the sensitivity analysis, considering a lower rate of membranes replacement (once in the plant's lifetime), up to replacing all membranes five times during the lifetime (every 5 years).

RED specific costs: The costs related to the RED stacks (membranes, stack casing, electrodes) show the higher uncertainty, since this technology is not yet commercialized. Therefore, a market research has been conducted, in order to adopt a reliable estimation of the relevant specific costs. These data have been processed, using assumptions about how the costs will develop in the future, up to 2050, and are then used in the future scenarios. Moreover, the effect of the plant size on the specific costs is also included, in order to introduce this effect in the calculations. The "small" plant size corresponds to a plant with 1,000 m^2 of membranes, and the "large" one with 10,000,000 m^2 of membranes, with appropriate correlations defined for using size-appropriate membrane and stack values in the calculations. These cost figures are shown in Table 2.8. The same membrane cost figures have been used for current membranes and for future membranes.

Table 2.8: Specific costs of the RED stack parts as a function of the future year and plant size

Year	Plant size	Membrane specific cost (€/m^2)	Stack casing specific cost (€/m^2)	Electrode specific cost (€/m^2)
2020	Small	30	15	500
	Large	15	7.5	500
2030	Small	16	7.5	250
	Large	8	3.5	250
2050	Small	10	3.5	200
	Large	5	1.5	200

MD specific cost: A similar approach is also followed for the estimation of the membrane module specific cost of the MD regeneration. This specific cost is given only as a function of the year, since no effect is applied on the plant size. These specific costs are given in Table 2.9.

Table 2.9: Specific cost of the membrane module of the MD regeneration as a function of the future year

Year	Membrane module specific cost (€/m²)
2020	100
2030	50
2050	30

2.5 System sizing parameters

The next step of this analysis is the sizing of each part of the plant, according to the total number of stacks. A separate tab in the spreadsheet is included that calculates the sizing based on the data inputs by the process simulator [36]. The sizing is divided into:

- RED part that includes the membranes (membrane pairs, electrodes and casing) and the RED pumps.
- The regeneration technology part (e.g. MED or MD) that includes the pumps, the heat exchangers, etc.
- Other auxiliary parts that include the piping, the working fluid, etc.

The sizing of the multi-stack system includes the main specifications, by multiplying the technical parameter for one stack with the total number of stacks, appropriately adjusting the sizing of the regeneration and auxiliaries parts. These specifications are presented in Table 2.10.

Table 2.10: System sizing and main specifications

Nr.	Variable	Units	Comments
1	Membrane surface per cell pair	m^2	The surface of each membrane is multiplied by 2 to account for the cell pair.
2	Membrane surface per stack	m^2	Calculated according to the membrane surface and the number of cell pairs per stack.
3	Total membrane surface	m^2	Parameter nr. 2 multiplied with the total number of stacks.
4	RED pumping power	kW	Total pumping power of RED pump.
5	Gross power production	kW	Gross power production of each stack multiplied with the total number of stacks.
6	Pumping power of the regeneration technology	kW	Total pumping power of the regeneration technology.

7	Total HEX (and membrane) surface of the regeneration technology	m^2	Total HEX of the regeneration technology. Applicable for all three technologies considered. The total membrane surface is considered only for the MD.
8	Total heat input	kW	Required heat input of each stack multiplied with the total number of stacks.
9	Net power production	kW	Total net power production.
10	Thermal efficiency	%	Calculated according to Eq. (2.9).
11	Piping length	m	An empirical expression is used: the length in meters is ten times the net power production in kW.
12	Piping mean diameter	m	Estimated based on empirical correlation and is equal to ¼ of the inch
13	Working fluid amount	kg	Calculated based on the total piping volume, and fluid density. The result is increased by 50% to account for the fluid that is inside the system parts.
14	Salt amount	kg	Calculated based on the concentration of the high/low concentration mixture, considering that half of the working fluid amount (parameter nr. 13) has low concentration and the other half high concentration.

2.6 Capital cost parameters

The cost calculations of the system then follow for providing the capital costs. The relevant parameters are presented in the next sub-sections for the RED system parts and regeneration technologies.

2.6.1 RED capital cost parameters

The capital cost parameters of the RED stack with its necessary parts are shown in Table. 2.11.

Table 2.11: Capital cost parameters of RED

Nr.	Cost parameter	Units	Calculation method
1	Total membrane specific cost	€/m^2	Sum of membrane and stack specific costs (without the electrodes).

2	Total membrane cost per stack	€/stack	Cost per stack based on parameter nr. 1 (without the electrodes).
3	Electrode/electrolyte cost	€	Total cost of the electrodes based on their specific cost and total surface. The latter is calculated as follows: Two pairs are placed in each stack with surface equal to each membrane (length x width). The cost of each pair is then multiplied by the total number of stacks.
4	Total RED stack cost	€	Cost of each stack (including the membranes, casing and electrodes) multiplied by the total number of stacks.
5	Total RED stack cost per (net) kW	€/kW	Parameter nr. 4 divided by net power production.
6	RED pump specific cost	€/kW_p	Correlation as a function of pumping power [172] ($Pump\ sp.cost = 900\left(\frac{P_{pump}}{300}\right)^{0.25} / P_{pump}$).
7	RED pump cost	€/pump	Parameter nr. 6 multiplied by the RED pumping power.
8	Inverter specific cost	€/kW_{gross}	Correlation from commercial products as a function of gross power production (see next)
9	Inverter cost	€/inverter	Parameter nr. 8 multiplied by gross power production.

Inverter cost: A market study has been accomplished for producing a correlation of inverter cost as a function of its electrical capacity. Inverters manufactured by SMA [173] (similar to the ones used in PV systems) have been considered, which are available at a large range of power. The overall result of this study is shown in Fig. 2.1, depicting the inverter specific cost (€/kW_{gross}, no VAT included), as a function of (gross) electricity production by the RED stacks.

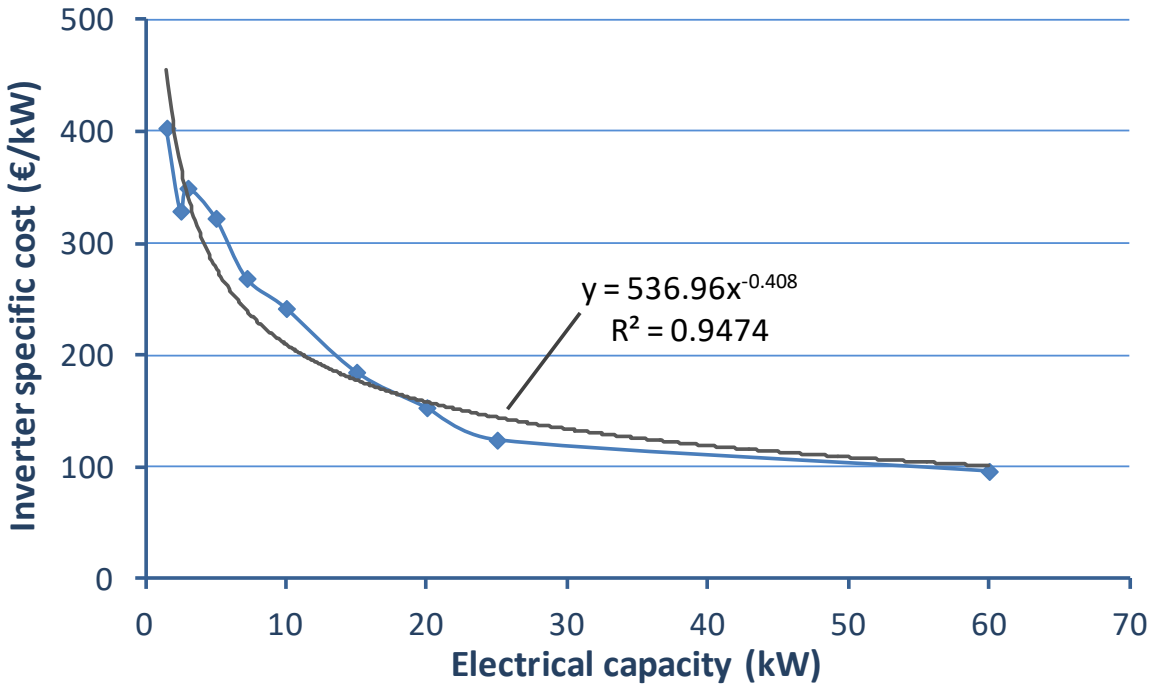

Figure 2.1: Inverter specific cost as a function of electrical capacity

The extracted numerical correlation based on the market data is also shown in Fig. 2.1, with a very good match with the available specific price values (R^2 approaching unity).

2.6.2 MED capital cost parameters

The capital cost parameters of the MED regeneration with its necessary parts are shown in Table. 2.12.

Table 2.12: Capital cost parameters of MED

Nr.	Cost parameter	Units	Calculation method
1	Number of effects	-	MED number of effects that affect the performance and cost
2	Total HEX surface	m^2	Total HEX surface of the effects
3	Distillate flow rate	kg/s	Total distillate flow rate
4	MED specific cost	€/(m^3/day)	Proposed correlation as a function of distillate flow rate and HEX surface (see later).
5	MED cost	€	Parameter nr. 4 multiplied by the distillate flow rate.

6	MED cost for RED	€	Parameter nr. 5 reduced by the fraction of the regeneration parts not used (not for desalination).

2.6.3 MED capital cost correlation

The work on developing the MED capital cost correlation was published in 2018:

G. Kosmadakis, M. Papapetrou, B. Ortega-Delgado, A. Cipollina, D.C. Alarcón-Padilla, Correlations for estimating the specific capital cost of multi-effect distillation plants considering the main design trends and operating conditions, Desalination. 447 (2018) pages 74-83. doi:10.1016/j.desal.2018.09.011*

Introduction

The most common method of estimating the capital cost of a MED plant is to correlate the specific cost with the plant capacity. This approach has been followed by many groups, in order to estimate the specific cost [23]. For that purpose, a conservative correlation has been proposed in Ref. [174], which is the outcome of processing the costs of many MED plants (in $) and is expressed as a function of the plant capacity, equal to the distillate flow rate (*D*). This correlation is given in Eq. (2.10) valid for a plant capacity up to 10,000 m^3/day.

$$C_{MED}(\$/m^3/day) = 3054D^{-0.0249} \quad (2.10)$$

The MED specific cost as a function of plant capacity is shown in Fig. 2.2 for the range of validity of Eq. (2.10). When applying this correlation for plants of higher capacity, this specific cost never moves to values below 2400 $/($m^3$/day), even for very large ones. Evidence shows that this is an overestimated value [99,175,176].

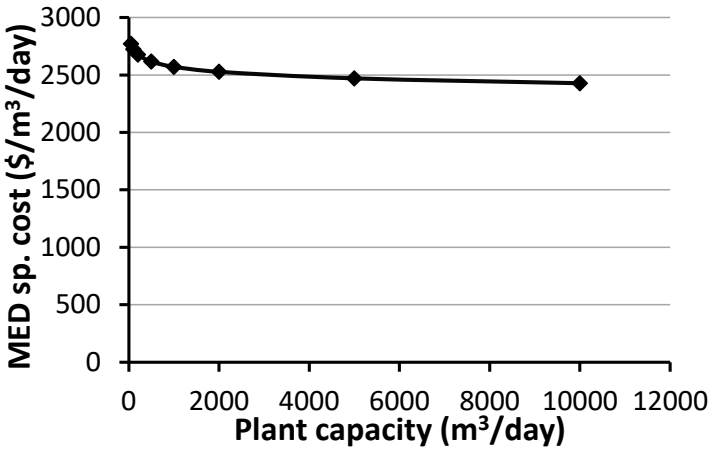

Fig. 2.2. Specific MED cost as a function of plant capacity up to 10,000 m3/day

Equation 2.10 has some other limitations, especially when the MED plant design deviates from the norm (recent designs introduce higher number of effects and/or higher temperatures of heat supply [177], as well as application of MED in fields other than seawater desalination [24]). The most important design parameters with a high contribution on the MED capital cost are the number of effects and the heat exchanger (HEX) area [178], which also define the top brine temperature (TBT).

Here additional elements are introduced in the correlation that take into account design characteristics of MED plants, aiming to increase the accuracy of the MED capital cost estimation. The first step was to apply a detailed MED model that correlates the following parameters with each other:

- Number of effects
- HEX area
- Distillate flow rate
- Heat source temperature

A regression analysis has been then conducted to correlate the HEX area and distillate flow rate with the number of effects, and heat source temperature. Polynomials of up to 4^{th} order have been fitted with accuracy almost 100%. These can be then used for comparative analysis based on a typical reference case.

The next step was to introduce the HEX cost fraction in a similar expression as Eq. (2.10) and use the above polynomials to examine the MED capital cost, when varying the main parameters. This allowed to derive a cost correlation as a function of both distillate flow rate and HEX area, using polynomial fitting.

The final step was to further simplify the cost correlation for quick and reliable estimations of the MED capital cost. The overall result is a general-purpose correlation that includes the impact of the factors having the highest contribution on the MED capital cost, and could be valuable for evaluating the cost of new MED designs and concepts under a large range of operating conditions.

Assessing the MED capital cost

Initially, the validity range of Eq. (2.10) is expanded to a higher plant capacity and approach the average values instead of the conservative ones. Therefore, a detailed literature review has been conducted that gathered various reported MED capital costs, supplemented by data from Desaldata database [23,174,175,179–185]. The available values have been processed and then grouped according to the plant capacity, in order to conclude to a numerical correlation of the MED specific cost similar to Eq. (2.10). Only the plants that are used for municipal fresh water supply are considered (not for power plants or industry). The ones used for dual-purpose have been also excluded. The outcome of this analysis is shown in Fig. 2.3 with a sample of 28 plants.

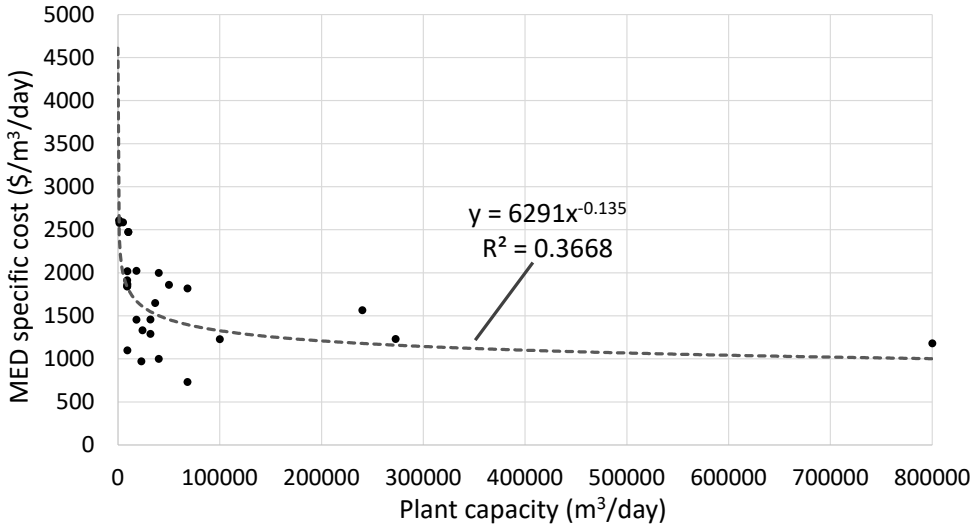

Fig. 2.3. MED specific costs and their fitting as a function of plant capacity

A fitting has been implemented from the data of Fig. 2.3 with a rather low accuracy (R^2 of about 0.37) that captures the trend of the varying capacity. The fitted correlation is given by Eq. (2.11), in \$/(m^3/day), being valid from 500 up to 800,000 m^3/day.

$$C_{MED,fit} = 6291D^{-0.135} \tag{2.11}$$

The outcome of this analysis and the fitted correlation of Eq. (2.11) reveals that for capacity over 4,000 m^3/day, corresponding to a small MED plant, the specific cost can be below 2,000 \$/(m^3/day). On the other hand, for very large MED plants with capacity over 200,000 m^3/day, the specific cost approaches the value of 1,000 \$/(m^3/day), which is in accordance to recently reported data [175].

As shown in Fig. 2.3, there is a large variation of the MED specific cost even for the same plant capacity. This variation reaches even a factor of 2 in extreme cases (values ranging from 1,000 to 2,000 \$/(m^3/day) for about 30,000 m^3/day capacity), causing the low accuracy of the fitting. Site-specific reasons contribute to these reasons, such as the plant location (different country with different market conditions), local labour cost, and feed water characteristics. Other reasons may vary to some extent over time, such as the material cost of the heat exchangers, and the operating/steam costs.

However, one main parameter affecting the cost that can be accounted for is the plant design [186], and especially the different number of effects and temperature of heat input, which bring a large variation to the evaporator's heat exchanger surface area [178].

In an effort to improve the accuracy of the correlation results, especially for cases deviating from the average (in terms of number of effects and heat source temperature), a similar methodology also adopted in Refs. [183,187] is followed. In those studies, the cost correlation has been broken down, introducing weighing factors, to take into account the cost variation of the components with the higher contribution to the capital cost. This method has proved its reliability to estimate the specific cost for various conditions and new designs/concepts [188,189], and is also followed

here. The aim is to decouple the evaporator cost from the other parts of a MED plant, since the evaporator accounts for the highest percentage of the MED capital costs, equal to 40% [190].

For this purpose, a validated numerical MED model has been applied for various operating and design conditions [191]. The results of this model are necessary, in order to identify how the number of effects and heat source temperature affect the HEX area and distillate flow rate, and finally conclude to correlations that introduce the effect of the design parameters to the MED capital cost. This procedure is presented in the next section, with the improved cost correlation further elaborated below.

MED numerical model

A mathematical steady-state MED model has been used [191], with the purpose to conduct multi-parametric studies of the main variables of MED plants. This model follows the standard approach for forward-feed MED plants and is already described with detail in Ref. [177]. The parameters and variables that are primarily examined are:

1. Number of effects, ranging from 3 up to 30. The maximum number is reduced where necessary to ensure that the temperature difference between effects is always over 2.5 °C. The number of effects reaches 30, in order to cover any possible future design option.
2. Heat exchanger area of each effect.
3. Distillate flow rate of each effect.

Other model input and parameters that are kept the same for all cases are:

- Constant heat rate input of 10 MW in the first evaporator.
- The end condenser temperature has been fixed to 35 °C.
- The intake seawater salinity and temperature are 40,000 ppm and 22 °C respectively.
- A terminal temperature difference (TTD) of 3 °C is imposed in the preheater associated with the first effect (temperature difference between the feed at the outlet and the condensing vapor in the preheater). Similarly, a TTD of 3 °C has been assumed at the end condenser.
- The recovery ratio is 38% according to Ref. [192].
- The temperature of the brine and distillate at the outlet of the plate heat exchangers has been considered to be 25 °C.

A regression analysis has been conducted using the results of the numerical model. This analysis concluded to polynomial functions with very high accuracy for the calculation of the distillate flow rate and HEX area only as a function of the heat source temperature, and the number of effects, within the range of the parameters considered here ($60 \leq T \leq 140$ °C, $3 \leq N \leq 30$). The fitted functions are given in Eqs. (2.12) and (2.13) for the distillate mass flow rate and HEX area respectively with a fitting accuracy of R^2=0.9998 and 0.9999. The coefficients of these correlations (a_i and b_i) are given in Tables 2.13 and 2.14 respectively.

$$\dot{m}_D = a_1 + a_2 T + a_3 T^2 + a_4 N + a_5 N^2 \quad (2.12)$$

$$A_{HEX} = b_1 + b_2T + b_3T^2 + b_4T^3 + b_5T^4 + b_6N + b_7N^2 + b_8N^3 + b_9N^4 + b_{10}TN + b_{11}TN^2 + b_{12}TN^3 + b_{13}T^2N + b_{14}T^2N^2 + b_{15}T^2N^3 + b_{16}T^3N + b_{17}T^3N^2 + b_{18}T^3N^3 \quad (2.13)$$

where *T* is the heat source temperature in Celsius degrees and *N* the number of effects.

Table 2.13. Coefficients of Eq. (2.12)

a_1	2. 70073708E+00
a_2	-2.821797340E-02
a_3	1.042603040E-04
a_4	3. 72683709E+00
a_5	-3.081884220E-02

Table 2.14 Coefficients of Eq. (2.13)

b_1	2.68586297E+04	b_{10}	-1.87082017E+02
b_2	-1.33645829E+03	b_{11}	-1.29048221E+01
b_3	2.44770182E+01	b_{12}	4.48279893E-01
b_4	-1.88924088E-01	b_{13}	1.98296987E+00
b_5	5.19451891E-04	b_{14}	7.11095569E-02
b_6	5.51003331E+03	b_{15}	-3.40892197E-03
b_7	7.50418119E+02	b_{16}	-6.58456815E-03
b_8	-1.97732653E+01	b_{17}	-1.06883451E-04
b_9	9.84824917E-03	b_{18}	8.38238282E-06

Proposed MED specific cost correlation

The methodology followed here requires the use of a reference MED plant. The main specifications and capital cost of the reference plant are presented next.

A reference MED plant is considered for the purpose of the developed methodology. Therefore, the main specifications of the reference MED plant are selected based on the most common design options used in MED desalination plants: heat source temperature of 70 °C and 8 MED effects, resulting to a TBT of 65.4 °C. The selection of 8 effects is based on the average number of effects from the reviewed papers relevant to MED plants, and represents a typical configuration that is valid for all locations with cold and hot seawater [193]. The main design specifications for these reference conditions are shown in Table 2.15. It is assumed here that the reported MED cost as a function of only the plant capacity (Eq. (2.11)) corresponds to this reference case.

Table 2.15: Specifications of the reference MED plant

Heat source temperature	70 °C
Number of effects	8
TBT	65.4 °C
Heat input	10 MW
Distillate mass flow rate	29.27 kg/s
Plant capacity	2,531.46 m^3/day
HEX area	8,841.0 m^2
Specific HEX area	302.01 m^2/(kg/s)
Feed water salinity	40,000 ppm
MED specific cost (using Eq. (2.11))	2,185.99 \$/(m^3/day)

The specific cost of a MED plant with the reference conditions as a function of the heat input, ranging from 1 up to 300 MW, is shown in Fig. 2.5.

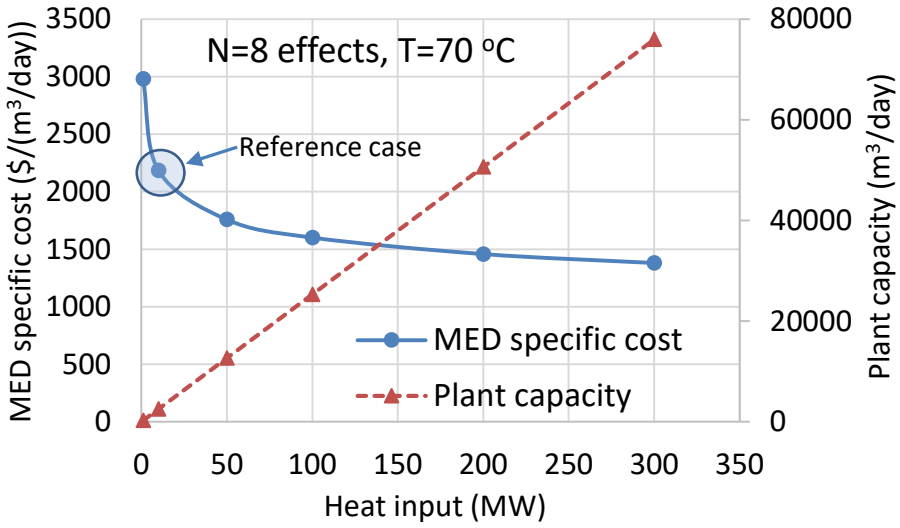

Fig. 2.5. MED specific cost and plant capacity as a function of the heat input amount for the reference case (8 effects, heat source temperature of 70 °C)

The heat input range covers the majority of existing and planned MED plants [23]. In Fig. 2.5 we see that for large plants the specific cost approaches a value of almost 1,350 $/(m^3/day), slightly reducing for very large plants.

The evaporator cost represents a large fraction of the total MED capital cost and therefore its contribution is separated. This decoupling is possible with the use of a weighting factor that represents the typical cost fraction of the evaporator. Thus, the first part of the improved correlation represents the costs of the plant components that depend only on the distillate flow rate (e.g. pumps, intake system, piping, etc.), including any other auxiliary and overhead costs, and its second part the cost of the evaporator, expressed through its HEX area. The general form of the proposed correlation is shown in Eq. (2.14) that includes the ratios of HEX area of the examined MED plant to the reference one, presented in section 4.1.

$$C_{MED} = 6291 D^{-0.135} \left[(1 - f_{HEX}) + f_{HEX} \left(\frac{HEX\ area}{HEX\ area,ref} \right)^{0.8} \right] \quad (2.14)$$

where f_{HEX} is the cost fraction of the evaporator, and the constant of 0.8 is used to take into consideration the plant scale/capacity, as also suggested in other related works [160,181,194]. The term (1-f_{HEX}) expresses the cost fraction of the components that do not depend on the HEX area.

The fraction of the capital cost that corresponds to the evaporator is considered to be 40% [190], as explained previously. However, this fraction could vary when the design conditions or scale/capacity change. The use of an exponent lower than unity reduces this uncertainty. In any case, this is examined in a sensitivity analysis that is presented later-on.

The HEX area of the reference MED plant and the one under consideration (with different design and operating parameters) can be calculated based on the results of the methodology presented in the previous section. The HEX area of the reference plant is given in Table 2.15, while the HEX area of a different design is calculated from the polynomial function given in Eq. (2.13), as a function of the heat source temperature and the number of effects. It should be stressed that both HEX areas should refer to the same heat input. For a variable heat input, the reference area

of Table 2.15 and the MED plant under investigation are adjusted, considering a linear variation (see Fig. 2.5).

The use of Eq. (2.14) allows to conduct parametric analysis for the MED specific capital cost as well, with main parameters the heat input and its temperature, by calculating the distillate flow rate based on the polynomial function given in Eq. (2.12) for a variable number of effects. This is very useful when the operating costs of a MED plant are also considered [195], for estimating the Levelized Cost Of Water (LCOW) [23,166,175], given in $/m^3, which is necessary for any MED plant developer.

Finally, Eq. (2.14) can be simplified by replacing the HEX area ratio with a simpler function of the heat source temperature and the number of effects. In order to do so, non-linear multi-variable regression analysis in Matlab has been conducted with the same MED numerical results. This analysis concluded to a very accurate expression (R^2 equal to 0.9935) as a function of the number of effects (N) and the heat source temperature (T), shown in Eq. (2.15).

$$C_{MED} = 6291 D^{-0.135} \left[(1 - f_{HEX}) + f_{HEX} \left(\frac{N}{N_{ref}} \right)^{1.277} \left(\frac{T_{ref}}{T} \right)^{1.048} \right] \quad (2.15)$$

where N_{ref} is the reference number of effects equal to 8, and T_{ref} the reference temperature of the heat source equal to 70 °C.

The expression of Eq. (2.15) is equivalent to Eq. (2.14) and shows a very small deviation, and both are derived from the processing of the same dataset. Moreover, Eq. (2.15) can be used for the same range of parameters (60 ≤ T ≤ 140 °C, 3 ≤ N ≤ 30) and provides in a more direct way the effect of the MED specific cost with the variable number of effects and heat source temperature presented previously. Finally, from the computational point of view it is less complex to apply Eq. (2.15) than Eq. (2.14) that includes a 4th grade polynomial function.

Validation of the proposed cost correlation

The proposed cost correlation is validated here, using available data of MED plant costs and their main design parameters. This process is not extended, due to lack of available data and the difficulty to find out the number of effects for each plant. Moreover, the validation about the heat source temperature is not examined, since all commercial MED plants operate with a similar temperature, dictated by the limitation of scaling phenomena in the evaporator (TBT up to 70 °C). Therefore, the validation concerns only the variation of the number of effects.

Table 4 shows the MED plants that have been used for validation purposes. Some main specifications are also provided for these plants [178,184,196–198]. Focus is given on having a sample with large enough differences so that the conclusions are as solid as possible. A larger sample of plants would be necessary to increase the confidence of the correlation accuracy.

Table 2.16. MED plants considered for validation purposes

Plant	Country	Capacity (m^3/day)	Number of effects
Al-Hidd	Bahrain	272,760	7

Trapani	Italy	18,000	12
Al-Jubail	Saudi Arabia	800,000	8
Yanbu	Saudi Arabia	68,190	9
Kalba	United Arab Emirates	9,090	4
Layyah	United Arab Emirates	36,368	5
Umm Al-Nar	United Arab Emirates	31,822	6

The specific costs of the plants of Table 2.16 are shown in Fig. 2.6. These include the actual specific cost, according to Desaldata [184], as well as the ones calculated by the standard correlation, Eq. (2.11), and its improvement, Eq. (2.15). The effect of heat source temperature is not included in this analysis, since all plants are considered to operate with the same heat source temperature of 70 °C.

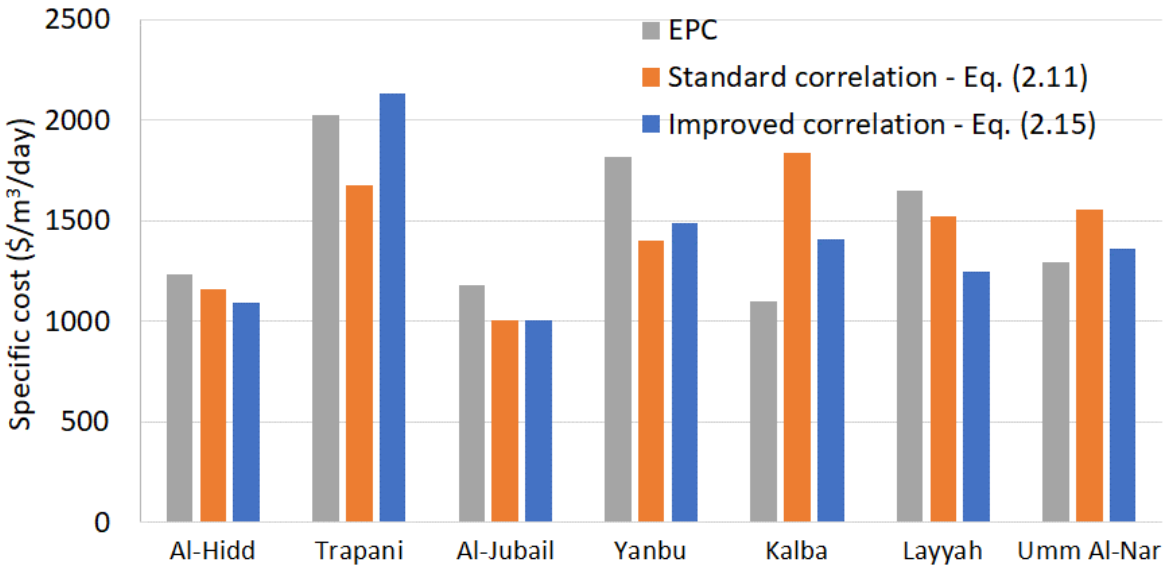

Fig. 2.6. Comparison of calculated MED specific capital cost with EPC costs

From this sample of MED plants, the improved correlation provides more accurate results for most of the plants. More specifically, the small cost difference in Al-Hidd is due to the use of 7 effects, which slightly decreases the specific cost calculated by the improved correlation (by 70 $/m^3/day), but still within a 10% variation. In Trapani and Yanbu, a higher number of effects is used compared to the reference of 8 effects (12 and 9 respectively), with the improved correlation giving higher values, which are closer to the actual specific cost. The MED plant in Al-Jubail has 8 effects (equal to the reference one) and this is why both correlations give the same result, about 15% lower than the actual one. The MED plant in Kalba has just 4 effects, and the improved correlation predicts with much higher accuracy the specific cost, going from a 67%

to 27% deviation from the actual specific price. The Layyah and Umm Al-Nar plants have similar plant capacity and number of effects (5 and 6 respectively), but their actual specific cost deviates by about 350 $/m^3/day. Therefore, it was expected that the improved correlation will show a mixed behavior, approaching the actual specific cost in one case (in Umm Al-Nar) and having a larger difference in the other (in Layyah).

Overall, the improved correlation reduces the deviation with the actual specific cost, and in most of the cases provides more accurate results, with about ±20% difference compared to the actual data, whereas the standard correlation has a higher relative difference. However, many significant parameters and design conditions contribute to these deviations, such as the different top brine and heat source temperatures, any possible intermediate steam extraction (in case of TVC-MED plants) reducing the specific cost, the feed seawater temperature and salinity.

Results

In this section are presented the results when using the improved correlation and they are compared with the ones of the correlation of Eq. (2.11). These results concern the MED specific capital cost for various designs and conditions. These conditions cover the variation of heat source temperature from 60 to 140 °C, and of the MED effects number from 3 up to 30 (the maximum number of effects is restricted by the imposed minimum average temperature difference between effects of 2.5 °C).

A constant number of effects equal to 8 is used (as in the reference case) to examine the effect of the heat source temperature on the MED specific cost. The heat input is equal to 10 MW and its temperature is varied from 60 up to 140 °C. The specific capital cost of a MED plant is shown in Fig. 2.7, using the standard calculation method (Eq. (2.11)) and the ones proposed here (Eqs. (2.14) and (2.15)).

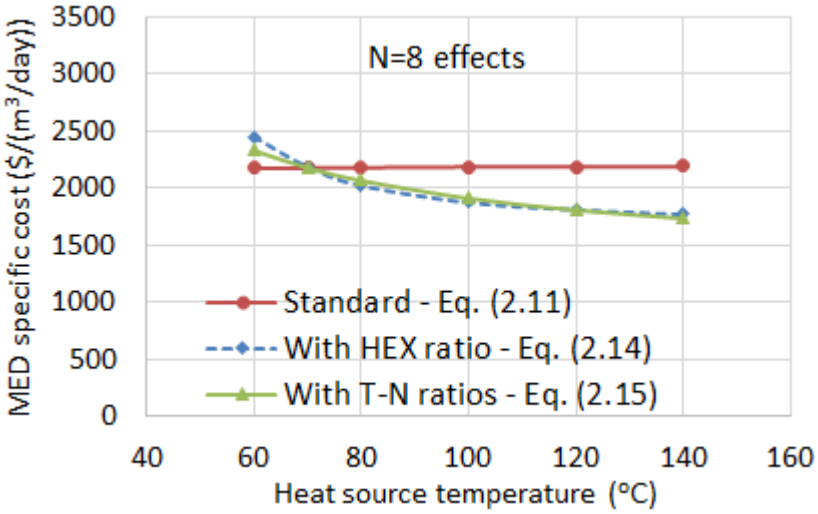

Fig. 2.7. MED specific cost for variable heat source temperature and 8 effects

Using a standard cost correlation, the MED specific cost is about the same for different temperatures, although the HEX area greatly decreases as temperature increases, with the plant capacity being almost the same. Specifically, the HEX area decreases from about 12,400 m^2 at 60 °C, to 9,000 m^2 at 70 °C, and to just 4,000 m^2 at 140 °C. The fact that the specific capital cost according to Eq. (2.11) remains almost constant for such high variation of the HEX area (which should be accounting for about 40% of the capital cost according to Ref. [190]), highlights the limitations of the standard approach [199]. The proposed correlation effectively handles this critical drawback, showing a specific capital cost variation of about 27% between the extreme cases of 60 °C and 140 °C, obtaining a more correct trend. Moreover, the results of the two proposed correlations (Eqs. (2.14) and (2.15)) are very similar and from now on only the calculations of Eq. (2.14) will be shown.

The large cost decrease for higher temperatures fully justifies the recent efforts to increase the MED operation temperature to over 70 °C and reach even 100 °C or higher by avoiding scaling phenomena in the evaporator [200]. This is the reason that in the present study such large temperature range has been considered. However, when operating at higher temperature, it is a common practice to use more effects, which has been shown to increase the specific cost. For the same temperature, there is a one-way relation of number of effects with HEX area. In Fig. 2.8 is shown the MED specific cost for a variable number of effects and heat source temperatures using the standard correlation and the one proposed here.

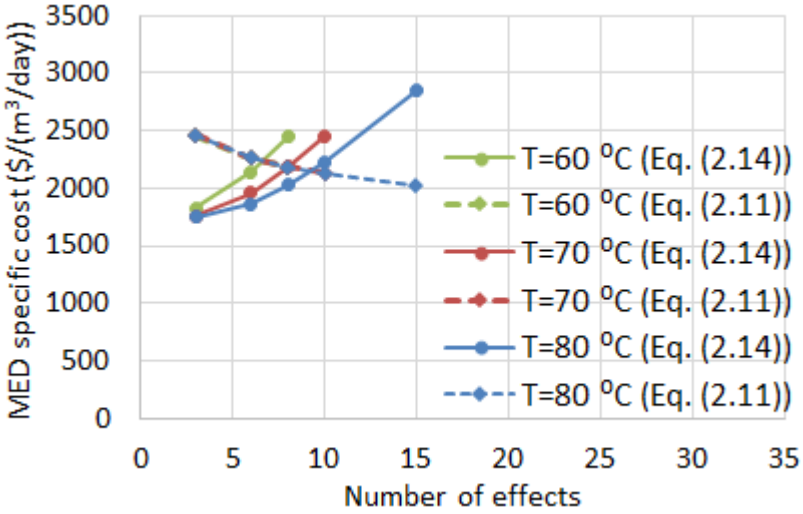

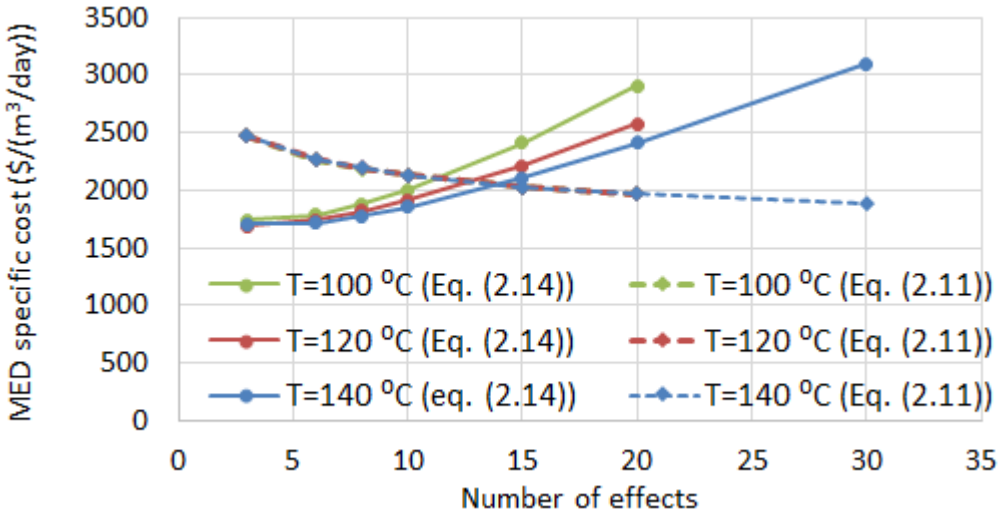

Fig. 2.8. MED specific cost for variable number of effects and heat source temperature (top: 60-80 °C, bottom: 100-140 °C)

For the same heat source temperature, a higher number of effects brings an increase to the specific cost, due to the increase of the required HEX area. The resulting effect is similar to the one presented in Ref. [178]. The standard correlation always predicts lower specific cost for increasing number of effects, due to the increase of the distillate flow rate, which is not a reliable outcome due to the higher HEX area for more MED effects, while the proposed correlation effectively overcomes this limitation.

2.6.4 MD capital cost parameters

The capital cost parameters of the MD regeneration and its parts are shown in Table 2.17.

Table 2.17: Capital cost parameters of MD

Nr	Cost parameter	Units	Calculation method
1	MD pump specific cost	€/kW$_p$	Correlation as a function of pumping power (see Table 2.11).
2	MD pump cost	€/pump	Parameter nr. 1 multiplied by the pumping power.
3	HEX specific cost	€/m^2	A standard value of 1800 €/m^2 is used [201].
4	HEX cost	€	Parameter nr. 3 multiplied by the total HEX surface.

5	Membrane module specific cost	€/m^2	The specific cost of the complete membrane module, used in the sensitivity analysis and for the extraction of future scenarios.
6	Membrane module cost	€	Parameter nr. 5 multiplied by the total membrane surface.
7	MD cost	€	The sum of the membrane module, HEX and pump costs (parameters nr. 2, 4, and 6).

2.6.5 Capital cost parameters of the thermolytic cost regeneration

The capital cost parameters of the thermolytic salts regeneration system are based on the technical parameters of the column, the shell and tube HEXs, the reboiler HEXs, and the pumps. These parameters are taken from a recent selection and design report [202], which provides detailed correlations of chemical process equipment, based on their main parameters and specifications. These correlations also consider the sizing of each component, in order to introduce this factor in the calculations.

The heat exchanger and reboiler costs are calculated according to their surface, materials, and capacity, while the pumps according to their flow rate, type, materials (depending on the handling fluids), and capacity. The distillation column cost depends on its dimensions (height, diameter), material, and packing volume and type.

These specifications defined through the process simulator [36] and are used in the cost calculations here. Further details of sizing this regeneration unit are provided in Section 3.

2.6.6 Auxiliaries capital cost parameters

The capital cost parameters of the auxiliaries are shown in Table. 2.18.

Table 2.18: Capital cost parameters of the system auxiliaries

Nr.	Cost parameter	Units	Calculation method
1	Civil & electrical infrastructure costs	€	Specific cost for Civil & electrical infrastructure multiplied by net power production.
2	Salt cost	€	Calculated from the specific cost of salt multiplied by the total salt amount.
3	Piping specific cost	€/kW$_e$	Correlation as a function of piping dimensions [172] (average diameter, length): $Piping\ sp.cost = 0.897 + 0.21(Pipe\ av.diameter)1000(Pipe\ length)/P_{net}$
4	Piping cost	€	Calculated from parameter nr. 3 multiplied by the net power production.

2.7 Running cost parameters

The running cost parameters of the system are defined here, relevant to operation and maintenance costs, as well as the heating costs in case the necessary heat is purchased. The running cost parameters that are included in the analysis are shown in Table. 2.16.

Table 2.19: Running cost parameters

Nr.	Cost parameter	Units	Description and calculation/estimation method
1	Operating costs	€/year	Costs including personnel cost, consumables and materials and indirect costs. Calculated by the expression: $(4000(P_{net})^{0.5})$, derived from data in [203]
2	Membranes replacement factor	%	Calculated according to the number of RED membrane replaced during the plant lifetime. It is included in the sensitivity analysis.
3	Maintenance cost (for RED membranes replacement)	€/year	Calculated according to the total RED membrane surface and the membrane replacement factor (parameter nr. 2).
4	Maintenance labour cost	€/year	Calculated according to the membranes replaced each year and an estimated labour effort per stack equal to 20 €/stack.
5	Heating costs	€/year	Running cost for heat supply based on the specific cost and amount required per year.

3. Cost results and evaluation

This section includes a detailed cost analysis, broken down in three subsections, one for each regeneration technology. The combination of RED with MED is presented first. This analysis is carried out in detail, identifying the most promising set-ups, mainly concerning the RED specifications. Then, the most promising RED specifications identified are used for the other regeneration technologies as well, in order to focus on the most cost-effective solutions without repeating all calculations. For each case, a parametric analysis is conducted for evaluating the effect of various parameters, focusing mostly on the system capacity, which is given as a function of the number of RED stacks.

3.1 RED-MED financial performance

The RED-MED cost model results are included in a paper that is under submission:

M. Papapetrou et al "Environmental and techno-economic analysis of the RED Heat Engine"

3.1.1 RED-MED reference case

A RED-MED reference case is introduced and analysed, presenting all relevant results. This case will be used as benchmark in the next sections, where the effect of various parameters will be examined, including the sensitivity analysis and future scenarios. The main (reference) design data are given next:

- Cell pairs per stack: 1000
- Membrane geometry ratio (length/width): 4
- Number of MED effects: 26
- Heat source temperature: 100 ^{o}C

The technical specifications of the reference case are shown in Table 3.1 with MED as the regeneration technology and using current membranes. The RED specific costs are referred to the year 2020, and the temperature of the heat input is 100 ^{o}C.

Table 3.1: Technical specifications of the reference RED-MED Heat Engine

Nr.	Specification	Value	Units
1	Number of stacks	500	-
2	RED pump power	4.77	kW
3	Power production, gross	224.4	kW
4	RED piping length	1,262.75	m
5	Working fluid amount	239.70	kg

6	Amount of salt	35.19	kg
7	MED total pump power	93.36	kW
8	MED HEX surface	111,065.57	m^2
9	MED distillate flow rate	470.81	m^3/h
10	Heat input (at 100 °C)	11,815.0	kW
11	Net power production	126.28	kW
12	Thermal efficiency	1.07	%

According to the methodology presented in Section 2, the capital cost of the reference case is presented in Table 3.2.

Table 3.2: Capital cost of the reference RED-MED Heat Engine

Nr.	Costs	Cost (€)
1	RED stacks (including membranes, casing, electrodes)	6,589,221
2	Pumps for RED	1797
3	Inverter for RED	13,207
4	Pumps for MED	12,327
5	MED unit	20,446,891
6	Heat supply (solar, geothermal)	0
7	Civil and electrical infrastructure	31,568
8	Piping	4,500
9	Salt of working fluid (NaCl)	7
	Total:	**27,087,193**

The total system cost is about 27 million € and corresponds to a specific cost of 214,000 €/kW, which is much higher than other heat-to-power conversion units, such as the ORC which shows a cost of about 2,500-3,000 €/kW for the same scale and heat source temperature [204,205]. The main reasons for this are the low thermal efficiency and the large MED size that leads to a very high MED cost. The cost break-down of the system capital cost is shown in Fig. 3.1.

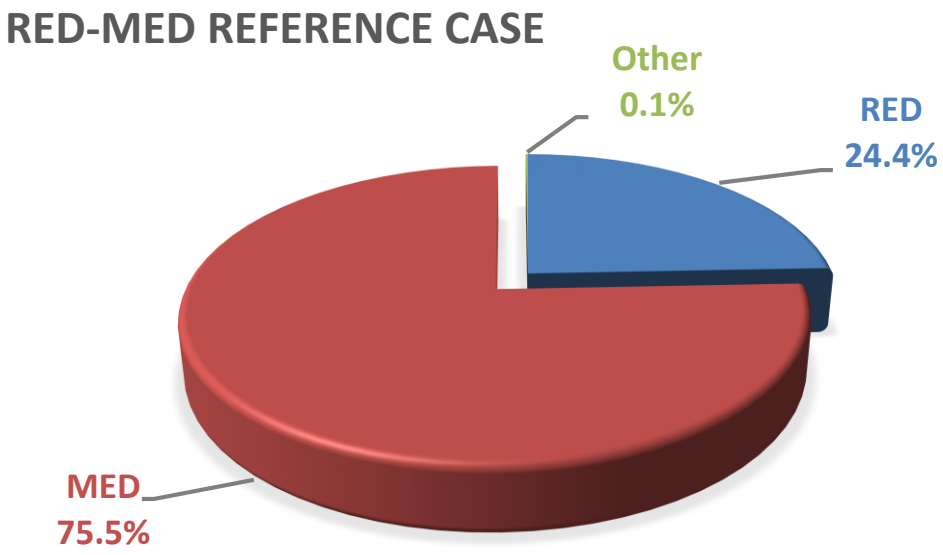

Figure 3.1: Cost break-down of the RED-MED reference case

The total cost is mostly divided between the MED (about 76%) and the RED (about 24%) with the other parts having a negligible contribution of 0.1%. The other parts include mostly the civil and infrastructure cost and the piping cost.

The annual balance that includes the income from the electricity sales and all running costs (maintenance, operating, etc.) is presented in Table 3.3.

Table 3.3: Annual balance of the reference RED-MED Heat Engine

Nr.	Annual cash flows	Annual cash flow (€/year)
1	Maintenance for membrane replacement (membranes)	500,000
2	Maintenance for membrane replacement (labour)	667
3	Operating costs	44,948
4	Heating costs	0
	Annual running costs:	**545,615**
5	Income from electricity sales	99,555
	Annual income:	**99,555**
	Annual (net) balance:	**-446,060**

The financial performance of the reference case is not sustainable, since the annual balance is negative, bringing losses during operation, and does not recover the initial investment cost presented in Table 3.1. In this case no payback period is reached, even if the system lifetime is expanded. This is clear from the cumulative cash flows during the whole lifetime of about -35 million €, which include both annual cash flows and investment cost. The annual balance and cumulative cash flows during the system lifetime are shown in Figs. 3.2 and 3.3 respectively.

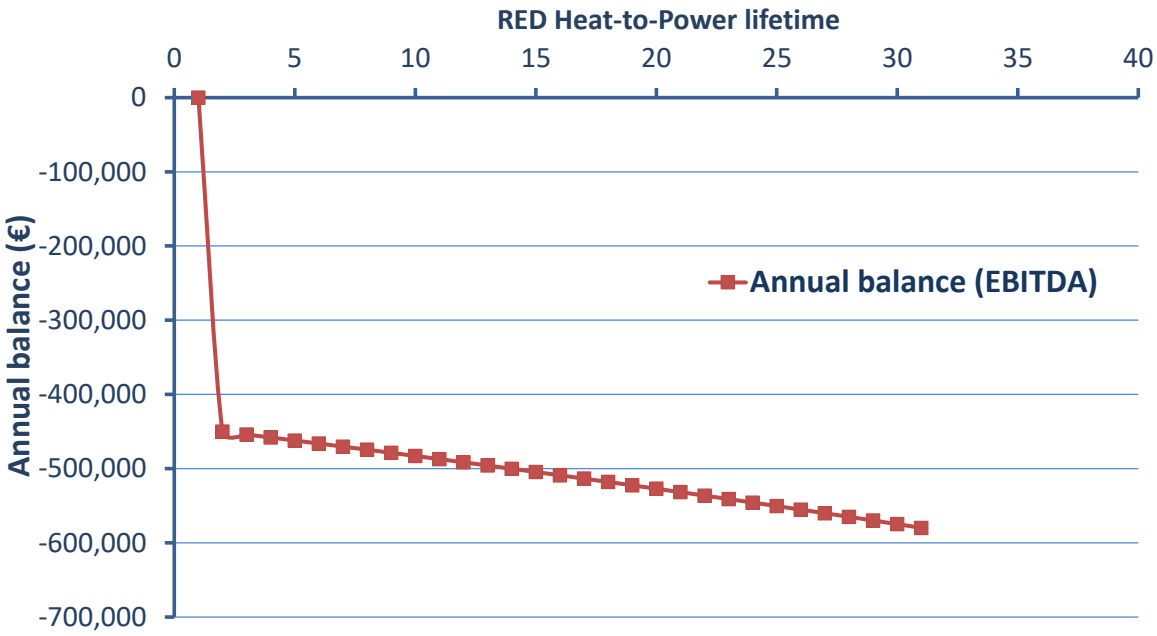

Figure 3.2: Annual balance during the system lifetime of the RED-MED reference case

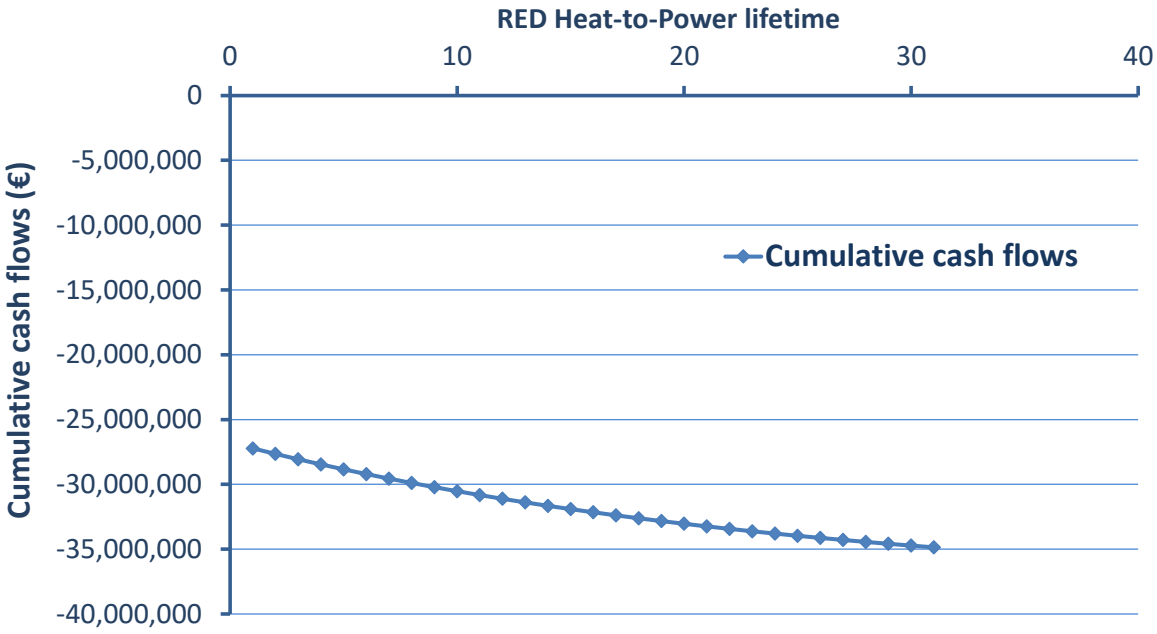

Figure 3.3: Cumulative cash flows during the system lifetime of the RED-MED reference case

The annual balance is not constant due to the discount rate and inflation parameters that have been considered in this analysis. For year 1 the annual balance is equal to the one presented in Table 3.3 (equal to -446,000 €/year), which is then decreased and reaches almost -600,000 €/year. These conditions lead to a **LCOE value of 2.252 €/kWh**, which is not competitive.

Even if the size/capacity of the plant is increased by using more RED stacks, the system is not cost-effective, although the LCOE decreases by almost 25% when increasing its size by about 10 times, as shown in Fig. 3.4.

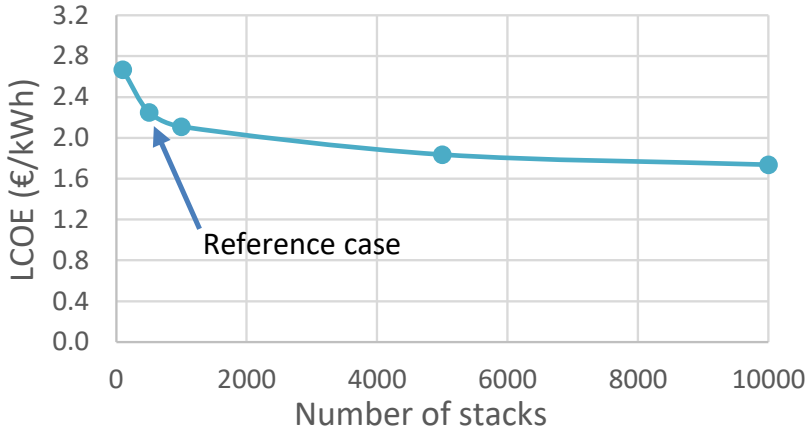

Figure 3.4: LCOE of the reference RED-MED case as a function of the number of RED stacks

Although the economics of the reference case presented are not sustainable from the financial point of view, this is a system in very early stages of development and the focus has been on exploring alternatives and identify the direction of development towards the goal of a cost-competitive LCOE value.

For that purpose, the effect of various parameters have been examined, in order to evaluate the current, but mostly the future, perspectives of this technology, as a promising alternative to the standard one for low-temperature heat exploitation, which is the ORC technology [206]. Two different types of RED membranes have been examined: the current ones and the future ones, as described in the introduction to this thesis (section 3.2). The analysis is provided for both membrane types, and including the effect of various parameters, with the future membranes expected to have higher efficiency, increasing the competitiveness of this technology. The effect of various design parameters is examined as well, such as the cell pairs per stack, membrane geometry, number of MED effects, temperature of heat input, and the system sizing/capacity.

The effect of the above system parameters on financial performance of the RED-MED case is presented next, using the LCOE as criterion.

3.1.2 RED-MED with current membranes

As mentioned before, the reference case efficiency of 1% for a heat source temperature of 100 ^{o}C is very low. For comparison the ORC technology that an efficiency of about 4-5% for the same temperature level [207]. The main limitation on increasing the efficiency of the Heat Engine

further is the performance of the ion exchange membranes. Still, in this section we stick with the current membranes and explore first the effect of various other parameters, in order to identify the best design of the system when using current membranes. Within the analysis, the reference case of section 3.1.1 is highlighted for comparison.

Effect of cell pairs per stack

The number of cell pairs per stack is varied from 500 up to 10000, with a reference value of 1000. This effect on LCOE is shown in Fig. 3.5.

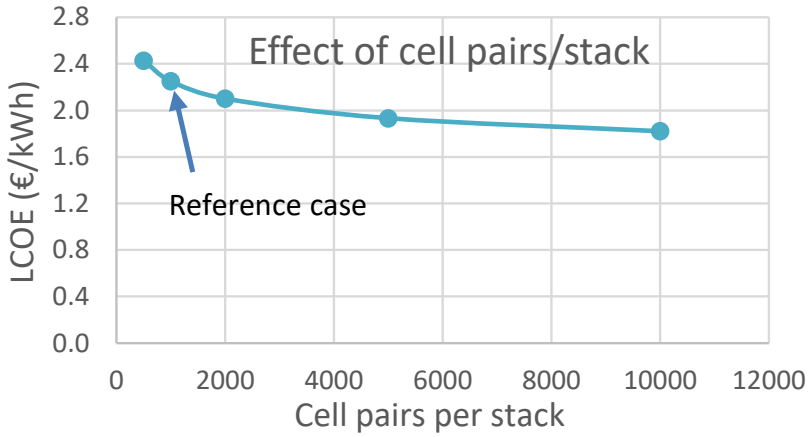

Figure 3.5: Effect of cell pairs per stack on LCOE for the RED-MED with current membranes

As the number of cell pairs increases, the power production of each stack also increases. Therefore, the trend shown in Fig. 3.5 is similar to the effect when changing the number of stacks/size of the system. Therefore, the actual improvement of the financial performance with the varying number of cell pairs is negligible, since for the same net power production, the differences of LCOE are below 1%. Moreover, thermal efficiency is kept constant for all cases and equal to 1.07%.

For very high number of cell pairs, operational limitations can occur, such as high pressure losses (greatly increasing the pumping power). Therefore, the reference value of 1000 cell pairs per stack can be considered as fixed in the following sections, as the LCOE value does not depend on this parameter.

Effect of RED membrane geometry

The length and width of the RED membrane geometry is varied with their ratio ranging from 0.1 up to 16. The effect of this ratio on the LCOE is shown in Fig. 3.6.

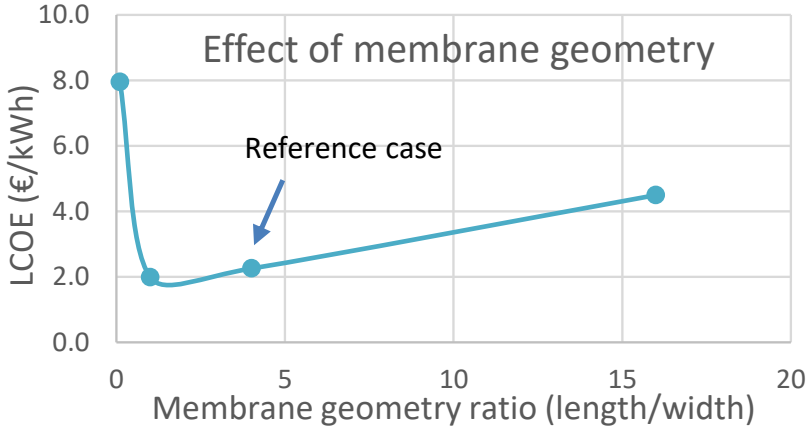

Figure 3.6: Effect of membrane geometry on LCOE for the RED-MED with current membranes

A membrane geometry ratio in the range of 1-4 maximizes the thermal efficiency, as also shown in [36], and at the same time brings a very low LCOE. The effect of the geometry on the financial performance is very clear and a constant ratio of 4 will be kept from now on.

Effect of number of MED effects

As presented previously, the cost of the regeneration represents a very large fraction of the total capital cost. Therefore, there are significant efforts on reducing this cost and making the system more cost-competitive. The main modification to the MED that decreases the cost is by reducing the number of effects. Figure 3.7 shows the effect of the number of MED effects on LCOE.

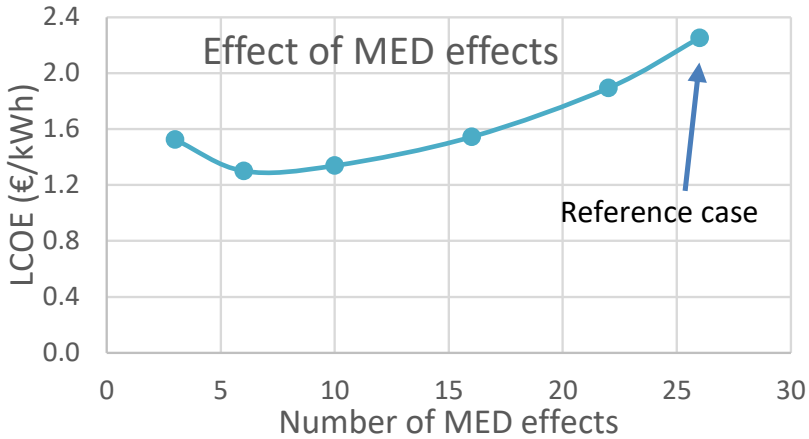

Figure 3.7: Effect of number of MED effects on LCOE for the RED-MED with current membranes

Up to now, 26 MED effects have been considered because the high number of effects leads to the highest thermal efficiency. However, it is very clear in Fig. 3.7 that this number maximizes the LCOE as well. By reducing the number of effects to 6, the thermal efficiency is reduced from 1 to less than 0.5%, but at the same time the LCOE is reduced by almost 2 times. The net power production is about the same in both extreme cases, but the required heat input is increased.

For even lower number of effects equal to 3, the LCOE increases again. Therefore, an optimized condition exists that minimizes the LCOE. The critical conclusion is that it is preferable to use few effects so as to reduce the LCOE in case there is a source with adequate heat amount, with the aim to maximize the financial performance.

3.1.3 RED-MED with future membranes

For the future membranes the same trends are examined as for the current ones, and additionally the variation of the heat source temperature (from 60 up to 140 °C) is investigated, in order to cover as many applications as possible.

Effect of heat source temperature

The effect of the temperature on the LCOE is presented in Fig. 3.8. The parameters of this case are the same as in the reference case with the only difference the use of the future membranes and the variation of the heat source temperature (a ratio of membrane geometry is equal to 4 and 1000 cell pairs per stack are considered). For 60 and 80 °C, less MED effects are used (14 and 20 respectively), due to constraints to the temperature difference of each effect.

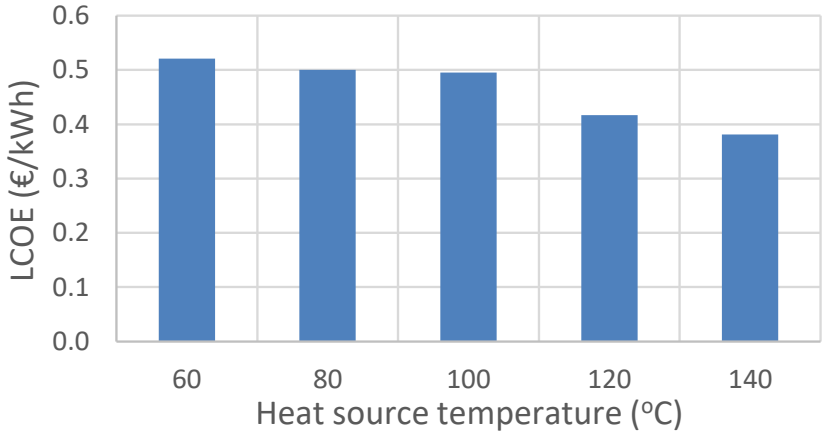

Figure 3.8: Effect of heat source temperature on LCOE for the RED-MED with future membranes

As the source temperature increases, the LCOE decreases, due to the decrease of the MED cost, which has a very high contribution on the total cost, as presented in the previous section. Even if at 60 and 80 °C less MED effects are used, decreasing the MED capital cost, this is not adequate to keep a lower LCOE value than at higher temperature. For the higher temperatures (over 100 °C), 26 MED effects are considered in all cases, reaching a thermal efficiency of up to about 15.5% for 140 °C. For all cases, the gross power production of the RED stacks is the same, while the pumping power is slightly higher for higher temperatures. This leads to a slightly lower net power production for high temperatures, with reduced heat input.

Effect of cell pairs per stack

The number of cell pairs per stack is again varied from 500 up to 10000. This effect on LCOE is shown in Fig. 3.9 for various heat source temperatures.

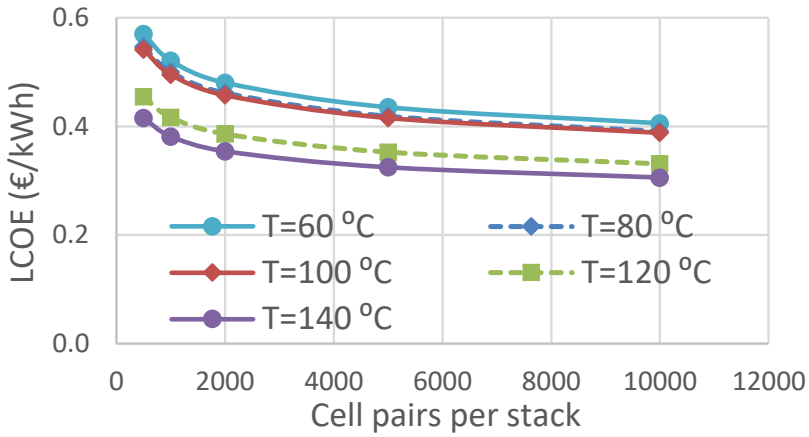

Figure 3.9: Effect of cell pairs per stack and heat source temperature on LCOE for the RED-MED with future membranes

A similar trend as with the current membranes is observed. Moreover, as the heat source temperature increases, the LCOE decreases. The main conclusion reached here is the same as with the current membranes that the reference value of 1000 cell pairs per stack can be used, since this parameter does not affect the financial performance and ensures a trouble-free operation to the membranes.

Effect of RED membrane geometry

The ratio of length to width of the RED membrane is varied from 0.1 up to 16. The effect of this ratio for various heat source temperatures on the LCOE is shown in Fig. 3.10.

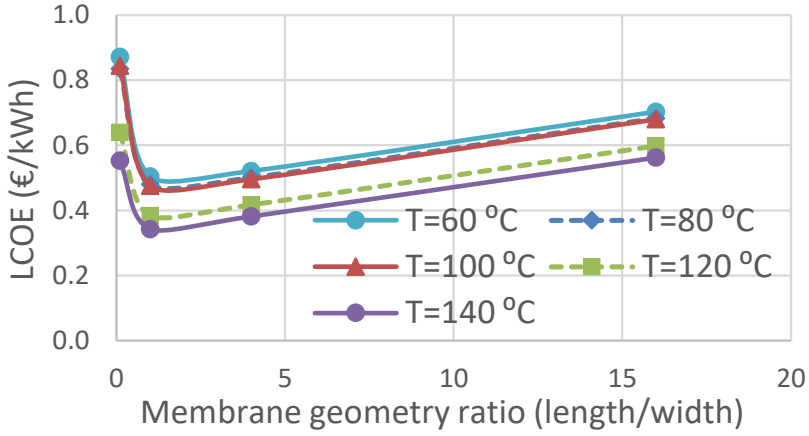

Figure 3.10: Effect of membrane geometry and heat source temperature on LCOE for the RED-MED with future membranes

The main conclusion here is that for high geometry ratio the LCOE shows a smoother increase compared to the case with the current membranes. But again the ratio within the range of 1-4 minimizes the LCOE and fully justifies the selection of the ratio equal to 4.

Effect of number of MED effects

Reducing the number of MED effects, did have an important impact on LCOE as we have seen in Fig. 3.7, where current membranes were used. Figure 3.11 shows the effect of the number of MED effects on LCOE, which is similar to the one seen before. In Fig 3.11 is shown the effects also for different waste heat temperature levels and it is noticed that for higher temperatures, the effects of lower LCOE for lower number of MED effects is still valid, but less pronounced. In Fig. 3.12, we can see that by lowering the number of MED effects, the efficiency of the RED Heat Engine decreases as well.

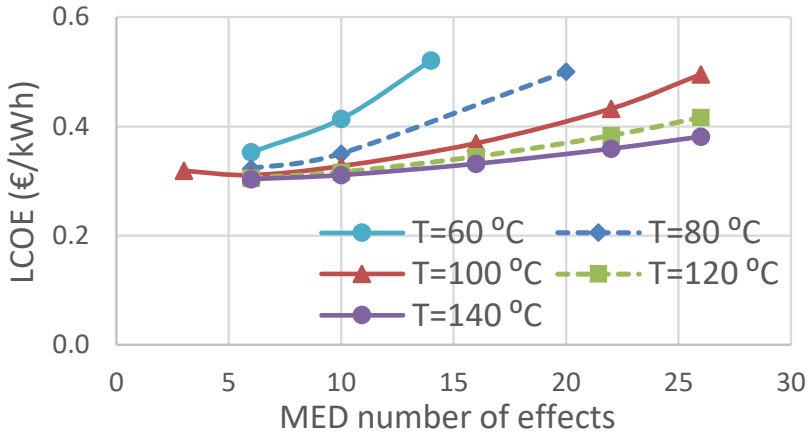

Figure 3.11: Effect of number of MED effects and heat source temperature on LCOE for the RED-MED with future membranes

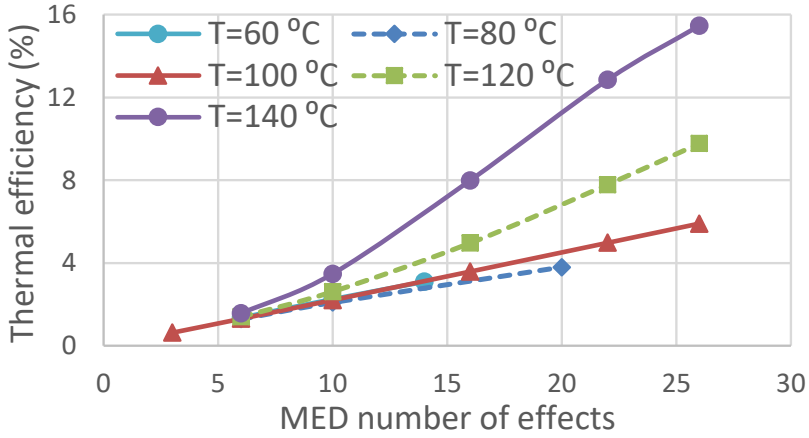

Figure 3.12: Effect of number of MED effects and heat source temperature on thermal efficiency for the RED-MED with future membranes

By using 6 MED effects, the LCOE is decreased to about 0.31 €/kWh, being very similar for all heat source temperatures. This is a crucial advantage of this technology, making it possible to exploit very low heat sources, with the potential to limit the LCOE. At the same time, the thermal efficiency converges to about 1.3%. It becomes clear here, that there is a trade-off between performance and cost. This is presented in Fig. 3.13, indicating the use of less MED effects.

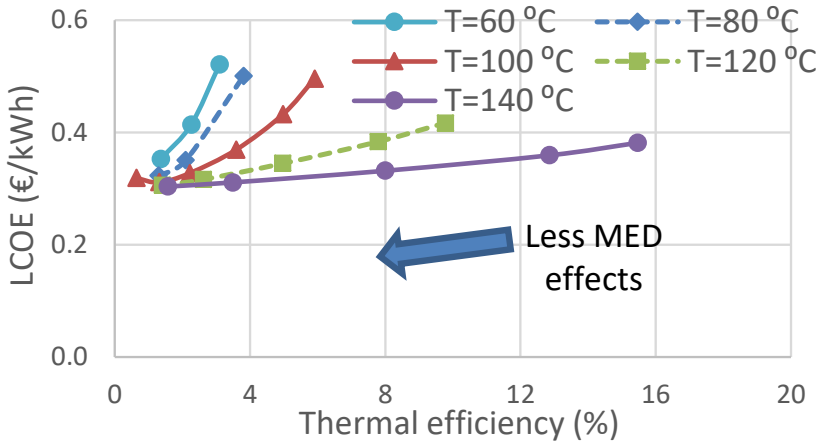

Figure 3.13: Thermal efficiency-LCOE trade-off for various heat source temperatures and number of MED effects for the RED-MED with future membranes

In order to reach a low LCOE value, it is necessary to design the MED configuration with few MED effects, especially at low heat source temperatures. This leads to low thermal efficiency of about 1.3%, which is about the same for all heat source temperatures. On the other hand, very high thermal efficiency can be reached, even 15.5% for a heat source temperature of 140 °C and 26 MED effects, which is much higher than alternative heat to power technologies, such as the ORC that shows thermal efficiency of about 10% for the same temperature range [208]. Finally, for 140 °C the LCOE does not show an important increase when using more MED effects and efficiency is increased, making it possible to obtain both high performance and low/moderate LCOE at the same time.

Effect of number of RED stacks

The number of RED stacks defines the system capacity, as explained previously. This effect has been presented in the previous section for the RED-MED reference case (Fig. 3.4), and is also shown here when using future membranes. A case similar to the reference one is examined (heat source temperature of 100 °C, 26 MED effects, etc.), with the only difference the use of future membranes. The LCOE values as a function of the number of RED stacks is shown in Fig. 3.14.

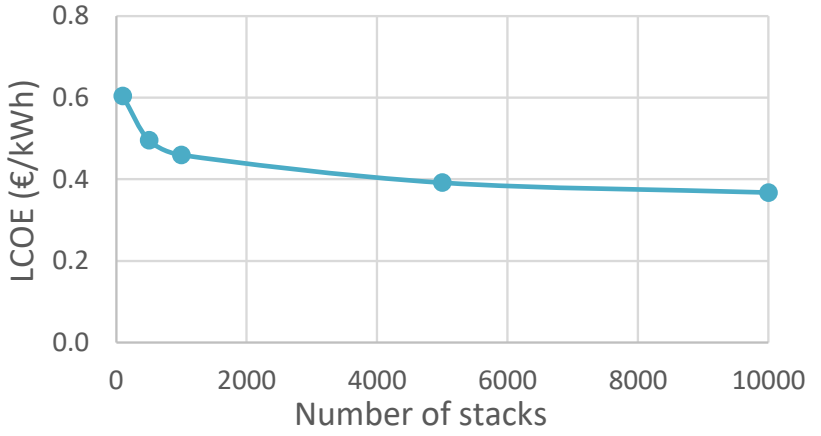

Figure 3.14: LCOE of the RED-MED with future membranes as a function of the number of RED stacks

For very large plants the LCOE is reduced by about 25% compared to the standard case with 500 RED stacks (net power capacity of 728 kW), reaching LCOE values of 0.37 €/kWh. On the other side, when reducing the number of stacks from 500 to 100, the LCOE increases by about 22%.

3.1.4 Cost break-down of various cases

The capital cost break-down of the RED-MED reference case has been presented in Fig. 3.1. Here, focus is given on the break-down of both capital and running costs for some representative cases, which are the following:

- The RED-MED reference case with current membranes (T=100 °C, 26 MED effects).
- The above case but with future membranes (T=100 °C, 26 MED effects).
- RED-MED with future membranes at T=60 °C and 6 MED effects.
- RED-MED with future membranes at T=100 °C and 6 MED effects.
- RED-MED with future membranes at T=140 °C and 6 MED effects.

Capital costs

The capital cost break-down for the above representative cases is presented in Fig. 3.15, divided into RED, MED and other capital costs.

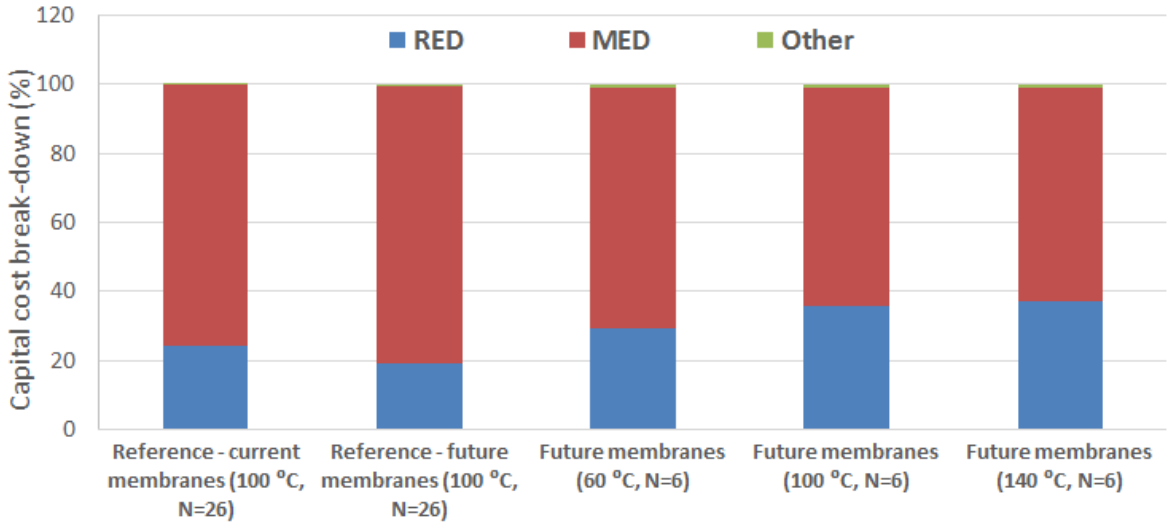

Figure 3.15: Capital cost break-down of representative RED-MED cases

In case 26 MED effects are used with either current or future membranes, the MED cost fraction represents 75-80% of the total one. This is the main reason that less MED effects are favoured, in order to greatly reduce the total capital cost. For 6 MED effects, the situation is more balanced, with the MED cost fraction reducing to about 60-65%. In all cases, the contribution of the other costs is very low and up to 1.1%.

Running costs

The contribution of the different parts to the running costs is examined through their effect on the LCOE, for the above five representative cases. The effect of capital and running costs on the LCOE is shown in Fig. 3.16.

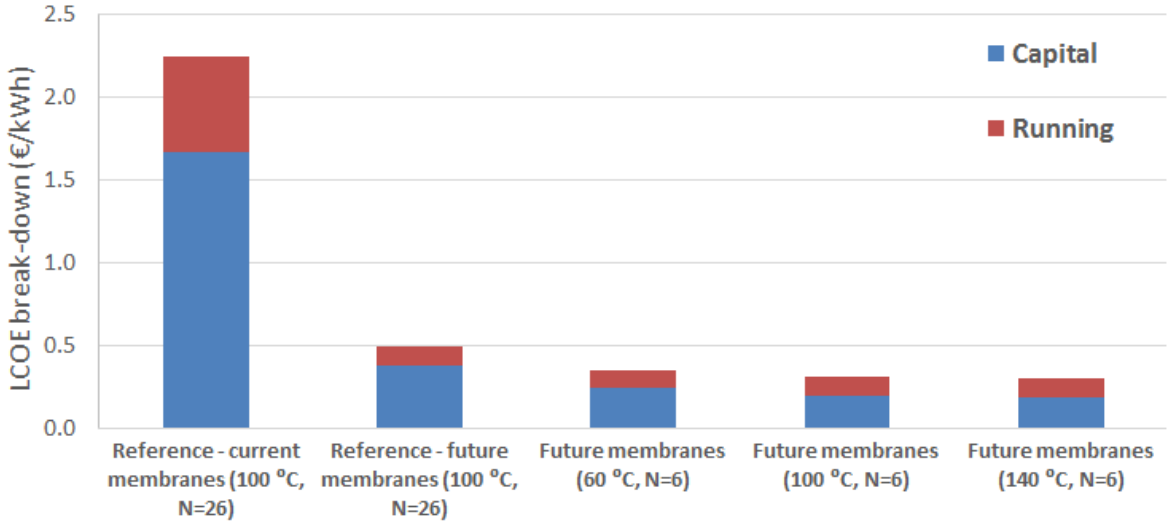

Figure 3.16: Capital and running cost break-down through the LCOE of representative RED-MED cases

The higher contribution to the LCOE is from the capital cost. This outcome was expected due to the high capital cost of the RED-MED configuration, even when the future membranes are considered. When considering the future membranes, the LCOE part of the running costs is the same and equal to about 0.11 €/kWh (about 35% of the total one when using 6 MED effects), even if the membrane replacement is included. This value is low and fully justifies one of the core advantages of this technology of low maintenance needs and low operational costs.

3.1.5 High temperature RED-MED with future membranes and NaCl

In an effort to increase the performance, while keeping about the same capital cost, the use of warmer solutions in the RED stack has been examined. This set-up assumes the preheating of the concentrate (two cases of 50 and 80 °C have been examined) enhancing the RED stack performance and is referred to as "*high-temperature RED-MED*". The system performance data are taken from the process simulator [36], as was the case with all system performance data in this thesis. The same cost analysis model is used as previously, with the only addition the cost of the two reheaters that are necessary, with a typical specific cost of 150 €/kW [202].

A case similar to the reference one is examined, with a heat input at 100 °C, keeping the same RED system specifications (e.g. cell pairs per stack), while the results are analysed for two number of MED effects, equal to 6 and 21, and two reheating temperatures. The effect of the number of effects on LCOE for this high-temperature RED-MED configuration with NaCl is shown in Fig. 3.17. The LCOE of the case operating at the standard temperature of 25 °C is also shown for reference and to reveal the added benefits that come from this configuration.

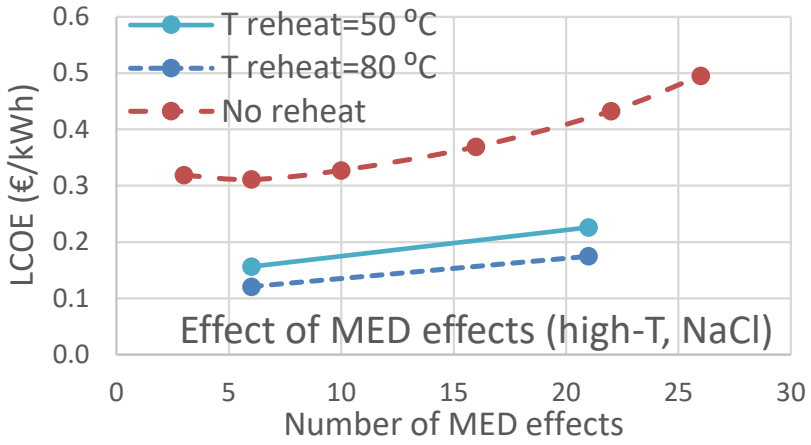

Figure 3.17: Effect of number of MED effects on LCOE for the high-temperature RED-MED with future membranes and NaCl

With the increase of the number of MED effects, a small increase of the LCOE is introduced. For all cases with reheating, the LCOE is much lower than the previous ones for the standard RED-MED, which showed a lowest LCOE value of 0.31 €/kWh. The LCOE here reaches even 0.12 €/kWh for 6 MED effects. The reheating temperature has a small effect on the LCOE. Moreover, the thermal efficiency is greatly enhanced, from 1.3% for the same conditions without reheating to over 2% for 6 effects, and reaching even 8% for the case with 21 MED effects. This is mostly attributed to the performance enhancement of the RED stacks.

The effect of the plant size on the LCOE, as a function of the number of RED stacks, is shown in Fig. 3.18 for both reheating temperatures, and for 6 MED effects.

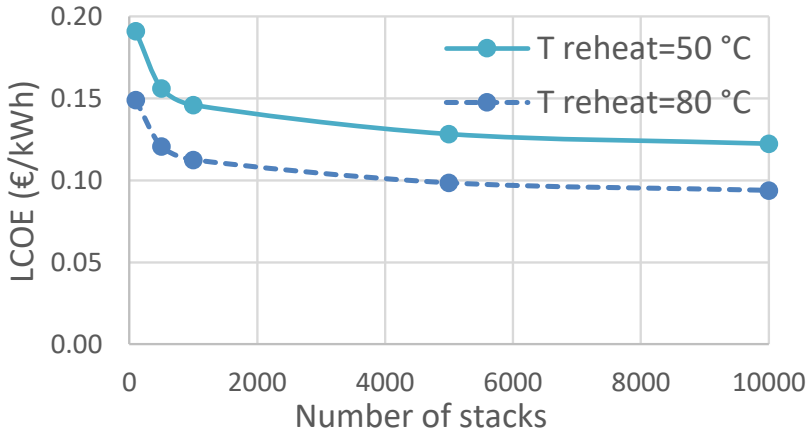

Figure 3.18: LCOE of the high-temperature RED-MED with NaCl and future membranes as a function of the number of RED stacks

The LCOE is further reduced for larger plants, than when using 500 stacks (net capacity of 1.9 MW). The trend is exactly the same between the two cases with different reheating temperature. The LCOE of a plant with 100 stacks (net capacity of 380 kW) is still low, in the range of 0.15-0.19 €/kWh in 2020, making it possible to reach competitive costs even for small-scale systems in 2030 or after that.

3.1.6 RED-MED with future membranes and KAc

Another very promising configuration is to use potassium acetate instead of NaCl. This set-up has been examined in the RED Heat-to-Power project and very promising results have been obtained concerning the performance of this configuration. Here, the relevant technical input has been processed, in order to identify whether the superior performance leads also to a reduced LCOE.

The heat source temperature is assumed again to be 100 °C and three operating temperatures of the RED part are considered, at 25 °C (no reheating), 50 °C and 80 °C. A power plant with 500 RED stacks is used. The maximum number of MED effects is restricted to 16 for operation at 25 °C, reducing to 11 with reheating, in order to respect the minimum temperature difference between the effects. The LCOE of the RED-MED with future membranes with KAc is shown in Fig. 3.19.

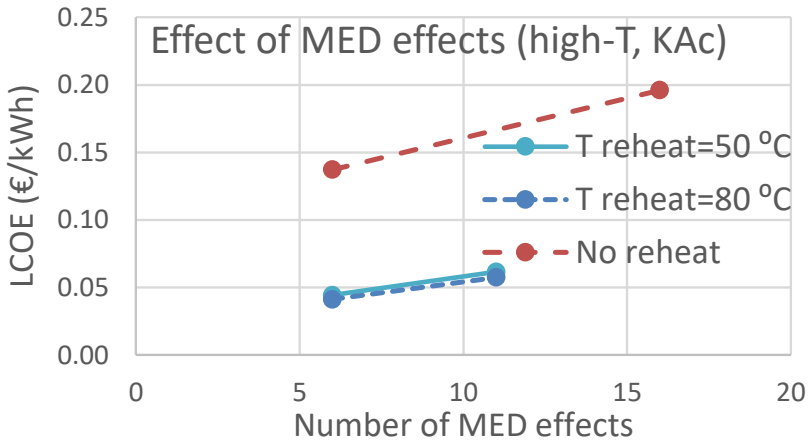

Figure 3.19: Effect of number of MED effects on LCOE for the high-temperature RED-MED with future membranes and KAc

The LCOE is greatly reduced by reheating the KAc solution, while the reheating temperature has a negligible effect on the LCOE, which additionally follows the same trend for varying the number of MED effects. With this configuration it is possible to reduce the LCOE up to about 0.05 €/kWh in 2020 for a 500-RED stack power plant (net power capacity of about 8 MW). This LCOE is the lowest observed among the different RED-MED set-ups, as well as among the other regeneration technologies presented in the next sections, and reveals the potential of this technology.

Since the power production of each stack is high, the effect of the plant size is also examined here. The range of the stack number is expanded to include also lower numbers (as low as 10 stacks, which corresponds to net capacity of 29.1 kW without reheating, 160-172 kW with reheating), to cover the whole range of possible applications. The number of MED effects is 6 and the LCOE results as a function of size are shown in Fig. 3.20 with no reheating and two reheating temperatures.

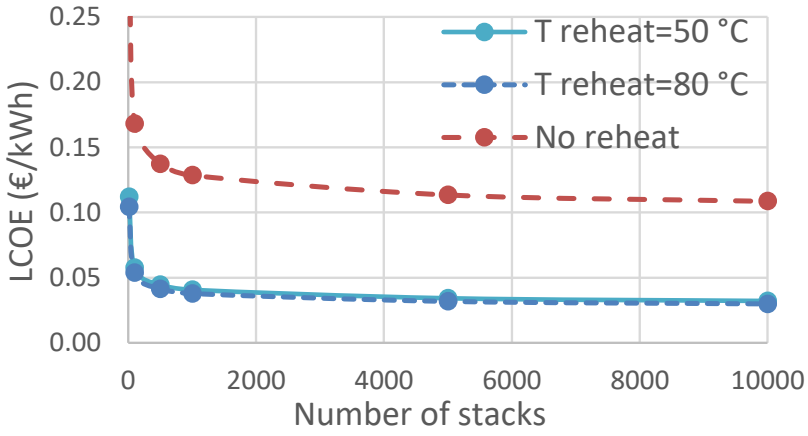

Figure 3.20: LCOE of the RED-MED with KAc (with and without reheating) and future membranes as a function of the number of RED stacks

The LCOE of even the small plants with KAc reheating is below 0.12 €/kWh, increasing to 0.25 €/kWh without reheating. Moreover, the LCOE with KAc reheating is below 0.06 €/kWh for plants with net capacity of over 160 kW, indicating that this configuration is very promising for reaching competitiveness even in relatively small systems.

3.2 RED-MD financial performance

The RED-MD cost model results were included in a paper that was published in 2018:

M. Micari, A. Cipollina, F. Giacalone, M. Papapetrou G. Kosmadakis, G. Zaragoza, G. Micale, A. Tamburini, "Towards the First Proof of Concept of a Reverse Electrodialysis – Membrane Distillation Heat Engine" Desalination 453 (2019), Pages 77-88, https://doi.org/10.1016/j.desal.2018.11.022

An alternative regeneration technology is the membrane distillation (MD), which is also used in desalination and water treatment plants [209]. This desalination technology is mostly applicable for small-scale systems[210] with the main advantage of keeping the costs low even for this type of systems [201].

The cost correlation of the MD part has been presented in Section 2, while the financial performance of the RED part has been examined in the RED-MED part of Section 3. Therefore, here the focus is on the financial performance of the RED-MD configuration, using the future RED membranes and the specifications of the RED stacks (e.g. membrane geometry ratio in the range of 1-4) that can lead to low cost values.

3.2.1 RED-MD cost analysis

The MD process has been simulated by Aquastill with the results further processed by other colleagues at the University of Palermo, in order to couple them with the appropriate RED part, considering as before one RED stack. For that purpose, different salinities and fluid velocities have been considered, resulting to different MD performances. These conditions lead to the same cost, since the equipment sizing is the same. Therefore, only the best performing MD case

has been included in the cost calculations, without conducting any parametric study on the MD part.

For adjusting the system capacity, the number of stacks is varied, having a small effect on the LCOE, since the MD cost is more or less the same. This effect is shown in Fig. 3.21.

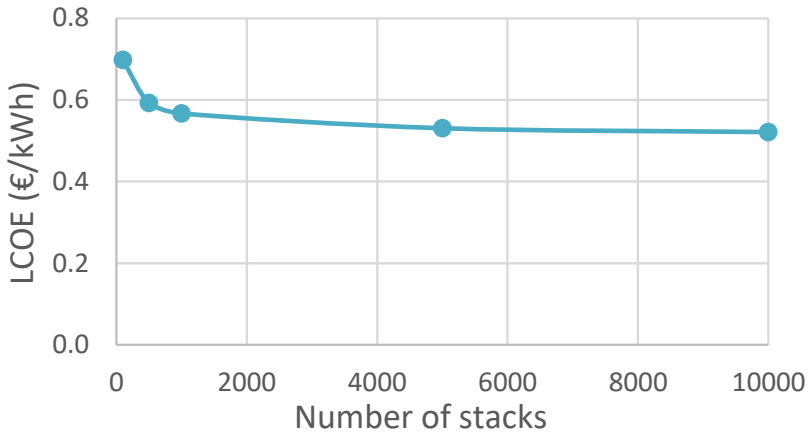

Figure 3.21: LCOE of the RED-MD with future membranes as a function of the number of RED stacks

The LCOE is almost 0.7 €/kWh for very small plants, reducing to almost 0.5 €/kWh for large plants. This range is similar to the one of the RED-MED case, shown in Fig. 3.14. The only advantage of the RED-MD configuration is the more rapid decrease of LCOE for few RED stacks (up to 1000), as well as the applicability of the MD down to the kW scale (MED units are currently available for over 500 m^3/day capacity).

3.2.2 RED-MD cost break-down

The cost break-down of the RED-MD system capital cost is shown in Fig. 3.22.

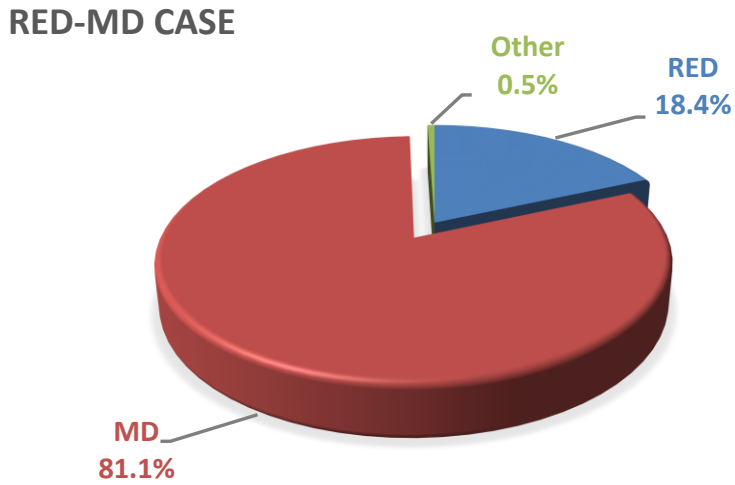

Figure 3.22: Cost break-down of the RED-MD case

The highest share of the total cost is attributed to the MD (about 81%) followed by the RED (about 18%) with the other parts having a negligible contribution of 0.5%. This break-down is similar to the RED-MED with future membranes, shown in Fig. 3.15. In this figure becomes very clear the future potential of this configuration, since it is expected that the MD specific cost will be reduced by more than 3 times over the next 3 decades, as will be shown in a next section.

3.3 RED-thermolytic salts financial performance

A preliminary version of the results presented in this section regarding the RED-thermolytic Heat Engine cost analysis were published in 2017:

M. Bevacqua, A. Tamburini, M. Papapetrou, A. Cipollina, G. Micale, A. Piacentino, Reverse electrodialysis with NH4HCO3-water systems for heat-to-power conversion, Energy. 137 (2017) 1293–1307. doi:https://doi.org/10.1016/j.energy.2017.07.012

For the financial performance of the system configuration that uses thermolytic salts and distillation/absorption columns for regeneration, the RED specifications are not examined. The future membranes are considered in the analysis and focus is given on the combined cost and LCOE potential.

A different approach has been followed here, since the initial simulations for this configuration have been conducted for a typical column with its necessary heat exchangers and pumps, adjusting the number of RED stacks, in order to match the flow rate of the concentrate. This has led to the cost calculation of the thermolytic salts regeneration per RED stack, with a strong declining rate as the stack number increases.

3.3.1 RED-thermolytic salts cost analysis

Three different cases of the thermolytic salts set-up have been considered, in order to identify the most cost-effective one. These cases are shown next:

1. Single-column, heat source temperature of 80 ^{o}C.
2. Single-column, heat source temperature of 100 ^{o}C.
3. Four-column, heat source temperature of 100 ^{o}C.

The cost of each regeneration set-up has been calculated separately as a function of the number of RED stacks. Appropriate correlations have been then developed, with the regeneration costs given in Fig. 3.23 for the two single-column cases and the four-column case. As shown, reliable correlations have been produced (with R^2 over 92%), which are then inserted in the cost analysis model, for the calculation of the regeneration cost, and finally the system LCOE.

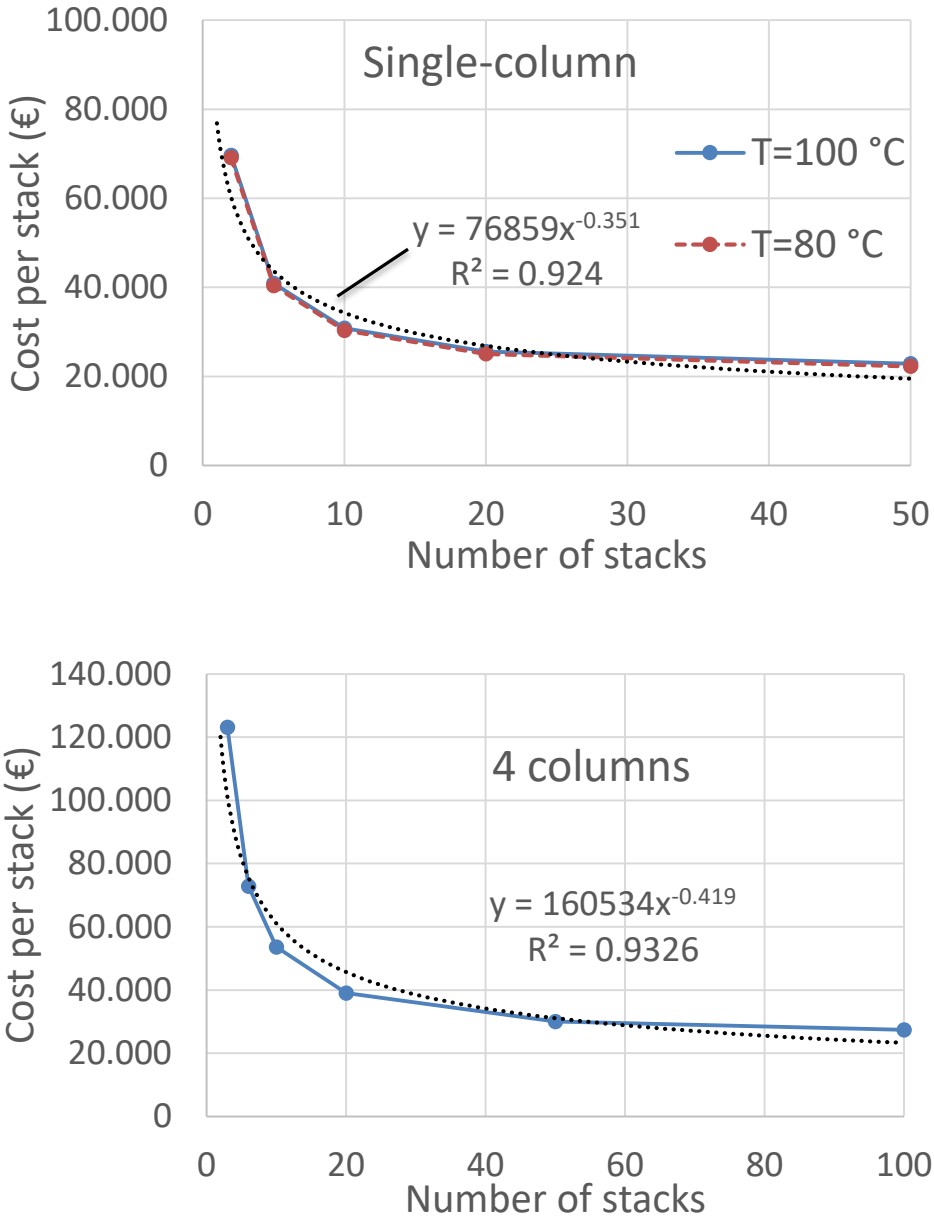

Figure 3.23: Regeneration unit cost per stack of the two single-column (top) and the four-column (bottom) case as a function of the number of RED stacks

For a small number of RED stacks, the cost per stack of the single-column cases is much lower than for the four-column one. This range corresponds to a power capacity of less than 10-20 kW. Therefore, in very small applications, the use of a single column is favoured. However, as the number of stacks increases, both costs are approaching to a common value of about 25,000 €/stack. Moreover, the heat source temperature has a negligible effect on this cost, as shown in Fig. 3.23, with the cost difference between the two cases being lower than 1%.

The LCOE values for a variable number of RED stacks, adjusting accordingly the system capacity are shown in Fig. 3.24. The single- and four-column cases are presented.

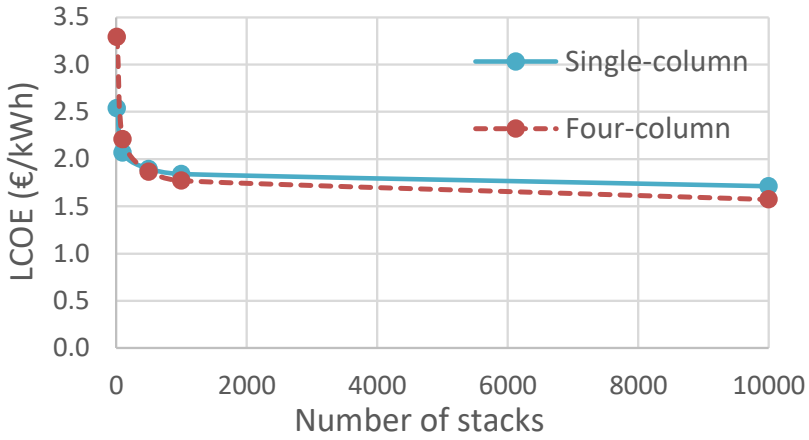

Figure 3.24: LCOE of the RED-thermolytic salts (single- and four-column, heat source at 100 °C) with future membranes as a function of the number of RED stacks

There is a very rapid decrease of the LCOE for low number of RED stacks, since both the stack cost and the regeneration unit cost greatly decrease, when their scale increases. This leads the LCOE from the value of about 2.5 €/kWh for few stacks and to even less than 1.80 €/kWh for a moderate number of RED stacks. However, these cost figures and not cost-competitive. In the future scenarios section it will be investigated whether they can become more competitive in the future. .

Finally, both cases show a similar LCOE, with the four-column case giving a slightly lower LCOE for medium/large-scale plants with over 1000 RED stacks.

3.3.2 RED-thermolytic salts cost break-down

The cost break-down of the RED-thermolytic system capital cost is shown in Fig. 3.25. The case of a single-and four-column case are examined here with a heat source temperature of 100 °C.

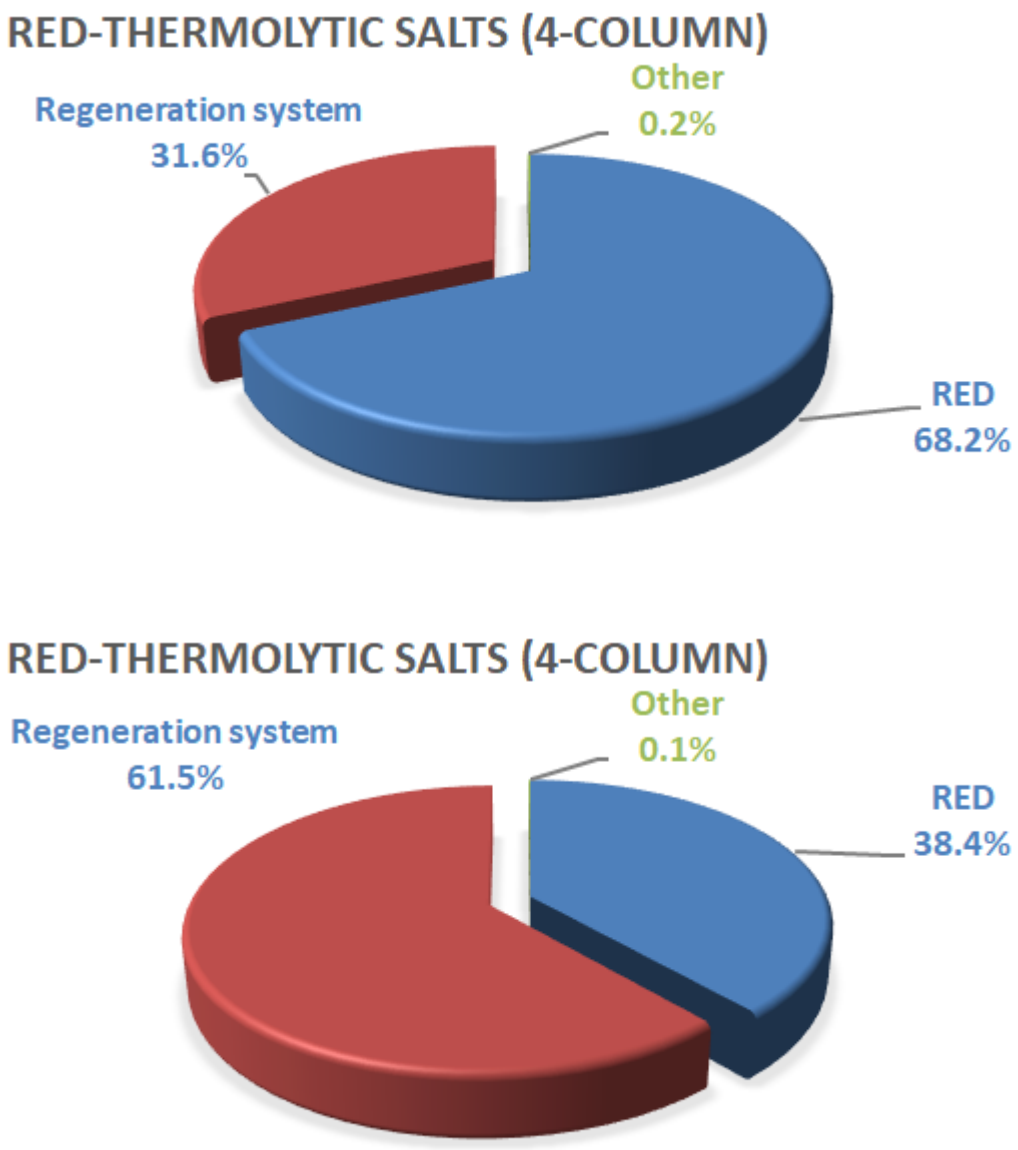

Figure 3.25: Cost break-down of the RED-thermolytic case. Top: single-column. Bottom: four-column (heat source temperature of 100 °C)

For the single-column case, the total cost is shared between the regeneration unit (about 31%) and the RED system (about 68%) with the other parts having a minor contribution of 0.2%. This break-down is not similar with the previous cases, in which the regeneration cost had the larger contribution by over 60%. This pattern though appears again for the four-column case, for which the larger contribution is from the regeneration unit (about 61%).

The large contribution of the RED in the system cost (single-column case) is beneficial for the economics of this configuration, since it is expected that the cost of this regeneration unit will not be greatly reduced in the future, since it is a common one in chemical processes. However, the cost of the RED part will be greatly reduced, driving down the whole system cost. Further details are shown later, when the future scenarios are presented.

3.4 Conclusions

The cost analysis of the RED with various regeneration technologies identified the design trends that should be followed in order to reach low LCOE values. Specifically, for the RED part:

- The membrane geometry ratio should be kept to values between 1 and 4, which also maximizes the thermal efficiency.
- The number of cell pairs per stack has a negligible effect on LCOE and its selection should be based on practical aspects, determined by the stack manufacturers and the preferences of the end-users.
- The use of current membranes with any possible set-up leads to unattractive LCOE values. On the other hand, the use of future membranes increases thermal efficiency and subsequently brings down the capital cost per kW produced, making it possible to lead to financial sustainable solutions.

Various regeneration technologies have been examined, in order to operate the RED stacks in a closed cycle. Most of them are used in desalination plants (MED and MD) with a similar function here. The overall conclusions reached are highlighted next:

- The number of MED effects should be kept relatively low, in order to limit the MED cost fraction to the total cost. However, this design option decreases the thermal efficiency (much higher heat input is required for the same net power production) and a trade-off should be found between performance and cost.
- The reheating of the NaCl solution in the RED-MED greatly increases the performance and reduces the LCOE.
- The use of KAc instead of NaCl can further enhance the performance and drive the costs down, resulting to a very low LCOE of even 0.05 €/kWh.
- The use of MD leads to slightly higher LCOE values compared to the standard MED, but it is preferred in smaller applications, since its specific cost is not affected much by the scale of the system.
- The use of thermolytic salts leads to high LCOE values. However, the configuration where a single-column is used shows a small contribution of the regeneration unit to the total capital cost, which indicates that it might be a promising configuration in case the RED stack cost greatly decreases in the future.

The use of future membranes in the RED stacks and its potential for reaching competitive LCOE values, even below 0.05-0.10 €/kWh, is further examined in the sensitivity and future scenarios sections, where the full potential of this technology is demonstrated. Finally, a comparative analysis between all presented configurations is provided in in the next chapters, after the future potential of this technology is identified.

4. Sensitivity analysis

The specifications of the RED Heat Engine presented in Section 3 include some parameters that either have some uncertainty or can be varied to some extent. Therefore, a sensitivity analysis of the LCOE is necessary to identify the key parameters that have the main effect on the cost performance of the system. This is conducted in the current section.

The sensitivity analysis of the RED-MED configuration is initially presented in detail, while the results for the other configurations are presented more briefly. The use of current membranes is not investigated further here since the results are not so promising; all configurations explored in that section use future membranes.

4.1 Parameters of sensitivity analysis

The sensitivity analysis considers all uncertain parameters that can have an impact on the costs and productivity of the RED Heat Engine. These parameters are presented in Table 4.1, together with their reference value and the minimum and maximum one, when using the future RED membranes and NaCl solution at 25 ^{o}C..

Table 4.1: Parameters of sensitivity analysis

Nr.	Parameter	Reference value	Units	Minimum value	Maximum value
1	Total number of stacks	500	-	100	10,000
2	Membrane specific cost	30	€/m^2	5	40
3	Stack casing specific cost	15	€/m^2	3	20
4	For RED-MED: Reduction of MED cost (not for desalination)	35	%	30	60
	For RED-MD: Reduction of MD membrane module specific cost	100	€/m^2	20	120
	For RED-thermolytic: Reduction of thermolytic salts regeneration system cost and optimization aspects	20	%	5	30
5	Capacity factor	90	%	50	100
6	Economic lifetime	30	Years	15	40
7	Discount rate	5	%	3	10
8	Lifetime of RED membranes	10	Years	5	20

For each parameter the range between the minimum and maximum values has been equally divided into 50 discrete steps, in order to identify any non-linear effects on the system costs and LCOE value.

4.2 Sensitivity analysis of RED-MED with NaCl

The effect of the sensitivity parameters on the LCOE of the RED-MED with NaCl is presented here in detail. Two extreme cases of the MED unit are assumed, using 6 and 26 effects. The heat source temperature is 100 ^{o}C and future membranes for the RED are considered.

The effect of all parameters considered on the LCOE for the two cases examined with different number of MED effects is presented in Fig. 4.1.

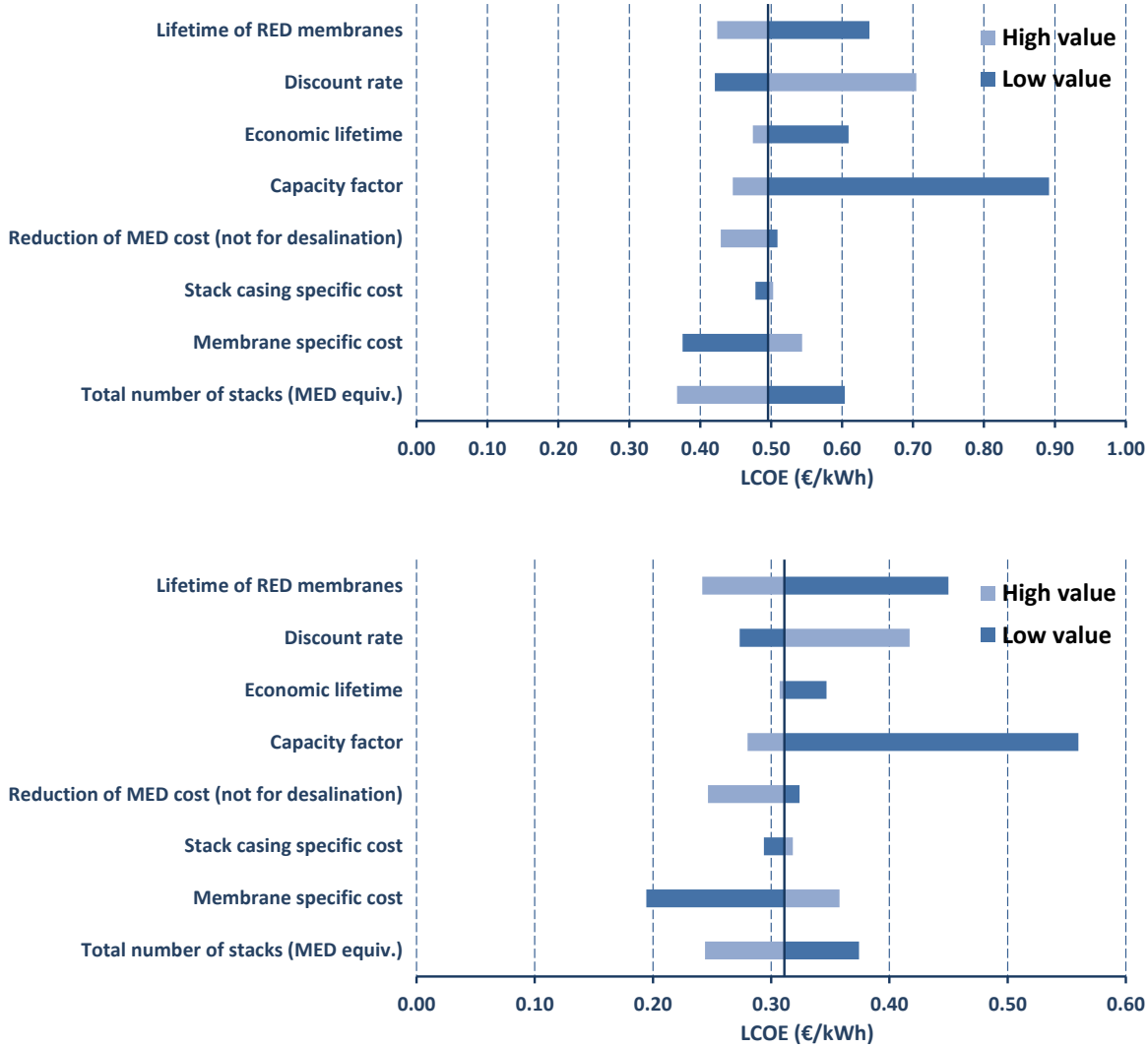

Figure 4.1: Overview of the effect of parameters considered on the LCOE for the RED-MED case. Top: MED with 26 effects. Bottom: MED with 6 effects

It appears that the system size (through the total number of stacks), capacity factor, the discount rate and the membranes (specific cost and lifetime) have a major role in the financial

performance of the system. By reaching the MW scale of net power output (over 1000 stacks), the LCOE is reduced to about 0.36 and 0.25 €/kWh for the 26 and 6 MED effects respectively. Further details for all parameters considered are provided next. The results with 6 MED effects will be only shown in the following sections, since this design is the most cost-competitive.

4.2.1 Effect of number of stacks

The total number of stacks has a major role in the sizing and specific cost of the regeneration technology and a minor one on inverter(s) and pumps. By increasing the number of stacks to 10,000 the net power output reaches 14.5 MW, while LCOE decreases to 0.24 €/kWh. Moreover, there is a non-linear effect of stack number on financial performance, as shown in Fig. 4.2.

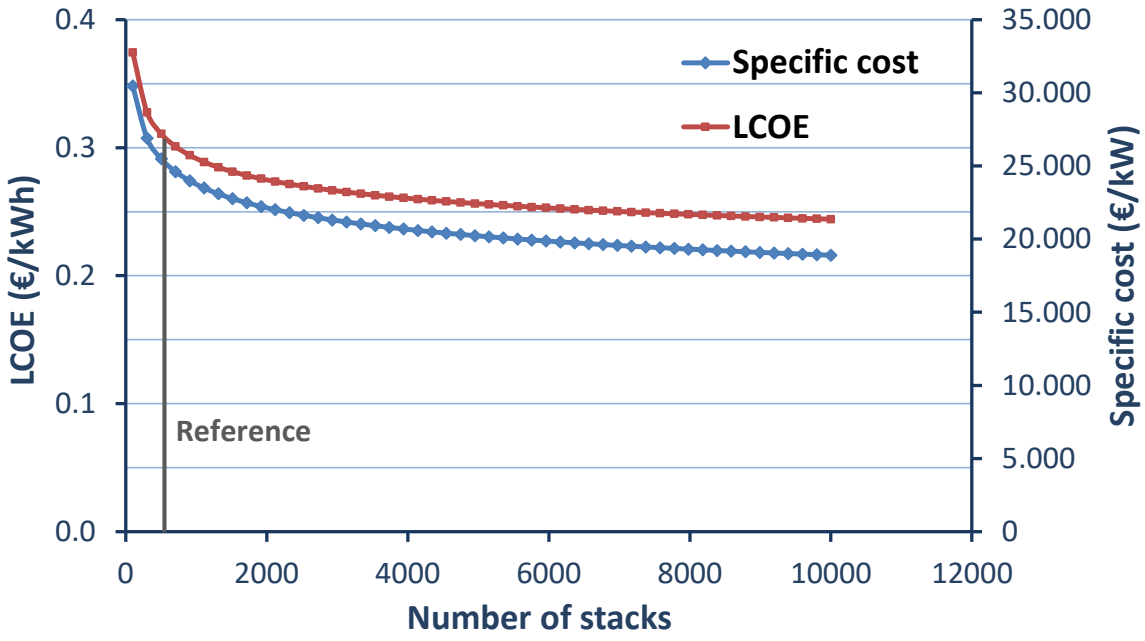

Figure 4.2: Effect of number of stacks on LCOE and specific cost

For over 5,000 stacks, the variation on LCOE is low, since the system size is already large and is favoured by economies of scale. The specific cost of MED rapidly decreases for over 200 RED stacks (net power production of 291 kW), making it an alternative solution even for low/medium capacity systems. For lower than 100 stacks (about 145 kW of net power production), the LCOE is close to 0.37 €/kWh and it is suggested to use an alternative regeneration technology for this system scale, such as MD or thermolytic salts. A further investigation of the exact limitations of each regeneration technology mostly concerning their size and heat source temperature is presented in the next sections.

4.2.2 Effect of membrane specific cost

The membrane specific cost has a more straightforward effect on the system's financial performance. As shown in Fig. 4.3, there is a perfect linear variation, reaching higher LCOE as the membrane specific cost increases, as expected.

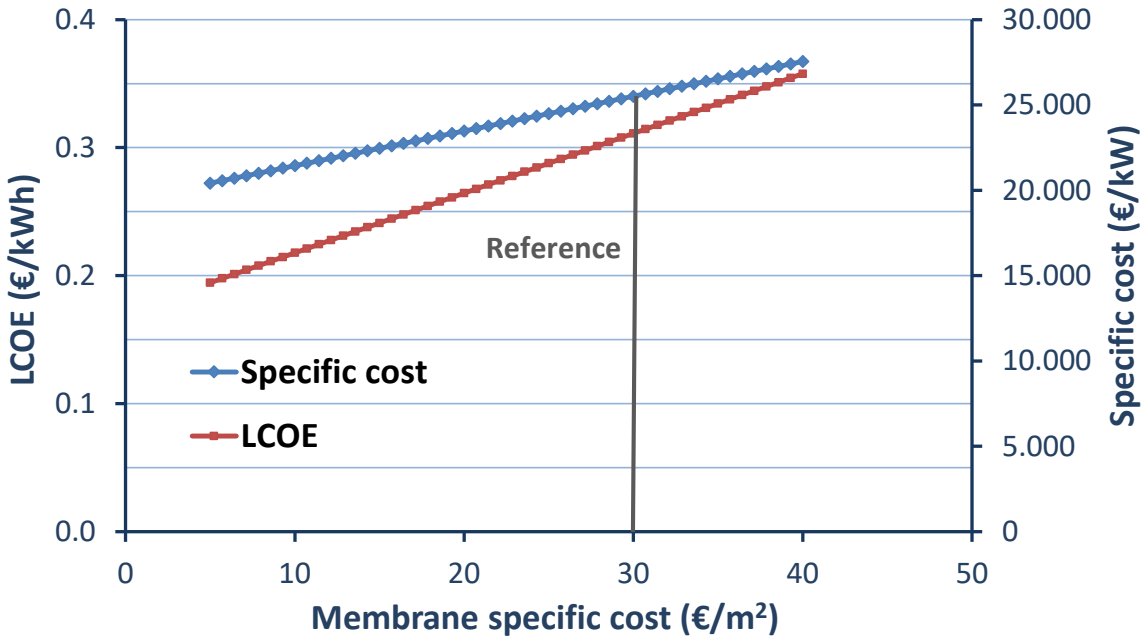

Figure 4.3: Effect of membrane specific cost on LCOE and specific cost

Since the MED cost has a major contribution to the overall capital costs, the effect of membrane specific cost on the LCOE is rather moderate. Still, this cost has the largest uncertainty and large efforts are given during the RED Heat-to-Power project for both increasing the membranes performance decreasing their costs.

Finally, the membrane specific cost is included in the analysis of future scenarios with the projected specific prices, in order to identify its cost reduction potential in case this technology moves to commercial level and is produced in mass.

4.2.3 Effect of stack casing specific cost

The stack casing specific cost has a low contribution on the system cost and brings a minor variation on the financial criteria, as shown in Fig. 4.4.

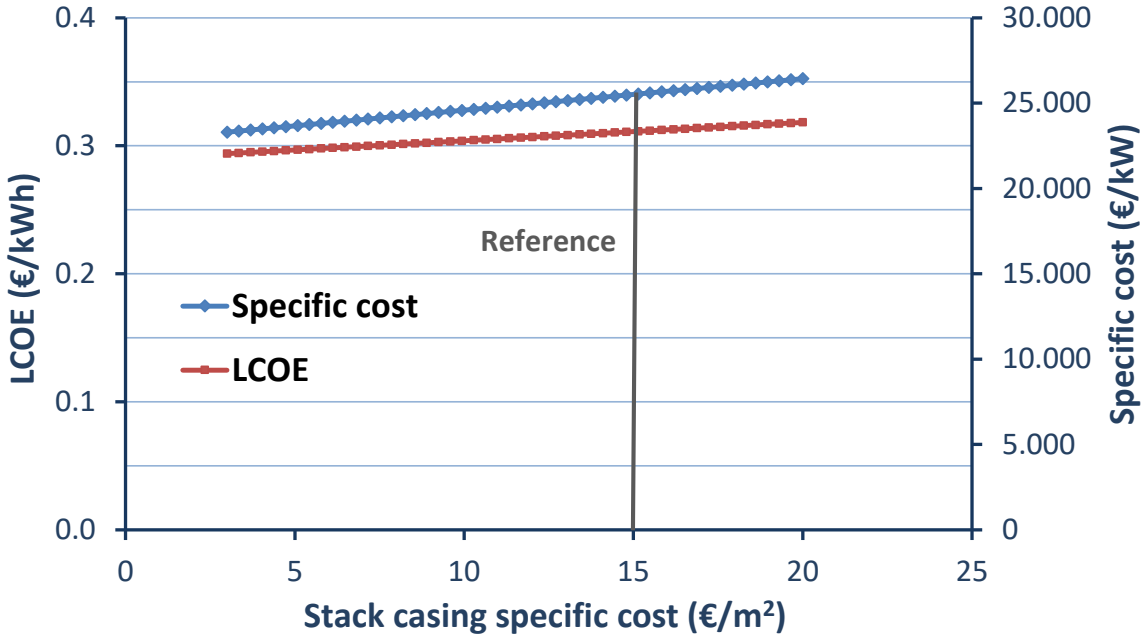

Figure 4.4: Effect of stack casing specific cost on LCOE and specific cost

Even if there is a large variation, the LCOE is increased by just 0.01 €/kWh. Moreover, the materials and design of this component are standard and its specific cost can be only decreased due to mass production. This parameter is also included in the future scenarios with the projected prices.

4.2.4 Effect of MED reduction factor

As already discussed, the MED cost considered is reduced by a factor to take into account the simpler design compared to MED units for seawater desalination (e.g. no pre- or post-treatment of seawater required, no intake structures etc). The reference value used in section 3 was 35%. The effect of this reduction factor on the LCOE and system specific cost is depicted in Fig. 4.5.

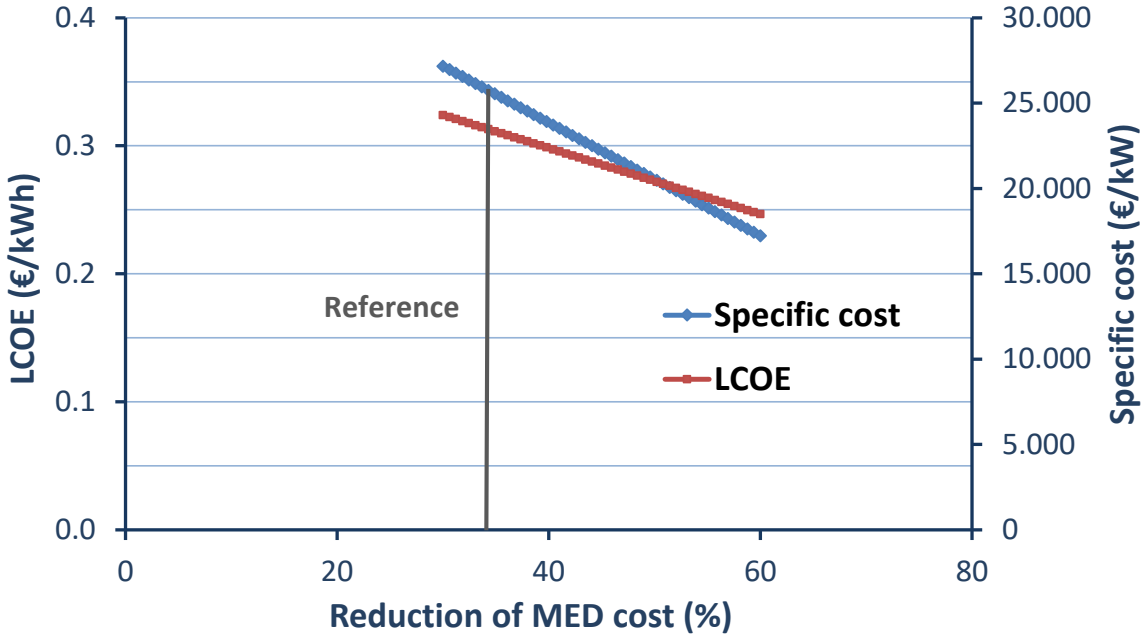

Figure 4.5: Effect of MED reduction cost on LCOE and specific cost

This effect is important, since the MED cost represents the largest fraction of the system cost, as presented in Section 3. By increasing this factor from 35 to 60%, LCOE is reduced by 20% with a similar relative reduction of the system specific cost.

Finally, the MED reduction factor is included in the analysis of future scenarios, in order to identify its cost reduction potential in case this technology moves to commercial level and mass produced, mostly related to seawater MED reduction costs as well.

4.2.5 Effect of capacity factor

The capacity factor reflects the total hours of operation per year. Therefore, it has no effect on specific cost, as clearly shown in Fig. 4.6, but rather a large one on the LCOE.

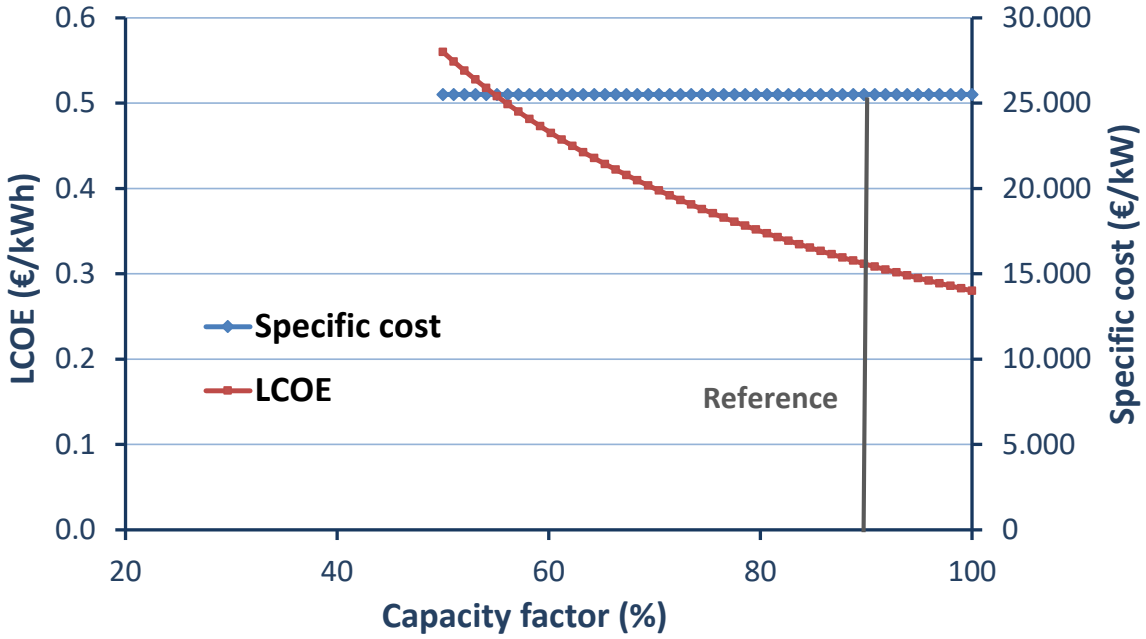

Figure 4.6: Effect of capacity factor on LCOE and specific cost

For capacity factor of 50% that corresponds to solar applications, LCOE is over 0.55 €/kWh, providing a first indication on the potential combination with solar thermal collectors. It becomes clear that the RED-MED system is necessary to operate many hours per year, in order to be profitable. An important advantage of biogas or industrial waste heat recovery applications is the high capacity factor, which can reach values of 90% or even slightly higher, keeping a low LCOE.

4.2.6 Effect of economic lifetime

Similar as the capacity factor, the system lifetime does not have any effect on system specific cost, and only on the LCOE value, as shown in Fig. 4.7. By increasing the lifetime, the initial investment is used over a longer period of time and apart from that, the discount factor changes.

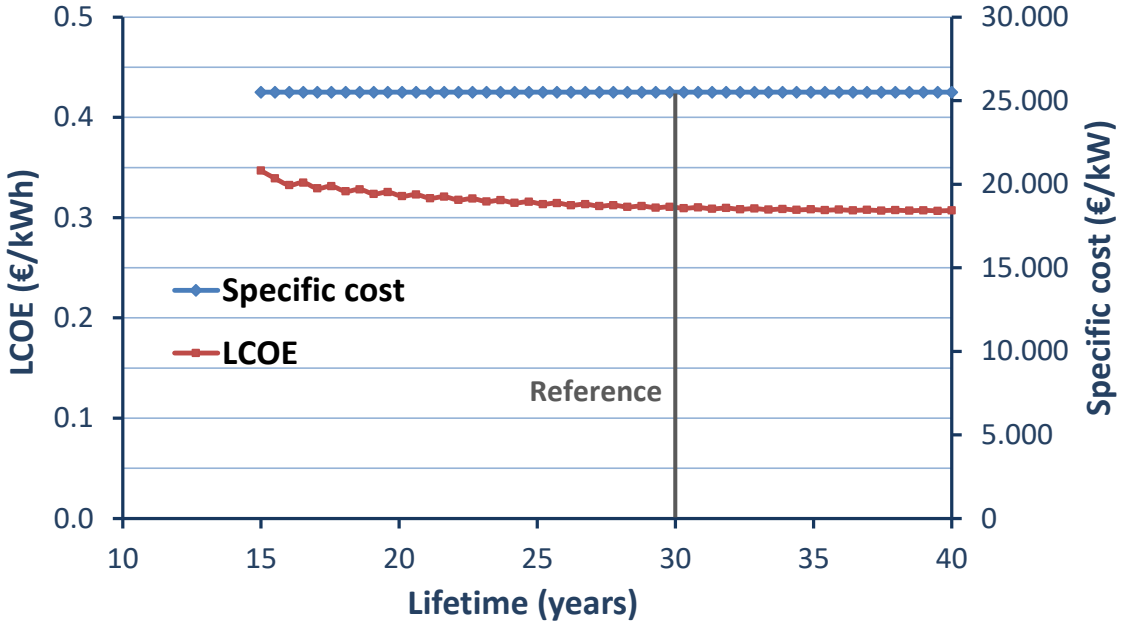

Figure 4.7: Effect of economic lifetime on LCOE and specific cost

The effect of lifetime on LCOE is low, with an approximate 3% reduction when increasing lifetime from 30 to 40 years. On the other hand, for much lower lifetime of 15 years, the LCOE rapidly increases and reaches 0.35 €/kWh, which is 13% higher than the one of the reference case.

4.2.7 Effect of discount rate

The discount rate does not have any influence on system specific cost but only on the LCOE value, as shown in Fig. 4.8.

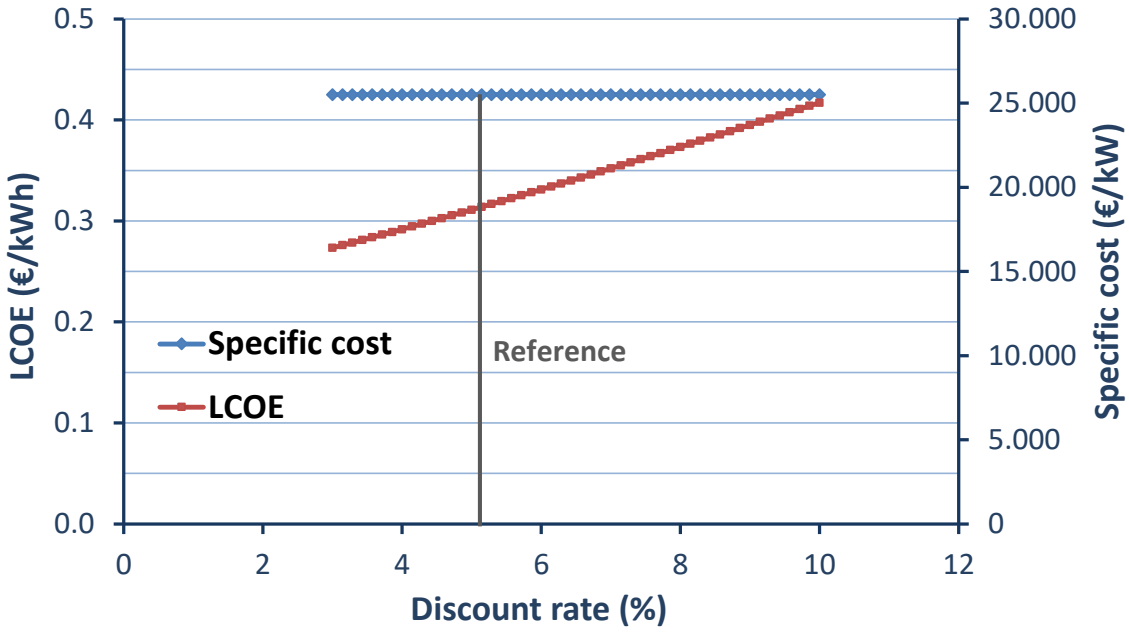

Figure 4.8: Effect of discount rate on LCOE and specific cost

The discount rate is included in the expression for calculating LCOE, having a non-linear dependence. The effect of discount rate is strong, reducing the LCOE by more than 10% (to 0.27 €/kWh) when moving from the reference value of 5%.to a lower rate of 3%.

4.2.8 Effect of RED membrane lifetime

The frequency of the ion exchange membranes replacement has a major effect on annual maintenance costs (for membranes and labour). This is introduced in the calculations through the membrane's lifetime. This parameter does not bring any change to the system specific cost but only to the LCOE, as shown in Fig. 4.9.

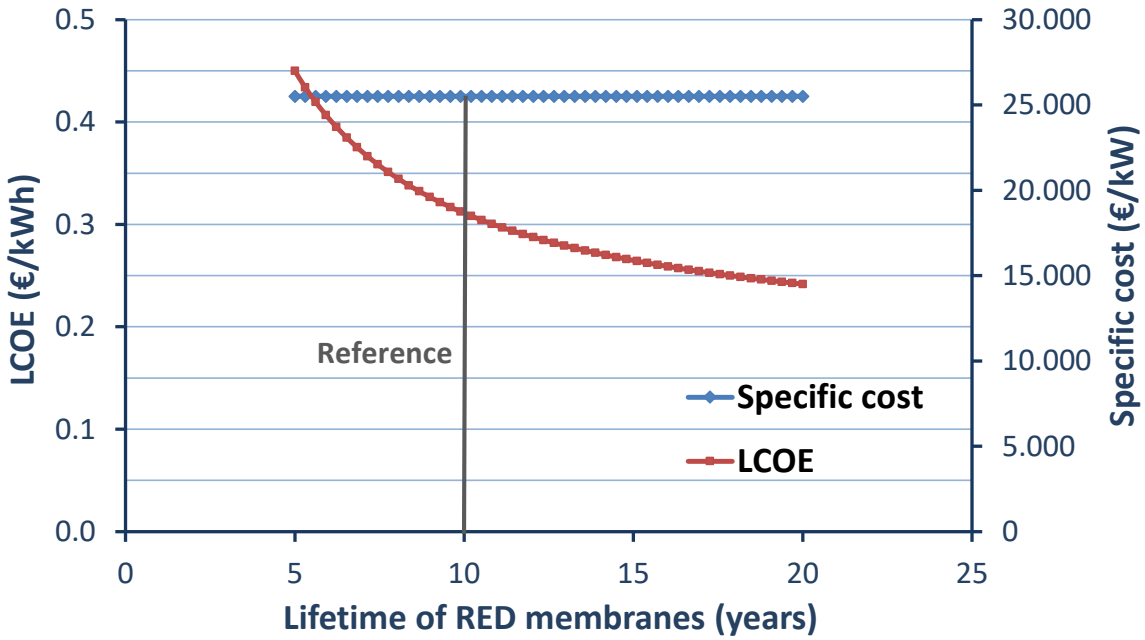

Figure 4.9: Effect of membrane replacement factor on LCOE and specific cost

The effect of this factor is high and can increase the LCOE by up to 45% for a more frequent membrane replacement every 5 years. This makes it necessary to verify a long lifetime, even more than 10-15 years, in order to contribute to the system cost-effectiveness in the future.

4.3 Sensitivity analysis of high-temperature RED-MED with NaCl

The effect of the sensitivity parameters on the LCOE of the RED-MED configuration with NaCl solutions that are fed in a RED (with future membranes) at higher temperatures is presented here. This effect is presented in Fig. 4.10 for a reheating temperature of 50 ^{o}C and 6 MED effects.

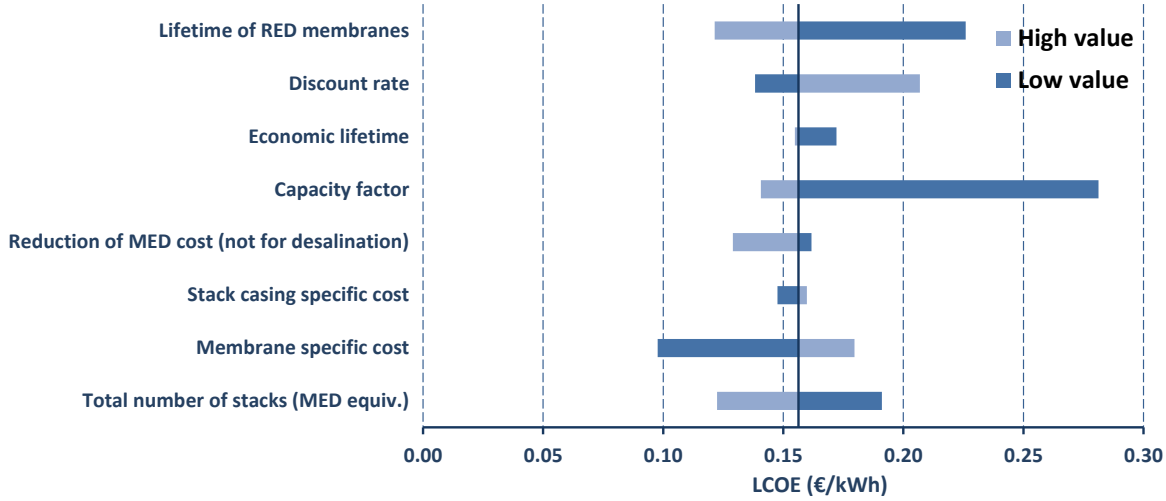

Figure 4.10: Overview of the effect of parameters considered on the LCOE for the high-temperature RED-MED case with NaCl

The trends observed here are similar with the RED-MED case examined before, but the overall LCOE values are lower, as was already explained in section 3. By increasing the system scale, the LCOE can be reduced to 0.12 €/kWh, while a low specific cost of the RED membranes can bring the LCOE down to even 0.10 €/kWh.

4.4 Sensitivity analysis of high-temperature RED-MED with KAc

The effect of the sensitivity parameters on the LCOE of the high-temperature RED-MED configuration with KAc and with future membranes is presented here. This effect is presented in Fig. 4.11 for a reheating temperature of 50 °C and 6 MED effects.

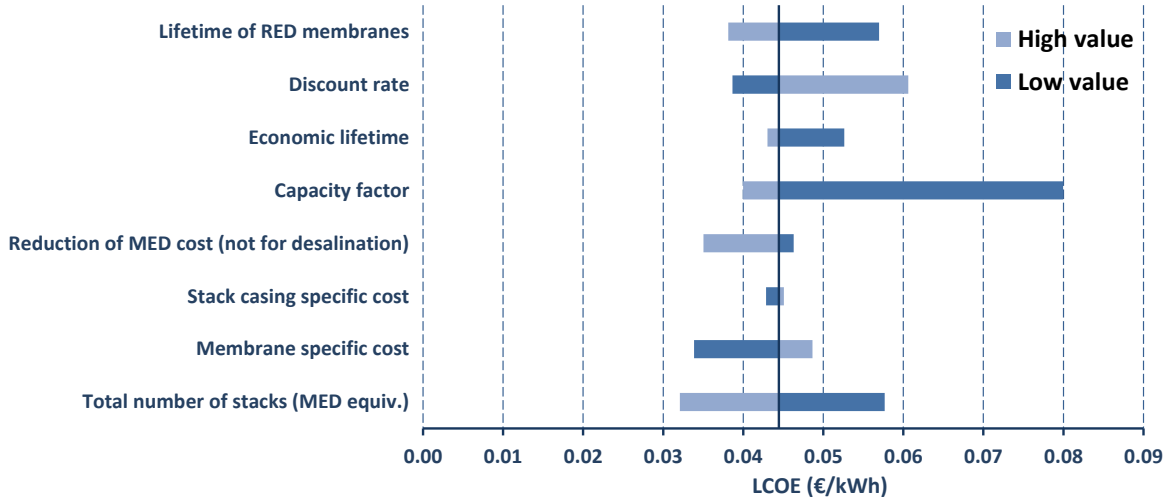

Figure 4.11: Overview of the effect of parameters considered on the LCOE for the high-temperature RED-MED case with KAc

The same parameters as before affect the LCOE of this case. However, its variation is restricted within a small range, usually from 0.03 up to 0.06 €/kWh, revealing the future potential of this configuration.

4.5 Sensitivity analysis of RED-MD

The effect of the sensitivity parameters (presented in Section 4.1) on the LCOE of the RED-MD configuration (with future ion exchange membranes) is presented here. This effect is presented in Fig. 4.12.

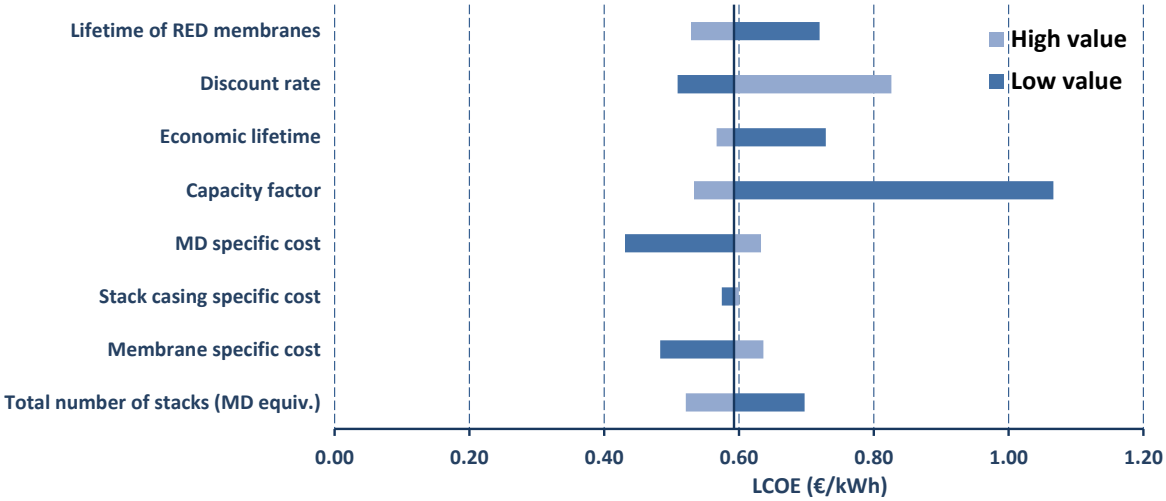

Figure 4.12: Overview of the effect of parameters considered on the LCOE for the RED-MD case

As in the RED-MED case, the system size (through the total number of stacks), the capacity factor, the discount rate and the membranes (lifetime and specific costs) play the most important role in the LCOE. The MD specific cost also has a large effect on the LCOE. By increasing the system scale, the LCOE can be reduced to almost 0.45 €/kWh, while a low specific cost of the RED membranes can bring the LCOE down to 0.47 €/kWh.

4.6 Sensitivity analysis of RED with thermolytic salts

The effect of the sensitivity parameters on the LCOE of the RED-thermolytic salts configuration (with future membranes) is presented here. This effect is presented in Fig. 4.13 for both single- and four-column regeneration unit.

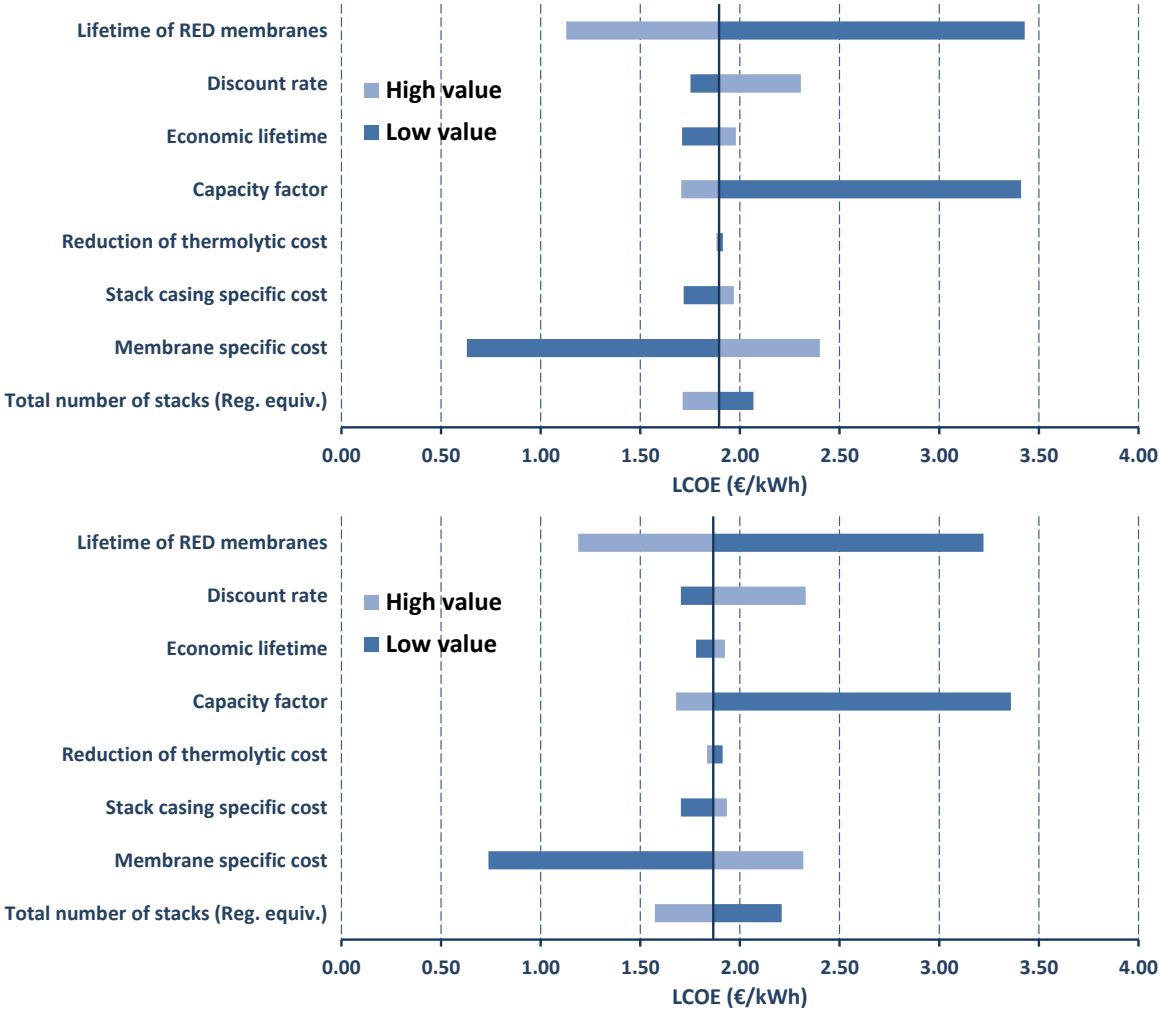

Figure 4.13: Overview of the effect of parameters considered on the LCOE for the RED-thermolytic salts case. Top: single-column. Bottom: four-column

The system size has a moderate effect on the LCOE, while the main effects are through the membrane specific cost and their lifetime for both cases. This is because the RED has a high contribution on the system capital cost, as presented previously. Moreover, the capacity factor has a large effect on the LCOE as well, which is expected for any power production technology.

Specifically, the reduction of the membrane specific cost can bring down the LCOE by a factor of 2, while the increase of membrane lifetime reduces the LCOE by up to 20%.

4.7 Conclusions

The main parameters of the RED Heat Engine have been included in the sensitivity analysis, considering all possible regeneration technologies and set-ups. The relevant results for the RED-MED configuration have been presented in detail, while the main outcomes have been presented for the other configurations. From this process, the key parameters with the highest effect on the LCOE have been identified, which are common in most system configurations. These parameters are the following:

- System size

- Capacity factor
- Membrane specific cost
- Lifetime of RED membranes
- Discount rate

The first two parameters (system size and capacity factor) depend on the application (size and type) and the heat source (e.g. industrial waste heat, solar thermal). The other two (RED membrane specific cost and lifetime) depend on the technological advancements of the membranes and their production method and volumes, which affect their cost. The membrane specific cost has been projected in future scenarios, and is further examined in the next section, together with additional parameters. Finally the discount rate is a factor that reflects the general economic situation (national and global) at a certain time when an investment is considered and the perception of the investor of the risks associated with a certain project.

5 Future scenarios of the RED Heat Engine

The main components with the higher contribution on the system cost are the RED part (mostly the membranes) and the regeneration technology. It is expected that the costs of these two parts will decrease over time, especially for the RED part, which is a new technology and the scaling up of the production can bring important savings. These projections have been used to examine future scenarios of the RED Heat Engine. In addition to that, electricity prices or FiTs are also included in this analysis, since it is expected to be increased in the future, contributing to the competitiveness of the RED Heat Engine for a variety of applications.

The effect of these parameter's cost developments in future scenarios is introduced in this section. A realistic scenario for the wide application of the technology in 2020 and beyond (in 2030 and 2050) is presented, accompanied by a more conservative and a more optimistic scenario, in order to have a better understanding of the potential of this technology. The methodology and results of this analysis are based on the projected cost reduction factor in case of mass production, and they are presented next. This analysis is conducted for the case of future RED membranes only, considering all regeneration technologies, solutions, and reheating options.

5.1 Parameters of the future scenarios

The RED-related parameters that have been included in the analysis of the future scenarios of the RED Heat Engine are listed in Table 5.1. Their values are projected to 2020, 2030, and 2050. A realistic scenario is included, together with a conservative and an optimistic one.

Table 5.1: Parameters and their values of the RED part considered in the future scenarios

Parameter	Reference value	2020			2030			2050		
		Conservative	Realistic	Optimistic	Conservative	Realistic	Optimistic	Conservative	Realistic	Optimistic
Membrane specific cost (€/m^2)	30	32	30	28	20	16	12	12	10	6
Stack casing specific cost (€/m^2)	15	18	15	12	9	7.5	6	4	3.5	3
Electrode specific cost (€/m^2)	500	550	500	450	270	250	220	220	200	180
Increase of thermal efficiency (-)	1	0.9	1.0	1.1	1.0	1.1	1.3	1.1	1.3	1.5

The values presented in table 5.1 are the ones for "small" systems as defined in section 2.4. The values for larger systems and the correlations for calculating the prices for systems of any size are calculating keeping same ratios and using the same approach introduced in section 2.4 (Table 2.8).

The parameter "increase of thermal efficiency" is introduced in order to account for the possibility of more efficient IEMs in the future, or other improvements of the design that can increase the overall efficiency.

The projected cost reduction relevant to the regeneration systems in the future years are shown in Table 5.2.

Table 5.2: Parameters and their values of the regeneration unit considered in the future scenarios

Parameter	Reference value	2020			2030			2050		
		Conservative	Realistic	Optimistic	Conservative	Realistic	Optimistic	Conservative	Realistic	Optimistic
Reduction of MED cost (%)	35	30	35	45	40	45	50	45	50	55
MD membrane module specific cost (€/m^2)	100	110	100	90	60	50	40	35	30	25
Reduction of thermolytic salts cost (%)	20	15	20	25	20	25	30	25	30	35

The financial performance of the system is presented next. The LCOE value is calculated for all examined configurations. The RED-MED is presented in detail, while the main outcomes are only presented for the RED combined with the other regeneration technologies.

5.2 Future scenarios of the RED-MED

The RED-MED with future membranes and 6 MED effects is considered for the projection of the system cost-effectiveness in future scenarios (with NaCl, no reheating). The temperature of the heat source is 100 °C and the number of RED stacks is 500 (equal to the reference value). The effect on the LCOE of the parameters considered in future scenarios is presented next.

5.2.1 Future cost of RED membrane specific cost

Using the above parameters, the effects of the future projections of the RED membrane specific cost on the LCOE is calculated with the same methodology as presented previously. The results are shown in Fig. 5.1.

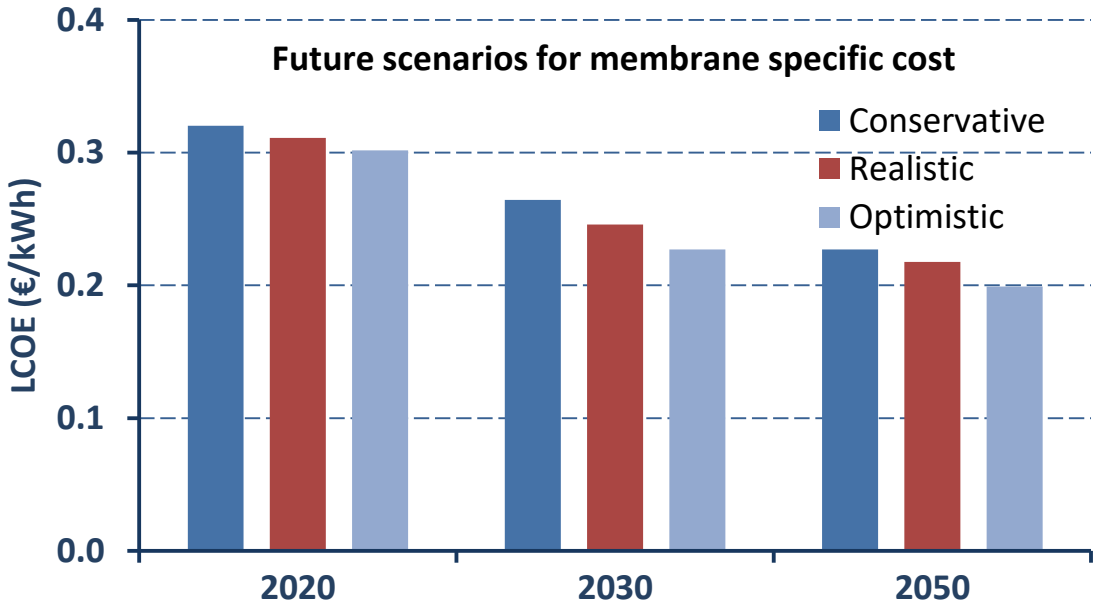

Figure 5.1: Future scenarios for membrane specific cost and its effect on LCOE of the RED-MED

It is expected that the LCOE will decrease to 0.25 €/kWh by 2030 and to about 0.20 €/kWh by 2050. The LCOE variation over time is high, reducing by about 33% reduction over a period of 30 years.

This effect on LCOE is only due to the cost reduction of the membranes. However, other factors that contribute to the LCOE reduction are also foreseen. This combined effect will be examined later.

5.2.2 Future cost of RED stack casing specific cost

The effect of the future projections of the RED stack casing specific cost on the LCOE is shown in Fig. 5.2.

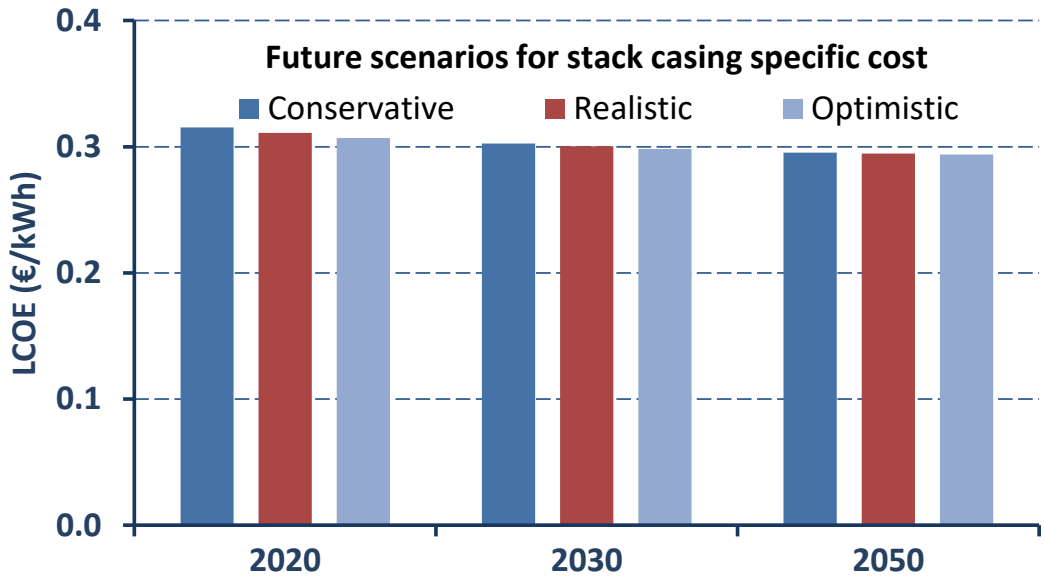

Figure 5.2: Future scenarios for stack casing specific cost and its effect on LCOE of the RED-MED

The effect of the stack casing specific cost on the LCOE is minor (up to 5% reduction in 2050). Although this specific cost is expected to reduce by 4 times in 2050, its contribution on the total capital cost is small.

5.2.3 Future cost of electrode specific cost

Next, the projected electrode specific cost is examined. Its effect on the LCOE in future scenarios is shown in Fig. 5.3.

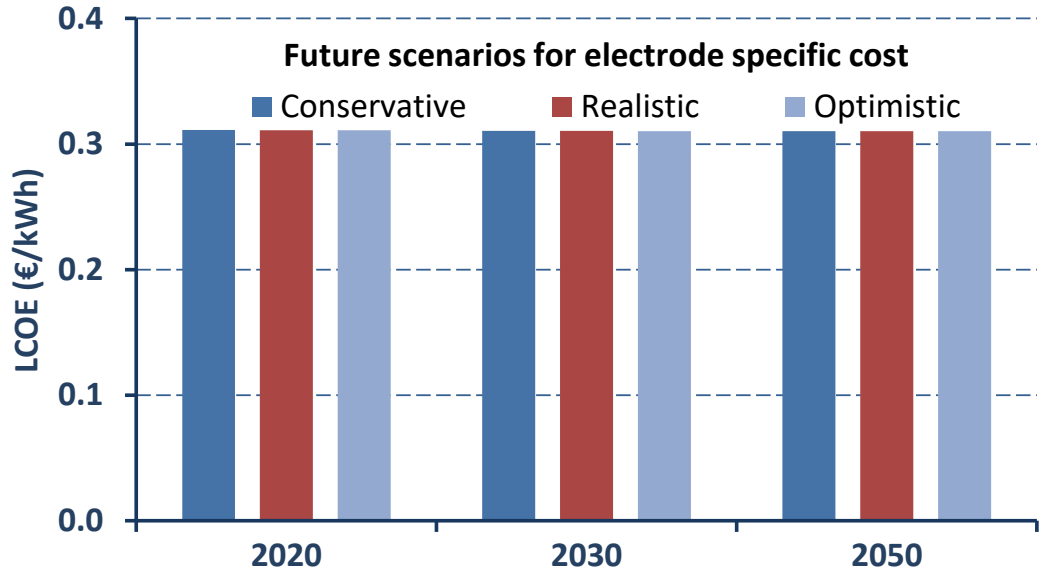

Figure 5.3: Future scenarios for electrode specific cost and its effect on LCOE of the RED-MED

This specific cost has an even lower effect on the LCOE as the stack casing cost. A negligible cost reduction is expected, reducing the LCOE by less than 0.3% in 2050.

5.2.4 Future RED thermal efficiency

There is continuous research on membranes, which is expected to reach much higher performance in the future, even higher than the "future membranes" that have been considered here. The effect of the RED thermal efficiency on the LCOE is presented in Fig. 5.4.

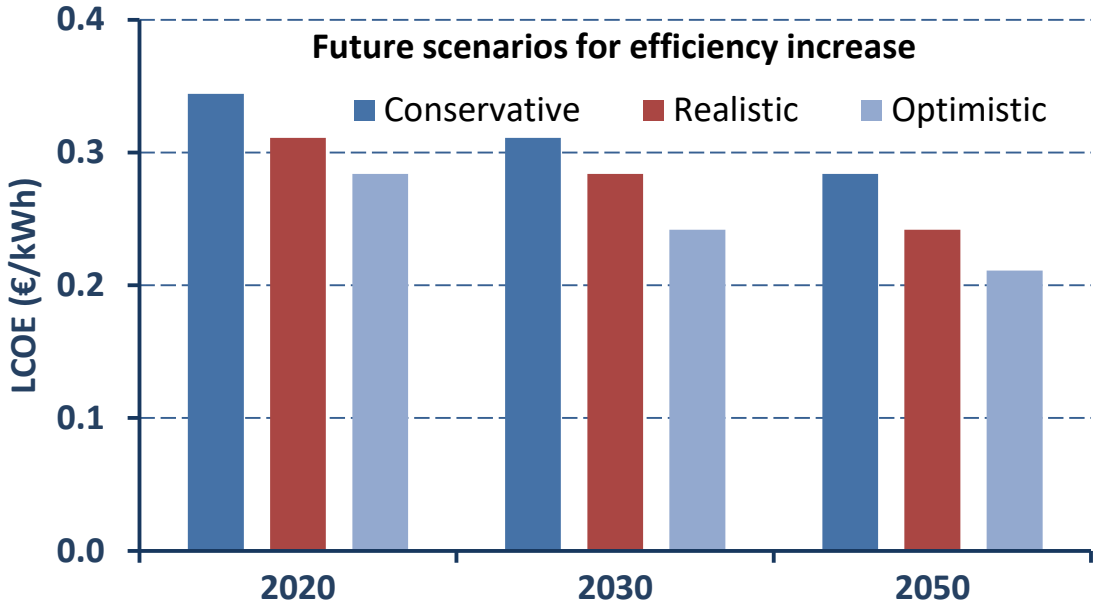

Figure 5.4: Future scenarios for system thermal efficiency and its effect on LCOE of the RED-MED

A significant LCOE reduction can be reached through the increase of the performance, reaching values as low as 0.21 €/kWh in 2050. The LCOE variation between the three scenarios for the same year reveals the large uncertainty of this parameter. In any case, it is clear that the increase of efficiency can affect the LCOE more than possible reductions of the equipment's specific costs.

5.2.5 Future cost of the MED

The cost of MED units is expected to decline over the next years, mostly due to the larger number of projects. Therefore, the future scenarios consider a cost decrease for regeneration, which is introduced in the model through a higher reduction factor for MED compared to MED for seawater desalination. Its effect on the LCOE is shown in Fig. 5.5.

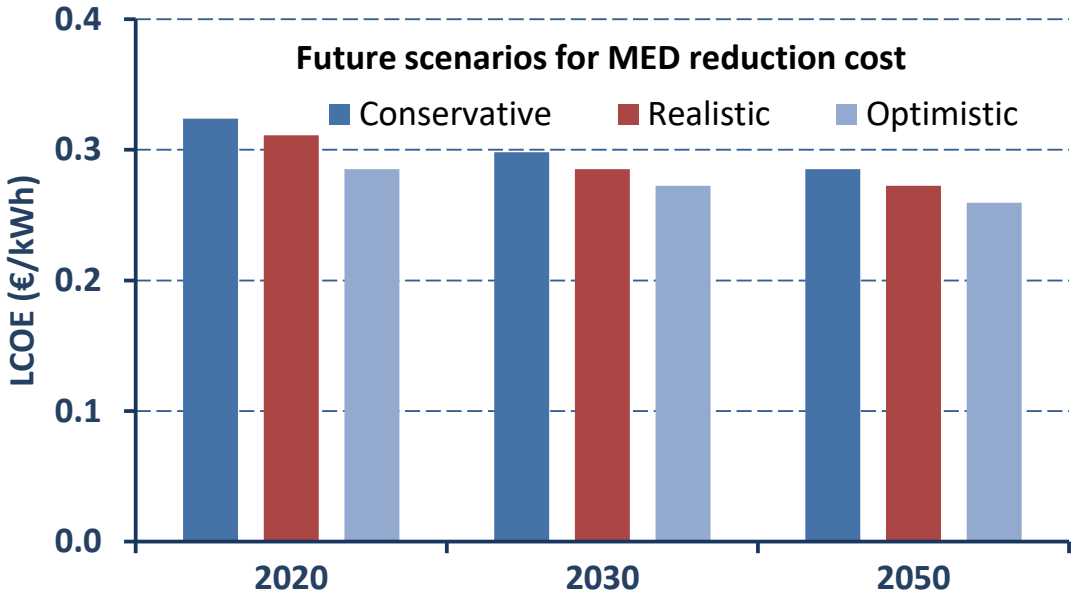

Figure 5.5: Future scenarios for MED cost reduction and its effect on LCOE of the RED-MED

By 2050, the MED cost for RED will be decreased by more than 50% compared to current MED costs for desalination. This has a moderate effect on LCOE, resulting to a decrease of LCOE to 0.27 €/kWh in 2050 (realistic scenario) and slightly lower with the optimistic one. The fact that the effect of the MED cost decrease is only moderate reflects the success of the strategy to use a MED with low number of effects, restricting in the contribution of the MED cost to the LCOE.

5.2.6 Combined effect of future scenarios for the RED-MED

In this section is studied the effect on the LCOE when the future scenarios for each component are combined. The effects of all parameters on the LCOE is depicted in Fig. 5.6.

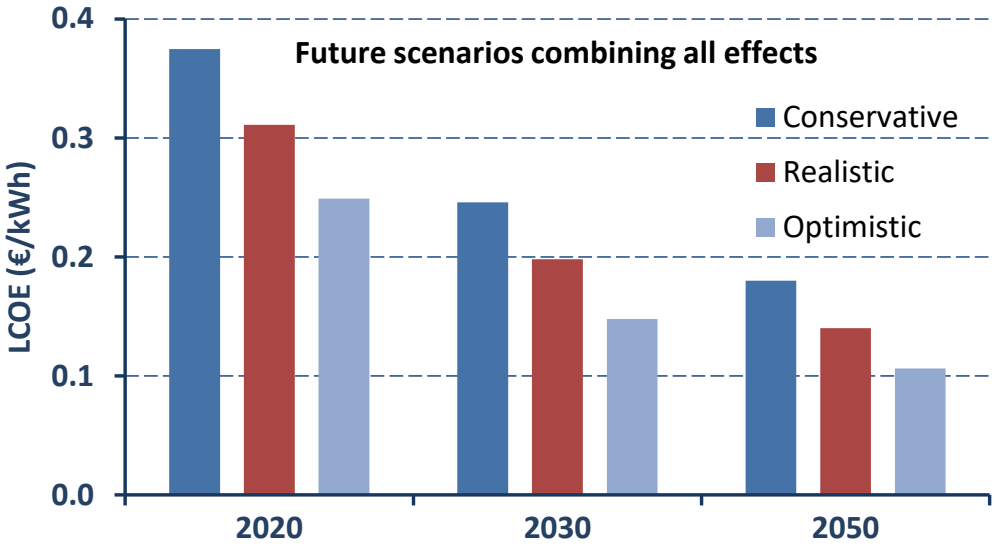

Figure 5.6: Future scenarios of all parameter and their effect on LCOE of the RED-MED

The combined effect brings a reduced LCOE that reaches 0.13 €/kWh by 2050, and even 0.10 €/kWh for the optimistic scenario. Therefore, there is plenty of room for making the RED Heat Engine a competitive solution in the future, if the scenarios considered are realised.

5.2.7 Combined effect of future scenarios for the RED-MED of large-scale

The main difference here is to consider a very large RED-MED plant with 5000 RED stacks (10 times larger than before, net capacity of 7.28 MW), in order to additionally identify the size effects of future scenarios. The effects of all parameters on the LCOE of this large plant is depicted in Fig. 5.7.

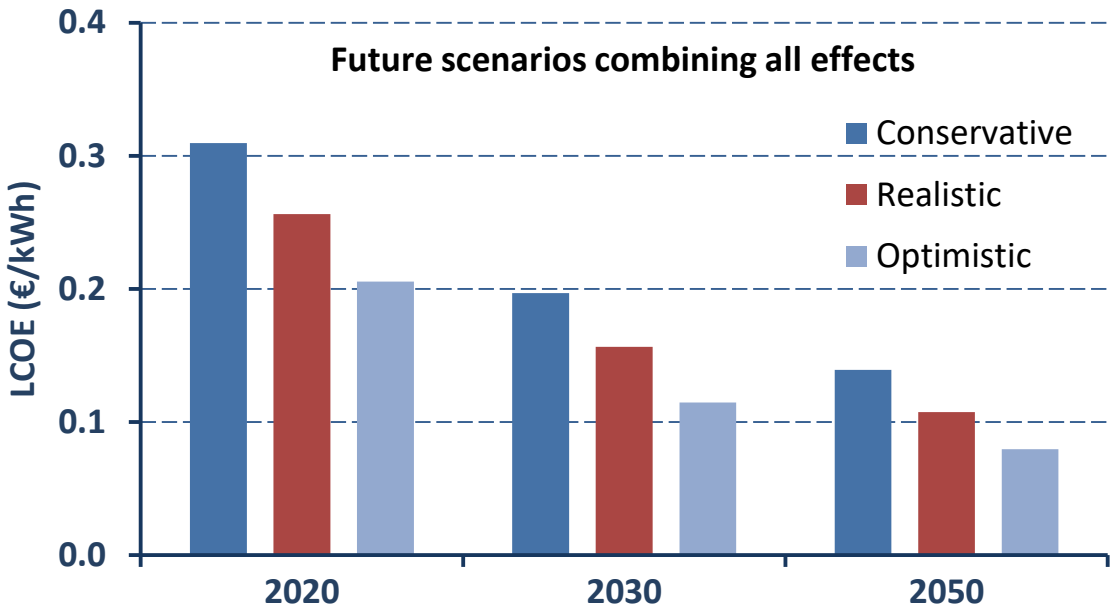

Figure 5.7: Future scenarios of all combined parameters and their effect on LCOE of the large RED-MED

The LCOE is reduced to 0.10 €/kWh in 2050 for the realistic case, about 20-25% lower than for the medium-scale RED-MED plant, presented in the previous section.

5.2.8 Combined effect of future scenarios for the high-temperature RED-MED with NaCl

The future cost-competitiveness of the high-temperature RED-MED configuration with NaCl is presented here. The system uses 500 RED stacks and 6 MED effects are considered. The combined effect of all parameters on the LCOE is shown in Fig. 5.8 for two reheating temperatures of 50 and 80 ^{o}C.

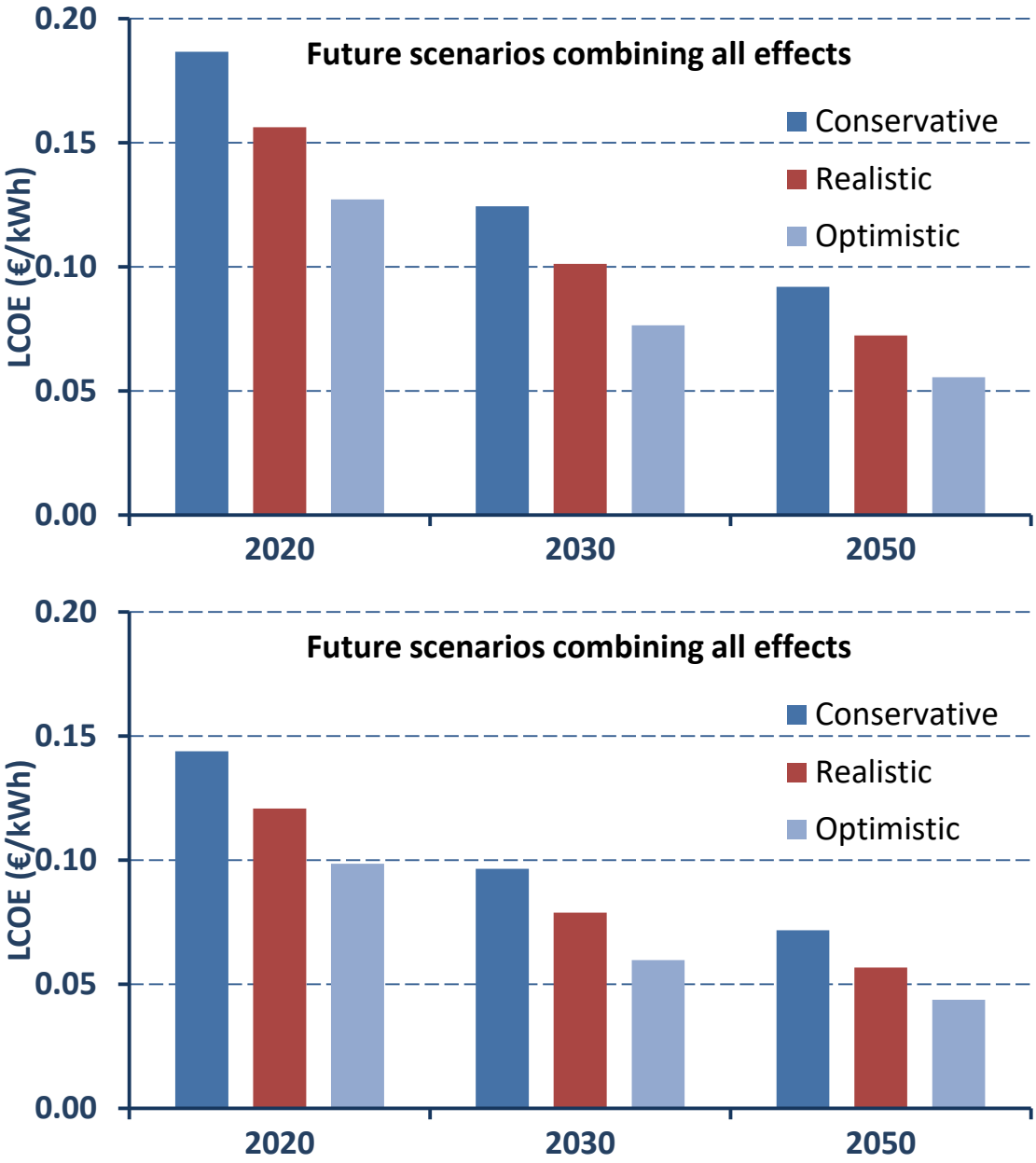

Figure 5.8: Future scenarios of all combined parameters and their effect on LCOE of the high-temperature RED-MED with NaCl. Top: reheating at 50 °C. Bottom: reheating at 80 °C

The LCOE can be reduced to 0.07 €/kWh in 2030, reaching even 0.04 €/kWh for the most optimistic case in 2050. This value is very competitive and if achieved would fully ensure the future commercial success of this technology.

This value can be further reduced by:

- 20-25%, when considering a larger plant (as in the previous section), approaching 0.03 €/kWh in 2050, and
- 10-20% for higher temperature of the heat source (e.g. 120 or 140 °C).

The overall result is to achieve a LCOE in the range of 0.03-0.05 €/kWh in 2050, which is much lower than any other heat to power technology, being close to current conventional (fossil-fuel) power plants.

5.2.9 Combined effect of future scenarios for the RED-MED with KAc

The future cost-competitiveness of the RED-MED configuration with KAc is presented here. The system uses 500 RED stacks and 6 MED effects are considered. The combined effect of all parameters on the LCOE is shown in Fig. 5.9 for two reheating temperatures of 50 and 80 °C, as well as with no reheating.

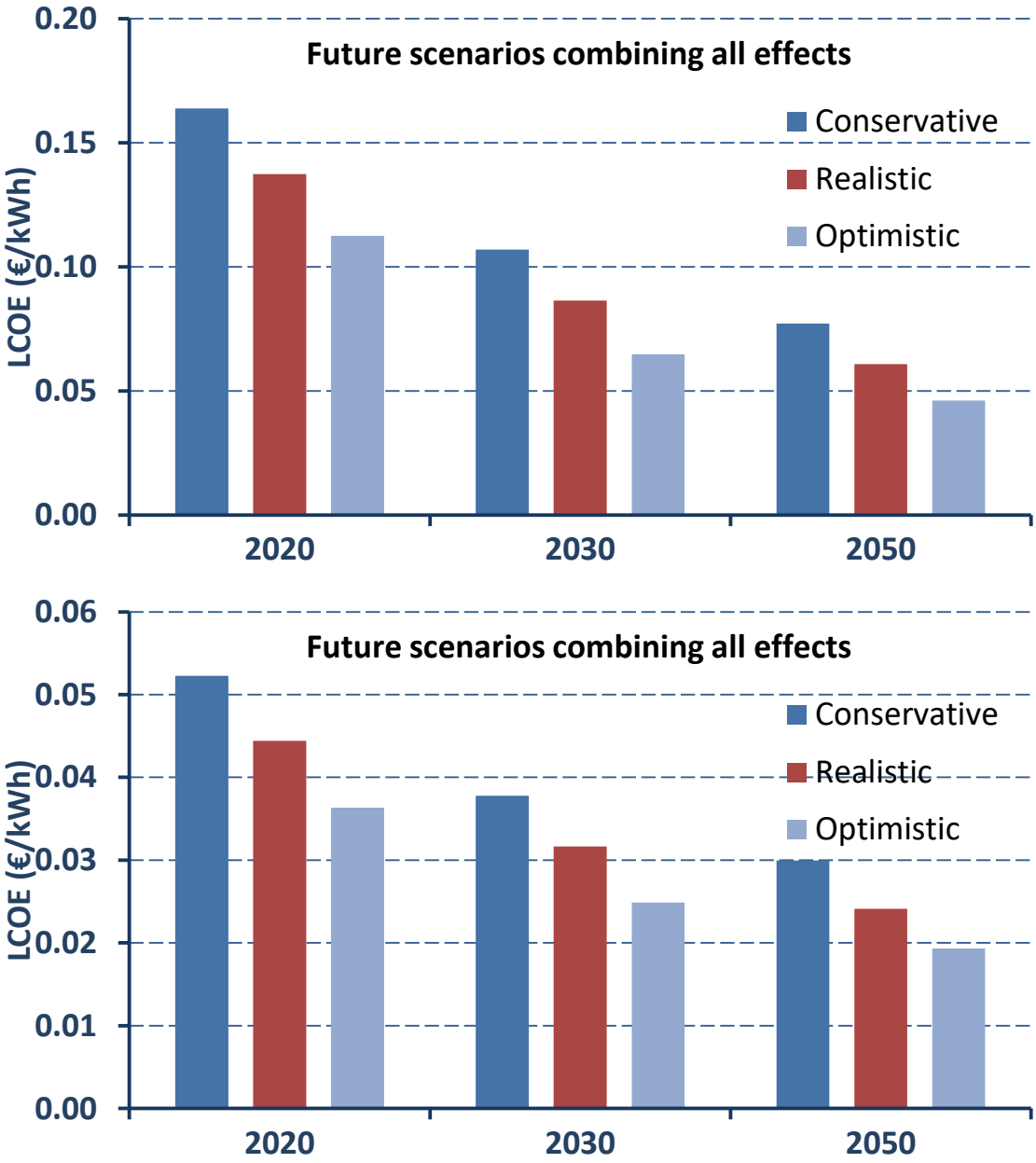

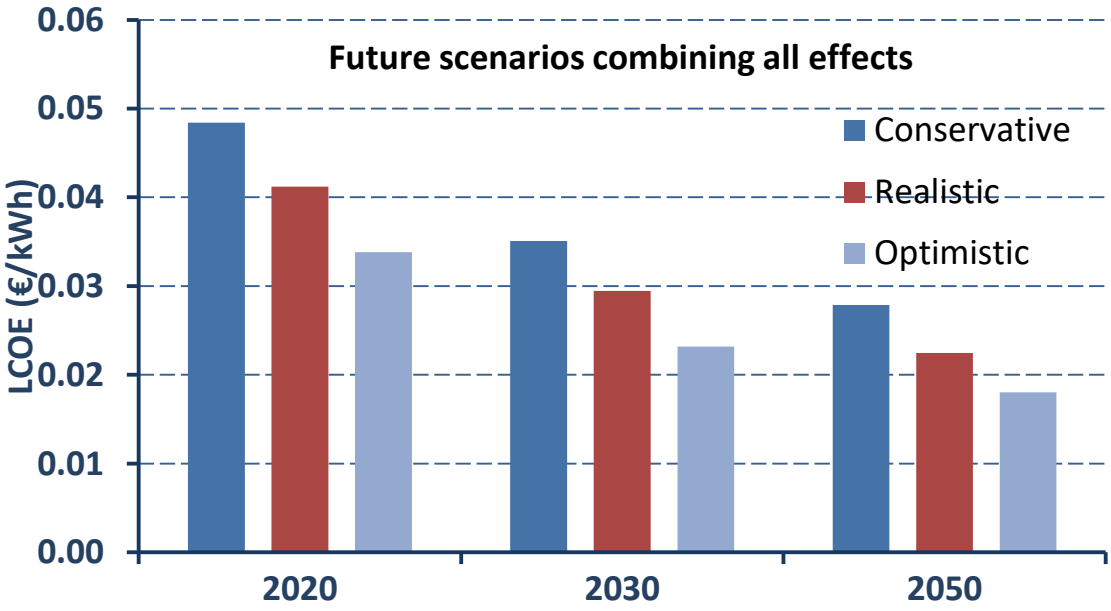

Figure 5.9: Future scenarios of all combined parameters and their effect on LCOE of the RED-MED with KAc. Top: no reheating, Middle: reheating at 50 °C. Bottom: reheating at 80 °C

As presented in the previous sections, the LCOE for the high-temperature RED-MED with KAc is expected to be about 0.05 €/kWh in 2020, making it possible to reduce to 0.03 €/kWh in 2030 and even to 0.02 €/kWh in 2050. The case without reheating (top of Fig. 5.9) is still competitive with a LCOE of 0.05-0.06 €/kWh in 2050.

For even larger plants, the LCOE of the high-temperature RED-MED with KAc can be reduced to about 0.015-0.02 €/kWh in 2050, while for very small ones (net power capacity of 170 kW, equivalent to 10 RED stacks) the LCOE is 0.07 €/kWh in 2050, which is still very competitive.

Finally, the LCOE differences between the cases with different reheating temperatures are rather small, bringing confidence that even if not all technical challenges are fulfilled concerning the long-term efficient operation of the membranes at elevated temperatures, still the reheating temperature can be restricted to 50 °C with significant performance and financial advantages.

5.3 Combined effect of future scenarios for the RED-MD

For the RED-MD case, the combined effect of all parameters is shown in Fig. 5.10.

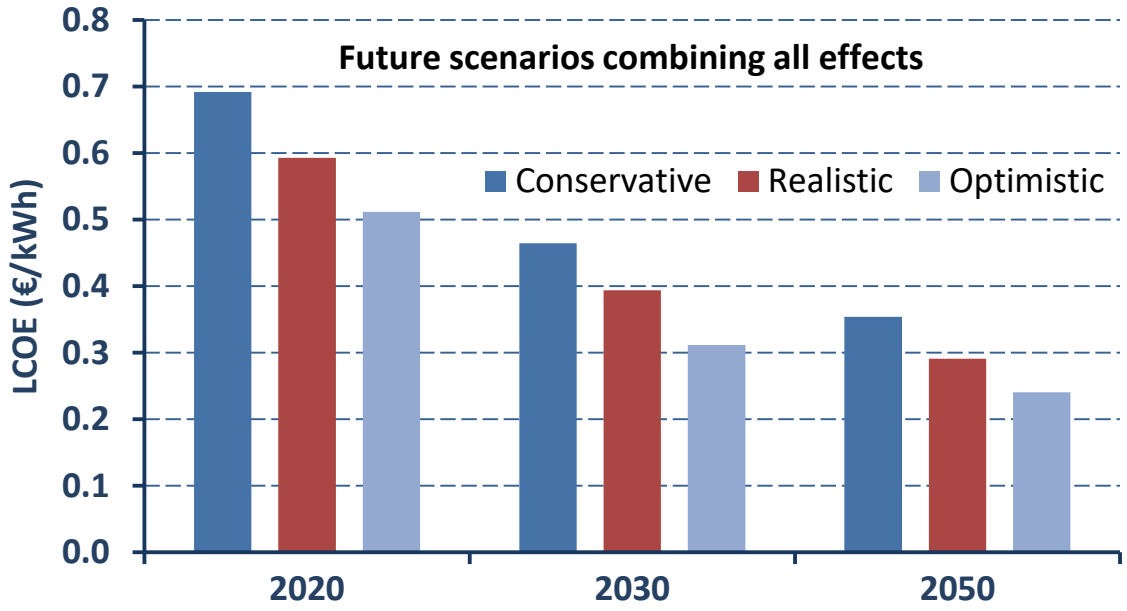

Figure 5.10: Future scenarios of all combined parameters and their effect on LCOE of the RED-MD

Even if the LCOE reduces by over two times from 2020 to 2050, still its value is around 0.29 €/kWh in 2050, making it difficult for this configuration to find a place in the market, making it necessary to focus on the further MD specific cost reduction.

5.4 Combined effect of future scenarios for the RED-thermolytic salts

For the RED-thermolytic salts case, the combined effect is shown in Fig. 5.11 for both single- and four-column cases.

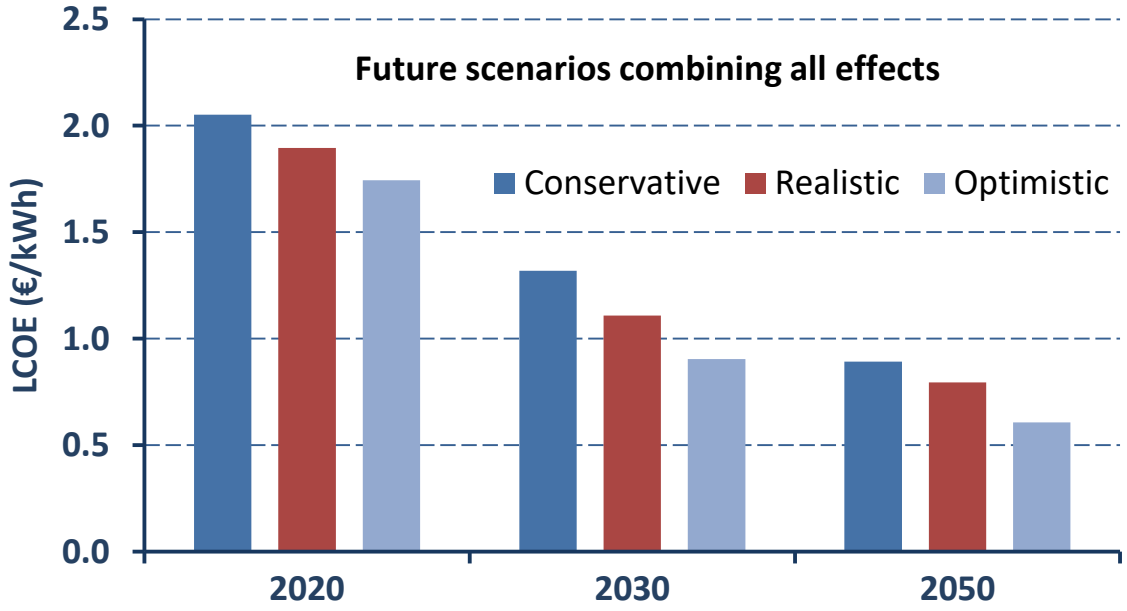

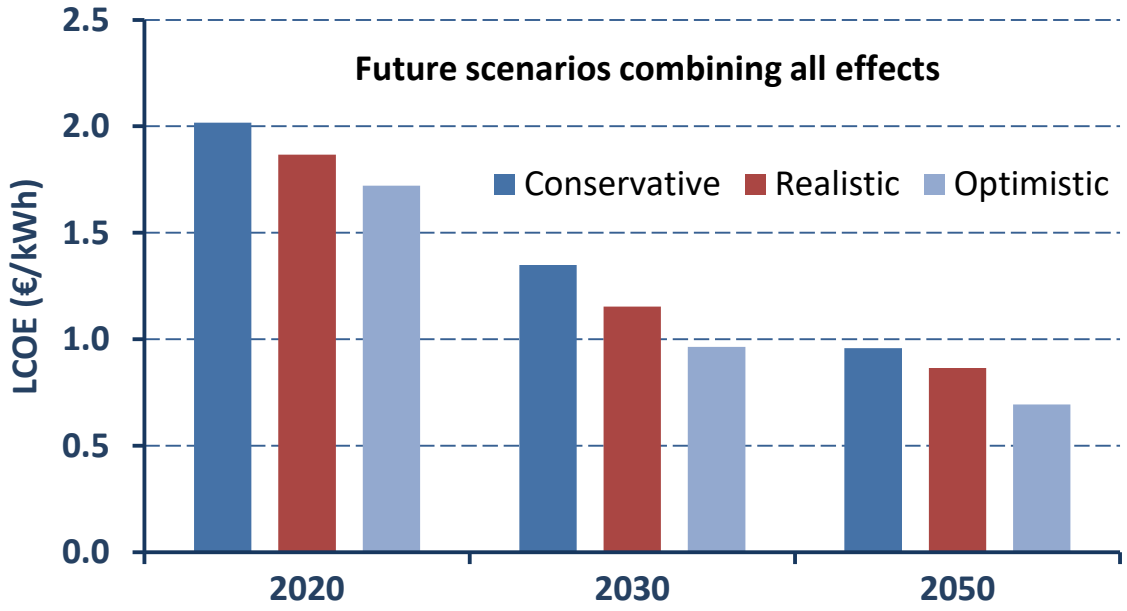

Figure 5.11: Future scenarios of all combined parameters and their effect on LCOE of the RED-thermolytic salts. Top: single-column. Bottom: Four-column

The LCOE is reduced by almost three times from 2020 to 2050, but still its value is around 0.8 €/kWh in 2050. The LCOE for the single-column case is reduced, since the RED cost contribution is higher, and it is expected to be reduced more than the cost of the regeneration unit cost. In any case, this solution is not financially sustainable, although this combination has the potential to be applied in the small-scale as well.

5.5 Conclusions

The future projections of the LCOE for various configurations have been presented. Focus was in the years 2020, 2030, and 2050. Appropriate parameters have been estimated, and the analysis considered their separate effect and their combined effect on the LCOE.

The results show that promising set-ups are the RED-MED of at least medium scale, and the high-temperature RED-MED with both NaCl and KAc. The RED-MD and the RED-thermolytic salts even if their LCOE is greatly reduced in 2050, they are still not competitive. However, the RED-MD could be applied in specific applications, mostly of small size, in which the RED-MED is not applicable, and for recovering very low temperature waste heat. A comparative analysis of all examined configurations is provided in the next section, summing-up the main highlights and conclusions.

6 Comparison of financial performance of RED with various regeneration technologies

The main highlights of all previous results are gathered in this section, in order to provide a comparative analysis of the financial performance of the different system configurations, focusing on the different regeneration technologies with the use of the RED stacks. This analysis is based on the best-performing cases of each regeneration unit, while the future scenarios are also included. The cases examined are the following:

- RED-MED with 6 MED effects.
- RED-MED with 26 MED effects.
- High-temperature RED-MED with NaCl and 6 MED effects (reheating temperature of 50 °C).
- High-temperature RED-MED with KAc and 6 MED effects (no reheating).
- High-temperature RED-MED with KAc and 6 MED effects (reheating temperature of 50 °C).
- RED-MD.
- RED-thermolytic with a single-column.

The system capacity in terms of the number of RED stacks is considered in this comparative analysis, in order to identify the limitations of each regeneration technology and its applicability limits. Therefore, the results are presented starting from a medium-scale system, and then expanded to small- and large-scale systems.

6.1 Comparative analysis of medium-scale systems

The results presented in the previous section concerning the use of a different regeneration technology with the RED stacks are gathered here, in order to gain an overview of the potential and limitations of each configuration.

For all cases examined, the future membranes are considered and 500 RED stacks are used (net capacity of 0.7-1 MW with MED, up to 8 MW with high-temperature RED-MED with KAc, 50 kW with MD -the stacks used with the MD are smaller as explained previously to fit the fixed MD module size, and 0.3 MW with thermolytic salts). The resulting LCOE of the above cases is shown in Fig. 6.1, including their future scenarios as well (only the realistic case is shown).

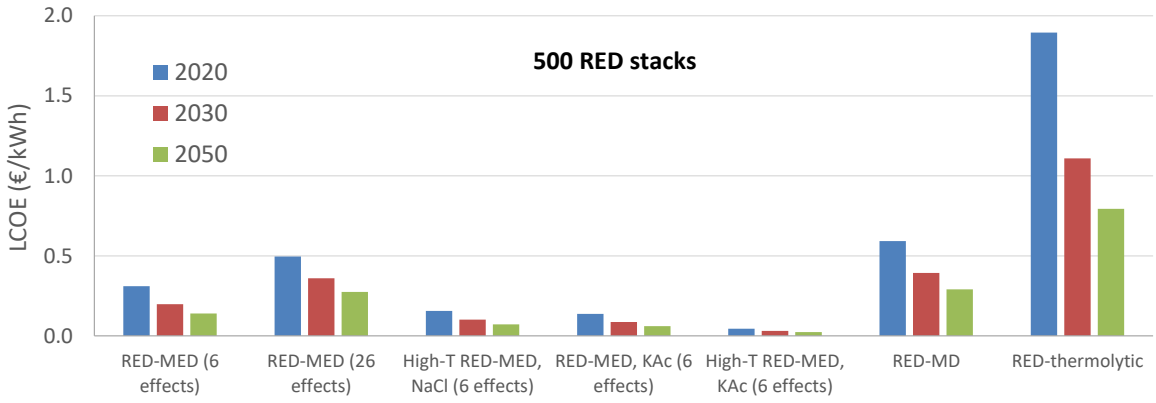

Figure 6.1: LCOE comparison of medium-scale RED with 500 stacks and different regeneration units, including future scenarios

The most cost-competitive configuration is the high-temperature RED-MED with KAc, reaching a LCOE lower than 0.03 €/kWh in 2050. The second most promising is the RED-MED with KAc and 6 effects followed by the high-temperature RED-MED with NaCl. The RED-thermolytic salts, even in future scenarios retains much higher costs than the other options.

6.2 Comparative analysis of small-scale systems

A similar comparative analysis as previously is conducted, when using less RED stacks, equal to 50 (10 times less). This capacity corresponds to below 100 kW for the configurations with the MED unit, 850 kW for the high-temperature RED-MED with KAc, 5 kW for the MD, and 30 kW for thermolytic salts. The resulting LCOE of the above cases is shown in Fig. 6.2, including their future scenarios as well (only the realistic case is shown).

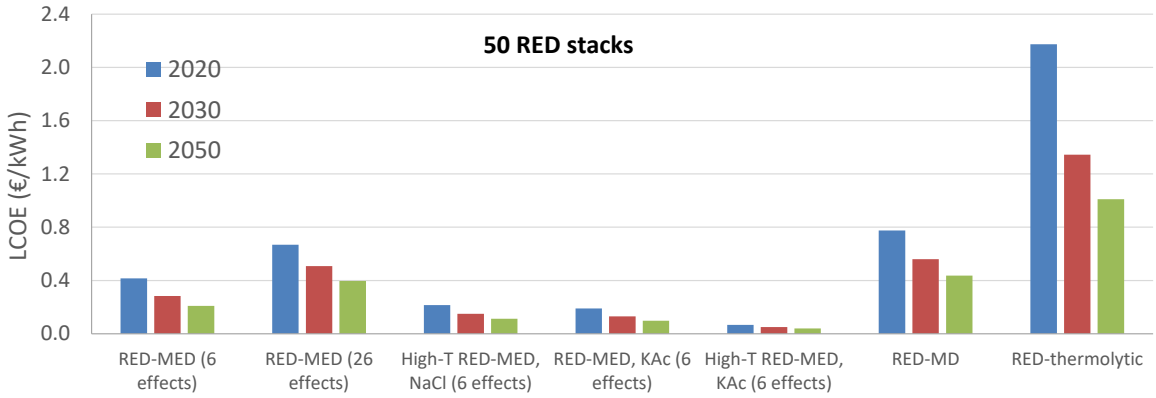

Figure 6.2: LCOE comparison of small-scale RED with 50 stacks and different regeneration units, including future scenarios

Again, the most cost-competitive configuration is the high-temperature RED-MED with KAc with a LCOE of 0.04 €/kWh in 2050. The RED-MED with KAc and 6 effects can reach a LCOE of just below 0.10 €/kWh in 2050, similar to the high-temperature RED-MED with NaCl. All the other configurations have much higher LCOE, over 0.20 €/kWh in 2050.

6.3 Comparative analysis of large-scale systems

A similar comparative analysis as previously is conducted, when using more RED stacks, equal to 5000, reaching the MW scale. The resulting LCOE of the above cases is shown in Fig. 6.3, including their future scenarios as well (only the realistic case is shown).

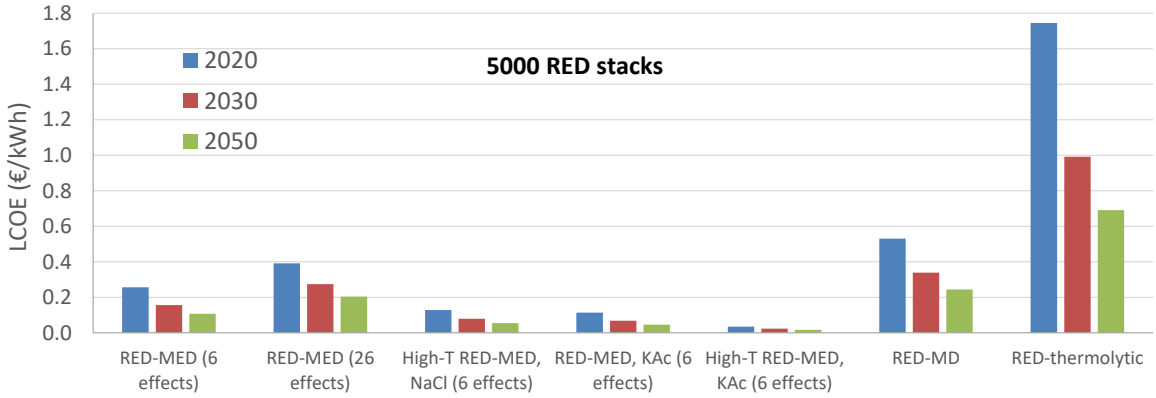

Figure 6.3: LCOE comparison of large-scale RED with 5000 stacks and different regeneration units, including future scenarios

The large-scale high-temperature RED-MED with NaCl and the RED-MED with KAc (with or without reheating) can become cost-competitive even in 2030, with a LCOE lower than 0.07 €/kWh, further reduced to below 0.05 €/kWh in 2050. Moreover, the RED-MED with 6 effects also has a good potential for becoming cost-effective in 2050 with a low LCOE value of about 0.10 €/kWh. The other configurations are not competitive even in 2050 and for large capacities.

6.4 RED Heat Engine cost-effectiveness for various scales

From the previous analysis it is clear that the best performing configuration is the RED-MED with KAc without reheating or reheated at 50 °C (both with 6 MED effects). For very small-scale systems though, the MED system becomes very expensive, while the MD keeps its specific cost constant. For these three configurations, a mapping of their LCOE has been developed and presented here, as a function of the heat availability, rather than keeping fixed the number of stacks as in the previous sections.

The results are also projected in future years, as before, while a high capacity factor of 90% and a heat source temperature of 100 °C are considered for all cases. The LCOE as a function of heat capacity is shown in Figs. 6.4-6.7 for mini (up to 0.5 MW_{th}), small (0.5-2 MW_{th}), medium (2-10 MW_{th}) and large scale (over 10 MW_{th}) systems, in order to better visualize the best performing configuration at each scale.

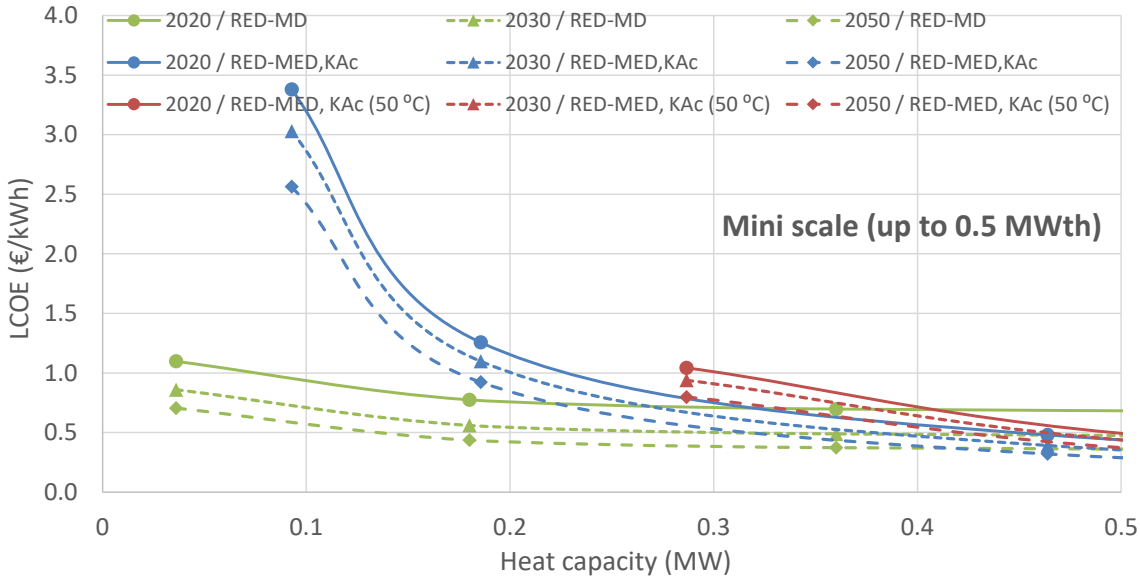

Figure 6.4: LCOE of the three best performing configurations as a function of heat capacity (mini-scale)

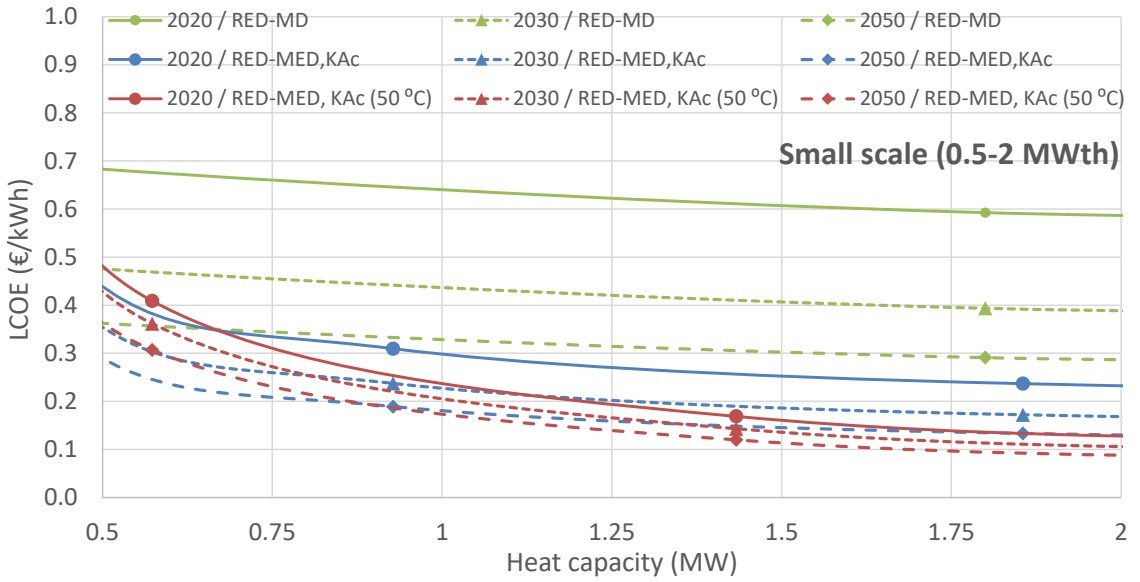

Figure 6.5: LCOE of the three best performing configurations as a function of heat capacity (small-scale)

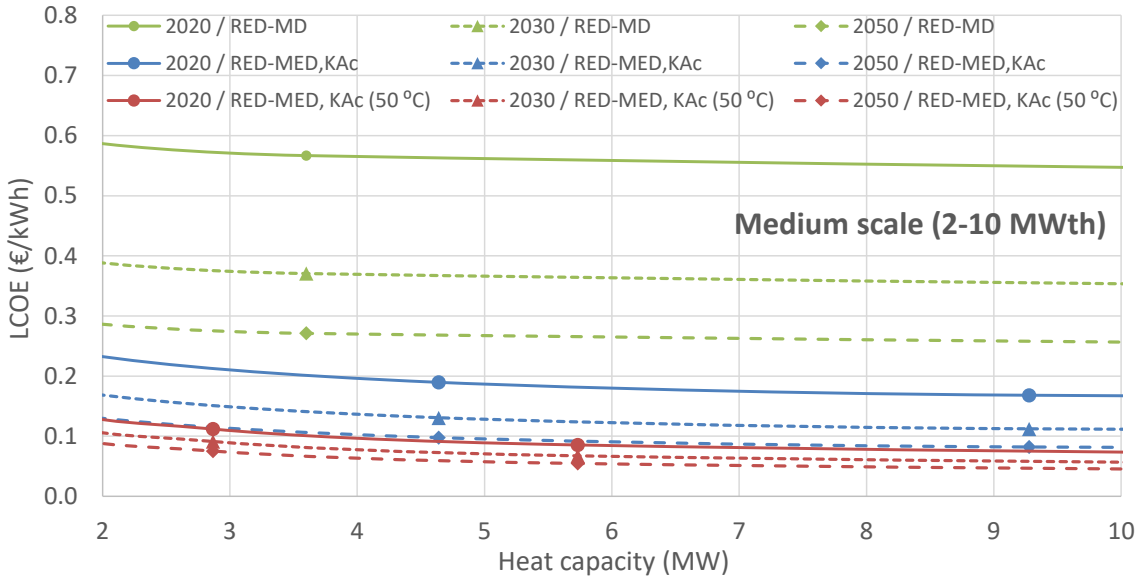

Figure 6.6: LCOE of the three best performing configurations as a function of heat capacity (medium-scale)

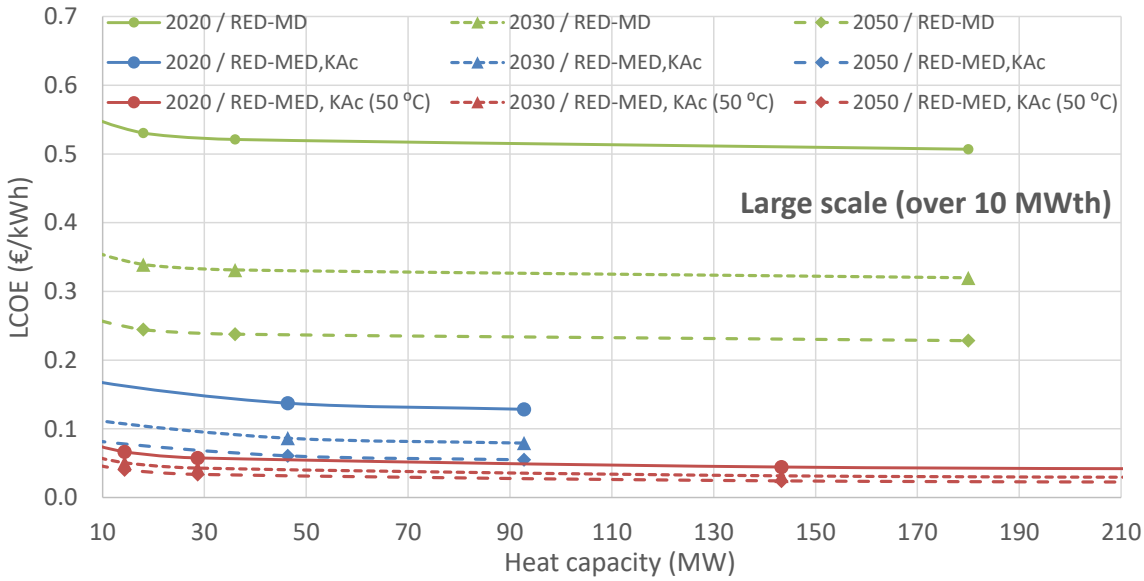

Figure 6.7: LCOE of the three best performing configurations as a function of heat capacity (large-scale)

For very small scale in terms of heat capacity (up to 0.4 MW_{th}), the RED-MD shows the lowest LCOE. However, this scale does not allow this configuration to become cost effective even by 2050, showing LCOE values over 0.35 €/kWh.

In the scale of 0.4-0.9 MW_{th}, the lower LCOE is observed by the RED-MED with KAc. This LCOE is over 0.19 €/kWh in 2050, which is possibly quite high for commercial applications but could be interesting under certain circumstances.

For even higher scale, over 0.9 MW_{th}, the RED-MED with KAc and reheated at 50 °C shows the lowest LCOE, reaching a value below 0.10 €/kWh in 2050 for a heat capacity over 1.6 MW_{th}. This LCOE threshold is reached in 2030 for a heat capacity over 2.6 MW_{th}.

In conclusion, the RED-MD shows a lower LCOE compared to RED-MED at very small scales, but still not low enough to become competitive. The RED-MED with KAc comes after that, but the LCOE values for the micro and small-scale applications are still relatively high compared to the current industrial electricity supply prices. Finally, the RED-MED with KAc solutions at higher temperatures shows the lowest LCOE for a heat capacity of over 0.9 MW_{th} and is the most promising configuration to be applied in medium and large scale applications, with the LCOE reaching values even below 0.02-0.03 €/kWh from 2030 and afterwards for very large applications.

6.5 Conclusions

Some promising regeneration technologies have been compared as a function of the number of RED stacks. In total 5 RED-MED variants have been included, as well as the RED-MD and the RED-thermolytic salts. The LCOE results have been projected in future years, and the system scale considered in the calculations. The main conclusions are listed next:

- As already presented in previous sections, the RED combined with thermolytic salts leads to very high LCOE values. These greatly drop once projected in 2050, but still far from considered a potential regeneration unit for the RED.
- The RED-MD shows a high LCOE value for all scales. However, its power production per stack differs from the other configurations. Therefore, it will be further examined in Section 8, where the system scale is examined as a function of heat input.
- The RED-MED with NaCl and 26 MED effects leads to moderate/high LCOE values. Its main advantage is its high thermal efficiency, but the use of many MED effects greatly increases the capital cost and the resulting LCOE. The similar configuration with 6 effects greatly reduces the LCOE by about 40%, making it more financially attractive.
- The high-temperature RED-MED (reheated at 50 ^{o}C) with NaCl and 6 effects lead to even lower LCOE values. This configuration is in direct competition with the best performing configurations employing KAc, highlighted next.
- The RED-MED with KAc with/without reheating shows the best financial performance at all system scales, and especially the variant with reheating at 50 ^{o}C and 6 MED effects. It has the potential to reach a LCOE of even less than 0.05 €/kWh in 2050.

7. RED Heat Engine at peak power mode

The inspiration to explore the peak power mode came from my contribution to the work on flexible industrial users of electricity that was published in 2018:

D. Papadaskalopoulos, R. Moreira, G. Strbac, D. Pudjianto, P. Djapic, F. Teng, M. Papapetrou, Quantifying the Potential Economic Benefits of Flexible Industrial Demand in the European Power System, IEEE Transactions on Industrial Informatics (Volume: 14, Issue: 11), Page(s): 5123 – 5132, Date of Publication: 08 March 2018, DOI: 10.1109/TII.2018.2811734

The configuration of the RED Heat Engine can be adjusted to operate at peak power mode. This will become a more interesting option, as the percentage of variable renewable energy connected to the grid increases, which leads to higher requirements for flexibility both on the side of electricity generation and consumption [211].

The peak power concept involves the continuous operation of the regeneration system, using all available heat for creating the salinity difference between the two solutions. Two reservoir tanks are included for storing the two solutions (of low and high concentration), after the regeneration system. The size of these two tanks can vary to accommodate the level of flexibility required. The RED system then is oversized, for converting the chemical energy of salinity gradient to electricity in a shorter period of time. In other words, when applying the peak mode configuration, the same amount of electricity is generated as in the continuous operation mode explored in the thesis up to now, but in a shorter period of time, providing higher power. The, time fraction that the RED operates is a variable that defines the level of flexibility, the size of the storage tanks and the size of the RED system. For example, if the time fraction is 50%, the size of the RED system should double.

For analysing the cost effectiveness of this mode, the same approach is followed here, as presented in the previous sections. The main differences concern:

1. The introduction of an additional parameter, expressing the time fraction that the RED part operates. In case this is unity, the previous results apply (continuous operation of both RED and regeneration parts). For time fraction lower than unity, the number of RED stacks is increased, compared to the previous cases.
2. The adjustment of the working fluid amounts and salt. This has a negligible effect on the capital cost and can be even ignored.
3. The addition of the two reservoir tanks for storing the two solutions. Their cost is added in the capital cost of the system.

A very important feature of this technology is that it shows no losses of its round-trip conversion efficiency, since the potential energy is stored in the form of salinity differences of the two solutions in the tanks. This feature gives it an advantage compared to other solutions, where the stored potential energy deteriorates over time.

7.1 Specific cost of storage tanks

Reservoir tanks have been considered, whose size ranges from a up to thousands few cubic meters. In general, the cost of the tanks is low and they have very low maintenance requirements. The specific cost of reservoir tanks has been estimated based on a recent study [212]. This specific cost is given as a function of their capacity. The results of this study have

been processed, in order to produce a fitted correlation (with R^2 approaching unity) that is shown in Fig. 7.1.

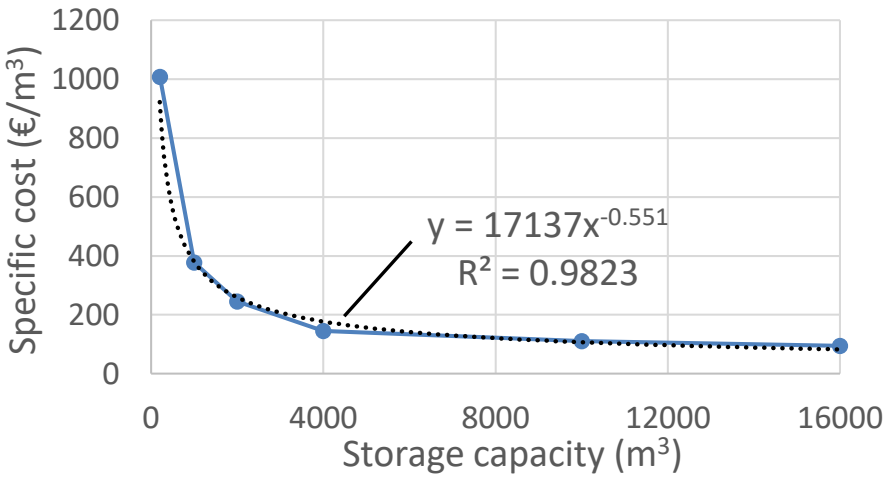

Figure 7.1: Reservoir tank specific cost as a function of its storage capacity

The above correlation is included in the cost analysis model for calculating the cost of the two storage tanks of the solutions, which have the same capacity.

7.2 Cost analysis at peak power mode

The RED-MED configuration has shown the most promising results in the previous sections, and therefore it is the only configuration for which the peak mode results will be presented in this section. Similar results are derived, when the other two regeneration technologies are considered. Two configurations are considered with future membranes and a heat source temperature of 100 °C, presented next:

1. RED-MED with NaCl without reheating and with 6 MED effects.
2. RED-MED with KAc with reheating at 50 °C and 6 MED effects.

The main parameter is the time fraction that the RED system operates compared to the MED unit, exploiting the salinity difference of the two solutions stored in the tanks. A daily storage capacity is considered, adjusting the size of the tanks (2 storage cycles per day). In case a higher storage capacity is needed, this has a negligible effect on the LCOE, since the cost of the tanks is very small compared to the total system cost, allowing at the same time to offer backup services to the grid.

The LCOE is shown in Figs. 7.2 and 7.3 for the two RED-MED cases as a function of the time fraction that the RED operates. These values are also projected to future scenarios, considering the estimated specific costs of the RED stacks.

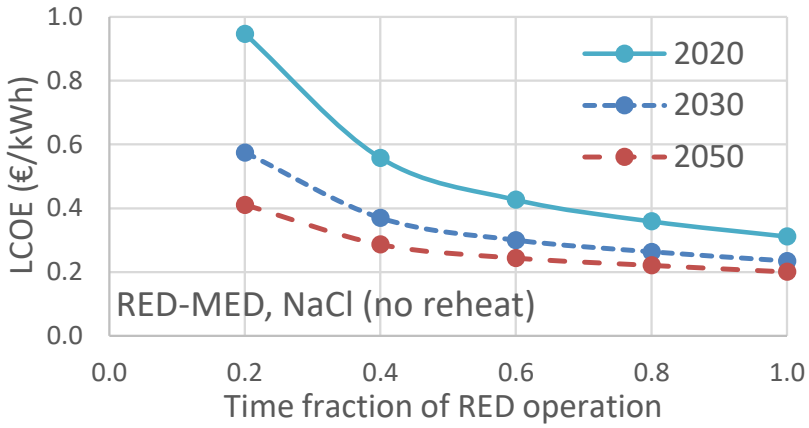

Figure 7.3: LCOE of the RED-MED with future membranes and NaCl (no reheating) at peak power production mode as a function of the time that RED operates

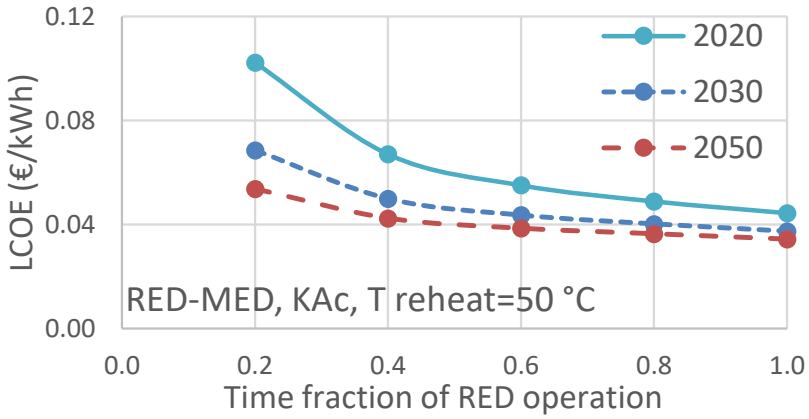

Figure 7.3: LCOE of the RED-MED with future membranes and KAc with reheating at 50 °C at peak power production mode as a function of the time that RED operates

As expected, the shorter the time fraction, the higher the LCOE, since the number of the RED stacks increases from 500 for the standard operation up to 2500 for a time fraction of 20%, keeping the same capacity for the MED. The idea is that the higher LCOE values will be compensated as the electricity (and power) will be supplied at the moments when they are most valuable, balancing the system at the moments of lower wind and/or solar energy generation.

The RED-MED with NaCl is not cost-competitive even in 2050 for operation at peak power mode. On the contrary, the RED-MED with KAc and reheating shows a LCOE below 0.10 €/kWh even for 2020 and for a time fraction of 20%, making it ideal for this kind of operating mode.

The capital cost-break-down for the projected case to 2020 and for a time fraction of 50% is shown in Fig. 7.4 for the RED-MED case with NaCl.

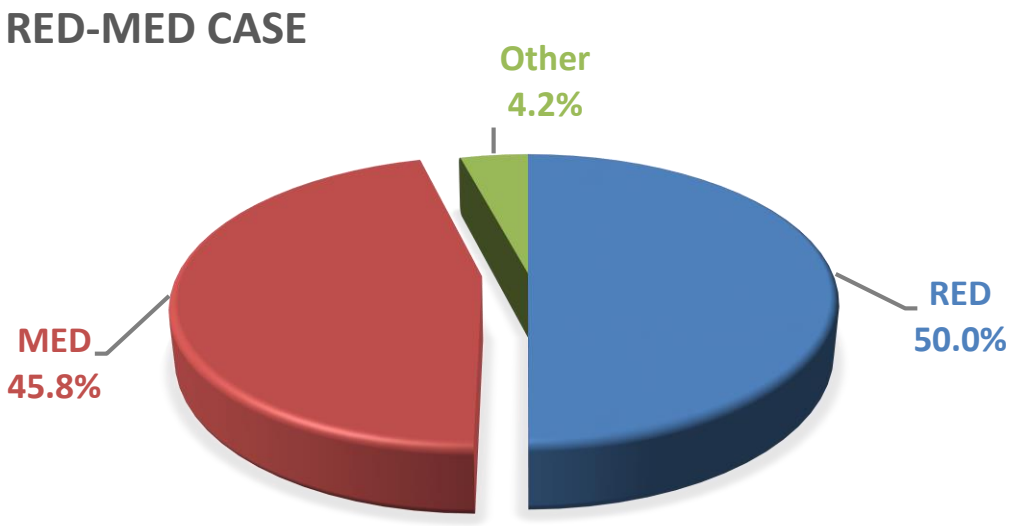

Figure 7.4: Cost break-down of the RED-MED case with NaCl and future membranes at peak power mode (time fraction of 50%)

For the standard RED-MED case, the MED capital cost represented more than 65% of the total system cost. However, as shown in Fig. 7.4, this fraction is reduced to less than 46% for a time fraction of 50%, making stronger the effect of the RED specific cost. This is one of the main reasons that a more rapid LCOE reduction is observed for 2030 and 2050 (see Fig. 7.3) compared to the cases presented in the future scenarios section (in Section 5). Similar conclusions are also reached for the RED-MED case with KAc and reheating.

Finally, the peak power production of this configuration is shown in Fig. 7.5, as a function of the time fraction that the RED operates for both configurations.

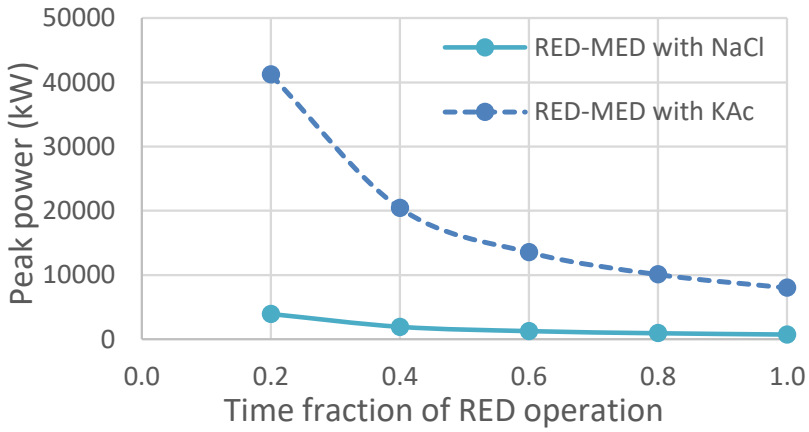

Figure 7.5: Peak power production by the RED stacks as a function of the time fraction of their operation for both configurations

For the RED-MED with NaCl at standard operation, the net power production is 728 kW, increasing to almost 4 MW for a 20% time fraction, 5 times higher. The storage capacity of each tank for the extreme case of 20% time fraction is 848 m^3, with a specific cost of 417 €/m^3. Its cost is included in the "other costs" of Fig. 7.4. For the RED-MED with KAc at similar conditions, the storage tank is 1460 m^3, with a lower specific cost of 309 €/m^3.

The peak power should be decided at the design stage, selecting the number of RED stacks and the size of the two tanks. However, the system can produce any power between its nominal capacity and its capacity without peak power mode, by adjusting the number of RED stacks that are fed with the two stored solutions. This provides the system an additional degree flexibility, which adds on the inherent flexibility of RED which can ramp-up and down from maximum to minimum capacity within seconds, without the need to warm up or, making it a valuable tool not only for balancing but also for frequency regulation and other network services that might be required in the future.

7.3 Future scenarios of the RED-MED at peak power mode

Similar as in Section 5, the future scenarios are calculated to provide the projected LCOE of the two RED-MED configurations at peak power mode. All parameters are considered in these calculations. The results are based on a time fraction of 50%, and are shown in Figs. 7.6 and 7.7 for the two RED-MED cases respectively.

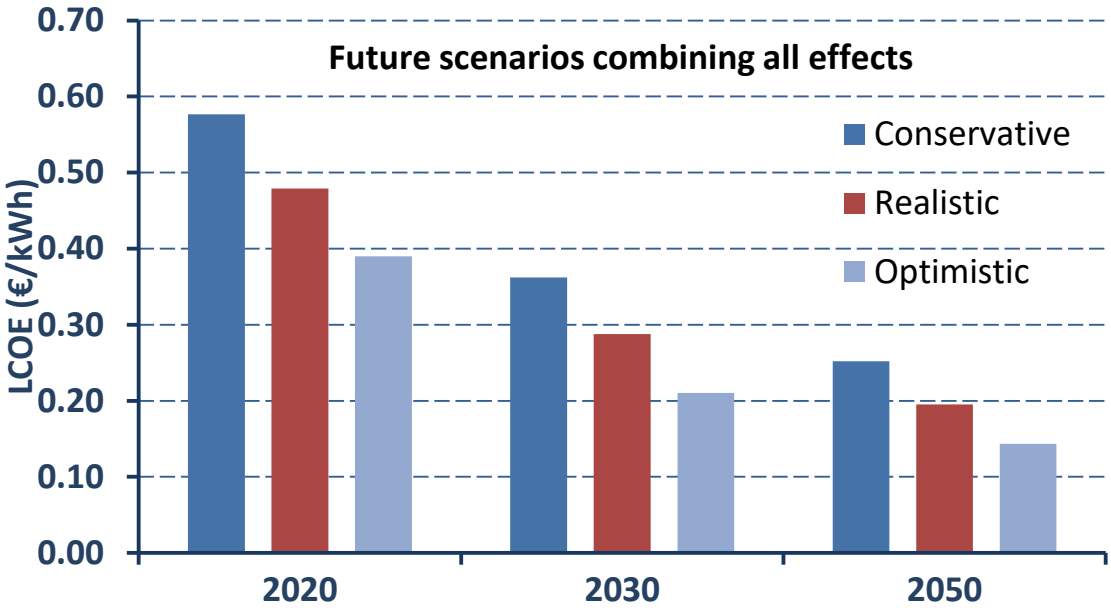

Figure 7.6: Future scenarios of all parameters and their effect on LCOE of the RED-MED with future membranes and NaCl (no reheating) at peak power mode with a time fraction of 50%

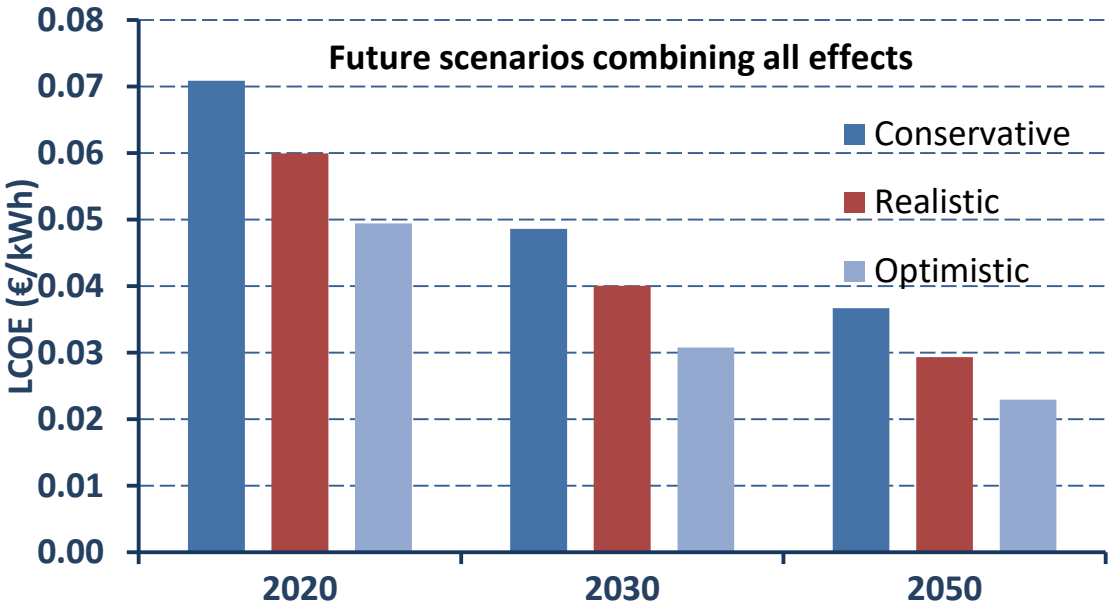

Figure 7.7: Future scenarios of all parameters and their effect on LCOE of the RED-MED with future membranes and KAc reheated at 50 °C at peak power mode with a time fraction of 50%

The system LCOE rapidly decreases in the future, due to the large cost fraction of the RED compared to the MED, as presented previously. The potential of the RED-MED with NaCl is to reach a LCOE of 0.19 €/kWh in 2050, which is rather high, but might be competitive in a market with very high shares of variable renewable energy where flexibility will be a desirable feature of both generation and consumption. On the other hand, the RED-MED with KAc and reheating can reach by 2050 a much lower LCOE of about 0.03 €/kWh, which combined with its favourable services to the grid, could be a very attractive solution for both short and long term storage.

7.4 RED Heat Engine at peak power mode for various scales

Up to now in this section, the financial performance of the RED-MED at peak power mode was examined for a fixed system scale, from 500 up to 2500 RED stacks, depending on the time fraction parameter. However, it becomes clear that the scale has a major impact on the LCOE values. Therefore, the most promising configuration of RED-MED with KAc at 50 °C and 6 MED effects is further examined, when adjusting its scale. A constant time fraction of 50% is used, and the LCOE results are projected to the future years. The system scale is expressed here as the available heat input, divided into small/medium scale for a heat input less than 10 MW_{th}, shown in Fig. 7.8, and large scale for higher heat input, shown in Fig. 7.9.

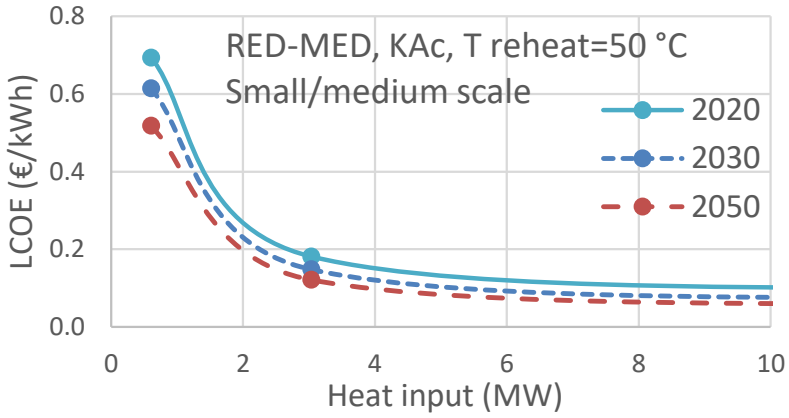

Figure 7.8: Future scenarios of all parameters and their effect on LCOE of the RED-MED with future membranes and KAc reheated at 50 °C at peak power mode with a time fraction of 50% as a function of heat input (small/medium scale)

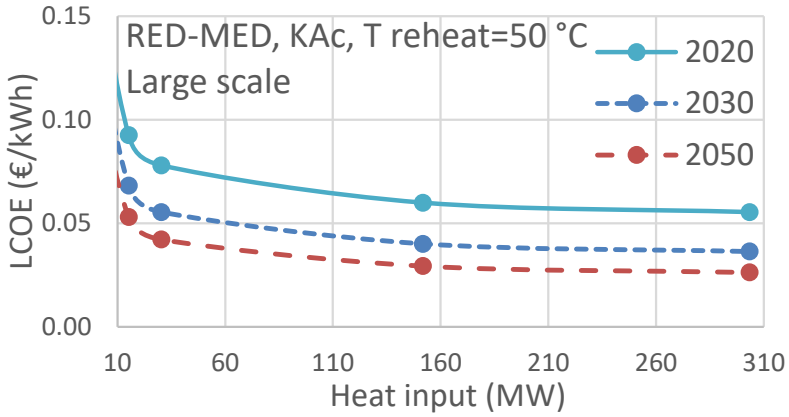

Figure 7.9: Future scenarios of all parameters and their effect on LCOE of the RED-MED with future membranes and KAc reheated at 50 °C at peak power mode with a time fraction of 50% as a function of heat input (large scale)

The system at peak power mode starts to become cost efficient for a heat input higher than 3 MW_{th}, having a LCOE lower than 0.20 €/kWh in 2020 and 0.12 €/kWh in 2050. For a heat input of 10 MW_{th}, the LCOE is already lower than 0.10 €/kWh in 2030 and for very large systems it drops to 0.04-0.06 €/kWh.

Having in mind that the majority of heat sources are up to few tens of MW, there can be concrete opportunities for this technology to be deployed for peak power production, demonstrating a low LCOE even in the 2020-2030 period.

7.5 Conclusions

The cost analysis model has been expanded to account for operation at peak power mode. The main modification was the addition of the two storage tanks and a parameter that expresses the time fraction that the RED operates. Two promising RED-MED configurations have been then examined, showing the resulting LCOE at this mode. Their LCOE values have been projected,

concluding that the RED-MED with KAc solutions reheated at 50 ^{o}C can be a very competitive solution.

For this set-up, the effects of the system scale, expressed through the available heat input, on LCOE has been explored. It has been shown that for reaching LCOE values lower than 0.10 €/kWh within the 2020-2030 period the heat input should be more than 10 MW_{th}, for a time fraction of 50%. For higher time fractions, the heat input limit is reduced, while for lower time factions the heat input limit increases. However, the LCOE threshold for the technology to be competitive is also not fixed. It will increase over time, as more variable renewable energy will get connected to the European grid, while the lower the time fraction, the more valuable the energy and power supplied, as they can be delivered only at the moments when the energy prices in the wholesale market are at a peak.

The overall conclusion is that the RED-MED with KAc can be exploited for peak power production with its financial performance depending on the system scale and time fraction of operation. In any case, low LCOE values can be obtained that can be in direct competition with electrical storage systems, such as batteries, or power plants for peak production, such as gas turbines.

This is a particularly interesting solution for large industrial energy users, who are trading in the wholesale energy market for covering the needs of their energy intensive operations. Such industries are looking for ways to hedge the risks of the energy price variations both seasonally but also for the medium to long term. These energy intensive industries have also typically large amounts of waste heat, as shown in Part I, and hence could be an early adopter of the peak power configuration of the RED Heat Engine.

8. Conclusions

A detailed tool/model has been developed for the economic analysis of the RED Heat Engine. This model includes all possible configurations with different regeneration units. The necessary technical input was obtained through the use of the process simulator, developed by other researchers at the University of Palermo [36], and the number of RED stacks was set as a free parameter to account for the system scale.

Appropriate correlations have been developed for each system component, with the main ones given as a function of their capacity/scale (e.g. the IEM, the MED unit, etc.). This allows to consider the scale of each solution in its financial performance.

Except from that, the main equipment costs have been projected in future years (2020, 2030, and 2050), which have been used in future scenarios, in order to demonstrate the potential financial sustainability of the system.

The presentation of the results started with the main set-up: the RED-MED. Various operating conditions have been examined for that purpose (e.g. number of effects, heat source temperature), including the main specifications of the RED membranes (e.g. current vs. future membranes, cell pairs per stack, membrane geometrical ratio), concluding to the parameters that lead to a reduced LCOE, which is used as the financial criterion in this study. This analysis showed that the use of future membranes is the only way for this technology to become cost-competitive and that by reducing the number of MED effects, the thermal efficiency is reduced, but at the same time the LCOE is decreased, since the MED cost fraction is lower. However, for many MED effects, the thermal efficiency could reach very high values, about 15% with a heat source temperature in the range of 100-140 ^{o}C, showing the performance potential of this technology. The RED-MED configuration has been extensively examined, with different set-ups (with or without reheating) and different salts (NaCl and KAc).

Using the main conclusions and design parameters from the previous analysis that led to low LCOE, the results of the RED-MD unit have been presented. Although its LCOE is higher for typical conditions and system sizes than the one of the RED-MED, its main advantage is its relatively low LCOE at very small-scale systems, with a capacity of few KW. This is because the MD specific cost is more or less the same as the MD size is varied.

Finally, the financial analysis of the RED-thermolytic salts has been presented. The cost of the regeneration unit has been estimated and correlated for a single- and a four-column unit as a function of the number of RED stacks. The next step was to provide the cost break-down and LCOE analysis of the system size, revealing that the resulting LCOE for this configuration is much higher than all other combinations for any system size.

The key parameters that either show some uncertainty or have a large effect on the LCOE have been included in the sensitivity analysis that followed. These parameters were mainly the system size, the capacity factor, the RED membrane specific cost, and the specific cost of the regeneration unit. The first two are related to the application, while the other two to the technological advancements of the system, which have been also included in the future projections. These projections concern the estimation of the LCOE in the years 2020, 2030, and 2050. The future scenarios showed that there is the potential to reach a LCOE below 0.10 €/kWh in various cases and applications in the future and as low as 0.02 – 0.03 €/kWh for specific large-scale applications in the period between 2030 to 2050.

Finally, the operation of the RED-MED at peak power mode can be a very interesting application of this technology, providing valuable services to the grid operators and avoiding the operation of expensive peaking power plants, usually fuelled with natural gas in gas turbines.

Part IV - Case Studies and Overall Conclusions

1. Case Studies

The performance of various typical cases is examined in this section, representing one case per sector of interest as identified in Part I of the thesis:

- Waste heat from industry, biogas plants, marine engines, and gas compression stations
- Solar thermal energy
- Geothermal energy

The RED is configured to match the sizing and heat source temperature for each case. Different system configurations are considered and their performance is compered for each case study, including all regeneration technologies, except the thermolytic salts, since it has been shown in Part III that its cost-effectiveness is very poor. The LCOE of each case is presented, including also future projections, in order to show the potential of the RED Heat Engine for each case study in future scenarios.

In the end of this section, a comparison with the ORC engine is provided, building on the results of the case studies.

1.1 Waste heat

1.1.1 Industrial waste heat – pulp and paper industry

A typical large-sized pulp and paper industry based in Sweden has been taken as an example, which includes a mill that produces bleached Kraft pulp with a production capacity of 250,000 t/year [213]. This industrial site has an average energy intensity of about 17,000 MJ/t (4722 kWh/t), which is close to the EU average value. About 84% of this energy demand concerns process heat. The annual heat demand is 1180 GWh/year. The waste heat recovery fraction for this industry type is 7.39%, as presented in Part I, resulting to a waste heat potential of 87.2 GWh/year at temperature in the range of 100-200 °C (closer to the lower limit of the range). This corresponds to a thermal capacity of about 12.44 MW_{th}, considering a capacity factor of 80%. By matching this thermal with the performance characteristics of each system configuration that is considered here, a different number of RED stacks and net power capacity is calculated for each configuration, as shown in Fig. 1.1. The resulting LCOE of each case, assuming that the waste heat is available at a temperature of 100 °C is presented in Fig. 1.2.

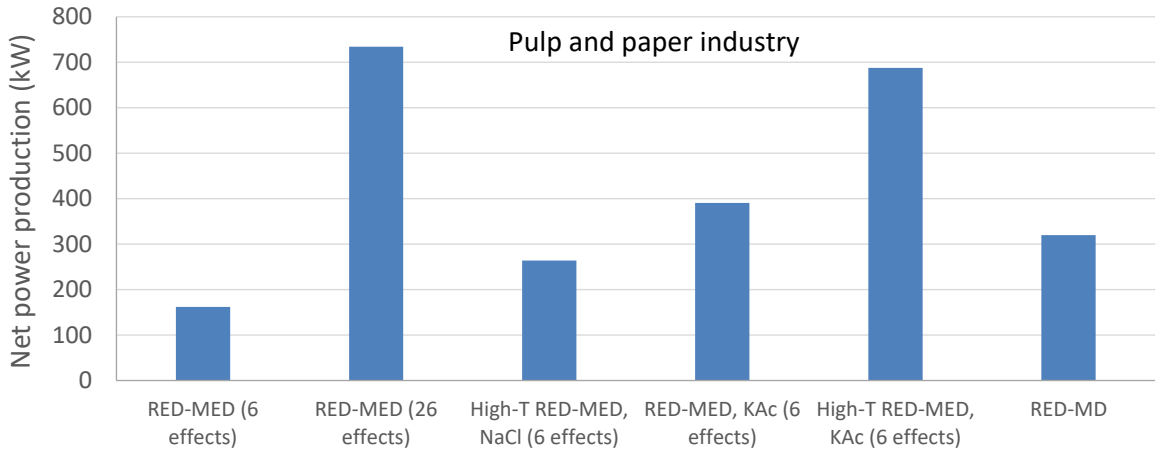

Figure 1.1: Net power capacity of each configuration for the pulp and paper industry

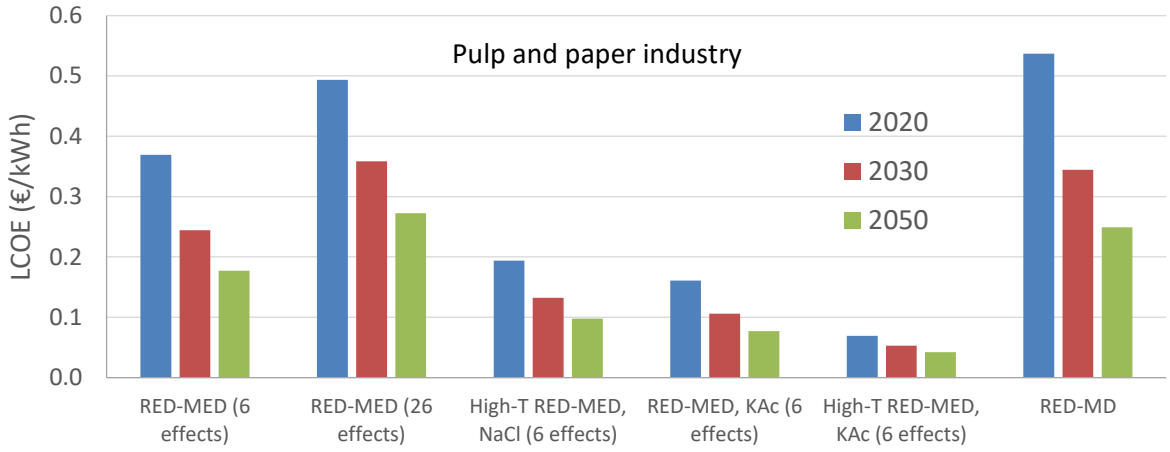

Figure 1.2: LCOE of each configuration for the pulp and paper industry in future scenarios

The RED-MED with 26 effects shows a high thermal efficiency, allowing to greatly increase its power production to similar values as the high-temperature RED-MED with KAc, having a net power production of 700 kW. However, this is not adequate to reach a low LCOE, as shown in Fig. 1.2. The high-temperature RED-MED with NaCl and RED-MED with KAc without reheating show a good financial performance, reaching a LCOE of 0.10 €/kWh in 2050, while the best performing case is the high-temperature RED-MED with KAc and 6 MED effects with a LCOE of about 0.05 €/kWh in 2030 reducing to 0.04 €/kWh in 2050.

1.1.2 Industrial waste heat – food industry

A typical medium-sized food industry has been described within the IEE project GREENFOODS [214]; this project performed energy audits in various food industrial sites of different type and size. About 6,300 MWh/year of heat from natural gas are required for high-pressure steam production and auxiliary heating, and another 800 MWh/year from heating oil for low-temperature steam. The waste heat losses are high especially from the gas boiler due to the high-temperature operation (from flue gases). They have been estimated at almost 2,800 MWh/year at approximate temperature of about 200-250 °C, with a waste heat potential of 1,500 MWh/year. The waste heat potential from the oil boiler is much lower and estimated to about 150 MWh/year at 180 °C.

The total waste heat potential is thus 1,650 MWh/year and considering a capacity factor of 80%, the waste heat capacity is 235.45 kW_{th}. With a typical pinch point temperature difference of 50 K in the case of a gaseous stream, as is the case here, and other heat losses, the heat input temperature is 120 °C.

Following the same process as in the previous section, the resulting net power production of each configuration, once matched with the above waste heat capacity, is shown in Fig. 1.3 and the LCOE of each solution in Fig. 1.4.

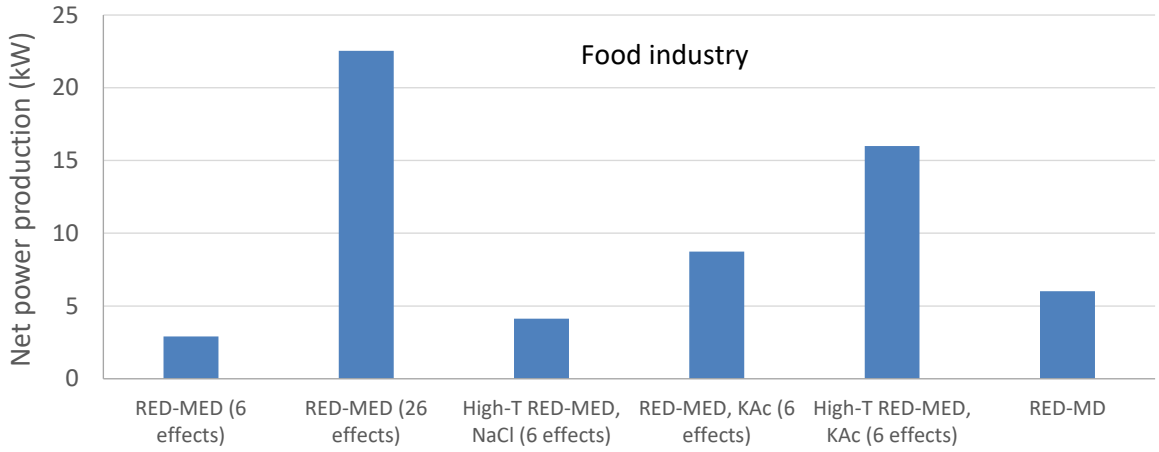

Figure 1.3: Net power capacity of each configuration for the food industry

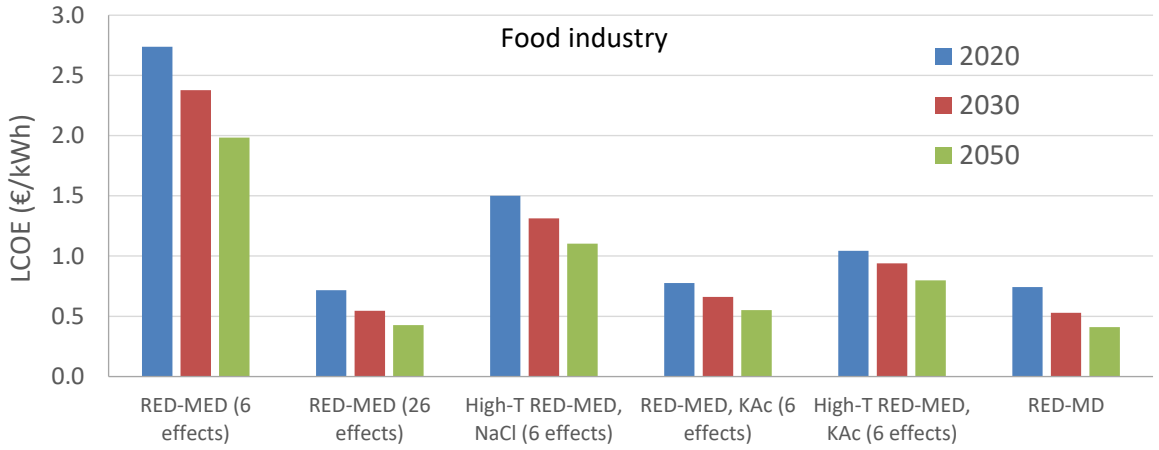

Figure 1.4: LCOE of each configuration for the food industry in future scenarios

This application is rather small for the RED Heat Engine, resulting to small-scale systems of less than 22 kW of net power production with 26 MED effects, reducing to less than 15 kW for 6 effects. This small size is not competitive especially for the RED-MED configurations with few MED effects, due to the very large specific cost of MED in such small scales. On the other hand, the RED-MD configuration performs better than the other ones, even though its LCOE is still high in 2050, at about 0.40 €/kWh. The financial performance for the RED-MED with 26 MED effects is similar to the one of the RED-MD, due to a better exploitation of the available heat and the increase of its scale that allows to reduce the specific costs. Similar results are also obtained with the RED-MED with KAc and more MED effects or with NaCl and reheating and 21 effects (not shown in Fig. 1.3 and 1.4).

It becomes clear that the developed system is not suitable for such small scales where its main competitor, the ORC, has proved its cost-effectiveness. Therefore, it is necessary to focus on larger systems for industrial waste heat recovery, as in the pulp and paper industry presented previously.

1.1.3 Waste heat from a biogas CHP plant

In 2006 a biogas plant was developed in a German farm [215], as shown in Fig. 2.46. This plant includes two gas engines with a capacity of 370 kW_e (gross) each for CHP operation. The electricity production is 5,800 MWh/year with parasitic losses – own consumption - about 10% of that (580 MWh/year). Heat production is 5,000 MWh/year with about 25% of this required by the anaerobic digester for its operation. The rest is partially used for drying purposes and the remaining is dissipated to the ambient.

Figure 1.5: Biogas plant in Germany for CHP operation (source [215])

It is estimated that the rejected amount of heat to the ambient is about 1,900 MWh/year, and considering that the capacity factor is 89.5%, heat capacity is 242 kW_{th}, with its temperature in the range of 90 to 150 °C. An average heat source temperature of 100 °C has been considered in the calculations. The resulting net power production of each configuration, once matched with the above waste heat capacity, is shown in Fig. 1.6 and the LCOE of each solution in Fig. 1.7.

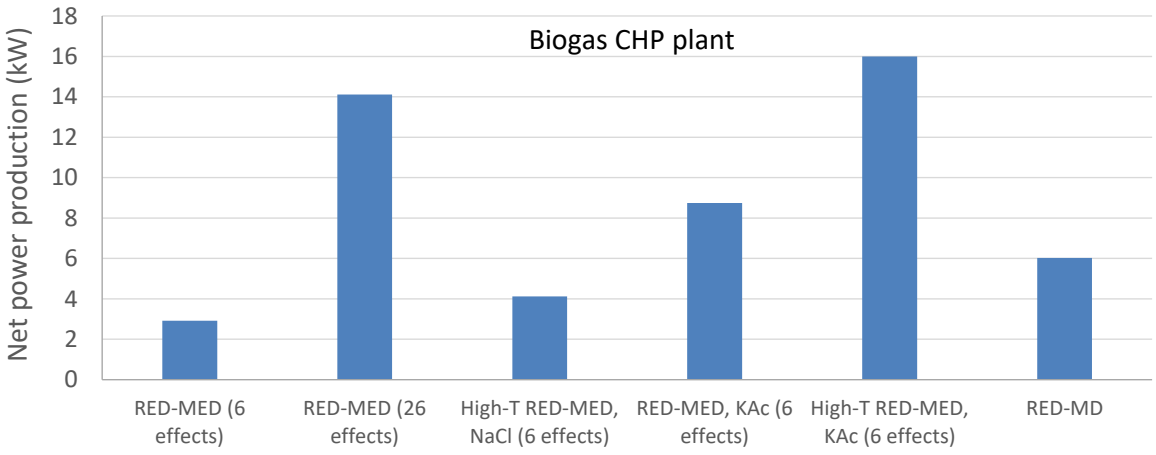

Figure 1.6: Net power capacity of each configuration for the biogas CHP plant

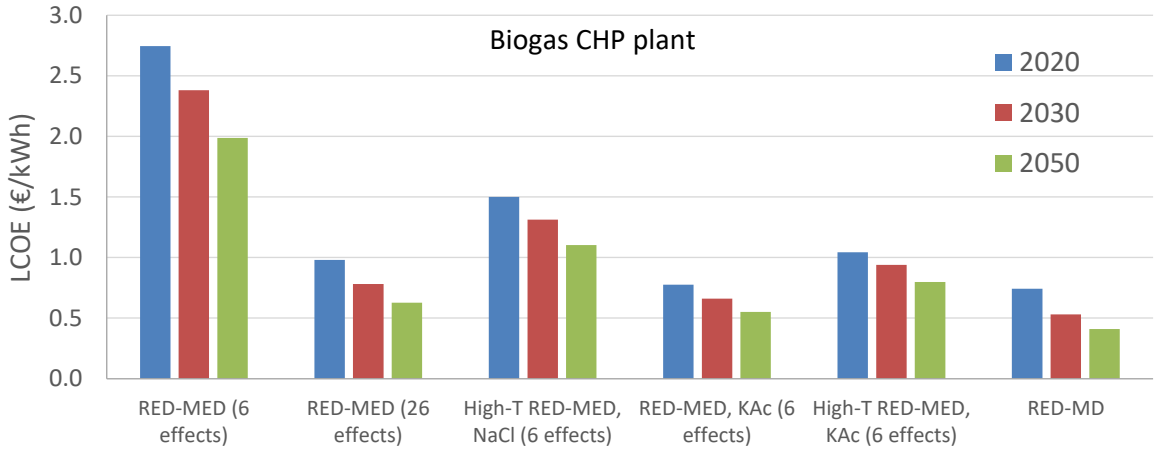

Figure 1.7: LCOE of each configuration for the biogas CHP plant in future scenarios

This case has many similarities with the previous food industry case, since the available waste heat is almost the same, with the maximum net power production of 16 kW. The RED-MED with 26 effects does not operate as well as in the previous case, due to the lower temperature of the available heat. The most promising solution is the RED-MD, but still far away from cost-effectiveness, since its LCOE is about 0.41 €/kWh in 2050. This is much higher, than the current feed-in-tariff of 0.169 €/kWh that the specific plant receives for the electricity that it provides to the grid.

1.1.4 Waste heat from auxiliary marine engines

A medium-sized bulk carrier of 35,000 deadweight tonnage (DWT) serves as a typical example for investigating the waste heat potential in ships [216]. This ship is depicted in Fig. 1.8.

Figure 1.8: Medium-sized bulk carrier (source [216])

This ship is equipped with three auxiliary engines for electricity production, each with a net capacity of 500 kW_e, which is the typical size of gensets in ships (two for standard operation and one for backup). According to the usual time distribution at sea, loading/unloading, and

manoeuvring, as well as the operating load and number of engines operating (most of the times only one), the electricity production is 3.95 GWh/year. The available waste heat from the cooling circuit (at temperature of 85-90 °C) of both auxiliary engines is 2.8 GWh/year, and if only the main auxiliary engine is considered then this potential decreases to 2.4 GWh/year. If the RED Heat Engine sizing is based on the maximum capacity, then the heat input is 625 kW_{th} (at 85-90 °C). In that case the system capacity factor needs to be adjusted to 51.1%, reducing the potential of this technology. The heat source temperature used in the calculations is 80 °C (heat input from liquid stream, the jacket water, with low pinch point temperature difference of 5-10 K), leading to a maximum of 20 MED effects for the 2nd configuration considered.

The resulting net power production of each configuration, once matched with the above waste heat capacity, is shown in Fig. 1.9 and the LCOE of each solution in Fig. 1.10.

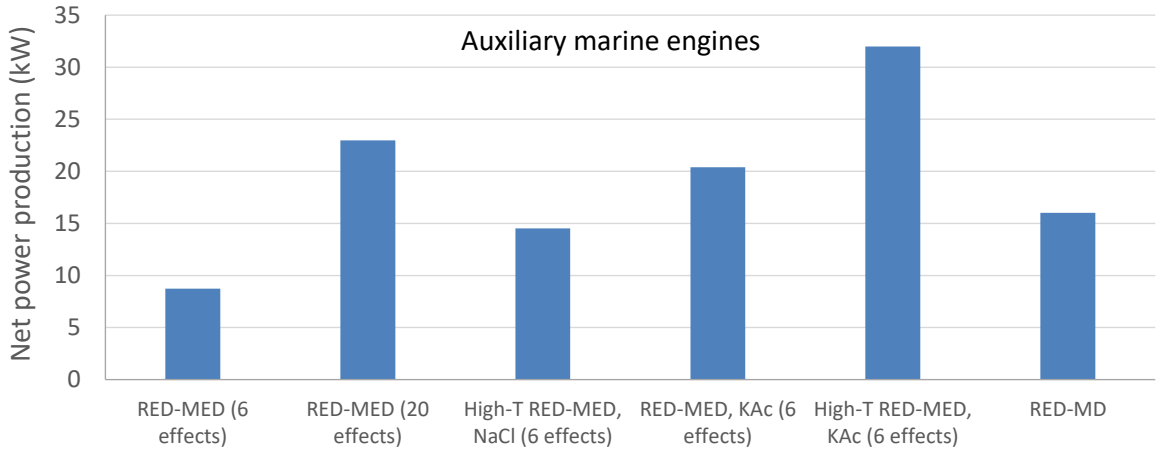

Figure 1.9: Net power capacity of each configuration for the auxiliary marine engines

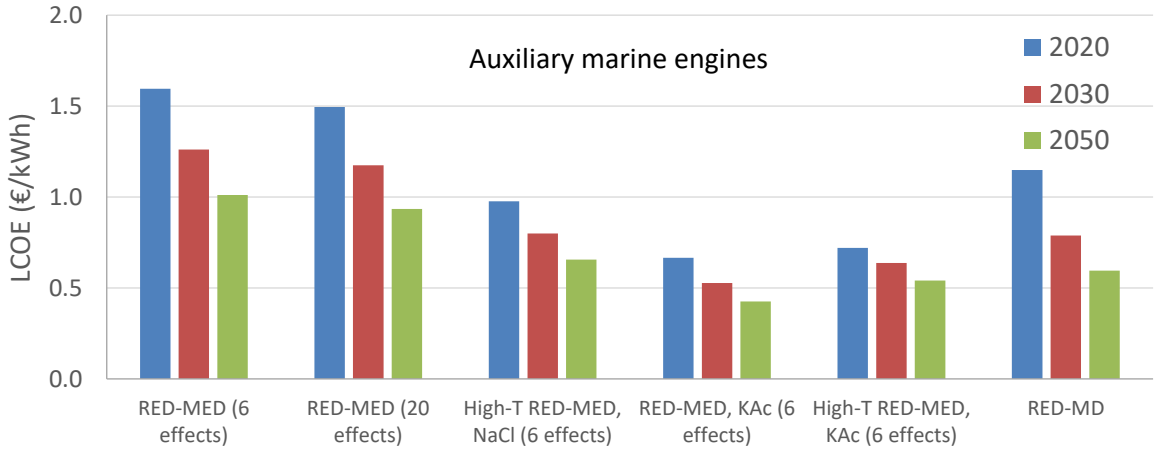

Figure 1.10: LCOE of each configuration for the auxiliary marine engines in future scenarios

The thermal capacity of this case study is more than two times higher than in the biogas CHP plant, leading to a similar increase of net power production. However, its reduced capacity factor and lower heat source temperature lead to less cost-competitive solutions. Even the RED-

MD solution shows LCOE values of up to 0.5 €/kWh in 2050, with the best-performing configuration being the RED-MED with KAc at 50 °C with a LCOE of 0.42 €/kWh in 2050.

8.1.5 Waste heat from a gas compression station

A gas compressor station in Poland serves as the case study to examine here. It is has a capacity of 51.3 MW in total and is located in Halberstadt [217]. It has two separate units; the first is equipped with 8 electric-driven compressors (2.5 MW_e each), and the second with two gas turbines of 31.3 MW capacity. The annual energy balance of this station is depicted in Fig. 1.11.

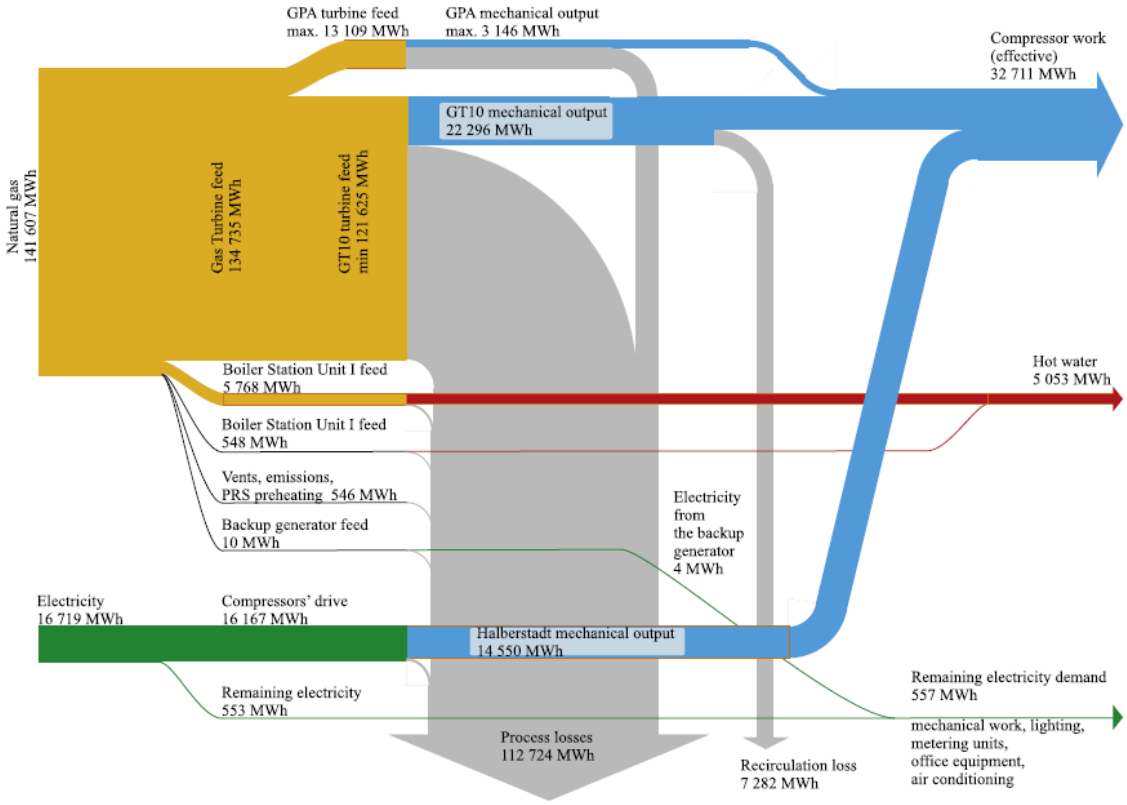

Figure 1.11: Annual energy balance of Halberstadt station (source: [217]*)*

The waste heat is about 112 GWh/year at temperature about 250-300 °C. However, the technical potential of this waste heat is reduced by almost 10%, leading to 100 GWh/year that can be recovered. The capacity factor of this station relevant to the gas turbines is very low, about 12%, since they operate at very low load, supported by the electric-driven compressors. The waste heat capacity is thus 95.1 MW_{th}, feeding with heat the RED Heat Engine. The main disadvantage of this application is the low capacity factor, since the other conditions are favourable (e.g. large-scale system, high temperature operation).

The resulting net power production of each configuration, once matched with the above waste heat capacity, is shown in Fig. 1.12 and the LCOE of each solution in Fig. 1.13.

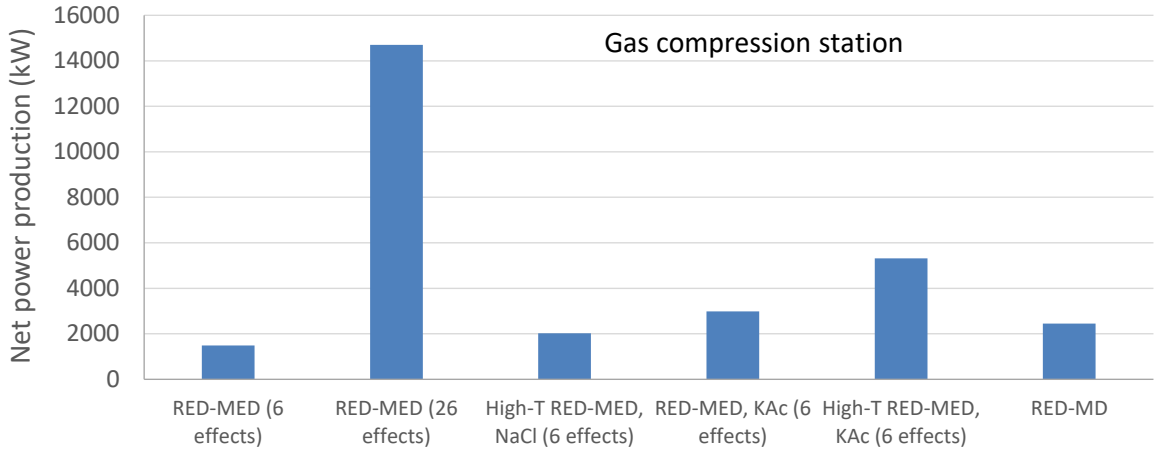

Figure 1.12: Net power capacity of each configuration for the gas compression station

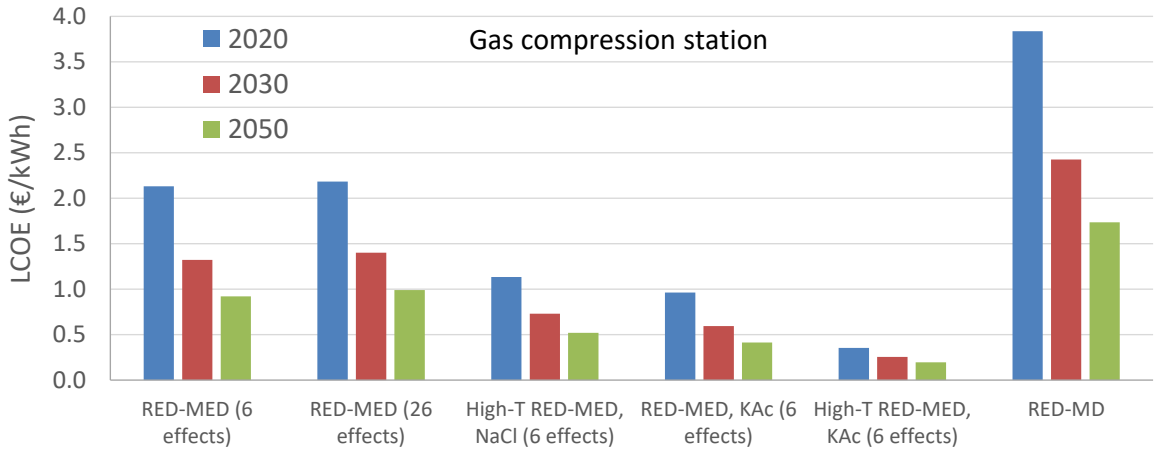

Figure 1.13: LCOE of each configuration for the gas compression station in future scenarios

The financial performance is weak, due to the very low capacity factor. All configurations with the MED give better results than with the MD, but still far from considered a sustainable solution. Only the RED-MED with KAc at 50 °C approaches cost-effective solutions with a LCOE of 0.19 €/kWh in 2050.

In case the capacity factor is increased by 5 times and reaches 60%, as is the case in other gas compression stations, the LCOE with the high-temperature RED-MED with KAc can reach the value of 0.04 €/kWh in 2050. If this factor is further increased to 90%, then very competitive solutions are reached with this set-up with the LCOE values reaching 0.03 €/kWh in 2050.

1.2 Heat from geothermal energy

A modern geothermal plant for CHP operation has been developed and initiated operation in Sauerlach, Germany (Munich area) [218] in 2014. Thermal water has a flow rate of about 110 l/sec and temperature 140 °C reaching a depth of 4,200 m, as shown in Fig. 1.14.

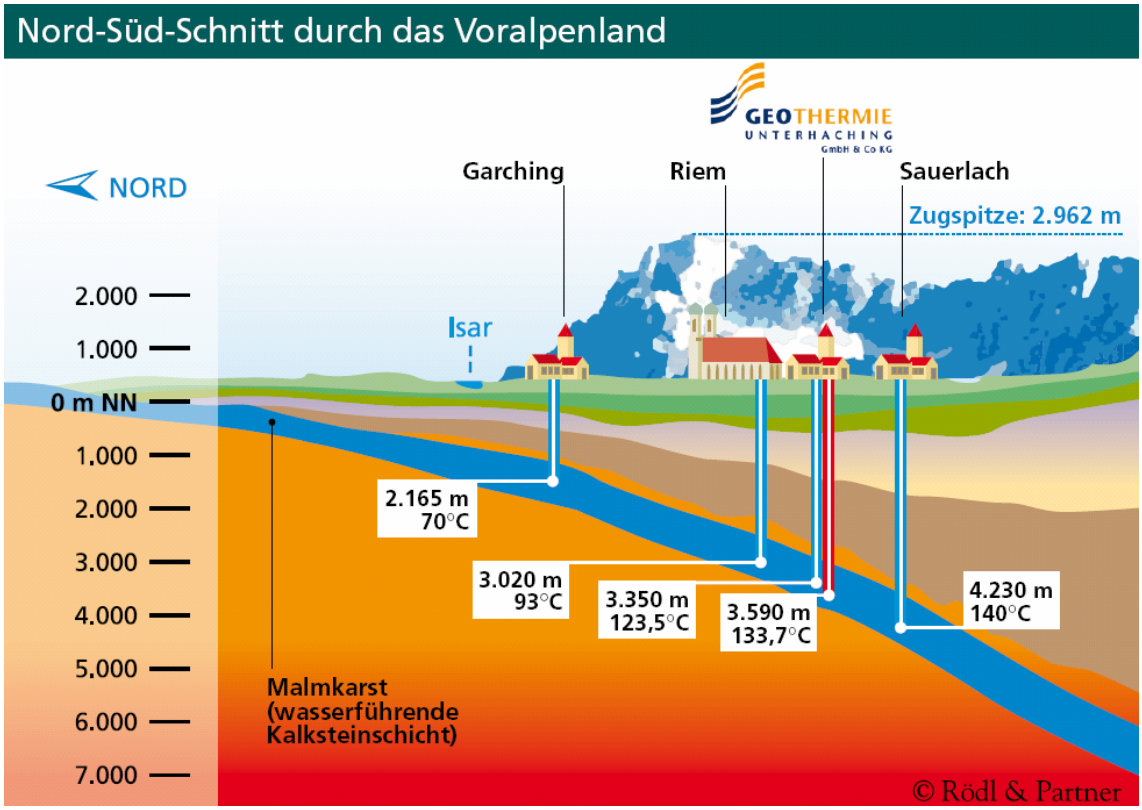

Figure 1.14: Sauerlach, Munich, geothermal field

The plant's thermal capacity is about 43 MW_{th} (1 production wells and 2 injection ones) and currently an ORC unit is used to produce electricity with capacity of 5 MW_e and efficiency of 11% [219]. A 2-step cycle has been used (high and low temperature), by-passing the second one in case heat supply is required. This configuration is used to maximize the annual electricity production, which is equal to 40 GWh/year.

The case study here considers is a power plant in Munich, Germany, following the successful example of the plant in the Sauerlach area. At a depth of about 3 km, the geofluid temperature can be about 100 °C, and hold a capacity as in the Sauerlach plant (of 43 MW_{th}) and a high capacity factor of 90%. The specific cost of geothermal infrastructure is 2,000 €/kW_{th}, as presented in Part I for new field installations.

The resulting net power production of each configuration, once matched with the above geothermal heat capacity, is shown in Fig. 1.15 and the LCOE of each solution in Fig. 1.16.

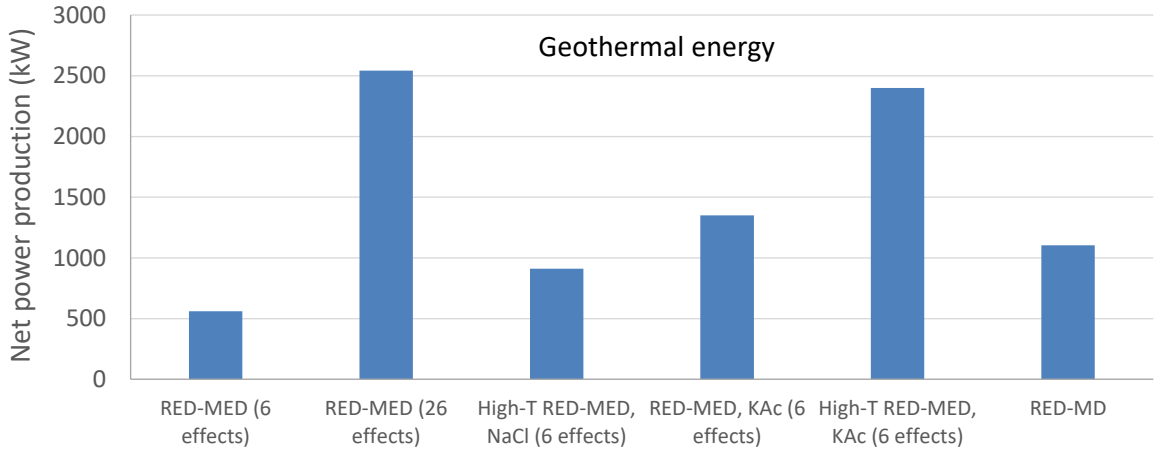

Figure 1.15: Net power capacity of each configuration supplied by geothermal heat

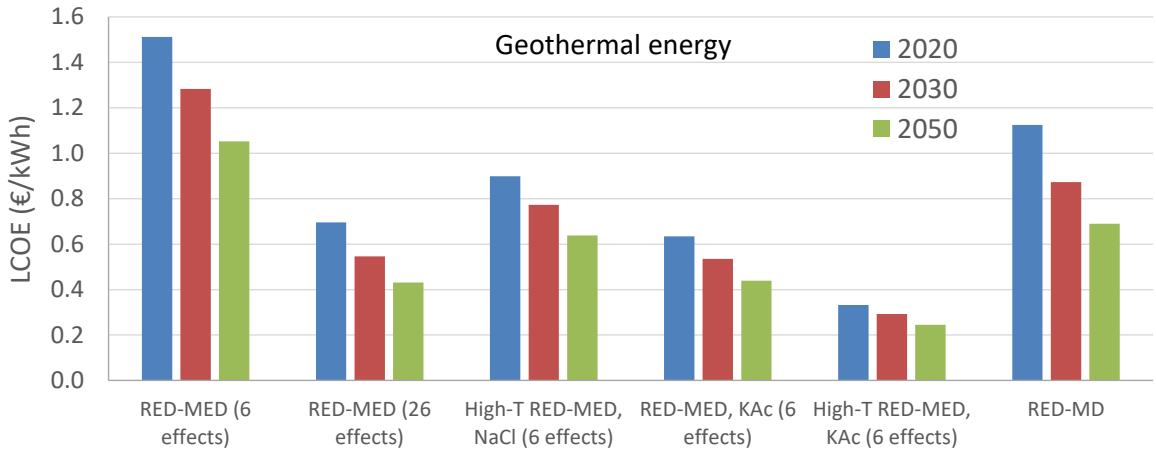

Figure 1.16: LCOE of each configuration supplied by geothermal heat in future scenarios

The capital cost of geothermal infrastructure is high, representing more than 70% of the total system cost. Therefore, a good heat exploitation is needed in this case, which can be achieved with the use of many MED effects in the RED-MED configuration, or with very high performing RED-MED with KAc. This is why these set-ups show the best financial performance. However, their LCOE in 2050 is still over 0.25 €/kWh, showing that they are not in the position of competing with other technologies, such as the ORC for exploiting geothermal heat, which is the prevailing technology. As mentioned in Part I, the only option might be to use the technology at sites where there are already (abandoned or operational) wells.

1.3 Heat from solar thermal collectors

A small-sized solar field of 1,000 m^2 with vacuum tube solar collectors is assumed for providing solar heat to the RED Heat Engine. A similar solar field is shown in Fig. 1.17 [220] as an example. The annual heat production is 820 MWh/year at temperature of 100 ^oC in Athens, Greece. Heat capacity is 600 kW_{th} (capacity factor of 16% of full load equivalent operation) and a typical specific cost of 300 €/m^2 is used. With an average collector efficiency of 50%, the resulting cost

is 600 €/kW_{th}. These cost figures have been included in the cost analysis model, adjusting the capital cost.

Figure 1.17: Solar field of vacuum tube solar collectors

The resulting net power production of each configuration, once matched with the above solar heat capacity, is shown in Fig. 1.18 and the LCOE of each solution in Fig. 1.19.

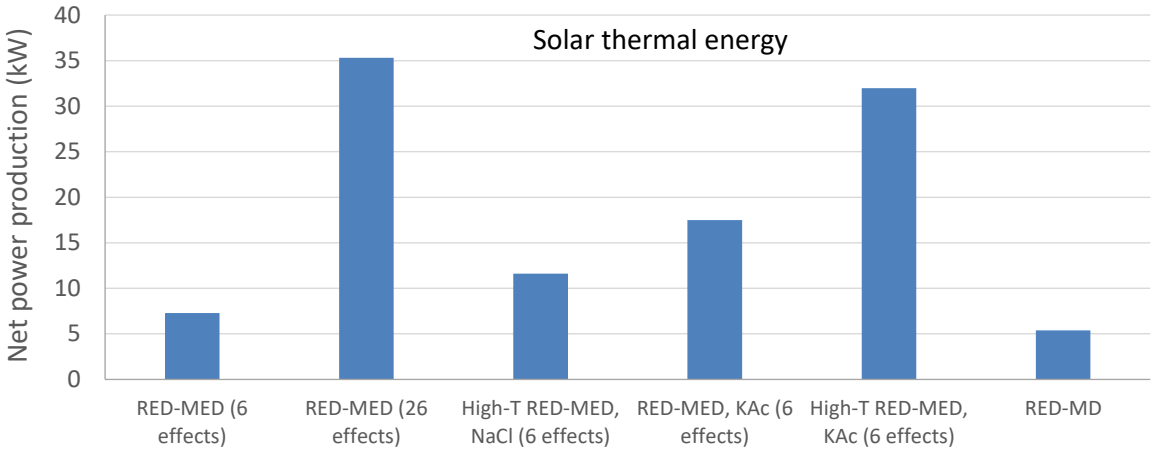

Figure 1.18: Net power capacity of each configuration supplied by solar heat

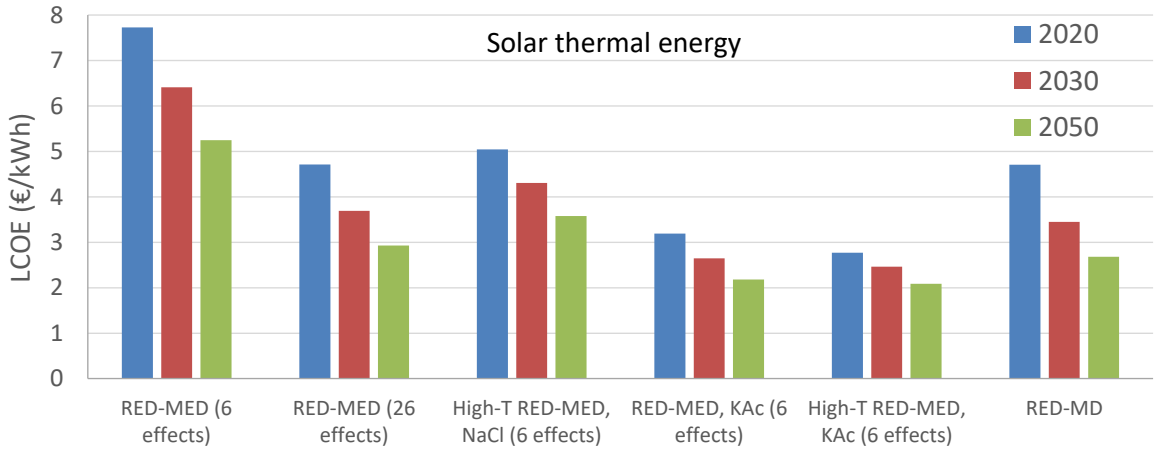

Figure 1.19: LCOE of each configuration supplied by solar heat in future scenarios

It becomes very clear that the RED Heat Engine is not suitable to be combined with solar collectors for exploiting their produced heat. The main reasons behind this is the additional capital cost needed for the collectors (about 20-30% of the system cost) and the low capacity factor, even in the sunny regions of south Europe. The resulting LCOE is always higher than 2 €/kWh, even in 2050. The small-scale considered also contributes on this poor financial performance. However, if a larger size is used with 100 times higher capacity (60 MW_{th}), the LCOE reduces but still always higher than 0.76 €/kWh in 2050.

1.4 Comparison of RED Heat Engine with ORC technology

The main competing technology is the ORC, which is also suitable for exploiting heat sources of low-temperature [221]. ORC is applicable for a heat input as low as 70-80 °C and can be scaled down to capacities of few kW [207]. ORC has already passed to commercial level with high growth [222], numerous manufacturers and existing installations in a variety of sectors (industry, biogas and geothermal plants, solar, etc.). One concern that ORC systems face is the use of organic fluids (e.g. refrigerants, hydrocarbons), which most of them have a significant environmental impact. In 2015, a new EU regulation (called "F-Gas regulation": Regulation (EU) No 517/2014 [223]) has been placed restricting the use of refrigerants with moderate/high Global Warming Potential (GWP) and non-zero Ozone Depletion Potential (ODP), and phasing-out many common ones. Although new ultra-low GWP fluids have been recently developed with GWP of less than 10, their cost is still high. There are on-going efforts for further reducing the environmental impact of the working fluids.

The ORC systems also need a high capacity factor to become cost-effective, while their specific cost (assuming a heat source temperature of 100 °C) is in the range of 3,000-3,500 €/kW for small-scale systems with capacity less than 100 kW, reducing to about 2,000 €/kW for large systems of over 0.5-1 MW.

The LCOE of ORC depends on various parameters similar to the RED Heat Engine (heat source temperature, size, capacity factor, etc.), typically in the range of 0.05-0.10 €/kWh, and demonstrating a payback period of about 3-4 years [137] in the most favourable conditions (e.g. when feed-in-tariffs are applied), increasing to 6-8 years for industrial waste heat recovery applications of medium/large scale.

The ORC technology is already applied with its global installed capacity constantly increasing, currently over 320 GWe. The cost reduction potential of ORC is limited, introduced mostly by the further increase of the relevant projects (economies of scale) and not from its performance increase. Therefore, the future projections of this technology concerning its LCOE can be slightly lower than the current one. This makes it possible to identify the cases, in which the RED Heat Engine is a favourable heat exploitation technology, when applying the LCOE values projected for the 2030 to 2050 period. An overview is provided in Table 8.1, based on the case studies presented previously, providing qualitatively the favourable technology per case study and scale (small/medium/large). The small scale here also includes the mini scale presented previously. The "plus" signs denote:

- "+": Limited or no potential (indicated on the table with red filling of the table cell)
- "++": Possible potential and moderate LCOE that could become cost-effective (indicated on the table with orange filling of the table cell
- "+++": High potential with low LCOE (indicated on the table with green filling of the table cell)

Table 1.1: Overview of favourable heat exploitation technologies in typical case studies according to the plant scale

Case study	Small scale		Medium scale		Large scale	
	RED HtP	ORC	RED HtP	ORC	RED HtP	ORC
Industrial waste heat	+	++	++	++	+++	++
Biogas CHP plant	+	+	++	++	+++	++
Auxiliary marine engines	+	+	+	++	+	++
Gas compression stations	+	+	+	+	+	+
Gas compression stations (with high capacity factor)	+	+	++	++	+++	+++
Solar thermal	+	+	+	+	+	+
Geothermal	+	+	+	++	++	+++

The opportunities of the RED Heat Engine become clear from the above table, showing the applications in which the developed technology can be a more favourable heat exploitation system than ORC (or equally favourable). These concern both medium and large-scale systems for exploiting heat in:

- Industries (waste heat)
- biogas CHP plants (excess/waste heat)
- gas compression stations with high capacity factor (waste heat)

These opportunities can be pursued by the partners of the RED Heat-to-Power project, according to the development and actual costs in future scenarios, using the results of this thesis to guide the next development stages.

2. Overall Conclusions

The RED Heat Engine operates as a closed-loop RED system, where limited amounts of artificial saline solutions are used as working fluids. The solutions exiting from the RED unit are regenerated by means of a separation step, which uses low-temperature heat as its energy source. Essentially the system converts low-grade heat to electricity

This thesis studied the RED Heat Engine perspectives in terms of:

- the sources that can provide the heat necessary for running the system, indicating the characteristics that the system should have to match the market requirements
- the life-cycle impacts, providing evidence for the environmental credentials of the technology, compared to alternative electricity supply options, and providing direction to system designs with the minimum environmental impacts.
- economic performance, improving the understanding of the factors that affect it, including the design options, operational choices as well as the development over time of the key components in terms of performance and cost

The available waste heat and its potential from various sectors was studied, such as industry, biogas plants, gas compressor stations and marine auxiliary engines. These four sectors show a total waste heat potential of about 700 TWh/year. The heat that is available at temperatures over 200 ^{o}C is still a valuable resource that can be used in other applications. If we focus only at the heat that is available at temperatures lower than that, the overall potential is reduced to 484.02 TWh/year. The potential at biogas plants and on marine auxiliary engines corresponds to small RED Heat Engines in the range of 7 to 15 kW_e. The potential at gas compression stations is for much larger systems, in the range of 6 to 10 MW_e, but the capacity factor is sometimes low. Finally, in industry the range can be very wide, but most would fall within the range of 280 to 700 kW_e. As shown in the case-studies, the industrial waste heat is the most interesting resource.

The geothermal resource analysis showed that such plants should be of large size, in order to compensate the initial investment costs and produce large amounts of electricity. Even for large plants, we have seen in the case study in section 1.2 that the costs are still high for being competitive with alternative solutions. The only possibility for reaching costs that are acceptable is to use existing geothermal fields of large scale.

The potential daily and seasonal solar heat production was calculated for different regions in Europe, representing the main climatic zones (south/central/north Europe). However, the case study showed clearly that this is an option that is not feasible, because of the high investment costs for collecting the heat and the low capacity factor.

The RED Heat Engine has lower environmental impacts compared to other energy generation technologies and compared to grid electricity. Between the different regeneration technologies, the distillation columns with the thermolytic salts give the highest environmental impacts and the MED gives the lowest environmental impact. The factors that affect mostly the environmental performance of the RED Heat Engine are the system lifetime, the performance of the ion exchange membranes and the metallic parts of the heat exchangers. The system efficiency is not that important from an environmental impact point of view. Reducing the number of MED effects has a positive impact to the environmental performance, even if it reduces the efficiency, because it leads to much lower use of metals for heat exchangers.

A detailed economic analysis of the RED Heat Engine has been performed. When using the RED-MED configuration, the results show that the use of ion exchange membranes that will be optimised for the RED Heat Engine application is necessary for this technology to become cost-competitive. By reducing the number of MED effects, the thermal efficiency is reduced, but at the same time the LCOE is also decreased. The salt that showed the best performance was KAc, while operation of the RED with the working fluid at 50 ^{o}C has also a very positive effect on the LCOE. The LCOE for the RED-MD configuration is higher than the one of the RED-MED, for typical conditions and system sizes. The main advantage of the RED-MD is that it can be scaled down for use at systems with capacity of few KW without a very negative effect on its LCOE, because the MD specific cost is more or less the same as the MD size is varied, which is not the case for the MED. The result is that the RED-MD is in general most cost-efficient than RED-MED for systems that are below 20-30 kW_e. But the LCOE is at levels that are not competitive with other technologies. For the RED-thermolytic salts configuration it has been shown that the LCOE is much higher than all other combinations for any system size.

The sensitivity analysis and the assessment of future scenarios showed that there is the potential to reach LCOE values below 0.10 €/kWh in various cases and applications in the future. In general, relatively large system sizes and high capacity factors are necessary to reach LCOE values that can make the system competitive. However, when it is necessary to install infrastructure for making the heat available to the RED Heat Engine (or when there is a charge for the heat supply) the values of LCOE are too high for the system to be financially viable.

Finally, the operation of the RED-MED at peak power mode can be a very interesting application of this technology, especially as more variable renewable energy sources are connected to the grid, making more volatile the wholesale energy prices and more valuable the provision of flexibility to the system.

Overall, we have seen that the following are among the main conditions that are necessary for the competitiveness of the RED Heat Engine:

- Optimised membranes that at least match the “future membrane” properties
- High capacity factors
- Medium to large scale applications
- Free availability of heat

For future research, the most important priority is the improvement of the ion exchange membranes, aiming for achieving the performance targets of “future membranes” and aiming to make them available at the membrane costs foreseen in Part III. This is a pre-condition for the commercial application in the future. Once this is achieved, the RED Heat Engine can enter the market, targeting applications where there is more than 1 to 2 MW_{th} of heat available at temperatures of at least 80 ^{o}C, with capacity factors over 60% without any associated costs. The most common setting where these conditions exist are the medium or large-scale industrial plants as well as the gas compression stations, provided that they operate with a high capacity factor.

The next priority, for widening the potential applications to sites where smaller systems can be installed, is the research on regeneration systems that are competitive at smaller scale. The one option is to develop MD systems with drastically reduced specific costs, through a combination of increased system performance and reduced costs of the main components. The other option

is to develop MED designs suitable for smaller scale applications, as proposed in Ref. [224]. One option for reducing the specific costs and the environmental impacts of smaller MED systems would be the development and use of polymeric heat exchangers.

Another issue that has to be examined once the RED Heat Engine is closer to commercial adoption is the integration of the system within an industrial plant and whether the required retrofitting will affect the operational characteristics of the plant. The most relevant points are the footprint of the engine and the heat extraction system. With regards to the footprint, the RED stacks are quite compact: a stack of 1 m^3 with future membranes and the conditions examined in this thesis could produce up to 17 kW; as a result, the stacks for a 1MW system would require 15 – 30 m^2 of floor area, depending on the height of the building. However, it would also require a 3000 m^3/day MED plant, which has an important footprint and could not fit within the current structures of standard industrial plants. The heat extraction system depends on the form in which the heat is available. If the heat is available in the form of hot water the extraction is not an issue. But if the heat is available in the form of exhaust gases, additional infrastructure would be required, such as special heat exchangers (economisers). Future research can focus on optimal integration approaches, where the relevant costs are minimised and potential concerns of the industrial plant operators for the heat engine affecting their processes are addressed.

Overall, the RED Heat Engine is a promising technology that could play a role in the future power system contributing to the decarbonisation targets set by the European Union.

Annexes and References

Annex I – Full results of the LCA

Full results of the LCA for the seven scenarios

Scenario 1										
Category	Unit	Total	kg/MWh	copper	nickel	steel	plastic	transport	end-of-life	
Mass	kg	121.0757259		1.96%	87.29%	5.03%	4.74%	0.09%	0.25%	99.37%
GWP potential	kg CO2 eq.	0.046667105	168.0015767	37.21%	34.27%	19.56%	5.87%	2.01%	0.59%	99.51%
Eutrophication Pc	kg Phosphate eq.	1.63133E-05	0.058727937	26.82%	48.65%	12.32%	3.90%	6.09%	1.96%	99.74%
Acidification Pote	kg SO2 eq.	0.000986101	3.549963296	7.14%	89.66%	2.17%	0.41%	0.39%	0.08%	99.85%
Terrestric Ecotoxi	kg DCB eq.	0.002414744	8.693078032	86.01%	12.69%	0.33%	0.62%	0.07%	0.15%	99.87%
Ozone Layer Depl	kg R11 eq.	1.33426E-09	4.80332E-06	99.98%	0.00%	0.00%	0.01%	0.00%	0.00%	100.00%

Scenario 2										
Category	Unit	Total	kg/MWh	copper	nickel	steel	plastic	transport	end-of-life	
Mass	kg	25.71880168		1.47%	65.32%	11.02%	18.86%	0.13%	0.69%	97.49%
GWP potential	kg CO2 eq.	0.012330619	44.39022801	22.39%	20.62%	32.75%	18.77%	2.33%	1.29%	98.15%
Eutrophication Pc	kg Phosphate eq.	4.01779E-06	0.014464029	17.31%	31.40%	22.47%	13.40%	7.60%	6.08%	98.25%
Acidification Pote	kg SO2 eq.	0.000167964	0.604669611	6.66%	83.67%	5.83%	2.05%	0.71%	0.26%	99.18%
Terrestric Ecotoxi	kg DCB eq.	0.000400981	1.443532965	82.33%	12.15%	0.97%	3.17%	0.13%	0.58%	99.32%
Ozone Layer Depl	kg R11 eq.	2.12221E-10	7.63997E-07	99.92%	0.00%	0.00%	0.08%	0.00%	0.00%	100.00%

Scenario 3										
Category	Unit	Total	kg/MWh	copper	nickel	steel	plastic	transport	end-of-life	
Mass	kg	6.72870735		1.62%	72.00%	9.20%	14.57%	0.12%	0.56%	98.06%
GWP potential	kg CO2 eq.	0.00303378	10.92160805	26.24%	24.17%	29.33%	15.42%	2.25%	1.10%	98.50%
Eutrophication Pc	kg Phosphate eq.	1.00722E-06	0.00362601	19.91%	36.12%	19.69%	10.80%	7.18%	4.95%	98.66%
Acidification Pote	kg SO2 eq.	4.72437E-05	0.170077307	6.83%	85.78%	4.54%	1.47%	0.60%	0.19%	99.42%
Terrestric Ecotoxi	kg DCB eq.	0.000113809	0.409713192	83.64%	12.35%	0.74%	2.26%	0.10%	0.43%	99.52%
Ozone Layer Depl	kg R11 eq.	6.1184E-11	2.20263E-07	99.94%	0.00%	0.00%	0.06%	0.00%	0.00%	100.00%

Scenario 4										
Category	Unit	Total	kg/MWh	copper	nickel	steel	plastic	transport	end-of-life	
Mass	kg	2.295891029		1.38%	61.52%	12.05%	21.30%	0.14%	0.77%	97.16%
GWP potential	kg CO2 eq.	0.001138093	4.097134283	20.39%	18.78%	34.53%	20.51%	2.37%	1.38%	97.96%
Eutrophication Pc	kg Phosphate eq.	3.672E-07	0.001321919	15.92%	28.88%	23.95%	14.78%	7.82%	6.68%	98.03%
Acidification Pote	kg SO2 eq.	1.43528E-05	0.051669907	6.56%	82.32%	6.66%	2.42%	0.78%	0.30%	99.03%
Terrestric Ecotoxi	kg DCB eq.	3.40655E-05	0.122635805	81.47%	12.03%	1.12%	3.76%	0.14%	0.68%	99.20%
Ozone Layer Depl	kg R11 eq.	1.78448E-11	6.42411E-08	99.90%	0.00%	0.00%	0.09%	0.00%	0.00%	100.00%

Scenario 5										
Category	Unit	Total	kg/MWh	copper	nickel	steel	plastic	transport	end-of-life	
Mass	kg	1.212436563		1.87%	83.23%	6.14%	7.35%	0.10%	0.33%	99.02%
GWP potential	kg CO2 eq.	0.00048842	1.758311818	33.95%	31.26%	22.47%	8.71%	2.08%	0.74%	99.21%
Eutrophication Pc	kg Phosphate eq.	1.68182E-07	0.000605455	24.84%	45.05%	14.43%	5.88%	6.40%	2.82%	99.43%
Acidification Pote	kg SO2 eq.	9.51245E-06	0.034244813	7.07%	88.74%	2.73%	0.66%	0.44%	0.10%	99.75%
Terrestric Ecotoxi	kg DCB eq.	2.32038E-05	0.083533724	85.45%	12.61%	0.42%	1.01%	0.08%	0.22%	99.79%
Ozone Layer Depl	kg R11 eq.	1.27397E-11	4.58628E-08	99.97%	0.00%	0.00%	0.02%	0.00%	0.00%	100.00%

Scenario 6										
Category	Unit	total	kg/MWH	MD	RED	pump	inverter	end-of-li	operatior	transport
Mass	kg	36.34185436		70.31%	22.97%	5.67%	0.00%	0.92%	0.00%	0.13%
GWP potential	kg CO2 eq.	0.016168497	58.20658762	33.28%	57.81%	4.64%	0.00%	1.86%	0.00%	2.41%
Eutrophication Pc	kg Phosphate eq.	4.43714E-06	0.015973714	30.51%	46.90%	5.55%	0.00%	7.70%	0.00%	9.35%
Acidification Pote	kg SO2 eq.	6.10339E-05	0.219722108	54.76%	33.92%	7.30%	0.00%	1.35%	0.00%	2.66%
Terrestric Ecotoxi	kg DCB eq.	0.000118501	0.426604061	51.13%	37.66%	7.30%	0.00%	3.32%	0.00%	0.59%
Ozone Layer Depl	kg R11 eq.	3.12281E-11	1.12421E-07	99.69%	0.27%	0.04%	0.00%	0.00%	0.00%	0.00%

Scenario 6 - Alternative way of grouping the results										
Category	Unit	total	kg/MWH	copper	nickel	steel	IEM	MD mem	MD space	other pla
Mass	kg	36.34185436		0.33%	14.73%	40.38%	0.33%	0.17%	19.14%	24.90%
GWP potential	kg CO2 eq.	0.016168497	58.20658762	2.82%	2.60%	71.88%	0.51%	0.22%	10.26%	11.72%
Eutrophication Pc	kg Phosphate eq.	4.43714E-06	0.015973714	2.85%	5.17%	63.57%	0.48%	0.37%	12.38%	15.19%
Acidification Pote	kg SO2 eq.	6.10339E-05	0.219722108	3.17%	39.77%	45.66%	0.21%	0.11%	5.67%	5.42%
Terrestric Ecotoxi	kg DCB eq.	0.000118501	0.426604061	44.90%	6.63%	9.45%	0.04%	0.06%	2.60%	36.32%
Ozone Layer Depl	kg R11 eq.	3.12281E-11	1.12421E-07	99.59%	0.00%	0.01%	0.00%	0.00%	0.00%	0.40%

Scenario 7										
Category	Unit	total	kg/MWH	steel	PVC	IEM	pump	transport		
Mass	kg	128.3330855								
GWP potential	kg CO2 eq.	0.055395302	199.4230879	88.71%	6.74%	1.39%	0.43%	1.60%		
Eutrophication Pc	kg Phosphate eq.	2.21514E-05	0.079745036	86.97%	5.61%	0.39%	0.35%	4.13%		
Acidification Pote	kg SO2 eq.	0.000343247	1.235689764	95.99%	1.56%	0.33%	0.41%	1.00%		
Terrestric Ecotoxi	kg DCB eq.	0.000302174	1.087826876	92.60%	1.37%	0.27%	0.90%	0.73%		
Ozone Layer Depl	kg R11 eq.	3.55866E-13	1.28112E-09	4.31%	94.58%	0.06%	1.01%	0.01%		

Full outcomes of the sensitivity analysis of the LCA results

transport - low								
Category	Unit	Total	copper	nickel	steel	plastic	transport	end-of-life
Mass	kg	1.211445908	1.87%	83.29%	6.14%	7.36%	0.02%	0.33%
GWP potential	kg CO2 eq.	0.000480335	34.52%	31.79%	22.84%	8.86%	0.35%	0.75%
Eutrophication Pc	kg Phosphate eq.	1.59589E-07	26.17%	47.48%	15.21%	6.20%	1.12%	2.97%
Acidification Pote	kg SO2 eq.	9.47877E-06	7.09%	89.05%	2.74%	0.67%	0.07%	0.11%
Terrestric Ecotoxi	kg DCB eq.	2.31892E-05	85.50%	12.62%	0.43%	1.01%	0.01%	0.22%
Ozone Layer Depl	kg R11 eq.	1.27397E-11	99.97%	0.00%	0.00%	0.02%	0.00%	0.00%

transport high								
Category	Unit	Total	copper	nickel	steel	plastic	transport	end-of-life
Mass	kg	1.214814134	1.87%	83.06%	6.13%	7.34%	0.29%	0.33%
GWP potential	kg CO2 eq.	0.000507823	32.65%	30.07%	21.61%	8.38%	5.99%	0.71%
Eutrophication Pc	kg Phosphate eq.	1.88805E-07	22.12%	40.13%	12.86%	5.24%	17.11%	2.51%
Acidification Pote	kg SO2 eq.	9.59326E-06	7.01%	87.99%	2.71%	0.66%	1.32%	0.10%
Terrestric Ecotoxi	kg DCB eq.	2.32388E-05	85.32%	12.59%	0.42%	1.01%	0.23%	0.21%
Ozone Layer Depl	kg R11 eq.	1.27397E-11	99.97%	0.00%	0.00%	0.02%	0.00%	0.00%

lifetime -low								
Category	Unit	Total	copper	nickel	steel	plastic	transport	end-of-life
Mass	kg	1.614719362	1.87%	83.32%	6.15%	7.25%	0.10%	0.33%
GWP potential	kg CO2 eq.	0.000648702	34.08%	31.39%	22.55%	8.38%	2.07%	0.73%
Eutrophication Pc	kg Phosphate eq.	2.23461E-07	24.92%	45.21%	14.48%	5.70%	6.38%	2.72%
Acidification Pote	kg SO2 eq.	1.26792E-05	7.07%	88.77%	2.73%	0.64%	0.44%	0.10%
Terrestric Ecotoxi	kg DCB eq.	3.09358E-05	85.46%	12.61%	0.43%	1.00%	0.07%	0.21%
Ozone Layer Depl	kg R11 eq.	1.69862E-11	99.97%	0.00%	0.00%	0.02%	0.00%	0.00%

lifetime - high								
Category	Unit	Total	copper	nickel	steel	plastic	transport	end-of-life
Mass	kg	0.810153764	1.87%	83.03%	6.13%	7.55%	0.10%	0.35%
GWP potential	kg CO2 eq.	0.000328138	33.69%	31.02%	22.29%	9.36%	2.09%	0.76%
Eutrophication Pc	kg Phosphate eq.	1.12903E-07	24.67%	44.74%	14.33%	6.23%	6.44%	3.02%
Acidification Pote	kg SO2 eq.	6.34574E-06	7.06%	88.68%	2.73%	0.72%	0.45%	0.11%
Terrestric Ecotoxi	kg DCB eq.	1.54718E-05	85.44%	12.61%	0.42%	1.01%	0.08%	0.23%
Ozone Layer Depl	kg R11 eq.	8.49311E-12	99.97%	0.00%	0.00%	0.02%	0.00%	0.00%

Capacity Factor - low								
Category	Unit	Total	copper	nickel	steel	plastic	transport	end-of-life
Mass	kg	1.818664281	1.87%	83.23%	6.14%	7.35%	0.10%	0.33%
GWP potential	kg CO2 eq.	0.000732634	33.95%	31.26%	22.47%	8.71%	2.08%	0.74%
Eutrophication Pc	kg Phosphate eq.	2.52274E-07	24.84%	45.05%	14.43%	5.88%	6.40%	2.82%
Acidification Pote	kg SO2 eq.	1.42687E-05	7.07%	88.74%	2.73%	0.66%	0.44%	0.10%
Terrestric Ecotoxi	kg DCB eq.	3.48059E-05	85.45%	12.61%	0.42%	1.01%	0.08%	0.22%
Ozone Layer Depl	kg R11 eq.	1.91096E-11	99.97%	0.00%	0.00%	0.02%	0.00%	0.00%

Capacity Factor - low								
Category	Unit	Total	copper	nickel	steel	plastic	transport	end-of-life
Mass	kg	1.091191774	1.87%	83.23%	6.14%	7.35%	0.10%	0.33%
GWP potential	kg CO2 eq.	0.000439577	33.95%	31.26%	22.47%	8.71%	2.08%	0.74%
Eutrophication Pc	kg Phosphate eq.	1.51364E-07	24.84%	45.05%	14.43%	5.88%	6.40%	2.82%
Acidification Pote	kg SO2 eq.	8.56119E-06	7.07%	88.74%	2.73%	0.66%	0.44%	0.10%
Terrestric Ecotoxi	kg DCB eq.	2.08834E-05	85.45%	12.61%	0.42%	1.01%	0.08%	0.22%
Ozone Layer Depl	kg R11 eq.	1.14657E-11	99.97%	0.00%	0.00%	0.02%	0.00%	0.00%

Membrane frequncy - low								
Category	Unit	Total	copper	nickel	steel	plastic	transport	end-of-life
Mass	kg	1.21803737	1.86%	82.84%	6.11%	7.75%	0.10%	0.36%
GWP potential	kg CO2 eq.	0.000495998	33.43%	30.79%	22.12%	10.00%	2.10%	0.78%
Eutrophication Pc	kg Phosphate eq.	1.70529E-07	24.50%	44.43%	14.23%	6.58%	6.48%	3.21%
Acidification Pote	kg SO2 eq.	9.52486E-06	7.06%	88.62%	2.73%	0.77%	0.45%	0.11%
Terrestric Ecotoxi	kg DCB eq.	2.32119E-05	85.42%	12.61%	0.42%	1.02%	0.08%	0.24%
Ozone Layer Depl	kg R11 eq.	1.27398E-11	99.97%	0.00%	0.00%	0.02%	0.00%	0.00%

Membrane frequncy - high								
Category	Unit	Total	copper	nickel	steel	plastic	transport	end-of-life
Mass	kg	1.210569653	1.87%	83.35%	6.15%	7.22%	0.10%	0.33%
GWP potential	kg CO2 eq.	0.000485894	34.12%	31.43%	22.58%	8.27%	2.07%	0.73%
Eutrophication Pc	kg Phosphate eq.	1.674E-07	24.95%	45.26%	14.50%	5.64%	6.38%	2.69%
Acidification Pote	kg SO2 eq.	9.50831E-06	7.07%	88.78%	2.73%	0.63%	0.44%	0.10%
Terrestric Ecotoxi	kg DCB eq.	2.32011E-05	85.46%	12.61%	0.43%	1.00%	0.07%	0.21%
Ozone Layer Depl	kg R11 eq.	1.27396E-11	99.97%	0.00%	0.00%	0.02%	0.00%	0.00%

Nomenclature

The main abbreviations and symbols used throughout the text are presented here. The list is non-exhaustive, but in general the symbols and subscripts, where not self-explanatory, are define in the text when used:

Abbreviations	
AEM	Anion Exchange Membrane
BAT	Best Available Technologies
BPE	Boiling Point Elevation
CEM	Cation Exchange Membrane
CHP	Combined Heat and Power
CPV	Concentrated Photovoltaic
CSP	Concentrated Solar Power
EES	Engineering Equation Solver
EI	Energy Intensity
ETC	Evacuated tube collector
EU	European Union
FiT	Feed in Tariff
FPC	Flat Plate Collector
GWP	Global Warming potential
HEX	Heat Exchanger
	Ionic Exchange Membrane
LCA	Life Cycle Assessment
LCOE	Levelized Cost of Electricity
MD	Membrane Distillation
NG	Natural Gas
O&M	Operation and Maintenance
ODP	Ozone Depletion Potential
ORC	Organic Rankine Cycle
PBP	Payback Period
	Pressure Retarded Osmosis
PV	Photovoltaics
	Reverse Electrodialysis
	Reverse Electrodialysis Heat Engine
	Salinity Gradient Power
T	Temperature (K or °C)
TBT	Top Brine Temperature
TRL	Technological readiness level (
TTD	Terminal Temperature Difference

WHF	Waste Heat Fraction
MED	Multi-Effect Distillation,
OHE	Osmotic heat engine

Symbols	
Cf	Capacity Factor
c_p	Specific heat capacity
D	Distillate flow rate
E	Electricity generated
G	Incident (global) irradiation
I	Capital Cost
inf	inflation
m	Mass
M	Running costs
n	efficiency
N	System lifetime in years
P	Pressure
r	Discount factor
T	Temperature
TD	Transport Distance
TL	Total Life
Q	Heat

References

[1] R.E. Pattle, Production of electric power by mixing fresh and salt water in the hydroelectric pile [19], Nature. (1954). doi:10.1038/174660a0.

[2] S. Loeb, F. Van Hessen, D. Shahaf, Production of energy from concentrated brines by pressure-retarded osmosis, J. Memb. Sci. (1976). doi:10.1016/S0376-7388(00)82271-1.

[3] S. Loeb, A method and apparatus for generating power utilizing reverse electrodialysis, US US4171409, 1979.

[4] A. Tamburini, G. La Barbera, A. Cipollina, M. Ciofalo, G. Micale, CFD simulation of channels for direct and reverse electrodialysis, Desalin. Water Treat. (2012). doi:10.1080/19443994.2012.705084.

[5] M. Tedesco, A. Cipollina, A. Tamburini, G. Micale, J. Helsen, M. Papapetrou, REAPower: use of desalination brine for power production through reverse electrodialysis, Desalin. Water Treat. 53 (2014) 3161–3169. http://www.tandfonline.com/doi/abs/10.1080/19443994.2014.934102#.VdDFnrM2tZ4.

[6] M. Tedesco, E. Brauns, A. Cipollina, G. Micale, P. Modica, G. Russo, J. Helsen, Reverse electrodialysis with saline waters and concentrated brines: A laboratory investigation towards technology scale-up, J. Memb. Sci. (2015). doi:10.1016/j.memsci.2015.05.020.

[7] A. Daniilidis, D.A. Vermaas, R. Herber, K. Nijmeijer, Experimentally obtainable energy from mixing river water, seawater or brines with reverse electrodialysis, Renew. Energy. 64 (2014) 123–131. doi:10.1016/j.renene.2013.11.001.

[8] A. Tamburini, M. Tedesco, A. Cipollina, G. Micale, M. Papapetrou, W. Van Baakc, A. Piacentino, Reverse Electrodialysis Heat Engine (REDHE) for sustainable power generation, Appl. Energy. Under revi (2017).

[9] M. Papapetrou, K. Kumpavat, Environmental aspects and economics of salinity gradient power (SGP) processes, in: A. Cipollina, G. Micale (Eds.), Sustain. Energy from Salin. Gradients, Elsevier, 2016: pp. 315–335. http://www.sciencedirect.com/science/book/9780081003121.

[10] H. Fang, J. Xia, K. Zhu, Y. Su, Y. Jiang, Industrial waste heat utilization for low temperature district heating, Energy Policy. (2013). doi:10.1016/j.enpol.2013.06.104.

[11] S. Bhawan, R. Puram, Chapter 8 - Waste Heat Recovery, in: Energy Effic. Therm. Util., 2003. doi:10.2460/ajvr.77.2.127.

[12] J. Swithenbank, K.N. Finney, Q. Chen, Y. Bin Yang, A. Nolan, V.N. Sharifi, Waste heat usage, Appl. Therm. Eng. (2013). doi:10.1016/j.applthermaleng.2012.10.038.

[13] D.M. van de Bor, C.A. Infante Ferreira, A.A. Kiss, Low grade waste heat recovery using heat pumps and power cycles, Energy. (2015). doi:10.1016/j.energy.2015.06.030.

[14] C. Forman, I.K. Muritala, R. Pardemann, B. Meyer, Estimating the global waste heat potential, Renew. Sustain. Energy Rev. (2016). doi:10.1016/j.rser.2015.12.192.

[15] G. Panayiotou, G. Bianchi, G. Georgiou, L. Aresti, M. Argyrou, R. Agathokleous, K. Tsamos, S. Tassou, G. Florides, S. Kalogirou, P. Christodoulides, Preliminary assessment of waste heat potential in major European industries, Energy Procedia. 123 (2017) 335–45.

[16] G.P. Hammond, J.B. Norman, Heat recovery opportunities in UK industry, Appl. Energy. (2014). doi:10.1016/j.apenergy.2013.11.008.

[17] US Department of Energy - Energy Efficiency and Renewable Energy, What is the energy payback for PV ?, Int. J. (2004). doi:DOE/GO-102004-1847.

[18] European Commission, Biofuels in the European Union A vision for 2030 and beyond, 2006. doi:10.2308/iace.2006.21.4.345.

[19] G.R. Timilsina, A. Shrestha, Biofuels Markets , Targets and Impacts, World Bank. (2010). doi:10.1596/1813-9450-5364.

[20] H.M. Upadhyaya, S. Senthilarasu, M.H. Hsu, D.K. Kumar, Recent progress and the status of dye-sensitised solar cell (DSSC) technology with state-of-the-art conversion efficiencies, Sol. Energy Mater. Sol. Cells. (2013). doi:10.1016/j.solmat.2013.08.031.

[21] M. Tedesco, A. Cipollina, A. Tamburini, G. Micale, Towards 1 kW power production in a reverse electrodialysis pilot plant with saline waters and concentrated brines, J. Memb. Sci. (2017). doi:10.1016/j.memsci.2016.09.015.

[22] RES LEGAL, Renewable energy policy database and support - Legal sources on renewable energy, (n.d.). http://www.res-legal.eu/search-by-country/.

[23] M. Papapetrou, A. Cipollina, U. LaCommare, G. Micale, G. Zaragoza, G. Kosmadakis, Assessment of methodologies and data used to calculate desalination costs, Desalination. 419 (2017) 8–19. doi:http://dx.doi.org/10.1016/j.desal.2017.05.038.

[24] A. Tamburini, M. Tedesco, A. Cipollina, G. Micale, M. Ciofalo, M. Papapetrou, W. Van Baak, A. Piacentino, Reverse electrodialysis heat engine for sustainable power production, Appl. Energy. 206 (2017). doi:10.1016/j.apenergy.2017.10.008.

[25] M. Bevacqua, A. Tamburini, M. Papapetrou, A. Cipollina, G. Micale, A. Piacentino, Reverse electrodialysis with NH4HCO3-water systems for heat-to-power conversion, Energy. (2017). doi:10.1016/j.energy.2017.07.012.

[26] R.L. McGinnis, M. Elimelech, Energy requirements of ammonia–carbon dioxide forward osmosis desalination, Desalination. 207 (2007) 370–382. doi:10.1016/j.desal.2006.08.012.

[27] J.R. McCutcheon, R.L. McGinnis, M. Elimelech, A novel ammonia—carbon dioxide forward (direct) osmosis desalination process, Desalination. 174 (2005) 1–11. doi:10.1016/j.desal.2004.11.002.

[28] R.L. McGinnis, J.R. McCutcheon, M. Elimelech, A novel ammonia–carbon dioxide osmotic heat engine for power generation, J. Memb. Sci. 305 (2007) 13–19. doi:10.1016/j.memsci.2007.08.027.

[29] M. Papapetrou, A. Cipollina, F. Giacalone, M. Bevacqua, Selection Report for the First Phase of the Project, 2016.

[30] Conversion of Low Grade Heat to Power through closed-loop Reverse Electro-Dialysis, RED Heat-to-Power, Horizon 2020, GA number 640667, (2015). http://www.red-heat-to-power.eu/.

[31] D.A. Vermaas, S. Bajracharya, B.B. Sales, M. Saakes, B. Hamelers, K. Nijmeijer, Clean energy generation using capacitive electrodes in reverse electrodialysis, Energy Environ. Sci. (2013). doi:10.1039/c2ee23562e.

[32] D.A. Vermaas, M. Saakes, K. Nijmeijer, Power generation using profiled membranes in reverse electrodialysis, J. Memb. Sci. (2011). doi:10.1016/j.memsci.2011.09.043.

[33] F. Giacalone, F. Vassallo, A. Cipollina, F. Scargial, G. Micale, G. Zaragoza, J.A.A. Mañas, K.

Goeting, S. Grasman, P. Jager, D. Kunteng, Experimental System Testing, 2018. http://www.red-heat-to-power.eu/.

[34] R.A. Tufa, S. Pawlowski, J. Veerman, K. Bouzek, E. Fontananova, G. Di Profio, S. Velizarov, J.G. Crespo, K. Nijmeijer, E. Curcio, Progress and prospects in reverse electrodialysis for salinity gradient energy conversion and storage, Appl. Energy. 225 (2018) 290–331.

[35] R.S. Kingsbury, S. Zhu, S. Flotron, O. Coronell, Microstructure determines water and salt permeation in commercial ion exchange membranes, ChemRxiv. (2018) 1–36. doi:10.26434/chemrxiv.6987248.

[36] Francesco Giacalone, M. Micari, P. Catrini, L. Gurreri, A. Cipollina, A. Piacentino, A. Tamburini, G. Micale, W. Van Baak, Report on the development and validation of the advanced process simulator for simulation and design of the RED HtP lab-prototype, 2017.

[37] International Organization for Standardization, Environmental management — Life cycle assessment — Requirements and guidelines ISO14044, Br. Stanards. 3 (2006).

[38] H. Tian, G. Shu, H. Wei, X. Liang, L. Liu, Fluids and parameters optimization for the organic Rankine cycles (ORCs) used in exhaust heat recovery of Internal Combustion Engine (ICE), Energy. (2012). doi:10.1016/j.energy.2012.09.021.

[39] S. Lecompte, S. Lemmens, H. Huisseune, M. Van Den Broek, M. De Paepe, Multi-objective thermo-economic optimization strategy for ORCs applied to subcritical and transcritical cycles for waste heat recovery, Energies. (2015). doi:10.3390/en8042714.

[40] S. Karellas, A. Schuster, A.D. Leontaritis, Influence of supercritical ORC parameters on plate heat exchanger design, Appl. Therm. Eng. (2012). doi:10.1016/j.applthermaleng.2011.09.013.

[41] DECC, The potential for recovering and using surplus heat from industry Final Report The potential for recovering and using surplus heat from industry, 2014.

[42] Eurostat, Database - Energy, (2016). http://ec.europa.eu/eurostat/web/energy/data/database.

[43] Electric Power Research Institute–EPRI, Power Plant Cooling System Overview for Researchers and Technology Developers., 2013. http://www.mcilvainecompany.com/Decision_Tree/subscriber/Tree/DescriptionTextLinks/EPRIoverview.pdf.

[44] H.L. Zhang, J. Baeyens, J. Degrève, G. Cacères, Concentrated solar power plants: Review and design methodology, Renew. Sustain. Energy Rev. (2013). doi:10.1016/j.rser.2013.01.032.

[45] K. Lovegrove, J. Pye, Fundamental principles of concentrating solar power (CSP) systems, in: Conc. Sol. Power Technol. Princ. Dev. Appl., 2012. doi:10.1016/B978-1-84569-769-3.50002-9.

[46] Eurostat, Archive: Consumption of energy, (2015).

[47] EU-Project-Odyssee-Mure, Energy efficiency trends in EU industry: Sectoral Profile - Industry, 2016.

[48] EU-Project-Odyssee-Mure, Energy efficiency trends in EU industry, 2016. http://www.odyssee-mure.eu/publications/efficiency-by-sector/industry/industry-eu.pdf.

[49] DBDH, S. Report, JRC, Heat and cooling demand and market perspective, Hot&Cool - Int. Mag. Dist. Heat. Cool. (2015). doi:10.2790/56532.

[50] M. Pehnt, J. Bödeker, M. Arens, Industrial waste heat – tapping into a neglected efficiency potential, in: ECEE 2011 Summer Study, 2011: pp. 691–700.

[51] C. Lauterbach, B. Schmitt, U. Jordan, K. Vajen, The potential of solar heat for industrial processes in Germany, Renew. Sustain. Energy Rev. (2012). doi:10.1016/j.rser.2012.04.032.

[52] S. Brückner, S. Liu, L. Miró, M. Radspieler, L.F. Cabeza, E. Lävemann, Industrial waste heat recovery technologies: An economic analysis of heat transformation technologies, Appl. Energy. (2015). doi:10.1016/j.apenergy.2015.01.147.

[53] S. Brueckner, L. Miró, L.F. Cabeza, M. Pehnt, E. Laevemann, Methods to estimate the industrial waste heat potential of regions - A categorization and literature review, Renew. Sustain. Energy Rev. (2014). doi:10.1016/j.rser.2014.04.078.

[54] T. Naegler, S. Simon, M. Klein, H.C. Gils, Quantification of the European industrial heat demand by branch and temperature level, Int. J. Energy Res. (2015). doi:10.1002/er.3436.

[55] Diesel and Gas Turbines Worldwide, (2016). https://dieselgasturbine.com/2016-power-generation-order-survey/#.WOovSKIlGM8.

[56] Brandon Owens, The Rise of Distributed Power, Gen. Electr. (2014). https://www.ge.com/sites/default/files/2014 02 Rise of Distributed Power.pdf.

[57] TU Delft, Enipedia, European power generation and emissions summary by fuel type, 2017. http://enipedia.tudelft.nl/wiki/Europe/Powerplants (accessed July 20, 2006).

[58] Eurostat, Electricity and heat statistics, (2016).

[59] R.A. of Engineering, FUTURE SHIP POWERING OPTIONS Exploring alternative methods of ship propulsion, 2013. http://www.raeng.org.uk/publications/reports/future-ship-powering-options.

[60] UNCTAD, Review of Maritime Transport, 2018, 2018. doi:978-92-1-112841-3.

[61] MAN Diesel and Turbo, Energy Efficiency Design Index, (n.d.). https://marine.mandieselturbo.com/docs/default-source/shopwaredocumentsarchive/eedi.pdf?sfvrsn=4.

[62] Entec, Market Survey of Marine Distillates with 0.2% Sulphur Content, 2002. http://ec.europa.eu/environment/air/pdf/chapter3_end_ship_emissions.pdf.

[63] International Maritime Organisation, Third IMO Greenhouse Gas Study 2014, (2014). http://www.imo.org/en/OurWork/Environment/PollutionPrevention/AirPollution/Documents/Third Greenhouse Gas Study/GHG3 Executive Summary and Report.pdf.

[64] F. Campana, M. Bianchi, L. Branchini, A. De Pascale, A. Peretto, M. Baresi, A. Fermi, N. Rossetti, R. Vescovo, ORC waste heat recovery in European energy intensive industries: Energy and GHG savings, Energy Convers. Manag. (2013). doi:10.1016/j.enconman.2013.07.041.

[65] Joint Research Centre, Reference documents under the IPPC Directive and the IED, (2018).

[66] T. Fleiter, D. Fehrenbach, E. Worrell, W. Eichhammer, Energy efficiency in the German pulp and paper industry - A model-based assessment of saving potentials, Energy. (2012).

doi:10.1016/j.energy.2012.02.025.

[67] S. Karellas, A.D. Leontaritis, G. Panousis, E. Bellos, E. Kakaras, Energetic and exergetic analysis of waste heat recovery systems in the cement industry, Energy. (2013). doi:10.1016/j.energy.2013.03.097.

[68] R. Law, A. Harvey, D. Reay, Opportunities for low-grade heat recovery in the UK food processing industry, Appl. Therm. Eng. (2013). doi:10.1016/j.applthermaleng.2012.03.024.

[69] A. Thekdi, S.U. Nimbalkar, Industrial Waste Heat Recovery : Potential Applications, Available Technologies and Crosscutting R&D Opportunities, 2015. doi:10.1111/bjc.12063.

[70] P. Tello, R. Weerdmeester, SPIRE Roadmap, (n.d.). https://www.spire2030.eu/sites/default/files/pressoffice/spire-roadmap.pdf.

[71] G. Bianchi, S. Tassou, Y. Ge, H. Jouhara, K. Tsamos, A. Leroux, M. de Miol, Design considerations on a small scale supercritical CO2 power system for industrial high temperature waste heat to power recovery applications., in: 1st Eur. Semin. Supercrit. CO2 Power Syst., Wien, Austria, 2016.

[72] SINTEF, Heat Up project - High temperature heat pumps for efficient utilisation of low temperature surplus heat, (2015). http://www.sintef.no/projectweb/heatup/.

[73] EUROHEAT & POWER, ECOHEATCOOL, (2006). https://www.euroheat.org/our-projects/ecoheatcool-european-heating-cooling-market-study/.

[74] ECOHEATCOOL, Possibilities with more district heating in Europ, (2006). https://www.euroheat.org/wp-content/uploads/2016/02/Ecoheatcool_WP4_Web.pdf.

[75] Enova, Utnyttelse av spillvarme fra norsk industry – en potensialstudie, (2009).

[76] G. Latz, O. Erlandsson, T. Skåre, A. Contet, S. Andersson, K. Munch, Performance analysis of a reciprocating piston expander and a plate type exhaust gas recirculation boiler in a water-based Rankine cycle for heat recovery from a heavy duty diesel engine, Energies. (2016). doi:10.3390/en9070495.

[77] IAPWS Working Group: Industrial Solutions and Requirements, IAPWS Certified Research Need - ICRN, (2008). http://www.iapws.org/icrn/ICRN23.pdf.

[78] K. Senary, A. Tawfik, E. Hegazy, A. Ali, Development of a waste heat recovery system onboard LNG carrier to meet IMO regulations, Alexandria Eng. J. (2016). doi:10.1016/j.aej.2016.07.027.

[79] Opcon Energy Systems, Typical fuel savings potential on a 15 MW vessel, (2017). http://opconenergysystem.com/en/opcon-marine-3/ (accessed June 1, 2017).

[80] GE Power, JENBACHER TYPE 3, (2017). https://www.gepower.com/gas/reciprocating-engines/jenbacher/type-3 (accessed June 1, 2017).

[81] M. Chaczykowski, Organic Rankine Cycle for Residual Heat to Power Conversion in Natural Gas Compressor Station. Part II: Plant Simulation and Optimisation Study, Arch. Min. Sci. (2016). doi:10.1515/amsc-2016-0019.

[82] U. Persson, Quantifying the Excess Heat Available for District Heating in Europe, 2015. http://stratego-project.eu/wp-content/uploads/2014/09/STRATEGO-WP2-Background-Report-7-Potenital-for-Excess-Heat.pdf.

[83] R.C. McKenna, J.B. Norman, Spatial modelling of industrial heat loads and recovery

potentials in the UK, Energy Policy. (2010). doi:10.1016/j.enpol.2010.05.042.

[84] S.C. Land AL, H. Feldhusen, A. Tvaerme, L. Cronholm, Industriell Spillvärme – Processer och potentialer, (2012).

[85] A. Land, H. Feldhusen, A. Tvaerme, L. Cronholm, C. Sundloef, Industriell Spillvärme – Processer och potentialer, (2002).

[86] I-THERM, D 2.1 Literature review of energy use and potential for heat recovery in the EU28, 2016. http://www.itherm-project.eu/wp-content/uploads/2017/10/I-ThERM_D2.1.pdf.

[87] European Commission, Electricity interconnection: Malta - Italy, (2014). http://ec.europa.eu/energy/eepr/projects/files/electricity-interconnectors/mt-it_en.pdf.

[88] Global Energy Observatory, (n.d.). http://globalenergyobservatory.org/analyze.php.

[89] Hellenic Electricity Distribution Network Operator – HEDNO, Πληροφοριακό δελτίο παραγωγής στα μη διασυνδεδεμένα νησιά για τον Φεβρουάριο 2017, (2017). https://www.deddie.gr/Documents2/MDN/PLIROFORIAKA DELTIA 2017/ΠΛΗΡΟΦΟΡΙΑΚΟ ΔΕΛΤΙΟ-2017 Φεβρουάριος.pdf.

[90] M. Panagiotidou, G. Xydis, C. Koroneos, Spatial Inequalities and Wind Farm Development in the Dodecanese Islands—Legislative Framework and Planning: A Review, Environments. (2016). doi:10.3390/environments3030018.

[91] T. Zachariadis, C. Hadjikyriakou, State of the Art of Power Generation in Cyprus, in: 2016: pp. 7–16. doi:10.1007/978-3-319-31535-5_2.

[92] MWM, Case Studies - Munich Airport, Germany, (2018). https://www.mwm.net/mwm-chp-gas-engines-gensets-cogeneration/gas-applications/references/infrastructure-projects-shopping-malls-airports/munich-airport-germany/.

[93] Eurostat, Cobined Heat and Power (CHP) data, (2016). http://ec.europa.eu/eurostat/documents/38154/4956229/CHP+data+2005-2013/62e87958-0b9a-4195-af70-356493e12233.

[94] EurObserv'ER, 17th annual overview barometer, (2017). https://www.eurobserv-er.org/category/all-annual-overview-barometers/.

[95] B. Kampman, C. Leguijt, T. Scholten, J. Tallat-Kelpsaite, R. Brückmann, G. Maroulis, J.P. Lesschen, K. Meesters, N. Sikirica, B. Elbersen, Optimal use of biogas from waste streams - An assessment of the potential of biogas from digestion in the EU beyond 2020, Optim. Use Biogas from Waste Streams. (2017). doi:10.13140/RG.2.2.14770.40643.

[96] European-Biogas-Association, Biomethane & Biogas Report 2015, 2015. http://european-biogas.eu/2015/12/16/biogasreport2015/.

[97] F. Campana, M. Bianchi, L. Branchini, A. De Pascale, A. Peretto, M. Baresi, A. Fermi, N. Rossetti, R. Vescovo, ORC waste heat recovery in European energy intensive industries: Energy and GHG savings, Energy Convers. Manag. 76 (2013) 244–252.

[98] M. Antics, B. Sanner, Status of Geothermal Energy Use and Resources in Europe, in: Eur. Geotherm. Congr., 2007.

[99] S. Loutatidou, H.A. Arafat, Techno-economic analysis of MED and RO desalination powered by low-enthalpy geothermal energy, Desalination. 365 (2015) 277–292. doi:10.1016/j.desal.2015.03.010.

[100] CESEN, BRGM, ETSU, GTN, ORKUSTOFNUN, Blue Book on GEOTHERMAL RESOURCES, 1999.

[101] S. Hurter, R. Schellschmidt, Atlas of geothermal resources in Europe, Geothermics. (2003). doi:10.1016/S0375-6505(03)00070-1.

[102] C. Augustine, J.W. Tester, B. Anderson, S. Petty, A Comparison of Geothermal with Oil and Gas Well Drilling Costs, Thirty-First Work. Geotherm. Reserv. Eng. (2006). doi:10.1111/ecca.12237.

[103] P. Dumas, M. Antics, P. Ungemach, Report on Geothermal Drilling, (2013). http://www.geoelec.eu/wp-content/uploads/2011/09/D-3.3-GEOELEC-report-on-drilling.pdf.

[104] GeoElec, A prospective study on the geothermal potential in the EU, (2013). http://www.geoelec.eu/wp-content/uploads/2011/09/D-2.5-GEOELEC-prospective-study.pdf.

[105] V.G. Gude, Geothermal source potential for water desalination - Current status and future perspective, Renew. Sustain. Energy Rev. (2016). doi:10.1016/j.rser.2015.12.186.

[106] C.R. Chamorro, J.L. García-Cuesta, M.E. Mondéjar, A. Pérez-Madrazo, Enhanced geothermal systems in Europe: An estimation and comparison of the technical and sustainable potentials, Energy. (2014). doi:10.1016/j.energy.2013.11.078.

[107] P. Olasolo, M.C. Juárez, M.P. Morales, S. Damico, I.A. Liarte, Enhanced geothermal systems (EGS): A review, Renew. Sustain. Energy Rev. (2016). doi:10.1016/j.rser.2015.11.031.

[108] S.K. Sanyal, S.J. Butler, An Analysis of Power Generation Prospects from Enhanced Geothermal Systems, in: Proc. World Geotherm. Congr., 2005. doi:10.4161/cib.3.5.12692.

[109] J. Limberger, J.-D. Van Wees, European temperature models in the framework of GEOELEC : linking temperature and heat flow data sets to lithosphere models, Eur. Geotherm. Congr. (2013).

[110] R. Arnold, D.B. Burnett, J. Elphick, J. Feeley III, Thomas, M. Galbrun, M. Hightower, Z. Jiang, M. Khan, M. Lavery, F. Luffey, P. Verbeek, Managing Water — From Waste to Resource, Oilf. Rev. (2004).

[111] J. McKenna, D. Blackwell, Geothermal electric power from Texas hydrocarbon fields, (2005) 121–8.

[112] T. Li, J. Zhu, W. Zhang, Cascade utilization of low temperature geothermal water in oilfield combined power generation, gathering heat tracing and oil recovery, Appl. Therm. Eng. (2012). doi:10.1016/j.applthermaleng.2012.01.049.

[113] X. Bu, W. Ma, H. Li, Geothermal energy production utilizing abandoned oil and gas wells, Renew. Energy. (2012). doi:10.1016/j.renene.2011.10.009.

[114] W.L. Cheng, T.T. Li, Y. Le Nian, C.L. Wang, Studies on geothermal power generation using abandoned oil wells, Energy. (2013). doi:10.1016/j.energy.2013.07.008.

[115] A.P. Davis, E.E. Michaelides, Geothermal power production from abandoned oil wells, Energy. (2009). doi:10.1016/j.energy.2009.03.017.

[116] R.J. Davies, S. Almond, R.S. Ward, R.B. Jackson, C. Adams, F. Worrall, L.G. Herringshaw, J.G. Gluyas, M.A. Whitehead, Oil and gas wells and their integrity: Implications for shale

and unconventional resource exploitation, Mar. Pet. Geol. (2014). doi:10.1016/j.marpetgeo.2014.03.001.

[117] E. Soldo, C. Alimonti, From an Oilfield to a Geothermal One : Use of a Selection Matrix to Choose Between Two Extraction Technologies, World Geotherm. Congr. 2015. (2015).

[118] N. Ghaffour, J. Bundschuh, H. Mahmoudi, M.F.A. Goosen, Renewable energy-driven desalination technologies: A comprehensive review on challenges and potential applications of integrated systems, Desalination. 356 (2015) 94–114. doi:10.1016/j.desal.2014.10.024.

[119] M.Z. Lukawski, B.J. Anderson, C. Augustine, L.E. Capuano, K.F. Beckers, B. Livesay, J.W. Tester, Cost analysis of oil, gas, and geothermal well drilling, J. Pet. Sci. Eng. (2014). doi:10.1016/j.petrol.2014.03.012.

[120] V. Stefánsson, Investment cost for geothermal power plants, Geothermics. (2002). doi:10.1016/S0375-6505(01)00018-9.

[121] J. Bundschuh, N. Ghaffour, H. Mahmoudi, M. Goosen, S. Mushtaq, J. Hoinkis, Low-cost low-enthalpy geothermal heat for freshwater production: Innovative applications using thermal desalination processes, Renew. Sustain. Energy Rev. 43 (2015) 196–206. doi:10.1016/j.rser.2014.10.102.

[122] S. Sanyal, S. Butler, Geothermal power capacity from petroleum wells–some case histories of assessment, in: World Geotherm. Congr. 2010, 2010.

[123] J.P. Salmon, J. Meurice, N. Wobus, F. Stern, M. Duaime, Guidebook to Geothermal Power Finance, Energy. (2011). doi:10.1021/acssuschemeng.5b01453.

[124] T. Huld, R. Müller, A. Gambardella, A new solar radiation database for estimating PV performance in Europe and Africa, Sol. Energy. (2012). doi:10.1016/j.solener.2012.03.006.

[125] SOLARGIS - Download solar resource maps and GIS data for 180+ countries, (n.d.). https://solargis.com/maps-and-gis-data/download/.

[126] Joint Research Centre, Country and regional maps, Photovolt. Geogr. Inf. Syst. (2017). http://re.jrc.ec.europa.eu/pvg_download/map_index.html.

[127] European Solar Thermal Industry Federation, Solar Thermal Markets in Europe 2015, (2015). http://www.estif.org/publications/statistics/interactive_statistics_2015_solar_thermal_markets_in_eu28_and_switzerland/.

[128] E.S.T.I. Federation, Solar Thermal Markets in Europe - Trends and Market Statistics 2014, 2015. http://www.estif.org/fileadmin/estif/content/market_data/downloads/2014_solar_thermal_markets_LR.pdf.

[129] S.A. Kalogirou, Solar thermal collectors and applications, Prog. Energy Combust. Sci. (2004). doi:10.1016/j.pecs.2004.02.001.

[130] European Solar Thermal Industry Federation (ESTIF), THE Quality Label for Solar Thermal Products in Europe, (2017). http://www.estif.org/solarkeymarknew/images/downloads/brochures/New_brochures_2017/solar_keymark_a5_en.pdf.

[131] Solar Keymark, The Solar Keymark Database, (n.d.). http://www.solarkeymark.dk/.

[132] Calpak, Technical Manual - Solar Selective Collector M4, (2018).

[133] NCSR Demokritos, Summary of EN 12975 Test Results, (2014). http://www.estif.org/solarkeymark/Links/Internal_links/DQS Hellas/SKM-9954-1.pdf.

[134] Kingspan, Thermomax DF400 Evacuated Tube Collectors, (n.d.).

[135] ISFH, Summary of EN 12975 Test Results, (2013). http://www.dincertco.de/logos/011-7S1946 R.pdf.

[136] E. Skoplaki, J.A. Palyvos, On the temperature dependence of photovoltaic module electrical performance: A review of efficiency/power correlations, Sol. Energy. (2009). doi:10.1016/j.solener.2008.10.008.

[137] G. Kosmadakis, D. Manolakos, G. Papadakis, Simulation and economic analysis of a CPV/thermal system coupled with an organic Rankine cycle for increased power generation, Sol. Energy. (2011). doi:10.1016/j.solener.2010.11.019.

[138] Solimpeks, Solimpeks Volther PV/T collector, (2018). http://www.solimpeks.com/product/volther-powertherm/.

[139] L. Thermal Energy System Specialists, TRNSYS - Transient System Simulation Tool, (2018). http://www.trnsys.com/.

[140] Scientific Applications International Corporation (SAIC), Life Cycle Assessment: Principles and Practice, Ohio, 2006.

[141] Elsevier, ScienceDirect, Search for peer-reviewed journals, articles, book chapters and open access content, (2018). https://www.sciencedirect.com/.

[142] R. Turconi, A. Boldrin, T. Astrup, Life cycle assessment (LCA) of electricity generation technologies: Overview, comparability and limitations, Renew. Sustain. Energy Rev. 28 (2013) 555–565. doi:10.1016/j.rser.2013.08.013.

[143] C. Liu, C. He, H. Gao, H. Xie, Y. Li, S. Wu, J. Xu, The environmental impact of organic Rankine cycle for waste heat recovery through life-cycle assessment, Energy. 56 (2013) 144–154. doi:10.1016/j.energy.2013.04.045.

[144] A. Uusitalo, V. Uusitalo, A. Grönman, M. Luoranen, A. Jaatinen-Värri, Greenhouse gas reduction potential by producing electricity from biogas engine waste heat using organic Rankine cycle, J. Clean. Prod. 127 (2016) 399–405. doi:10.1016/j.jclepro.2016.03.125.

[145] T. Hoepner, S. Lattemann, Chemical impacts from seawater desalination plants — a case study of the northern Red Sea, Desalination. 152 (2003) 133–140. doi:10.1016/S0011-9164(02)01056-1.

[146] S. Lattemann, T. Höpner, Environmental impact and impact assessment of seawater desalination, Desalination. 220 (2008) 1–15. doi:10.1016/j.desal.2007.03.009.

[147] F. Vince, E. Aoustin, P. Bréant, F. Marechal, LCA tool for the environmental evaluation of potable water production, Desalination. 220 (2008) 37–56. doi:10.1016/j.desal.2007.01.021.

[148] Pré Consultants B.V:, SimaPro LCA software package, (2018). https://simapro.com/.

[149] G. Raluy, L. Serra, J. Uche, Life cycle assessment of MSF , MED and RO desalination technologies, Energy. 31 (2006) 2361–2372. doi:10.1016/j.energy.2006.02.005.

[150] L. Gerber, M. Gassner, F. Maréchal, Systematic integration of LCA in process systems design: Application to combined fuel and electricity production from lignocellulosic biomass, Comput. Chem. Eng. 35 (2011) 1265–1280.

doi:10.1016/j.compchemeng.2010.11.012.

[151] M. Papapetrou, K. Kumpavat, Environmental aspects and economics of salinity gradient power (SGP) processes, 2016. doi:10.1016/B978-0-08-100312-1.00010-9.

[152] K.L. Hickenbottom, L. Miller-Robbie, J. Vanneste, J.M. Marr, M.B. Heeley, T.Y. Cath, Comparative life-cycle assessment of a novel osmotic heat engine and an organic Rankine cycle for energy production from low-grade heat, J. Clean. Prod. 191 (2018) 490–501. doi:10.1016/j.jclepro.2018.04.106.

[153] Joint Research Centre, European Platform on Life Cycle Assessment, (2018). http://eplca.jrc.ec.europa.eu/?page_id=43.

[154] thinkstep AG, GaBi Software System and Database for Life Cycle Engineering, (2018). https://www.thinkstep.com/software/gabi-lca/.

[155] Pré Consultants B. V., Introduction to LCA with SimaPro 7, 2008.

[156] A. Ruiz-Aguirre, J.A. Andrés-Mañas, J.M. Fernández-Sevilla, G. Zaragoza, Experimental characterization and optimization of multi-channel spiral wound air gap membrane distillation modules for seawater desalination, Sep. Purif. Technol. 205 (2018) 212–222. doi:10.1016/j.seppur.2018.05.044.

[157] M. Bevacqua, A. Tamburini, M. Papapetrou, A. Cipollina, G. Micale, A. Piacentino, Reverse electrodialysis with NH4HCO3-water systems for heat-to-power conversion, Energy. 137 (2017) 1293–1307. doi:https://doi.org/10.1016/j.energy.2017.07.012.

[158] N. Palanov, Life-cycle assessment of Photovaltaic systems - Analysis of environmental impact from the production of PV system including solar panels produced by Gaia Solar, Lund University, 2014.

[159] F. Ueckerdt, L. Hirth, G. Luderer, O. Edenhofer, System LCOE : What are the costs of variable renewables ?, Energy. 63 (2013) 61–75. doi:10.1016/j.energy.2013.10.072.

[160] M.K. Wittholz, B.K. O'Neill, C.B. Colby, D. Lewis, Estimating the cost of desalination plants using a cost database, Desalination. 229 (2008) 10–20. doi:10.1016/j.desal.2007.07.023.

[161] A. Daniilidis, R. Herber, D.A. Vermaas, Upscale potential and financial feasibility of a reverse electrodialysis power plant, Appl. Energy. 119 (2014) 257–265. doi:10.1016/j.apenergy.2013.12.066.

[162] M. Papapetrou, G. Kosmadakis, A. Cipollina, U. La Commare, G. Micale, Industrial waste heat: Estimation of the technically available resource in the EU per industrial sector, temperature level and country, Appl. Therm. Eng. 138 (2018) 207–216. doi:10.1016/j.applthermaleng.2018.04.043.

[163] L. Bai, Life Cycle Assessment of Electricity Generation from Low Temperature Waste Heat, (2012).

[164] E. Bernier, F. Maréchal, R. Samson, Multi-objective design optimization of a natural gas-combined cycle with carbon dioxide capture in a life cycle perspective, Energy. (2010). doi:10.1016/j.energy.2009.06.037.

[165] X. Chen, Y. Su, D. Reay, S. Riffat, Recent research developments in polymer heat exchangers – A review, Renew. Sustain. Energy Rev. 60 (2016) 1367–1386. doi:10.1016/j.rser.2016.03.024.

[166] G. Kosmadakis, D. Manolakos, S. Kyritsis, G. Papadakis, Economic assessment of a two-stage solar organic Rankine cycle for reverse osmosis desalination, Renew. Energy. 34

(2009) 1579–1586.

[167] M. Papapetrou, A. Cipollina, U. La Commare, G. Micale, G. Zaragoza, G. Kosmadakis, Assessment of methodologies and data used to calculate desalination costs, Desalination. 419 (2017). doi:10.1016/j.desal.2017.05.038.

[168] R. Pili, A. Romagnoli, H. Spliethoff, C. Wieland, Techno-Economic Analysis of Waste Heat Recovery with ORC from Fluctuating Industrial Sources, in: Energy Procedia, 2017. doi:10.1016/j.egypro.2017.09.170.

[169] C. Sommariva, Desalination and Advance Water Treatment Economics and Financing, Balaban Desalination Publications, 2010. https://www.desline.com/Sommariva_book_flyer.pdf.

[170] eia - US Energy Information Administration, Capital Cost Estimates for Utility Scale Electricity Generating Plants, 2016. https://www.eia.gov/analysis/studies/powerplants/capitalcost/pdf/capcost_assumption.pdf.

[171] M. The true competitiveness of solar PV - A European case study, ETIP-PV, European Technology and Innovation Platform Photovoltaics, Energy Policy. (2016). doi:10.1016/j.enpol.2016.04.014.

[172] S. Quoilin, S. Declaye, B.F. Tchanche, V. Lemort, Thermo-economic optimization of waste heat recovery Organic Rankine Cycles, Appl. Therm. Eng. (2011). doi:10.1016/j.applthermaleng.2011.05.014.

[173] SMA, The SMA company, (2018). https://www.sma.de/en/.

[174] B. Rahimi, J. May, A. Christ, K. Regenauer-Lieb, H.T. Chua, Thermo-economic analysis of two novel low grade sensible heat driven desalination processes, Desalination. 365 (2015) 316–328. doi:10.1016/j.desal.2015.03.008.

[175] P. Palenzuela, D.C. Alarcón-Padilla, G. Zaragoza, Large-scale solar desalination by combination with CSP: Techno-economic analysis of different options for the Mediterranean Sea and the Arabian Gulf, Desalination. 366 (2015) 130–138. doi:10.1016/j.desal.2014.12.037.

[176] R. Olwig, T. Hirsch, C. Sattler, H. Glade, L. Schmeken, S. Will, A. Ghermandi, R. Messalem, Techno-economic analysis of combined concentrating solar power and desalination plant configurations in Israel and Jordan, Desalin. Water Treat. 41 (2012) 9–25. doi:10.1080/19443994.2012.664674.

[177] B. Ortega-Delgado, L. Garcia-Rodriguez, D.-C. Alarcon-Padilla, Opportunities of improvement of the MED seawater desalination process by pretreatments allowing high-temperature operation, Desalin. Water Treat. 97 (2017) 94–108.

[178] I.S. Al-Mutaz, I. Wazeer, Economic optimization of the number of effects for the multieffect desalination plant, Desalin. Water Treat. (2015). doi:10.1080/19443994.2014.960468.

[179] N. Wade, Distillation plant development and cost update1, Desalination. 136 (2001) 3–12. doi:10.1016/S0011-9164(01)00159-X.

[180] L. Tian, Y. Wang, J. Guo, Economic analysis of a 2×200 MW nuclear heating reactor for seawater desalination by multi-effect distillation (MED), Desalination. 152 (2003) 223–228. doi:10.1016/S0011-9164(02)01067-6.

[181] U.K. Kesieme, N. Milne, H. Aral, C.Y. Cheng, M. Duke, Economic analysis of desalination

technologies in the context of carbon pricing, and opportunities for membrane distillation, Desalination. 323 (2013) 66–74. doi:10.1016/j.desal.2013.03.033.

[182] M. Moser, F. Trieb, T. Fichter, J. Kern, Renewable desalination: a methodology for cost comparison, Desalin. Water Treat. 51 (2013) 1171–1189. doi:10.1080/19443994.2012.715446.

[183] M. Moser, F. Trieb, T. Fichter, J. Kern, D. Hess, A flexible techno-economic model for the assessment of desalination plants driven by renewable energies, Desalin. Water Treat. 3994 (2014) 1–15. doi:10.1080/19443994.2014.946718.

[184] Desaldata Desalination database, (2018).

[185] Personal communication with MED technology providers, (n.d.).

[186] M.A. Sharaf, A.S. Nafey, L. García-Rodríguez, Exergy and thermo-economic analyses of a combined solar organic cycle with multi effect distillation (MED) desalination process, Desalination. 272 (2011) 135–147.

[187] A. Christ, K. Regenauer-Lieb, H.T. Chua, Boosted Multi-Effect Distillation for sensible low-grade heat sources: A comparison with feed pre-heating Multi-Effect Distillation, Desalination. 366 (2015) 32–46.

[188] X. Liu, W. Chen, S. Shen, M. Gu, G. Cao, The research on thermal and economic performance of solar desalination system with evacuated tube collectors, Desalin. Water Treat. 51 (2013) 3728–3734.

[189] D. Zhao, J. Xue, S. Li, H. Sun, Q. Zhang, Theoretical analyses of thermal and economical aspects of multi-effect distillation desalination dealing with high-salinity wastewater, Desalination. 273 (2011) 292–298.

[190] C. Sommariva, Desalination and advanced water treatment: Economics and financing., Balaban Desalination Publications, Hopkinton, MA, 2010.

[191] B. Ortega-Delgado, P. Palenzuela, D.-C. Alarcón-Padilla, Parametric study of a multi-effect distillation plant with thermal vapor compression for its integration into a Rankine cycle power block, Desalination. 394 (2016) 18–29.

[192] A. Ophir, F. Lokiec, Advanced MED process for most economical sea water desalination, Desalination. 182 (2005) 187–198. doi:10.1016/j.desal.2005.02.026.

[193] F. Verdier, MENA Regional Water Outlook, Part II: Desalination Using Renewable Energy. Final report, Stuttgart, 2011.

[194] A.M. Helal, A.M. El-Nashar, E. Al-Katheeri, S. Al-Malek, Optimal design of hybrid RO/MSF desalination plants Part I: Modeling and algorithms, Desalination. 154 (2003) 43–66.

[195] K. V. Reddy, N. Ghaffour, Overview of the cost of desalinated water and costing methodologies, Desalination. 205 (2007) 340–353. doi:10.1016/j.desal.2006.03.558.

[196] I.S. Al-Mutaz, I. Wazeer, Current status and future directions of MED-TVC desalination technology, Desalin. Water Treat. 55 (2015) 1–9.

[197] A.O. Bin Amer, Development and optimization of ME-TVC desalination system, Desalination. 249 (2009) 1315–1331.

[198] M. Al-Shammiri, M. Safar, Multi-effect distillation plants: state of the art, Desalination. 126 (1999) 45–59.

[199] A.M. El-Nashar, The economic feasibility of small solar MED seawater desalination plants for remote arid areas, Desalination. 134 (2001) 173–186.

[200] N. Ghaffour, T.M. Missimer, G.L. Amy, Technical review and evaluation of the economics of water desalination: Current and future challenges for better water supply sustainability, Desalination. 309 (2013) 197–207. doi:10.1016/j.desal.2012.10.015.

[201] S. Al-obaidani, E. Curcio, F. Macedonio, G. Di, H. Al-hinai, E. Drioli, Potential of membrane distillation in seawater desalination : Thermal efficiency , sensitivity study and cost estimation, J. Memb. Sci. 323 (2008) 85–98. doi:10.1016/j.memsci.2008.06.006.

[202] J. Couper, W. Penney, J. Fair, S. Walas, Chemical Process Equipment-Selection and Design, 3rd ed., Elsevier, 2012.

[203] S. Kaplan, Power Plants: Characteristics and Costs, Congr. Res. Serv. (2008). https://fas.org/sgp/crs/misc/RL34746.pdf.

[204] M. Imran, B.S. Park, H.J. Kim, D.H. Lee, M. Usman, M. Heo, Thermo-economic optimization of Regenerative Organic Rankine Cycle for waste heat recovery applications, Energy Convers. Manag. (2014). doi:10.1016/j.enconman.2014.06.091.

[205] M.T. Whitea, O.A. Oyewunmia, M.A. Chatzopouloua, A.M. Pantaleoa, B.A.J. Haslama, C.N. Markidesa, Integrated computer-aided working-fluid design and thermoeconomic ORC system optimisation, in: Energy Procedia, 2017. doi:10.1016/j.egypro.2017.09.095.

[206] G. Kosmadakis, D. Manolakos, G. Papadakis, Experimental investigation of a low temperature organic Rankine cycle (ORC) engine under variable heat input operating at both subcritical and supercritical conditions, Appl. Therm. Eng. (2016). doi:10.1016/j.applthermaleng.2015.09.082.

[207] G. Kosmadakis, A. Landelle, M. Lazova, D. Manolakos, A. Kaya, H. Huisseune, C.S. Karavas, N. Tauveron, R. Revellin, P. Haberschill, M. De Paepe, G. Papadakis, Experimental testing of a low-temperature organic Rankine cycle (ORC) engine coupled with concentrating PV/thermal collectors: Laboratory and field tests, Energy. (2016). doi:10.1016/j.energy.2016.10.047.

[208] E. Ntavou, G. Kosmadakis, D. Manolakos, G. Papadakis, D. Papantonis, Experimental testing of a small-scale two stage Organic Rankine Cycle engine operating at low temperature, Energy. (2017). doi:10.1016/j.energy.2017.09.127.

[209] E. Guillén-Burrieza, G. Zaragoza, S. Miralles-Cuevas, J. Blanco, Experimental evaluation of two pilot-scale membrane distillation modules used for solar desalination, J. Memb. Sci. (2012). doi:10.1016/j.memsci.2012.03.063.

[210] G. Zaragoza, A. Ruiz-Aguirre, E. Guillén-Burrieza, Efficiency in the use of solar thermal energy of small membrane desalination systems for decentralized water production, Appl. Energy. (2014). doi:10.1016/j.apenergy.2014.02.024.

[211] D. Papadaskalopoulos, R. Moreira, G. Strbac, D. Pudjianto, P. Djapic, F. Teng, M. Papapetrou, Quantifying the Potential Economic Benefits of Flexible Industrial Demand in the European Power System, IEEE Trans. Ind. Informatics. 14 (2018) 5123–5132. doi:10.1109/TII.2018.2811734.

[212] D. of E. and Conservation, W.R.M. Division, Evaluation of Potable Water Storage Tanks in Newfoundland and Labrador and their Effect on Drinking Water, 2011. https://www.mae.gov.nl.ca/waterres/reports/drinking_water/Tank_Report_July_12_2011.pdf.

[213] ICF, STUDY ON ENERGY EFFICIENCY AND ENERGY SAVING POTENTIAL IN INDUSTRY AND ON POSSIBLE POLICY MECHANISMS, 2015. https://ec.europa.eu/energy/sites/ener/files/documents/151201 DG ENER Industrial EE

study - final report_clean_stc.pdf.

[214] C. Brunner, Low CO2 production in European food and beverage industry -Branch concepts, (2013). http://www.rhc-platform.org/fileadmin/user_upload/Structure/Solar_Thermal/Download/130315_Workshop_SPHI_Low_CO2_production_in_European_food_and_beverage_industry_-_C_Brunner.pdf.

[215] T. Patterson, S.R. Esteves, A.G. J., M.R. Dinsdale, CASE STUDY: Pellmeyer Biogas Plants, Eggertshofen, Munich, Germany, (2009). https://www.ifa.ie/wp-content/uploads/2013/10/Pellmeyer-Biogas-Case-Study-Germany.pdf.

[216] S. Schnack, 35.000 dwt bulk carrier exhaust gas emission reduction concept study, 2009. http://greenship.org/wp-content/uploads/2017/01/Green-ship-of-the-future_concept-study.pdf.

[217] W.J. Kostowski, J. Kalina, P. Bargiel, P. Szufleński, Energy and exergy recovery in a natural gas compressor station - A technical and economic analysis, Energy Convers. Manag. (2015). doi:10.1016/j.enconman.2015.07.002.

[218] E. Knapek, C. Pletl, Geothermal Energy in the Munich Metropolitan Area, (2014).

[219] J. Bonafin, M. Del Carria, M. Gaia, A. Duvia, Turboden Geothermal references in Bavaria : technology , drivers and operation, World Geotherm. Congr. (2015). doi:10.3389/fpsyg.2014.01195.

[220] Two-stage-RO-Rankine project, (n.d.). http://solar-orc-ro.aua.gr/en/.

[221] F. Vélez, J.J. Segovia, M.C. Martín, G. Antolín, F. Chejne, A. Quijano, A technical, economical and market review of organic Rankine cycles for the conversion of low-grade heat for power generation, Renew. Sustain. Energy Rev. (2012). doi:10.1016/j.rser.2012.03.022.

[222] Thomas Tartière, ORC market - A world overview, (2016). http://orc-world-map.org/analysis.html.

[223] European Commission, Regulation (EU) No 517/2014 of the European Parliament and of the Council of 16 April 2014 on fluorinated greenhouse gases and repealing Regulation (EC) No 842/2006, Off. J. Eur. Union. (2014). doi:https://doi.org/10.4271/1999-01-0874.

[224] P.K. Sen, P.V. Sen, A. Mudgal, S.N. Singh, S.K. Vyas, P. Davies, A small scale Multi-effect Distillation (MED) unit for rural micro enterprises: Part I—design and fabrication, Desalination. 279 (2011) 15–26. doi:10.1016/j.desal.2010.11.003.